CARDIOVASCULAR MONITORING AND DISEASE DIAGNOSIS USING ECG AND PPG FOR TELEMEDICINE APPLICATIONS

Thesis

Submitted by

Rashmi Rekha Sahoo

Doctor of Philosophy (Engineering)

Department of Electrical Engineering

Faculty Council of Engineering & Technology

Jadavpur University

Kolkata, India

2025

INDEX NO. : 284/21/E

1. Title of the thesis: **CARDIOVASCULAR MONITORING AND DISEASE DIAGNOSIS USING ECG AND PPG FOR TELEMEDICINE APPLICATIONS**

2. Name, Designation & Institution of Supervisor/s: **Dr. Palash Kumar Kundu**
Professor
Department of Electrical Engineering
Jadavpur University, Kolkata-700032, India

3. List of Publication:

Journal Publications:

[1] R. R. Sahoo, S. Ghosh, S. Mani, P. K. Kundu, "Prediction of ECG fiducial parameters from PPG signals for the analysis of cardiovascular diseases: A novel Gaussian process regression-based approach", Biomedical Signal Processing and Control, Volume 90,2024, 105838, ISSN 1746-8094, https://doi.org/10.1016/j.bspc.2023.105838**.**

[2] R. R. Sahoo, S. Bhowmick, D. Mandal, P. K. Kundu, "A novel approach of Gaussian mixture model-based data compression of ECG and PPG signals for various cardiovascular diseases", Biomedical Signal Processing and Control, Volume 96, Part B, 2024, 106581, ISSN 1746-8094, https://doi.org/10.1016/j.bspc.2024.106581.

[3] R. R. Sahoo, S. Ghosh, S. Mani, P. K. Kundu, "A composite feature Engineering approach for enhanced detection of cardiovascular diseases using ECG and PPG signals", Biomedical Signal Processing and Control (Submitted).

Conference Publications

[1] R. R. Sahoo, S. Ghosh, A. Lala and P. K. Kundu, "Classification of Cardiac Abnormality using PPG Fiducial Parameters and Probabilistic Neural Network," *2022 IEEE Calcutta Conference (CALCON)*, Kolkata, India, 2022, pp. 49-54, https://doi.org/10.1109/CALCON56258.2022.10059736.

[2] R. R. Sahoo, A. Lala, P. K. Kundu and S. Ghosh, "Data Compression of Photoplethysmogram Signal for IoT Application," *2022 IEEE International Conference of Electron Devices Society Kolkata Chapter (EDKCON)*, Kolkata, India, 2022, pp. 615-620, https://doi.org/10.1109/EDKCON56221.2022.10032860.

Book Chapter

[1] R.R. Sahoo, P.K. Kundu, "Prediction of Fiducial Parameter of PPG Signal—A Comparative Study Between Radial Basis and General Regression Neural Network Performance." In: Bhaumik, S., Chattopadhyay, S., Chattopadhyay, T., Bhattacharya, S. (eds) Proceedings of International Conference on Industrial Instrumentation and Control. Lecture Notes in Electrical Engineering, vol 815. (2022) Springer, Singapore. https://doi.org/10.1007/978-981-16-7011-4_10

4. List of Patents : NIL

5. List of Presentation in National/ International Conferences/Workshop:

[1] R.R. Sahoo, P.K. Kundu, "Prediction of Fiducial Parameter of PPG Signal—A Comparative Study Between Radial Basis and General Regression Neural Network Performance.", International Conference on Industrial Instrumentation & Control (ici2c-2021) 20-22nd August 2021.

[2] R. R. Sahoo, A. Lala, P. K. Kundu and S. Ghosh, "Data Compression of Photoplethysmogram Signal for IoT Application," 2022 IEEE International Conference of Electron Devices Society Kolkata Chapter (EDKCON), Kolkata, 26-27th November 2022.

[3] R. Sahoo, S. Ghosh, A. Lala and P. K. Kundu, "Classification of Cardiac Abnormality using PPG Fiducial Parameters and Probabilistic Neural Network," 2022 IEEE Calcutta Conference (CALCON), Kolkata, 10-11th December 2022.

Statement of Originality

I Rashmi Rekha Sahoo registered on 23rd July, 2021 do hereby declare that this thesis entitled **"CARDIOVASCULAR MONITORING AND DISEASE DIAGNOSIS USING ECG AND PPG FOR TELEMEDICINE APPLICATIONS"** contains literature survey and original research work done by the undersigned candidate as part of Doctoral studies.

All information in this thesis have been obtained and presented in accordance with existing academic rules and ethical conduct. I declare that, as required by these rules and conduct, I have fully cited and referred all materials and results that are not original to this work.

I also declare that I have checked this thesis as per the "Policy on AntiPlagiarism, Jadavpur University, 2019", and the level of similarity as checked by iThenticate software is (03)%.

Rashmi Rekha Sahoo

Signature of Candidate:

Date: 26/06/2025

26/06/2025

Certified by Supervisor(s):

(Signature with date, seal)

Professor
Electrical Engineering Department
JADAVPUR UNIVERSITY
Kolkata - 700 032

CERTIFICATE OF SUPERVISOR

This is to certify that, the thesis entitled "CARDIOVASCULAR MONITORING AND DISEASE DIAGNOSIS USING ECG AND PPG FOR TELEMEDICINE APPLICATIONS" submitted by Mrs. Rashmi Rekha Sahoo, who got her name registered on 23rd July 2021 for the award of Ph.D. (Engineering) degree of Jadavpur University is absolutely based upon her own work under the supervision of Dr. Palash Kumar Kundu and that neither her thesisnor any part of the thesis has been submitted for any degree/diploma or any other academicaward anywhere before.

26/08/2025

Professor
Electrical Engineering Department
JADAVPUR UNIVERSITY
Kolkata - 700 032

Signature of the Supervisor and date with office seal

Acknowledgement

The author would like to express her gratitude and sincere appreciation to everyone who has given of their time and encouraged me throughout the course of my Ph.D. tenure. Throughout this time, I am appreciative of their precious suggestions, invaluable constructive criticism, and cordial counsel. They provided me with honest and enlightening opinions on a variety of topics pertaining to my doctoral research, for which I genuinely thank them.

The author would like to express sincere gratitude to her supervisor , *Dr. Palash Kumar Kundu*, Professor, Electrical Engineering Department, Jadavpur University, for his unwavering support of Ph.D. research and study.

The author feels fortunate to have had such a mentor who gave her the freedom to pursue her interests while still providing guidance when her steps faltered. His advice has been helpful throughout the entire research and writing process for this dissertation. The author is also appreciative of him for morally supporting her while she was in trouble.

The author wishes to convey her profound gratitude to the faulty members Prof. Sugata Munshi, Prof Mita Dutta, Prof. Amitava Chatterjee, Prof. Debanghu Dey, Prof. Gautam Sarkar, and Biswajit Bhattacharyya of the Measurements and Instrumentation Laboratory, Electrical Engineering Department of Jadavpur University for their invaluable counsel and continued assistance in conducting the research.

The author is grateful to the present and former Heads Prof. Biswanath Roy and Prof. Saswati Mazumdar respectively of the Electrical Engineering Department at Jadavpur University for providing adequate research facilities in the department. The author also thanks the faculty and staff members of the Department of Electrical Engineering for their unwavering support and encouragement.

The author thanks Dr. Siddhartha Mani, Consultant Interventional Cardiologist, NH Rabindranath Tagore, International Institute of Cardiac Sciences, Kolkata, India for his insightful comments and important contribution to this research work. The author would always be grateful to him for giving sufficient time from his busy schedule and contributing his medical knowledge to the research project for cooperation to collect data samples of current signals from healthy and cardico vascular diseased people to carry out this research work.

The author wants to express her sincere gratitude to Mr. Saibal Ghosh for all of his help, encouragement, and support during her Ph.D. study. His wise counsel, helpful criticism, and extensive expertise have greatly influenced her work. Mr. Ghosh's perseverance, encouragement, and readiness to impart his knowledge have motivated her to improve academically. The author sincerely values his steadfast assistance and the time he invested in honing her concepts and resolving issues. Without his invaluable guidance and suggestions, this thesis would not have been feasible.

This research project would not have been possible to finish without the constant assistance from fellow researchers of the Measurements and Instrumentation Laboratory, Department of Electrical Engineering. In this regard, the author would like to thank his laboratory members Ms. Antara Ghosh, Mr. Anadi Biswas, Dr. Biswarup Ganguly, Dr. Sayanti Chaudhuri, and Ms. Pubali De for their continuous emotional support in overcoming the hardships during the Ph.D. journey.

The author would like to specifically thank to her parents Mr. Nakula Sahoo, Mrs. Kumudini Sahoo, Mr. Satyaban Bera, and Mrs. Subhadra Bera for their continuous encouragement, tireless motivation and taking enormous pains during her tenure of work. Without them, nothing would have been possible. The author would especially thank her husband Mr. Prabin Kumar Bera and her loving daughter Saanvi Sai Bera for their continuous encouragement to complete her Ph.D. To endwith, the author acknowledges all her well-wishers whom she could not mention and who have contributed directly and indirectly towards the completion of her work. Also, thank the almighty God for giving her mental patience and physical perseverance for the completion of the research work in the present form.

Rashmi Rekha Sahoo 26/06/25

Rashmi Rekha Sahoo
Measurements & Instrumentation Laboratory
Department of Electrical Engineering
Jadavpur University
Kolkata, India

Dedicated to…

My Parents

My Husband

&

My Daughter Sona

Who have always supported me in all my endeavors…

Contents

List of Figures

List of Tables

List of Abbreviations

Abbreviations	*Description*
SA	Sinoatrial
CVD	Cardiovascular disease
RBBB	Right Bundle Branch Block
ACC	American College of Cardiology
AHA	American Heart Association
DCM	Dilated Cardiomyopathy
CHB	Complete Heart Block
ECG	Electrocardiography
PPG	Photoplethysmography
AV	Atrioventricular
PD	Photo Resistor/Detector
PTT	Pulse Transit Time
ST	Systolic Time
DT	Diastolic Time
PT,PTIME	Pulse Time
PPGAI	PPG Augmented Index
HR	Heart rate
HRV	Heart rate variability
WT	Wavelet Transform
AR	Autoregressive
HMM	Hidden Markov Model
PCA	Principal Component Analysis
DTW	Dynamic Time Warping
BiLSTM	Bidirectional Long Short-Term Memory
FM	Fourier Model
GM	Gaussian Model
ATA	American Telemedicine Association
ICT	Information And Communication Technology

ANS	Autonomic Nervous System
AF	Atrial Fibrillation
ANF	Adaptive Notch Filter
EDR	ECG-Derived Respiration
IHR	Instantaneous Heart Rate
CNN	Convolutional Neural Network
MA	Motion Artifacts
TFS	Time-Frequency Spectrum
DFT	Discrete Fourier Transform
MIMO	Multi-Input-Multi-Output
LSTM	Long Short Term Memory
IBI	Interbeat Interval
SNR	Signal-to-Noise Ratio
AVCT	Atrioventricular Conduction Time
SCD	Sudden Cardiac Death
PWLL	P-Wave Locked Loop
AFT	Accelerated Failure Time
VT	Ventricular Tachycardia
ANN	Artificial Neural Networks
SVM	Support Vector Machines
RBF	Radial Basis Function
MLP	Multilayer Perceptions
CRNN	Convolutional Recurrent Neural Network
LSTM	Long Short-Term Memory
MI	Myocardial Infarction
CorNET	Cortical Neural Network
PR	Pulse Rate
SBP	Systolic Blood Pressure

DBP	Diastolic Blood Pressure
CR	Compression Ratio
KLT	Karhunen–Loeve Transform
AZTEC	Amplitude Zone Time Epoch Coding
RLE	Run-Length Encoding
HE	Huffman Encoding
CS	Compressive Sensing
SVD	Singular Value Decomposition
PCA	Principal Component Analysis
DCT	Discrete Cosine Transform
XDJDL	Cross-Domain Joint Dictionary Learning
LDA	Linear Discriminant Analysis
DT	Decision Tree
KNN	K-Nearest Neighbor
DCNN	Deep Convolution Neural Network
GACNN	Graph Attentive Convolution Neural Network
MIMIC	Medical Information Mart For Intensive Care
BIH	Beth Israel Hospital
MIT	Massachusetts Institute Of Technology
APG	Acceleration PPG
ICD-9-CM	International Classification Of Diseases, 9th Revision, Clinical Modification
VPG	Velocity PPG
WHO	World Health Organization
PRD	Percent root mean square difference
PRDN	Percentage Root Mean Square Difference Normalized
RMSE	Root Mean Square Error
CC	Pearson correlation coefficient
QS	Quality score

Exe. Time	Execution Time
FWHT	Fast Walsh-Hadamard Transform
AALO	Accelerated Ant Lion Optimizer
EZW	Embedded Zero Tree Wavelet
CHIO	Coronavirus Herd Immunity Optimizer
ACO	Ant Colony Optimizer
GPR	Gaussian Process Regression
EMD	Empirical Mode Decomposition
RNN	Recurrent Neural Networks
RRMSE	Relative Root Mean Square Error
LOA	Lower Limit Of Agreement
UOA	Upper Limit Of Agreement
CI	Confidence Interval
HYPER	Hypertension
ARYTH, ARYTH-ATRFAB	Arrhythmia-Atrial Fibrillation
RBNN	Radial Basis Neural Network
GRNN	General Regression Neural Network
PNN	Probabilistic Neural Network
1D-CNN	1-D Convolutional Neural Network
LR	Logistic Regression
LDA	Linear Discriminant Analysis
DT	Decision Tree
RF	Random Forest
DLP	Diastolic Phase
FPR	False Positive Rate
A-ROC	Area Under ROC Curve
A-PR	Area Under PR Curve
COPD	Chronic Obstructive Pulmonary Disease

List of Symbols

Symbols	*Description*
$e(n)$	Noise
$x(n)$	ECG/PPG signal
$z(x)$	Gaussian function
C_0	Average value of PPG signal
$Y(X)$	Output of GRNN
A_n	Sine wave amplitude in FM
B_n	Cosine wave amplitude in FM
a_m	Amplitude in Gaussian model (GM)
b_m	Center in Gaussian model (GM)
c_m	Variance in Gaussian model (GM)
σ_m	Standard deviation of m^{th} component of GM
$f(i)$	Gaussian process function
$m(i)$	Mean function
$k(.\ ,.\ ;\hbar)$	Arbitrary covariance function
$p(f\|I)$	Predictive distributor
σ_s	Scaling parameter of Gaussian process regressor (GPR)
l	Length parameter of GPR
ρ	Pearson's correlation coefficient
R^2	Coefficient of determination
N	Order of the Fourier Model (FM)
T	Time period of ECG/PPG wave

Abstract

The field of illness diagnosis, characterization, and classification using signal processing and feature extraction approaches has seen tremendous growth in recent years. This is a result of the global increase in the number of diseases. Among those globally, cardiovascular diseases (CVDs) are the most prevalent non-communicable health issues and one of the fundamental causes of death The dysfunction of the heart is the main cause of CVD, a condition with several symptoms. So, attention towards CVD is the root cause in the healthcare domain. The unavailability of enough health care systems and the work stress and casual lifestyle hinder routine health check-ups and precise diagnoses. A key issue has been the requirement for a prompt, affordable, and precise diagnosis, treatment, and cure at the early stage at a fair price to enhance human health. In the evolving landscape of telemedicine, the management of CVD patient data, particularly electrocardiogram (ECG) and photoplethysmogram (PPG) signals, requires efficient compression, prediction, and classification techniques. This study delves into advanced methodologies to address these challenges, ensuring optimized storage, transmission, and diagnostic capabilities for remote healthcare applications. The compression of PPG signals is critical for Internet of Things (IoT) applications, facilitating real-time monitoring through wearable devices. Efficient compression algorithms are developed to meet the demands of low-power devices, ensuring that essential diagnostic data is preserved. Fourier and Gaussian model-based compression techniques are also explored to optimize PPG data handling, with secure sharing implemented through cloud-based platforms like Dropbox. Furthermore, an integrated algorithm is proposed to compress both ECG and PPG signals effectively, ensuring compatibility with telemedicine frameworks while maintaining high diagnostic accuracy. Predicting fiducial parameters from ECG and PPG signals is essential for identifying critical markers of CVD. Neural network models, including Radial Basis Neural Networks (RBNN) and General Regression Neural Networks (GRNN), are employed to predict PPG fiducial parameters with high accuracy. Gaussian Process Regression (GPR) is introduced as a robust statistical method to accommodate inter-patient variability in physiological signals. Additionally, methods for extracting ECG fiducial parameters from PPG signals are developed, reducing the reliance on multiple monitoring devices and enhancing system scalability. Comprehensive results and analyses validate the effectiveness of these predictive techniques, demonstrating improved accuracy and reliability in clinical settings. Classification and authentication of CVD types form a cornerstone of this study. Machine learning techniques are applied to detect CVD, leveraging data-driven insights for precise identification. A one-dimensional Convolution Neural Network (1-D CNN) is designed to enhance detection accuracy by capturing temporal and spatial signal features. Composite feature engineering combines insights from both ECG and PPG signals, further improving detection performance. An algorithm is proposed for classifying unknown CVD types using the approaches of 1-D CNN and machine learning methods, ensuring adaptability to diverse clinical scenarios. The results demonstrate the superiority of these classification methods, showcasing their potential for early and accurate disease detection. This comprehensive study integrates state-of-the-art compression algorithms, predictive modeling, and classification frameworks to advance telemedicine for CVD management. By combining techniques such as Fourier and Gaussian models, RBNN, GRNN, GPR, and 1-D CNN, the proposed methodologies achieve significant improvements in data efficiency, prediction accuracy, and disease classification. The findings underscore the potential of these approaches to enhance the scalability, reliability, and accessibility of telemedicine solutions, paving the way for more effective healthcare services for CVD patients. The presented methods highlight the interplay between signal processing, machine learning, and IoT technologies, offering a robust foundation for future innovations in remote healthcare systems.

In a nutshell, the goal of this thesis is to build and develop methods for CVD detection, compression, characterization, and classification using signal processing, neural networks, machine learning, and deep learning. The development of more intricate structures to capture a variety of morphological patterns that can surpass the performance of current state-of-the-art frameworks has led to the invention and development of several machine learning and, more recently, deep learning frameworks.

Chapter 1

Introduction

This chapter gives a brief idea of the mechanism of the heart function. Malfunctioning of the regular action of the heart leads to many cardiovascular diseases. PPG and ECG provide two distinct viewing windows for the same heart activity, indicating their intrinsically strong physiological correlation. Here the narration of fiducial parameters of ECG and PPG are done with the different existing modeling. Also, this chapter explains the application of this signal analysis in telemedicine for remote areas.

1.1 Mechanism of heart and its functioning

The human body is regulated by various organ systems that generate bioelectric signals through continuous physiological activities. Among these, the cardiovascular system plays a significant role where the heart is the center of attraction and carries substantial weight [1]. The heart serves as a muscle pump, which ensures a perpetual supply of blood to the body's tissues and organs. The right atrium contains the sinoatrial node (SA node), often known as the heart's natural pacemaker, which generates electrical impulses and initiates the heart pumping [2]. These impulses circulate through the heart, coordinating contractions and facilitating the action potential spread quickly.

Electrical signals that originate in the heart and travel via the cardiac conduction system control the cardiac myocardium's contraction (systole) and relaxation (diastole), constituting a heartbeat. To facilitate the movement of blood fluid to the ventricles, the signals start at the SA node and cause atrial systole as they traverse through the atria. The signals then traverse through the atrioventricular node, giving the atrium enough time to transfer blood. Then they proceed to the ventricles, where they start ventricular systole and pump blood into the arteries. Atrial diastole and ventricular diastole are the relaxation and repolarisation of the atria and ventricles, respectively that occur before the cardiac cycle restarts [3]. A heartbeat results from the heart muscle contracting and relaxing, pumping blood throughout the body. A cardiac rhythm, on the other hand, is the pattern or series of heartbeats throughout time. Numerous cardiac disorders are determined by the electrical signals that control the heart's contractions [4]. The entire heart operation is portrayed in Fig. 1.1.

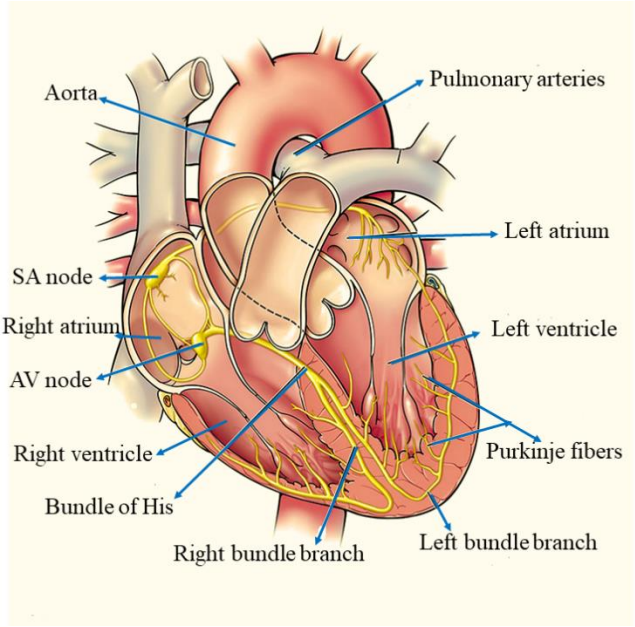

Fig. 1.1. Typical structure of the heart.

1.2 Cardiovascular diseases

The term cardiovascular diseases (CVDs) refers to a collection of conditions that impact the heart and blood arteries, such as hypertension, coronary artery disease, stroke, etc. Frequently associated with risk factors such as smoking, obesity, and bad lifestyle choices, they are the world's top cause of mortality. CVDs can be successfully prevented and managed with the support of medical care, good lifestyle choices, and early detection. Malfunctioning of the heart's regular action leads to various CVDs and few of them are listed below.

1.2.1 Right bundle branch block (RBBB)

It occurs when there's a delay in the electrical signal traveling through the right bundle branch of our heart. As a result, the signals on the left and right sides of the heart no longer move simultaneously. The signal has to pass throughout a block in the branch when there is a right bundle branch block as shown in Fig. 1.2 by which the right ventricle contracts after the left as the signal travels down the right bundle branch a bit more slowly than the left bundle branch. This is the result and the signal on the right side lags, leading to an irregular heartbeat [4]. The causes of this type of CVD may be, “Myocarditis, Trauma to our chest, heart attack (myocardial infarction), right heart catheterization or other procedures, changes in branch structure, such as stretching, etc.”

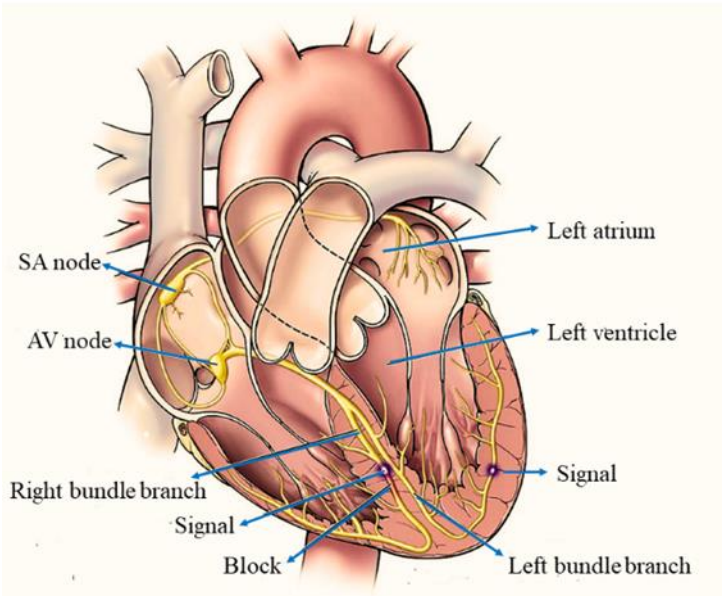

Fig. 1.2. Typical structure of the heart with right branch bundle block.

1.2.2 Hypertension

For healthy people because of their activity, emotion, posture, diet, and medicine blood pressure changes for a shorter duration, which is not hazardous. But for diseased people, when arteries are narrowed and exhibit greater strain when carrying blood away from the heart, the force acting on the arterial walls increases [5] as shown in Fig. 1.3. This causes the heart to pump more blood, causing hypertension, which drastically changes the systolic and diastolic pressure. In 2017, the American College of Cardiology (ACC) and the American Heart Association (AHA) made the guideline for different types of hypertension (high blood pressure) for 'systolic pressure by diastolic pressure' as- " Normal person=120/80 mm Hg, Elevated= 120-129/below 80 mm Hg, Stage 1= 130-139/80-89 mm Hg, Stage 2= 140/ 90 mm Hg or more".

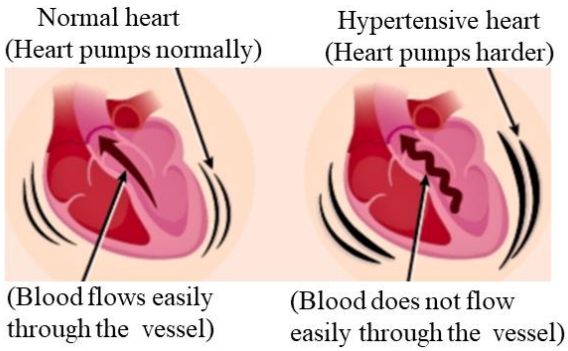

Fig. 1.3. Typical structure of the heart with hypertension.

1.2.3 Arrhythmia-Atrial fibrillation

A problem with our heartbeat's rhythm or pace is called an arrhythmia. It indicates that the rhythm of our heartbeat is irregular, too fast, or too sluggish [6]. The condition known as tachycardia occurs when the heart beats more quickly than usual. Bradycardia occurs when the heart beats too slowly. Atrial fibrillation, which results in an irregular and rapid heartbeat, is the most prevalent kind of arrhythmia [7]. Numerous factors, such as structural cardiac defects, electrolyte imbalances, cardiovascular illnesses, and other underlying medical disorders, might result in these rhythm abnormalities. Mostly, Atrial fibrillation is characterized by erratic and fast electrical activity in the heart's atria (upper chambers), where the atria quiver instead of contracting in unison, which results in rapid blood flow, and a change occurs in the heart's tissue ultimately in the electrical signal [8] as shown in Fig, 1.4.

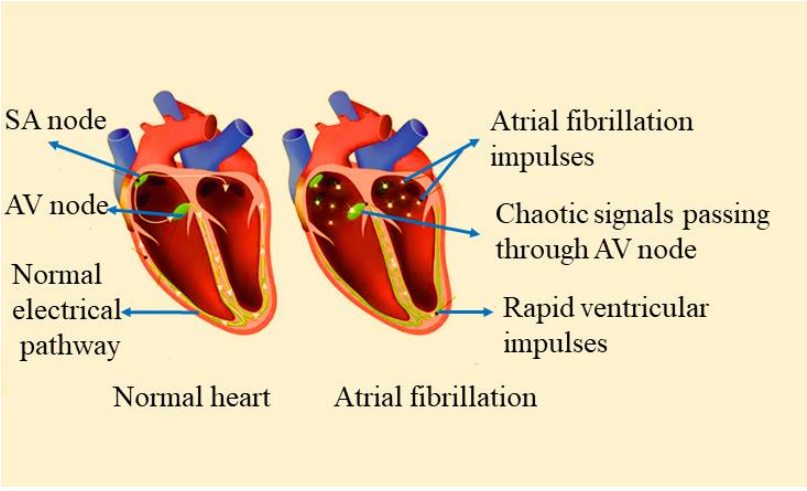

Fig. 1.4. Typical structure of the heart with arrhythmia-Atrial fibrillation.

1.2.4 Dilated cardiomyopathy (DCM)

The disease often begins in the heart's primary pumping chamber, the left ventricle. The heart muscle starts to expand and thin out as it dilates. Consequently, the chamber's interior expands. Frequently, the issue first affects the right ventricle before moving on to the atria. The heart muscle cannot contract normally as shown in Fig.1.5, when the heart chambers dilate making it difficult for the heart to pump blood effectively. Heart failure may develop as the heart weakens. DCM even can lead to blood clots, valve problems arrhythmias, etc. It occurs may be due to excessive alcohol consumption, viral infections that affect the heart muscle, diabetes etc.

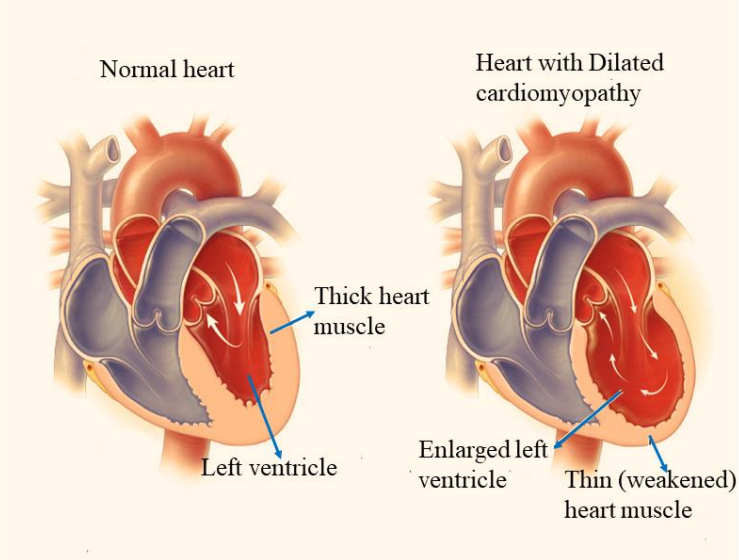

Fig. 1.5. Typical structure of the heart with DCM.

1.2.5 Complete heart block (CHB)

Atrial contraction is made possible by the SA node, ventricular contraction is made possible by the His-Purkinje system, and signal transmission between the atria and ventricles is made possible by the AV node. Blood can be pumped out to the body as long as the electrical impulse is transferred normally, which causes the heart to contract and behave normally. A form of heart block known as CHB happens when the electrical communication between the heart's atria and ventricles is disrupted. The conduction system becomes disconnected as a result, and the ventricles may begin to beat more slowly than the atria as shown in Fig.1.6. This may impair the heart's capacity to pump blood to the rest of the body and result in slow or irregular or sometimes skip heartbeats.

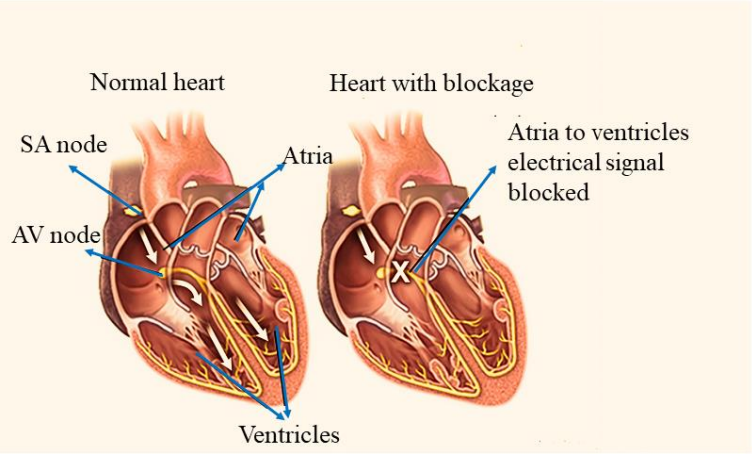

Fig. 1.6. Typical structure of the heart with CHB.

1.3 Electrocardiography (ECG) and Photoplethysmography (PPG)

These two visualizations and highly correlated windows portray the same cardiac activity of the heart function for detecting disorders and diseases related to the cardiovascular system with different working principles.

1.3.1 Electrocardiography (ECG)

The sinoatrial (SA) node, situated in the upper part of the right atrium, is the epicenter of the electrical activity of the heart muscles. At this node, a specialized subset of pacemaker cells spontaneously depolarizes and repolarizes 60–100 times each minute. At a rate of 4 m/s, the electrical impulses slowly dispersed across the atria, forcing them to contract collectively. This results in a discernible deviation on the ECG record known as the P wave. The electrical impulses go through the atria before arriving at the atrioventricular (AV) node, which is situated at the bottom of the right atria. The ECG record shows an equipotential line known as the PR segment, which is the result of the conduction at the AV node establishing a gap between the atrial and ventricular conductions. Electrical impulses from the AV node enter the bundle of His, which is divided into branches for the left and right bundles. Both the ventricles begin to contract (depolarize) together when the impulses pass through the bundle branches. This causes the QRS complex, a combination of abrupt upward and downward deflection in the ECG record. Purkinje fibers, which are dispersed to the left and right atria, gradually disperse the conduction. Hence overall QRS complex generates due to ventricular depolarization. Further, the atria enlarge (repolarize) during ventricular contraction. However, the ventricular activity suppresses the electrical activity that is produced

as a result of this, making it extremely weak. The ECG record shows no electrical activity for a short period between the ventricular contraction and expansion. The equipotential ST segment serves as a representation of this, and the ventricles then begin to expand (repolarise) simultaneously. Soon after this T wave generates because of ventricular repolarization. Following the T wave U wave is recorded due to the ventricular repolarization [9]. Fig. 1.7 and Table 1.1 depicts the index points and the typical signature of the ECG waveform.

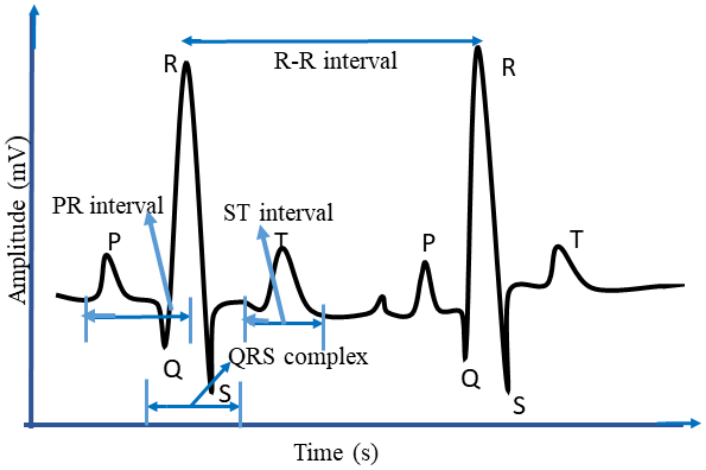

Fig. 1.7. ECG signal waveform with the index points.

Table 1.1. Typical ECG signature and the associated values.

Clinical signature	**Typical values**	**Nominal variations**
P width	110 ms	±20 ms
P amplitude	0.15 mV	±0.05 mV
T width	180 ms	±40 ms
T amplitude	0.3 mV	±0.2 mV
QRS width	100 ms	±20 ms
QRS amplitude	1.2 mV	±0.5 mV

The ECG signal is captured by placing suitable electrodes on the human body non-invasively. The 'three-limb leads- Lead I, Lead II, Lead III', 'three-augmented limb leads- aVR, aVL, aVF', and 'six chest leads-*v*1, *v*2, *v*3, *v*4, *v*5, *v*6' constitutes 12-lead ECG system. In a clinical setting, an electrocardiograph machine connected with electrodes attached to the patient's body establishes an electrocardiogram waveform, which in turn establishes the ECG recording.

1.3.2 Phphotoplethysmography (PPG)

Photoplethysmography (PPG) is a non-invasive, vivo optical technique for detecting disorders and diseases related to the cardiovascular system and measuring and monitoring physiological parameters such as blood pressure, Oxygen saturation(SpO2), heart rate (beat), and respiration in the blood [10,11].

As the radial artery is the best place to capture the pressure pulse wave, the proposal is to select the index fingertip for the placement of sensors in the setup. In PPG setup comprises of IR transmitter (typically a photodiode emitting light pulse at a wavelength of around 900 nm)) which emits the light pulse periodically into the skin of the fingertip, where some may be absorbed by tissue, some scattered and some reflected (Reflectance mode) to the photodetector (typically phototransistor) as shown in Fig. 1.8 [12,13]. The absorption intensity utilizes Beer-Lambert's law [11], which illustrates the amount of blood in the illuminated region, which in turn depends on the cardiac pressure. The more blood in the illuminated region (Systolic phase) i.e. when the heart muscle contracts, it pushes the blood out of the heart into the large blood vessel (artery) of the circulatory system, and BP increases), the more light is absorbed by hemoglobin (Hb), and less light is reflected and ultimately resistance of PD (photo resistor) increases. The PPG signal contains AC, DC components, and some noise components due to motion artifacts. It has a DC component caused by skin, bone, fat, and muscle, which is superimposed on the AC component caused by arterial blood in correspondence to every heartbeat. Using different filtering techniques [14] noise can be eliminated. In gist, the PPG waveform has 3 major components as shown in Fig. 1.9.

- Systolic part (pressure transmittance along a direct path from the aortic root to the finger [15].)
- Diastolic part (pressure transmittance from the ventricle along the aorta to the lower body from where it is reflected back along the aorta to the finger.
- Dicrotic notch (a consequence of a short period of backward flow of blood immediately before the aortic valve closes after the start of diastole)

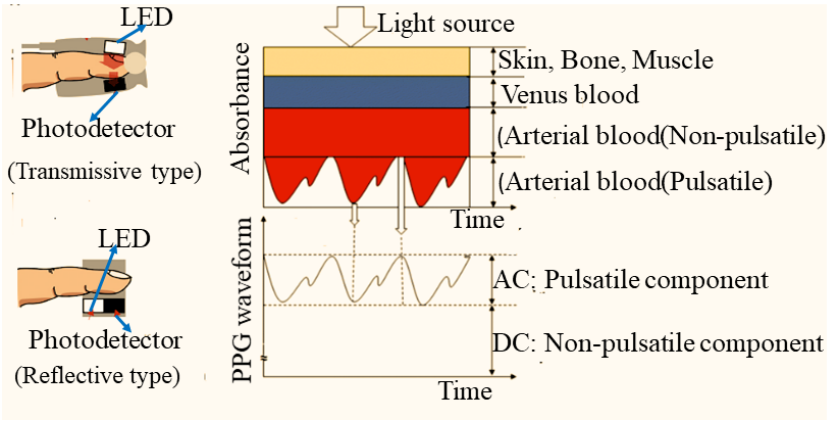

Fig. 1.8. Variation in light attenuation by tissue in PPG.

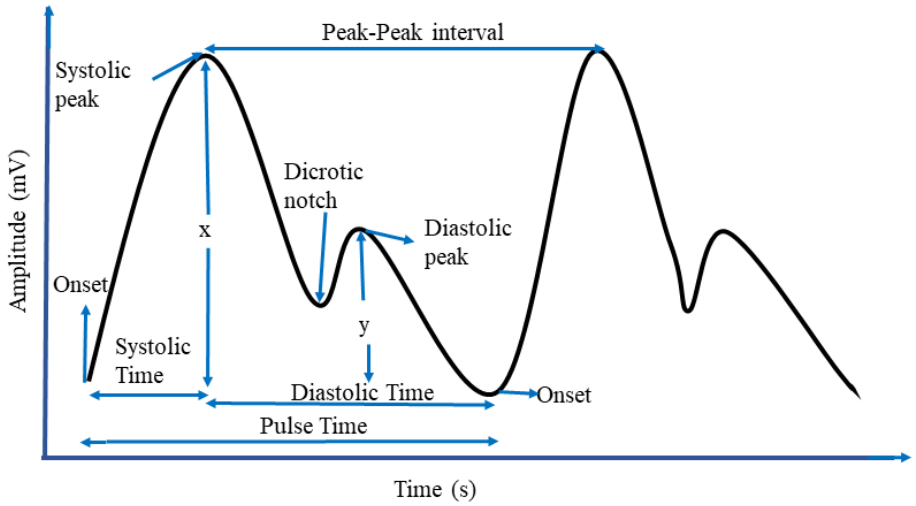

Fig. 1.9. PPG signal waveform with the index points.

1.4 Fiducial parameters of ECG and PPG signals.

Key characteristics or points in ECG and PPG signals that are utilized for feature extraction, analysis, and interpretation are referred to as fiducial parameters or index points. These metrics are essential for comprehending the cardiovascular system's physiological and pathological conditions.

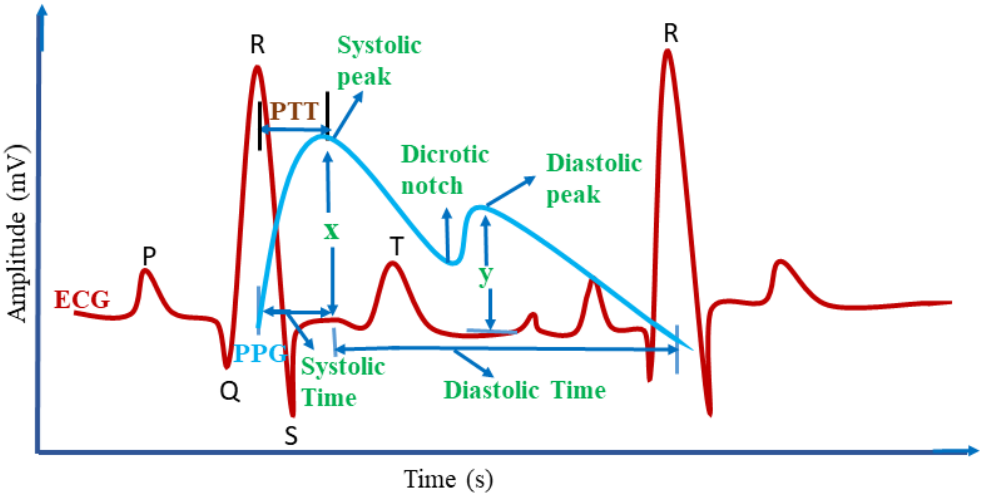

Fig. 1.10. Correlated ECG and PPG signal waveform with the index points.

- Key fiducial parameters of ECG signals are:

  Temporal parameters such as: "P wave duration, PR interval, QRS complex duration, R-R interval/heart rate, ST segment duration, number of P wave, etc."

  Amplitude parameters such as: "P wave amplitude, QRS amplitude, T wave amplitude, ST segment depression/elevation, etc."

Considering one case as an example where the absence of the P wave and shorter R-R interval indicates an arrhythmia case of atrial fibrillation and the cardiac ECG pattern known as 'irregularly irregular'. Likewise, tall R wave, ST depression, and sometimes T wave inversion indicate hypertension disease. For enlarged and weaker heart muscle defining characteristic of dilated cardiomyopathy (DCM) may be challenging for the heart to pump blood adequately when it grows strained leading to wide QRS duration. Wide S and indicate RBBB disease. More P waves than the number of QRS waves with a heart rate < 40 indicates CHB cardiac syndrome. For the diagnosis of arrhythmias, ischemia, myocardial infarction, and other cardiac disorders, parameters such as the PR interval, QRS duration, and QT interval are essential.

- Key fiducial parameters of PPG signals are:

Temporal parameters such as: “pulse transit time (PTT) [16], systolic peak-peak interval, systolic time, diastolic time, pulse time, PPG augmented index (PPGAI = y/x), etc.), Amplitude parameters such as: “systolic peak amplitude, diastolic peak amplitude, dicrotic notch amplitude, etc.” shown in Fig.1.10.

PTT indicates arterial stiffness. systolic peak-peak interval shows the heart rate and can be easily identify CHB cases with a heart rate < 40. High systolic peak amplitude detects the anomalies like hypertension. Diastolic time indicates blood pressure and SpO_2 level in blood and heart rate variability etc.

Hence it can offer comprehensive information about the whole health of the arteries as well as the electrical and mechanical functions of the heart.
Comprehensively fiducial parameters of ECG and PPG are beneficial in the following ways.

- Clinical diagnosis and monitoring
- Heart rate and heart rate variability (HRV) analysis
- Estimation of arterial stiffness and blood pressure
- Real-time monitoring of wearable devices
- Early detection of abnormalities
- Cardiovascular research
- Non-invasive health assessments
- Personalized medicine

These index parameters assist in filling the gap between unprocessed signal data and useful medical insights by serving as a basis for sophisticated algorithms and models.

1.5 Modeling of ECG and PPG signals.

The process of mathematically or computationally describing an ECG or PPG signal to efficiently analyze, interpret, and process its features is known as modelling. The objective is to meaningfully replicate the heart's electrical activity as recorded by the device for technological, scientific, or diagnostic purposes. So, ECG/PPG signal modeling is necessary to promote research and teaching, increase automated analysis, improve diagnosis accuracy, and deliver dependable and effective cardiac care. It binds those dots between

unprocessed physiological data and useful medical information. There are many existing methods available to model these physiological signals.

1.5.1 Wavelet Transform (WT)

To analyze non-stationary elements in PPG (such as pulse waves) and ECG (such as the QRS complex), the signals are broken down into time-frequency components. Though it is well good for noise reduction and transient feature extraction, but requires a keen selection of the wavelet [17].

1.5.2 Autoregressive (AR) Model

It is possible to express the ECG/PPG signal $x(n)$ at time instant n in an AR process of order L as a linear combination of the signal's L prior values as in the equation (1.1).

$$x(n) = \sum_{j=1}^{L} a(j)x(n-j) + e(n) \quad (1.1)$$

Where $a(j)$ is the jth coefficient of the AR model [18] having order L with $e(n)$ noise. Though it reveals information about the periodic features of the signal, it is inadequate to handle stochastic non-stationary signals like ECG/PPG.

1.5.3 Hidden Markov Model (HMM)

It depicts the ECG and PPG signals as hidden state sequences, such as pulse waves or heart cycles. It can adequately model the temporal pattern and heart rate variability of cardiac diseases but with high computational burden and minute tuning of parameters. It can solve the decoding, and evaluation in speech recognition and classification job as well [19].

1.5.4 Principal Component Analysis (PCA)

It eliminates distortion while concentrating on key features in multivariate ECG and PPG data by dimension reduction. It one can reduce the linear dimension that projects data in the directions of greatest variation. PCA algorithm [20] computes the covariance matrix from the extracted ECG/PPG features, decomposes the covariance matrix into eigenvalues and eigenvectors, sorts the eigenvectors in descending

order of eigenvalues, and then projects the original ECG/PPGfeatures in the directions of the sorted eigenvectors. Most of the variation in the data is represented by the first few components. Mostly used in feature extraction and compression assuming linear relationships in data.

1.5.5 Dynamic Time Warping (DTW)

Usually, it is used for speech or word authentication/ matching. However, it can extract the dynamic warping-based features depending on different cardiac conditions [21]. Little inadequate for large data sets and noisy signals.

1.5.6 Bayesian Models

Bayesian models are probabilistic methods that apply Bayes' theorem to update a hypothesis's probability based on new information or evidence. They are used to manage uncertainty, model variability, and integrate previous information for signal analysis, interpretation, and prediction [22]. Bayesian models are also used for ECG and PPG signals in noise or artifact removal, heart beat classification and arrhythmia detection, and heart rate monitoring /variability analysis, etc. Though not adequate for complex signals, they are the cornerstone in cardiovascular signal processing and wearable health monitoring applications.

1.5.7 BiLSTM (Bidirectional Long Short-Term Memory)

One type of recurrent neural network (RNN) that can process data both forward and backward is called BiLSTM [23]. As it captures both past and future contextual dependencies, this design is especially well-suited for sequential data, such as ECG and PPG signals. It is extensively used in multimodal fusion, segmentation, blood pressure estimates, artifact removal, and arrhythmia detection. Due to its robustness, it is critical for contemporary cardiovascular signal analysis and wearable health monitoring technology.

1.5.8 Fourier Model (FM)

As ECG/PPG is a periodic signal can be represented [24] with the sum of sines and cosines i.e. Fourier series model. The trigonometric form of the representation of the model is given in equation(1.2), (1.3) and (1.4). Where, $y(t)$ = time-instantaneous value of PPG signal, n= Total number of data points, C_0= Average value of PPG signal=Time period of PPG wave, $\omega_{0\,=}$ Angular frequency of fundamental

component 2π/T. Let's say twelve model parameters are proposed for each beat of PPG if it is of 4th order.

$$y(t) = C_0 + \sum_{n=1}^{n} A_n \sin(n\omega_0 t) + B_n \cos(n\omega_0 t) \quad (1.2)$$

$$A_n = \frac{2}{T}\int_0^T x(t) \sin(n\omega_0 t)dt \quad (1.3)$$

$$B_n = \frac{2}{T}\int_0^T x(t) \cos(n\omega_0 t)dt \quad (1.4)$$

1.5.9 Gaussian model (GM)

The basis of the Gaussian model is a combination of time-scaled, amplitude-scaled, and time-shifted Gaussian pulses to represent a real-time random signal. The bell shape of the Gaussian pulse is similar to the ECG's pulse components (P wave, QRS complex, and T wave) and PPG (forward wave and reflection wave) signal as well. Therefore, our proposed work aims to create effectively a linear combination of Gaussian pulses to depict the ECG and PPG waveform as well. Hence GM can be used to synthesize/simulate the ECG and PPG waveform [31] [25] as in equation (1.5). As Gaussian pulses are nonorthogonal in nature, it is a nontrivial challenge throughout the decomposition process by implying dependency between the component functions.

$$GM(x) = \sum_{m=1}^{N} a_m e^{-\left(\frac{x-b_m}{c_m}\right)^2} \quad (1.5)$$

Where, Amplitude a_m, center b_m, and variance c_m are the model parameters that need to be determined for $m = 1$ to N number of Gaussian pulses.

Furthermore, $a_{m} = \frac{1}{\sigma_m \sqrt{2\Pi}}$ and $c_m = \frac{1}{2\sigma_m}$

$\sigma_m$is the standard deviation of mth component of GM.

Let's take, $N = 2$ and the two-Gauss function will be synthesized by six parameters as in equation(1.6).

$$f = [\, a_1, b_1, c_1, a_2, b_2, c_2 \,] \quad (1.6)$$

Irrespective of sending all points beat-wise, only these six parameters including beat number and number of samples will be sent beat-wise depending upon the pattern of wave structure.

1.6 Telemedicine in healthcare

The widely used method of biotelemetry is gathering physiological data in one location and transmitting it to another via appropriate means of communication for recording, comprehension, and analysis.

However, the phrase "telemedicine" [26] is more commonly used in clinical practice. Telemedicine is an integrated technology platform that allows a distant doctor to evaluate and monitor a patient via a communication link. One of the top professional associations promoting the use of remote diagnostics to raise the standard, cost, and equity of healthcare globally is the American Telemedicine Association (ATA) [27], which defines telemedicine as:- "Telemedicine is the use of medical information exchanged from one site to another via electronic communications to improve patients' health status. Closely associated with telemedicine is the term ' telehealth,' which is often used to encompass a broader definition of remote health care that does not always involve clinical services. Videoconferencing, transmission of still images, e-health including patient portals, remote monitoring of vital signs, continuing medical education, and nursing call centers are all considered part of telemedicine and telehealth.'' In developed countries where the fundamental health and supporting infrastructure are sufficient to provide the general public with high-quality healthcare services, information and communication technology (ICT) is widely established. However, the patient-to-doctor ratio is quite high in the majority of emerging countries, such as India. The state-of-the-art medical facilities are focused on the city. The main drivers for the promotion of telehealth services in developing countries are as follows:

1. Disparity between rural and urban areas in the provision of health care services.
2. Inadequate infrastructure for rural health care.
3. There are not enough doctors and paramedics working in rural health facilities.
4. Inadequate road access between urban hospitals and outlying areas.
5. The propensity of urban-based medical professionals to work in highly populated urban areas.
6. A low ratio of doctors to patients.

1.7 Organization of the Thesis

Chapter 1 provides a comprehensive introduction to the thesis, which starts with the heart's mechanism and operation. Following that, it examines a number of cardiovascular conditions, such as complete heart block (CHB), dilated cardiomyopathy (DCM), atrial fibrillation, hypertension, and right bundle branch block (RBBB). The chapter also covers the importance of diagnostic methods in medical analysis, including photoplethysmography (PPG) and electrocardiography (ECG). A thorough examination of various modeling approaches, such as wavelet transform (WT), autoregressive (AR) models, hidden Markov models (HMM), principal component analysis (PCA), Bayesian models, BiLSTM, Fourier models (FM), and Gaussian models (GM), follows the introduction of key fiducial parameters of ECG and

PPG signals. Finally, the function of telemedicine in healthcare is discussed, with a focus on its increasing significance in remote diagnosis and monitoring.

Chapter 2, starts with a thorough review of the literature is presented in the application of ECG and PPG signals for heart rate estimate and their applicability in evaluating heart rate variability and cardiovascular disorders. The prediction of ECG fiducial parameters from PPG signals for cardiovascular disease (CVD) analysis is then examined, after which the compression of ECG and PPG signals for telemedicine applications is investigated. Concatenating ECG and PPG data for better CVD categorization is covered in more detail in this chapter. It outlines the rationale for the research, points out important research gaps in the previous studies, and ends with the thesis's specific goals.

Chapter 3 focuses on data acquisition and the extraction of fiducial parameters necessary for cardiovascular analysis. It starts with a short overview of important datasets, such as the MITBIH and MIMIC III datasets, and how ICD-9-CM codes are used to classify diseases. Next, the chapter describes how to acquire ECG data using the Bipac system and PPG data using the HRM-2511E Easy Pulse version 1.1. The procedure of extracting fiducial parameters from PPG signals is further explained, including beat extraction, preprocessing, and fiducial parameter identification. Likewise, beat-wise fiducial parameter extraction and ECG preprocessing are covered in relation to the extraction of ECG fiducial parameters. Finally, the chapter concludes with the formation of the 2-D beat matrix for signal analysis, compression, and classification algorithms.

Chapter 4 illustrates the compression of ECG and PPG signals for effective telemedicine applications, particularly in monitoring CVD. The importance of signal compression is explained at the outset, and then modeling-based compression methods such as Fourier modeling (FM) and Gaussian model (GM)-based techniques are covered. The chapter goes into additional detail about the segmentation and operation of GM-based compression techniques for ECG and PPG signals. The usefulness of these techniques is then evaluated by discussing quality evaluation indices for compression. Furthermore, a case study on CVD patients is presented together with dataset descriptions, hyperparameter sensitivity analysis, and result discussions for ECG and PPG compression. Gaussian mixture model-based compression is also offered for CVD monitoring. The chapter also explores data compression of PPG signals in an IoT-based healthcare platform, discussing data acquisition, cloud storage using Dropbox, and comparative analysis of FM and GM-based compression techniques. It concludes with a summary of the findings and their implications for telemedicine.

Chapter 5 mainly predicts the ECG fiducial parameters from PPG signals for the diagnosis of CVD. An overview of the importance of ECG fiducial parameter prediction in non-invasive cardiac monitoring is given at the outset. The chapter then conceptually describes a number of prediction models, such as Gaussian process regression (GPR), deep learning-based techniques, the Hidden Markov Model (HMM), and Empirical Mode Decomposition (EMD). The accuracy of GPR models is evaluated through a discussion of performance evaluation indices. The chapter goes into additional depth about the GPR model's prediction of ECG fiducial parameters from PPG signals, including comments, dataset descriptions, and analysis of the results. Additionally, it examines the prediction of PPG fiducial parameters using methodologies such as Gaussian modeling, Radial Basis Neural Network (RBNN), and General Regression Neural Network (GRNN), followed by an evaluation of their performance. The chapter concludes with a summary of key findings, emphasizing their importance in improving CVD diagnosis.

Chapter 6 emphasizes on the classification and authentication of cardiovascular diseases (CVD) using composite features derived from ECG and PPG signals. The significance of composite characteristics in enhancing CVD classification accuracy is introduced at the outset. The chapter then examines a number of classification techniques, including machine learning techniques like Support Vector Machines (SVM), Logistic Regression, Linear Discriminant Analysis, Decision Trees, Random Forest, and K-Nearest Neighbors, as well as deep learning techniques like 1D-Convolutional Neural Networks (1D-CNN). Furthermore, a classification technique called the Probabilistic Neural Network (PNN) is presented. In order to assess the efficacy of the model, performance assessment metrics are examined. The chapter goes into additional depth about the composite feature-based method for CVD detection, including feature creation, dataset description, and the use of Principal Component Analysis (PCA) to reduce dimensionality. The outcomes and conversations demonstrate how successful the suggested process is. Additionally, the use of PNN and PPG fiducial parameters to classify cardiac anomalies is investigated, including data collection, findings, and debates. The chapter ends with a synopsis of the main conclusions, highlighting how composite feature-based categorization can improve the diagnosis of CVD.

Chapter 7 concludes all the research works presented in this thesis. Moreover, this chapter highlights potential areas for future investigation. There are seven distinct chapters that comprise the complete work that is presented and illustrated in this thesis. The six chapters (Chapters 3 through 6) comprise the primary research efforts. In order to improve the diagnostic system, each chapter aims to tackle the signal processing, compression, prediction, and classification of CVD utilizing machine learning and the most recent deep learning techniques.

Chapter 2

Literature Surveys

This work focuses on the monitoring of cardiovascular diseases using ECG and PPG signals for telemedicine applications, which can be also used in remote areas. Therefore an exhaustive literature survey has been done on ECG and PPG signals and how they can help telemedicine applications for cardiac patients either in data compression, prediction, or in the classification domain. Below is a summary and discussion of significant contributions in these areas.

2.1 Literature survey related to the use of ECG and PPG in the estimation of heart rate

The devices can track heart rate (HR), which refers to the number of contractions of the heart per minute (beats per minute, or bpm), as well as heart rate variability (HRV) index, which quantifies the fluctuation in beat-to-beat intervals. HRV analysis is a non-invasive assessment of the autonomic nervous system (ANS) that has proven beneficial for both healthy individuals and cardiac disease patients [28].

The autonomic nerve system's (ANS) sympathetic and parasympathetic branches regulate heart rate (HR) [29]. Acetylcholine is released by the parasympathetic vagal nerves to reduce the heart rate, whereas noradrenalin is released by the sympathetic nerves to speed it up. The sympathetic and parasympathetic nervous systems work in harmony to produce the HR's fluctuation [30]. The parasympathetic response takes over and the heart rate decreases when you're at rest. The sympathetic response takes over during activity, and the heart rate rises [31].The HRV is the word used to describe the beat-to-beat variation in HR. Since the ANS is primarily responsible for controlling the heart rate, measuring the heart rate variability (HRV) yields valuable insights into sympathetic and parasympathetic cardiovascular function [32].

The most widely utilized of the many different approaches for R-peak detection [33] is the one put out by Pan and Tompkins [34] and its subsequent refinement [35]. The majority of the techniques, including those that are derivative-based [34], wavelet transform-based [36], [37], matching filter [38], artificial neural networks [39], and a lot more, are thoroughly reviewed in [40].

Poian *et al.* [33] employed the detection of R-peak on compressive sensing ECG wave by the correlation

between a known template with the compressed signal (without going through the signal reconstruction). It used compressive sensing with matched filter phenomena for heart rate estimation.

Shuai *et al.* [41] examined that ECGs should be obtained for at least 30 seconds in patients with Atrial Fibrillation (AF) since 10 seconds is not enough to provide a clinically reliable estimate of heart rate. When the heart rate is high, it is preferable to record the ECG for 60 seconds.

Cheng *et al*. [42] proposed a real-time heart-rate estimator using ECG data obtained by a wireless bluetooth receiver and monitored using steel textile wearable electrodes in a worn system. The heart-rate estimation process is a complex task since the measured ECG signals exhibit high baseline wandering phenomena and high noise aberrations, particularly when the wearer is moving, due to the moveable electrodes and the consequent unfixed contacts. They proposed heart rate estimation, which overcomes this issue by removing baseline wandering in ECG data using the subspace technique, and then obtaining the heart rate estimate using the adaptive notch filter (ANF) technique capable enough to remove the DC.

Sharan *et al.* [43] suggested a technique where ECG-derived respiration (EDR) and instantaneous heart rate (IHR) signals are used. The input signals are IHR and EDR to a neural network that uses a bidirectional gated recurrent unit (BiGRU) for learning the long-term dependencies between the windows in both forward and backward directions, and a 1-D convolutional neural network (CNN) to acquire the temporal and spectral characteristics in short-time windows. The multi-input network independently analyzes the IHR and EDR signals. To classify sleep stages, features gleaned from the examination of the IHR and EDR signals were typically combined.

Biswas *et al.* [44] described that in an ambulatory setting, PPG signals obtained from the wrist, earlobe, finger tip are prone to motion artifacts (MA). The sensor module moves to the skin and sensor deformation typically brings on MA after prolonged daily use. Consequently, the quality of the signal and the extraction of physiological indicators are affected. In recent years, several research projects have used machine learning-based methods and time/frequency domain signal processing techniques to successfully detect, eliminate, or attenuate MA and estimate HR [45]-[47].

Kong *et al.* [48] reported a method to estimate heart rate (HR) from motion artifact (MA)-corrupted PPG signals through: Time-Frequency Spectrum (TFS) estimation using variable-frequency complex demodulation (VFCDM) for high-resolution HR and amplitude detection [49], MA Removal by subtracting the TFS of accelerometer signals from PPG data, and Post-Processing to eliminate residual

noise and interpolate missing HR data. To eliminate sporadic noise, a moving average technique is frequently used. With varying degrees of success, more computationally demanding MA removal techniques have been employed, including adaptive filtering [50], Wiener filtering [51], independent component analysis [52], principal component analysis [53], and Kalman filtering [54].

Li *et al.* [55] employed a strong robust fusion method (SRFM) to improve the robustness of HR estimation by combining the discrete Fourier transform (DFT) with testers' HR attributes. The work was done with pre-processing using the db5 wavelet transform, which helped in eliminating baseline drift and power frequency noise.

Zhang *et al*. [56] calculated HR using a wrist-type PPG signal from a smart watch which was quite interesting and challenging for HR. Again a two-stage normalized-LMS adaptive noise canceller was proposed by Yousefi *et al*. [57] to reduce motion artifacts from PPG signals. This resulted in a PPG signal with reduced interference, which was subsequently used to calculate cardiovascular parameters. A nonlinear multi-input-multi-output (MIMO) model predictive controller was implemented in the literature [58] to handle HR [59].

Yen *et al*. [60] employed multi-scale convolution that was suggested as 'CNN-LSTM model', which combined the feature extraction skills of multi-scale convolution models with the benefits of a long short term Memory (LSTM) model and a CNN model for heart rate estimation by using combined ECG and PPG signals. Accurately estimating blood pressure and heart rate to avoid cardiovascular diseases requires verification in patients with CVDs. That was especially important for clinical applications, such as monitoring heart and stroke in critical-care postoperative patients.

2.2 Literature survey related to heart rate variability and cardiovascular diseases

An instantaneous heart rate (IHR) time series or an interbeat interval (IBI) time series derived from successive heartbeats are the two basic methods used to calculate HRV [61].

ECG and PPG are the gold standard for measuring HRV in this era. Furthermore, several studies have also used seismocardiography (SCG), ballistocardiography (BCG), and Doppler radar signals to measure HRV because developments in electromechanical sensors have made it possible to monitor the mechanical activity of the heart discreetly [62]-[64]. To extract the beat-to-beat variations, however, these signals need sophisticated signal processing techniques because their signal-to-noise ratio (SNR) is much lower than that of ECG and PPG signals [64]. IBIs are often retrieved by peak-based techniques [65], [66], and spectral-based techniques [67], learning-based techniques [68] [69]. To monitor the physiological

changes, a standard method for determining IBI necessitates the identification of the events of interest, such as the systolic peak in PPG or the QRS complex in ECG. the enhancement stage and the detection stage are the two main phases of this process [65].

Elgendi *et al.* [66] investigated how to improve the events of interest above other signal transitions, the first step was to employ several linear and nonlinear filtering techniques. The enhanced SNR enabled the detection step to determine the onset and offset of each event of interest by using a pertinent peak-detection technique followed by a decision logic. To reduce the algorithm's computational cost, simple thresholding in the detection stage was typically recommended.

Greiser *et al*. [70] realized that beyond conventional risk parameters, heart rate variability measurements provide prognostic information. Higher HRV, as determined by the conventional 10-second ECG, is a more reliable predictor of cardiac death in older adults than lower HRV. They concluded that there was a moderate to poor association between HRV estimations from 10-second ECGs and those from 5 or 20-minute.

Ahmad *et al.* [71] reported the impact of atrioventricular conduction time (AVCT) on short-term heart rate variability (HRV) by calculating HRV parameters for three groups of patients: those with normal heartbeats, arrhythmias, and sudden cardiac death (SCD) using the intervals between the onsets of successive P waves (PP time series). To identify PP, PR, and RR time series, an extremely accurate wavelet transform-based ECG delineator was created. When compared to the normal group, the mean PR variation in the arrhythmia and SCD groups was found to be considerably higher. It was shown that RR variability no longer offered a highly good estimate of HRV after PR fluctuations in arrhythmia and SCD instances exceeded a particular threshold. In these situations, PP variability was able to offer a more accurate HRV evaluation.

Balasubramanian *et al*. [72] designed a PWLL (p-wave locked loop) hardware unit that automatically locks to the p-wave of the provided ECG and delivers the p-p interval count in both analog and digital form. The PC received this count for additional analysis. As an alternative, a software system counted and displayed the time interval after an algorithm found the p-wave in the ECG readings for the prediction of arrhythmia.

González *et al.* [73] provided several multi-modal techniques that integrate 30-second ECG records with roughly long-term HRV data developed to estimate the probability of heart failure (HF) hospitalization. They presented two survival models: a ResNet model that learns from the raw ECG and an XGBoost model with Accelerated Failure Time (AFT) that incorporated extensive ECG features. They supplemented them with brand-new long-term HRVs that were derived from a mixture of beat-to-beat, ultra-short-term readings made throughout the day. They suggested a survival model that combined the Transformer and ResNet architectures (TFM-ResNet) to capture their temporal dynamics. High model performance for HF risk assessment was demonstrated.

Different AI models are being used by researchers to examine different HRV parameters, and AI has demonstrated its effectiveness and precision in this field [74]. For instance, Baumert *et al.* [75] developed a model that evaluated different HRV parameters to forecast the short-term occurrence of Ventricular Tachycardia (VT) by combining the Fast Fourier Transform (FFT) with the Blackman-Harris window technique. Furthermore, to predict the incidence of VT, the scientists created an Artificial Neural Networks (ANN) classifier [76] and trained it using the "PhysioNet Spontaneous Ventricular Tachyarrhythmia Database" [77]. Based on many criteria, they recorded accuracy, sensitivity, and specificity at 76.60%, 82.9%, and 71.4%, respectively.

Villegas *et al.* [78] employed Support Vector Machines (SVM), Radial Basis Function (RBF), and Multilayer Perceptions (MLP) to predict cardiovascular risk. The accuracy of their best model was 96.67%. Furthermore, Song *et al.* [79] developed a prediction model with an accuracy of 89% using SVM to predict cardiovascular risk following myocardial infarction. Additionally, Ebrahimzadeh *et al*. [80] used the Multilayer Perceptron Neural Network (MLP) and k-nearest Neighbor algorithms to develop models to predict Sudden Cardiac Death (SCD). The "PhysioNet Sudden Cardiac Death Holter database" [81] and the "PhysioNet Normal Sinus Rhythm database" [82] were used to train their models. The accuracy for the first, second, third, and fourth one-minute intervals was 99.73%, 96.52%, 90.37%, and 83.96%, respectively.

Murukesan *et al*. [83] predicted SCD two minutes before it started by using SVM and Probabilistic Neural Networks (PNNs). The "PhysioNet MIT Normal Sinus Rhythm database" [82] and the "PhysioNet Sudden Cardiac Death (SCD) Holter database" [81] were also used by the authors to train their models. SVM and PNN achieved prediction rates of 96.36% and 93.64%, respectively.

Mihandoost *et al.* [84] introduced a novel method that used cyclostationary analysis of ECG signals. Using the Spectral Correlation Function (SCF), it revealed a spectral hidden periodicity between the QRS-T complexes of the ECG signal, which are the primary wave components that represent electrical activity in the heart. The performance of the suggested approach was verified by applying the SCF coefficients from a single ECG to a Convolutional Recurrent Neural Network (CRNN), which was made up of convolutional and long short-term memory (LSTM) layers [84].

Choudhary *et al*. [85] presented a model where following the acquisition of the PPG signal, systolic peaks were identified by using a unique algorithm that has a 99.8% sensitivity and a 99.9% positive predictive power. The PPG and ECG data obtained from the same subjects were then used to compute heart rate variability parameters. The notion that PPG-derived HRV can be used in place of ECG-derived HRV is supported by analyses showing that the two approaches yield results that are essentially the same for normal and myocardial infarction (MI) affected people.

Ahamed *et al*. [86] approached a model, where each of the three axis acceleration signals was selected based on its highest band power to produce a motion artifact (MA) signal. The generated MA signal served as the reference signal for the adaptive noise cancellation based Recursive Least Square (RLS) filter, which excluded MA from the PPG signal. To provide accurate HR and HRV value over successive periods, a straightforward tracking and verification process was included in the excessive physical exercise condition.

Murthy *et al*. [87] reported that if the data was subjected to FFT spectral analysis, it revealed several spurious peaks. The usual peak of the normal is between 0.1 and 1.5 Hz. The PPG data underwent non-parametric spectral analysis to eliminate the spurious peaks. The Welch method was used to calculate the power spectral density (PSD) estimate. by using the common "PSD" function found in Matlab 5.3. The PSD estimate lacked the spurious peaks but displayed frequency contents comparable to the FFT. There was a notable variation in the HRV spectrums of cardiac patients (such as Myocardial Infarction (MI), Atrial Flutter(AF)) and normal as well. These findings demonstrated that PPG can be used as a substitute diagnostic method to examine the cardiovascular system, focusing on heart rate variability.

Ihsan *et al.* [88] described the most deadly type of heart disease called coronary heart disease (CHD), which develops when plaque in the coronary arteries or heart blood vessels blocks the flow of blood that carries oxygen and nutrients to the heart muscle. After using the FIR filter for signal processing, three

algorithms were explored for feature extraction: time domain features, HRV features, and respiratory rate (RR) interval to detect CHD. It was well proved that kurtosis, skewness, VLF, LF, HF carried the best HRV features and beat the other two mentioned methods.

Biswas *et al.* [89] proposed an innovative deep learning framework Cortical Neural Network (CorNET), which comprised of two-layers of CNN, two-layers of LSTM, and a final dense layer (DL) that can effectively execute biometric identification (BId) and estimate heart rate (HR) data using just a single-channel PPG signal obtained in an ambulatory setting and worn on the wrist. Using a four-layer deep neural network, the authors had developed a fully customized data-driven strategy. To mimic the temporal sequence found in the pulsatile signal indicative of heart activity, two-convolution neural network layers were combined with two long short-term memory layers, and then a dense output layer was applied.

Wang *et al*. [90] studied and the major goal was to determine whether it is feasible to create a fusion graph for physiological signals utilizing the multi-omics technique and the vertically stacked original time-domain sequences idea. Additionally, the study used the fusion graph of physiological information to improve the accuracy of blood pressure prediction during haemorrhage. This study used a novel multi-omics approach to demonstrate for the first time how time-frequency information and the spatial dependency of physiological signals can be integrated through physiological signal fusion. The suggested technique was a data-level fusion methodology that combined all ECG and PPG signal dimensions to produce a multi-omics fusion map of physiological signals for blood pressure measurement.

Aygun *et al*. [91] identified the actual IBIs from the morphological characteristics of ECG and PPG signals in the presence of motion artefact and suggested a combinatorial approach based on the shortest path. R-peaks were investigated as the most crucial characteristic point of ECG signals for reliable calculation of IBI and HRV, whereas systolic peaks, maximum slopes, and onsets were identified as the prominent and distinctive components of PPG signals. To make use of the many morphological characteristics of the one-channel physiological signal modality, a fusion technique was presented. The heartbeat detection problem was characterized as a shortest path search problem on a direct acyclic network that used the time-continuity of heartbeats—each heartbeat ends with the beginning of the subsequent pulse—and the morphological characteristics of the cardiac signals. Vertices and edges in the graph's construction stand for potential morphological traits and IBIs, respectively.

Shilpa *et al.* [92] examined the prediction of hypertension, the authors reported how well linear and non-linear BP estimation models based on pulse rate (PR) and pulse transit time (PTT) perform for monitoring mean arterial pressure (MAP), systolic blood pressure(SBP), and DBP(diastolic blood pressure) using the cuffless design. By calculating the MAP error between the estimated MAP using the MAP model and the MAP computed directly using the estimated SBP and DBP values, they showed the dependability of the estimated SBP and DBP values. According to evaluation results, the non-linear BP estimation approach outperformed the linear model. The results also demonstrated that BP estimation models required precise PTT and PR estimation from ECG and PPG signals, which might be difficult in the presence of various artifacts. Heart health assessment and arterial blood pressure estimation can be done using the pulse transit time (PTT), which calculates the amount of time it takes for an arterial pulse pressure wave to go from the aortic valve to a peripheral location [93]. PTT is defined as the interval of time between the photoplethysmogram's (PPG) systolic peak and the electrocardiogram's (ECG) R peak [94]. PTT and BP have an inverse relationship. There are relationships between BP and pulse rate (PR) as well [95]. Consequently, both linear and non-linear BP models were employed in this research together with the PTT and PR parameters.

Jarchi *et al.* [96] presented a model to offer an estimate of heart rate variability during exercise, a novel algorithm framework for extracting instantaneous heart rate from wearable PPG and ECG signals. The new spectral masking methodology for ECG signals involves altering a particle filter tracking technique, while for PPG signals, it limits the instantaneous frequency derived from the Hilbert transform to a region of interest surrounding a potential heart rate value. Accelerometry, wearable ECG, and PPG data from participants riding a bike and running on a treadmill were used to confirm the performance. This is helpful in a variety of clinical settings, such as diabetic neuropathy and sleep analysis, as well as more and more non-clinical settings, such as improving workout regimens.

2.3 Literature survey related to the compression of ECG and PPG signal for telemedicine

ECG signals are compressed when intrabeat redundancies (between consecutive beats) and interbeat redundancies (between beat samples) are reduced [97]. Compression tends to fall into two categories: lossy and lossless. Lossless techniques compress the signals without surrendering any information [98], while lossy compression approximates the original signal and yields a higher compression ratio (CR) with a lower CR value. Lossy ECG compression techniques have therefore been widely used [99] in order to

achieve high CR and improved data transmission. Beat correlation makes it easier to forecast signals, and eliminating redundancies results in superior compression efficiency [100].

Additionally, there are three types of ECG redundancy techniques: direct, modified, and parameter extraction [101]. The transformed approach analyzes energy compaction using frequency domain persuasion. The dominant features extracted from the original signal serve as the basis for applying the parameter extraction technique. Direct techniques are used to compress the data from the digitalized signal samples in the time domain. The direct compression group includes techniques like turning point (TP) [104], amplitude zone time epoch coding (AZTEC) [103], and delta pulse code modulation (DPCM) [102]. Despite their low computing complexity, all of these methods are less effective in terms of compression for a given level of reconstruction error. Discrete wavelet transform [105], discrete cosine transform (DCT), Karhunen–Loeve transform (KLT), Fourier transform [106], and Walsh transform [107] are all included in the changed approach once more. Other methods that have been created using the parameter extraction method include the peak determining and prediction method and neural-based or syntactic methods.

Bera et al. [108] reported a hybrid encoding scheme for real-time lossy ECG data compression scheme using plain and complex blocks to enhance entropy optimization, but the method fell short in adequately describing the computational complexity. The algorithm processed ECG signals in real-time strategy tailored for patient monitoring applications by detecting beats, dividing them into equal-sized "plain" or "complex" blocks based on complexity, and allocating bits using two different principles to optimize entropy.

Jha et al. [109] used an efficient Electrocardiogram (ECG) data compression algorithm designed for tele-monitoring cardiac patients, particularly in resource-limited settings. The work was done by using Savitzky-Golay filter to denoise ECG signals. They utilized, DCT to convert from the time domain to the frequency domain to condense energy, normalization, and rounding, after which they used run-length encoding (RLE) and Huffman encoding (HE) for data compression.

Yin et al. [110] proposed an ultra-low power ECG with an ASIC (application-specific integrated circuit) processor that has R-wave detection to detect arrhythmia and compression using modified swinging-door-trending (SDT), but has not been validated with a prototype device. Adaptive Detection Algorithm**,** a derivative-based algorithm is proposed for detecting arrhythmia and Hierarchical Data Buffer**, t**o optimize

the limited memory available in devices. Lastly, Data Compression**,** a modified Swinging-Door-Trending (SDT) method is used for efficient ECG data compression.

Kolekar et al. [111] applied wavelet transform at the first phase concentrating the majority of the signal's energy into a smaller number of coefficients by breaking down ECG data. Dead-Zone Quantization, where small coefficients that fell inside a dead zone were eliminated. Consequently, energy efficiency filtering was used to maximize compression. Lastly, the modified Run-Length Encoding methodology achieved greater compression ratios than traditional methods without sacrificing important information to achieve higher CR for Holter monitoring .

Mitra et al. [112] suggested compressive sensing (CS) and a unique Kronecker-based recovery strategy, which Quality improvement is mathematically linked to the reduction of mutual coherence. for detecting arrhythmia. Random Matrices, like Gaussian and Bernoulli distributions.and Deterministic Matrices (DBBD) were analyzed. The method was appropriate for continuous ECG monitoring applications since it guaranteed improved signal recovery quality and robustness against noise.

Kumar et al. [113] introduced a hybrid compression method for ECG signals using embedded zero tree wavelet (EZW) and singular value decomposition (SVD) approaches to achieve high compression with minimal signal distortion. However, it was limited to twelve ambulatory system data only and insufficient for verifying its resilience across various cardiac diseases. The algorithm was tested on the MIT-BIH arrhythmia database to ensure high-quality signal reconstruction.

Jha et al. [114] reported that DCT in combination with discrete orthogonal Stockwell transform (DOST) which merges frequency-dependent resolution of time-frequency space with local phase details, enabling effective ECG compression, but failing in giving the information of execution time and memory requirement for the compression process. The work was done with integer conversion, to increase compression efficiency, transformed coefficients are transformed into integers. RLE, achieved high compression without sacrificing important information by encoding integer coefficients by taking advantage of repetitive data occurrences.

Fathi et al. [115] employed discrete Krawtchouk moments for feature extraction followed by an accelerated Ant Lion Optimizer (AALO) for the selection of optimum features for ECG compression with

handsome processing time but lacking in the information of memory requirement for the said process. It enhanced the wearable device's storage capacity, processing speed, and energy efficiency.

Xiao et al. [116] proposed a transformer-based network for feature extraction and a residual multihead convolutional network make up the densely knowledge-aware network model. This model applied to ECG signals for anomaly detection, such as atrial fibrillation, rather than compression. Although compression work is not specifically addressed, Xiao et al. [117] developed a deep contrastive representation learning with the self-distillation model in which features are retrieved by residual networks and used to ECG datasets for classification and clustering frameworks. A capsule-based transformer was used by Xiao et al. [118] to implement the CapMatch feature extractor model, and feature-based knowledge distillation used in the healthcare system for data reduction tasks.

Pal et al. [119] utilized tunable-Q wavelet transform (TQWT) and coronavirus herd immunity optimizer (CHIO) for the self-controlled reconstruction of compressed signal. To improve compression performance, transform coefficients were quantized, thresholded, and encoded.

Mohebbian et al. [120] used an optimized Basis spline (B-spline) interpolation and ant colony optimizer (ACO) for a semi-lossless ECG compression, which failed in illustrating processing speed. The B-spline interpolation process compared to conventional approaches, it saved time by calculating B-spline coefficients as compressed data, allowing for direct signal display without decompression. ACO optimized the interpolation parameters for effective data representation, which improved the compression process.

Alam et al. [121] utilized the principal component analysis (PCA) to select the dominant features for quality control PPG compression for normal and CVD patients including the noisy environment without highlighting the SNR and correlation coefficient parameters. By choosing the ideal number of principal components (PC), eigenvectors (EV), and their quantization levels (Q), compression is accomplished by PCA.

Author Gupta [122] proposed a combination of methods of Huffman encoding for efficient data compression and second-order delta encoding scheme for reduction of redundancy for lossless PPG compression for real-time applications. The validation with MIMIC II data showed low CR because of motion artifacts, but the data captured by Biopac System yields better results.

Xu et al. [123] applied a two-Gauss based stochastic modeling for the PPG compression method to represent forward and backward waves for people in physical exercise conditions where respiration changes the signal amplitude and different morphological patterns not considered with diseases. In this topology, the signal representation was reduced to a small number of characteristics that were highly consistent across cardiac periods. Efficiency of Compression maintains a PRD below 9% while maintaining a clinically acceptable level of recovery quality.

Vadrevu et al. [124] proposed a novel quality-conscious quality-control data compression architecture for energy saving in the Internet of Things (IoT) and smartphone PPG monitoring equipment without highlighting the execution time with different cardiac syndromes. Before compression, noisy and pulse-free photoplethysmogram (PPG) signals were filtered away, guaranteeing that only noise-free data was processed effectively.

Alam et al. [125] introduced a modified delta encoding based on zonal complexity for PPG compression without mentioning the different cardiac anomalies. Classification of Zones was based on variations and energy content, the PPG signal was divided into "plain" and "complex" zones. Again adaptive compression used run-length encoding, adaptive hard thresholding, and zonal complexity-appropriate selective biasing of the initial difference array.

Reddy et al. [126] applied the first seven significant Fourier coefficients of the Fourier series to abolish the motion artifacts and compression job of PPG followed by that without calculating the speed of processing. It used cycle-by-cycle Fourier series analysis to eliminate motion artifacts brought on by patient movement.

Alam et al. [127] applied the on-board signal quality assessment through vector quantized with autoencoder to minimize reconstruction error for high fidelity and subsequently compression to reduce data size, but the limitation of validation through the variability of PPG morphological patterns. MIMIC-II and BIDMC dataset was used for that.

Banerjee et al. [128] introduced Second Order Delta Encoding, RLE, and buffer array for PPG compression, where the CR factor was taken into consideration without taking into account other performance indicators like PRD, PRDN, memory requirement, etc. An innovative application of a "buffer array" substantially reduces the amount of bits needed for storage.

Sahoo et al. [129] proposed also a two-Gauss model for PPG data compression only for IoT applications considering only three types of cardiac diseases from real-time hospital data and not verified by authorized open database like MIMIC III waveform or MIT-BIH Arrhythmia Database.

Banerjee et al.[130] reported a novel lossless compression technique utilized the run length encoding (RLE) and second order delta encoding (DE) was proposed by the authors. The addition of buffer arrays to the RLE approach to increase CR was carried out effectively. They had suggested an enhanced method of lossless compression for PPG and ECG signals (regardless of sampling frequency(SF) and data resolution), supporting clinical and scientific applications. Also Gaussian noise power was effectively considered for the high CR achievement with no reconstruction error.

2.4 Literature survey related to the prediction of ECG fiducial parameters from PPG signals for analysis of CVD

Prior research investigated the substantial link between heart rate variability measured by ECG signals and PPG signals. The RR, PR, QRS, and QT intervals of prominent dicrotic notch individuals can be more effectively derived from certain PPG fiducial features [131]. BIDMC datasets had a great performance [132] for a strong correlation between ECG and PPG (the onset of PPG is lagging behind 600-700 ms of P-peak, the systolic peak of PPG is lagging behind 600-700 ms of R-peak, the RR interval of ECG corresponds to a peak-peak interval of PPG, the P-peak maps to the onset of PPG, the PR interval refers to the systolic peak of PPG, and the RP interval correlates to the diastolic phase of PPG). Few earlier work has been done on estimating parameters and inferring ECG waveforms from PPG signals

Banerjee et al. [131] presented an empirical-based algorithm by using the maximal information coefficient (MIC) to select the vital range of some parameters of ECG from 15 PPG features. Though it retrieves some parameters of ECG, it fails to predict the total ECG waveform for cardiovascular syndrome patients. By choosing the most pertinent features for categorization, a feature selection algorithm Maximal Information Coefficient (MIC) was used to improve detection accuracy.

Kosasih *et al*. [133] suggested a cloud-based fully connected neural network-based system to predict ECG waveforms and focused on avoiding the computational burden on the device itself, rather, which used data

from the PPG, accelerometer, and gyroscope sensors. The system's fundamental flaw is its inability to accurately forecast ECG values in different individuals having different sizes and weights etc.

Zhu *et al*. [134] adopted a mathematical strategy and developed a discrete cosine transform (DCT) based model to infer the correlations between PPG and ECG to study heart action from affordable wearable Internet-of-Things (IoT) devices for mobile health monitoring. Because of the absence of non-linear information and 12-lead data, the representation lowers the models' ability to reconstruct an ECG accurately and restricts their applicability to incorporate into sophisticated actual medical situations.

Chiu *et al*. [135] proposed a transformed network for continuous ECG monitoring called Convolutional Neural Network (CNN) having an encoder-decoder architecture. Though the sequence transforms, attention network and loss function are implemented in the methodology there is a scope to improve the performance indices like sensitivity for the detection of QRS complex by implementing some robust learning skills. So for the waveform-level ECG reconstruction, this method opened the door for low-cost, continuous monitoring with PPG sensors, facilitating clinical-level research and diagnosis.

Sarkar *et al.* [136] used generative adversarial networks (GAN) as CardioGAN with generator and dual discriminators both in the time-frequency domain to avail high fidelity ECG signal from PPG signal. Still, challenges persist for multi-lead ECG investigation. Attention-based generator that picked up on the PPG signal's significant local characteristics and dual discriminators that preserved data integrity in the frequency and time frame domains

Tang *et al*. [137] proposed a subject-oriented model by using the methodology of bidirectional long short-term memory (BiLSTM) for the reconstruction of long ECG signals from the PPG signal. The model was trained and validated with 60-second PPG and ECG signals.The work focused on the frequency range of the reconstructed ECG mainly below 20 Hz, which cannot give a flavor to the frequency range of aberrant ventricular conduction, which is higher than 70 Hz. It gave clinicians a reliable way to measure only PPG while analyzing both signals.

Tian *et al.* [138] developed a cross-domain joint dictionary learning (XDJDL) platform to monitor ECG waveform for primary diagnosis in a cost-effective way from the optical-based PPG signal for preventive healthcare. To improve the expressive power of both PPG and ECG data, the (XDJDL) framework was presented, and the K-SVD (K-Singular Value Decomposition) approached to learn both signals

dictionaries with a transformation that converts the PPG sparse codes to ECG. However, the methodology outperforms various types of cardiovascular disease data including the ECG morphologies, but fails to aid its classification for the early stage detection.

2.5 Literature survey related to the concatenation of ECG and PPG signals for classification of CVD

- There are ample studies done for CVD classifications using only ECG signals.

Li et al. [139] used Empirical Mode Decomposition (EMD) methodology for the ECG image feature extraction representing the "heartbeat condition." and subsequently followed a 2-D Convolutional Neural Network (CNN) for the classification of cardiac diseases like “Right Bundle Branch Block(RBBB), Left Bundle Branch Block(LBBB), Paced beat (P)” only, but methods require a huge-scale signal. The three-minute ECG recording demonstrated how well domain-specific signal processing and deep learning work together to accurately classify heartbeats.

Likewise, Bhoi et al. [140] utilized two machine learning approaches namely, Linear Discriminant Analysis (LDA) and decision tree for Ischemia and arrhythmia classification incorporating their distinct clustering patterns to have time-frequency domain characteristics without considering the classification metrics such as sensitivity, F-1 score, etc.. Measures such as the QRS complex's interval and average rise and fall amplitude ratio were examples of time-domain features. Likewise, frequency-domain features, which took into account the mean QRS complex's peak frequency and power.

Authors Ramaswamy et al. [141] applied Fourier–Bessel series expansion (FBSE) and Jaya optimized ensemble random subspace KNN (JO-ERSKNN) model with a larger number of data beats for 5 types of arrhythmia classifications with Principal Component Analysis (PCA) to reduce the dimension to 12 numbers, but was not tested with various cardiac diverse patterns with the presence of ‘P’, R-R variability, and so on. The Model converted cardiac patterns into useful information that illustrates the structural soundness of arrhythmias.

Yao et al. [142] introduced ML methods as classifiers using time-domain features extracted from QT and ST-T segments for binary classification as coronary artery disease (CAD) or healthy person, without considering multiclass problem. The primary takeaways were that QT interval time-series characteristics

outperformed RR interval features in terms of classification performance. Performance was enhanced by combining characteristics from the RR and QT intervals. The highest accuracy was obtained by adding characteristics from ST-T segment waveforms.

- A couple of investigations have also focused on classifying cardiovascular diseases (CVDs) using only PPG signals.

Rios et al. [143] proposed a wavelet scattering transform as a feature selector followed by an ML approach with a Support Vector Machine (SVM) for only hypertension detection using PPG and some clinical data without going through the various cardiac syndromes with low accuracy and F1-score. The features are examined using early fusion, which integrates clinical and PPG data at the input level, and late fusion, which combines the results of various analyses.

Qananwah et al. [144] worked with a PPG database with 41 features along with four ML approaches followed by PCA for dimension reduction only for the classification of arrhythmias like tachycardia, bradycardia, and fibrillation only without taking care of performance evaluator as F1-score. Decision Tree (DT), k-nearest Neighbors (KNN), Support Vector Machine (SVM), and Ensemble Learning were the four ML methods used for high-accuracy arrhythmia classification.

Abdullah et al. [145] worked with only three ML classifiers to detect different stages of hypertension by using PPG signals along with clinical features without going through the emerging field of research of CNN. The features were extracted from acceleration photoplethysmography (APG) waveforms**.** The Decision Tree (DT) classifier demonstrates superior accuracy compared to both Linear Discriminant Analysis (LDA) and Linear Support Vector Machine (LSVM).

Fahoum et al. [146] used low-cost for screening of coronary artery disease (CAD) like cerebrovascular accident (CVA), deep vein thrombosis (DVT), heart failure (HF), and atrial fibrillation (AF) by selection of time-domain feature by seven types of ML classifiers. Still, they considered only accuracy performance evaluators. Seven classifier types were examined in this study: K-nearest neighbor (KNN), rule-based (J-Rip and PART), artificial neural network (ANN) (multilayer perceptron), decision trees (J48 and random forest), and Bayesian (Naïve Bayes) classifiers and Bayesian did the best performance in accuracy.

Praveen et al. [147] proposed a whole-based, non-invasive method for classifying blood pressure utilizing raw PPG signal values. Classifying blood pressure for hypertension syndrome using machine learning algorithms is a practical approach for analysis and outcome prediction. They used several machine-learning models in the work, including Random Forest, GradientBoost, and XGBoost. The authors employed repeated stratified k-fold cross-validation to prevent overfitting and were able to classify the BP with sufficient accuracy.

- A dearth of studies were conducted on CVD classification using both ECG and PPG signals.

Among those Pal et al. [148] conducted a thorough evaluation process of fused ECG and PPG signals to determine the kind of CVD through the deep convolution neural network (DCNN) methodology, compromised with poor performance evaluation parameters like precision, accuracy, and F1-score. A deep neural network with skip connections, multidimensional convolution, and self and cross-attention processes was created for classification. Reinforcement learning was utilized to improve the flexibility of the model.

Likewise, Aldughayfiq et al. [149] worked with a novel approach by employing the 1D-CNN and BiLSTMmodel for binary classification of whether AF or non-AF cases without going through the various cardiac diseases using non-invasive methods like ECG and PPG signals. The method combined PPG and ECG signals as multi-featured time-series data, and the hybrid model showed good prediction ability with a 95% accuracy on test data.

Suboh et al. [150] applied five ML algorithms to see the severity of Ischemic Heart Disease (IHD) by acquiring average accuracy and specificity values [150] without multi-class cardiac diseases. Eleven ECG fiducial points, four PPG fiducial points, and five second derivative PPG fiducial points were effectively identified by this computerized signal processing. Artificial neural networks (ANN), discriminant analysis, decision trees, k-nearest neighbors, and support vector machines are the five machine learning algorithms examined in the study and ANN outperformed among all.

Pal et al. [151] reported to separate patients with stenosis and identify the main coronary artery disease using PPG and ECG signals, cardiovascular disease (CVD) patients were selected from the cardiology department for this study. Following the preprocessing of these signals, templates were taken from each

cardiac cycle's dicrotic notch region of PPG and S-T segment of ECG. An algorithm that was suggested produced a new fused segment from two templates. To assess the condition of coronary arteries, the authors developed the Coronary Health Index (CHI) using data from three templates. Following determining the coronary health index (CHI) values, they classified the graph attentive convolution neural network (GACNN) for the patients. Later, they categorized the patients with CAD as either non-CAD or CAD.

2.6 Research Gap

Even though some state-of-the-art techniques produce remarkable outcomes, the following problems remain unaddressed or can be sorted by further study. The following are the primary issues identified after a summary of all the algorithms for CVD monitoring and diagnosis utilizing ECG and PPG for telemedicine applications:

- Previously reported works were to predict the ECG waveform from the PPG signal. Sending of ECG signal demands high data volume, increased power consumption, transmission delay, complexity of data processing, prone to noise, and greater bandwidth requirement.

- All approaches exclusively deal with compression for ECG or PPG data, as the literature study described in the previous subsection makes evident. No published research have been done on precisely compressing both PPG and ECG data. Once more, there isn't a thorough examination of different cardiac conditions that include arrhythmias like atrial fibrillation and other abnormalities like RBBB, hypertension, and DCM while taking normal or healthy people into account. Furthermore, the majority of previously published investigations are limited to MIT-BIH Arrhythmia Database records, which are intended solely for ECG. There are several published articles on the compression of ECG signals, but there is a dearth of studies on PPG compression. Additionally, data compression techniques based on Gaussian models have not been investigated for ECG signals. Furthermore, nothing is known about computational complexity, such as memory usage and compression/decompression process execution times.

- Cardiovascular diseases (CVDs) are mostly classified using PPG or ECG signals in the literature analysis previously addressed. Few researchers have tried to integrate features from both PPG and ECG signals, and the results typically yield poor performance. Furthermore, few studies have compared different cardiac conditions, such as arrhythmias like atrial fibrillation, with other

abnormalities like dilated cardiomyopathy (DCM), complete heart block (CHB), hypertension, and right bundle branch block (RBBB), against healthy subjects. Furthermore, the majority of previous research has focused on either contemporary deep learning methods or conventional machine learning strategies.

2.7 Motivation

The motivations are as follows:

- The motivation underlying this work is that fiducial parameters, which have a smaller data size than the entire ECG waveform, optimize transmission bandwidth and lower storage needs for real-time tele-monitoring applications over wired or wireless networks, including Internet of Things platforms. Additionally, they reduce processing time and energy usage, which makes them perfect for remote medical monitoring systems. Fiducial parameters, which use signal amplitude and time intervals to offer adequate information regarding cardiovascular problems, are simple, less susceptible to noise and baseline drift. By using fewer data samples than state-of-the-art techniques that necessitate enormous datasets, this method lowers expenses and facilitates simpler diagnosis. It also encourages the early identification and treatment of CVDs, such as RBBB, hypertension, arrhythmias, DCM, and CHB.

.

- Techniques for compressing ECG and PPG signals are being developed to overcome issues with storage, transmission bandwidth, and processing efficiency for remote healthcare monitoring. These techniques allow for effective transmission and storage over limited networks without baseline drift problems by reducing data size while maintaining therapeutically important information. This makes remote monitoring and diagnostics more convenient, which is especially advantageous in environments with limited resources. Additionally, compression makes it easier to integrate cloud computing and IoT, enabling real-time analysis and individualized medical care. Our suggested approach is to advance proactive healthcare management and public health by increasing the effectiveness, affordability, and accessibility of remote medical care. Compressing both signals while taking into consideration various CVD morphological patterns is still quite difficult, though.

  .

- Because AF episodes can happen suddenly and can be hard to pick up on brief ECG recordings, extended monitoring is frequently required, which can cause skin discomfort and sensor displacement. For ambulatory or home healthcare, on the other hand, PPG provides a non-invasive, practical option that is simple to use using wearable technology or smartphone apps. Alongside ECG, PPG is a helpful initial screening technique that detects changes in blood volume in peripheral microvascular arteries. Furthermore, machine learning (ML) and deep learning (DL) algorithms combined with PPG and ECG data allow for quick, automated, and precise analysis, filling in gaps and promoting the creation of trustworthy and clinically proven CVD detection systems.

2.8 Objectives of the Thesis

The main objective of the thesis is to monitor and diagnose different cardiovascular diseases having different morphological patterns by taking ECG and PPG signals for telemedicine applications. So, the objective focuses on the design and development of some neural network, machine learning, and deep learning algorithms and those are enlisted as follows:

- Comparative study of different Artificial Neural Networks for the prediction of fiducial parameters of PPG of high blood pressure patients.
- Development of a Data compression and retrieval system by incorporating Gaussian and Fourier modeling of PPG signal for IoT applications with CVD syndromes for remote areas.
- A novel approach of Gaussian mixture model-based data compression of ECG and PPG signals for various cardiovascular diseases for remote areas.
- Development of a regression-based model to predict ECG fiducial parameters from PPG signals for the analysis of cardiovascular diseases.
- Classification of cardiac abnormality using PPG fiducial parameters and probabilistic neural network (PNN).
- Implementation of machine learning and deep learning framework for the classification and detection of CVD using composite features of ECG and PPG signals for an improved diagnostic system.

The total objectives is illustrated through a unified system architecture diagram as shown in Fig. 2.1.

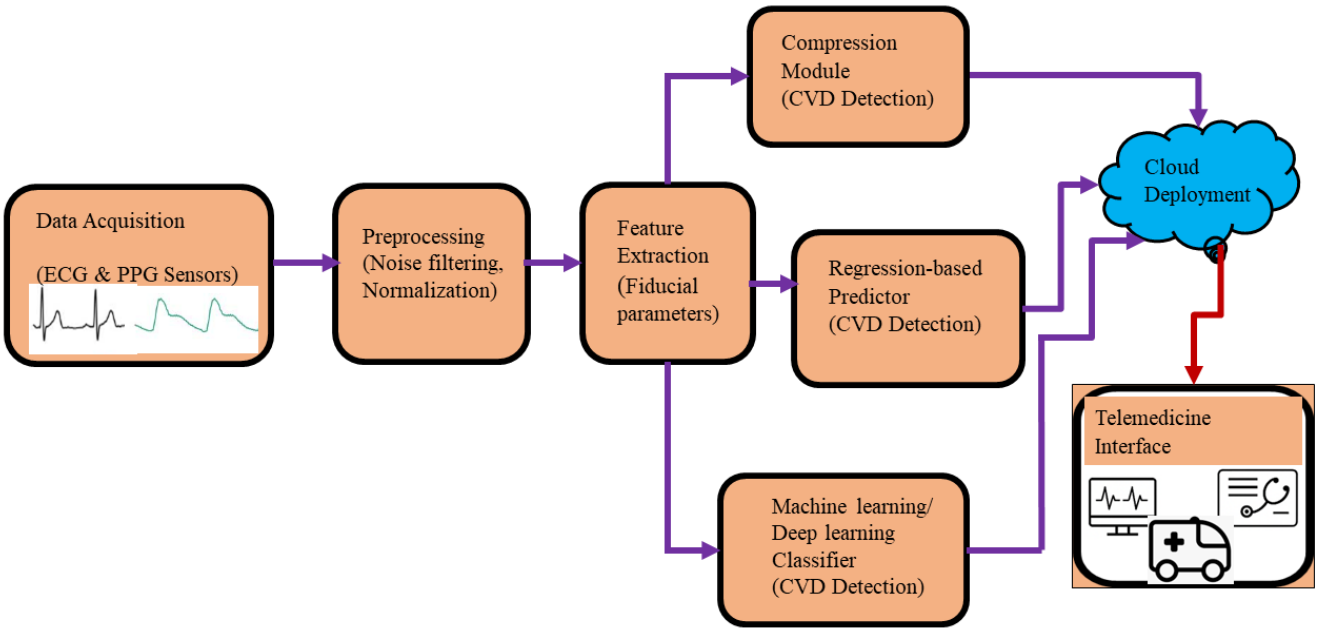

Fig. 2.1. Unified system architecture diagram.

The detailed illustration of compression module is given in Chapter 4. Similarly regression-based predictor through Gaussian model is described in Chapter 5. Likewise, classification is well described through machine learning and deep learning topology in Chapter 6 for early stage CVD detection.

Chapter 3

Data Acquisition/Collection and Extraction of Fiducial Parameters

To analyze Electrocardiogram (ECG) and Photoplethysmogram (PPG) signals for medical and biomedical applications, data collection and fiducial parameter extraction are essential procedures. By recording waveforms like P, QRS, and T waves that represent cardiac functioning, an ECG examines the electrical activity of the heart. Whereas, PPG, on the other hand, is an optical method that provides information on cardiovascular health by detecting changes in blood volume in microvascular tissues. To ensure precise and noise-free recordings, the procedure starts with signal gathering by utilizing specialized sensors or devices. Also. some databases are publicly available, which have comprehensive clinical datasets and are developed to support research in healthcare, machine learning, and data science. Advanced techniques are employed to preprocess these signals, removing artifacts caused by motion, baseline wander, power line noise, or other interferences. Fiducial parameters are then extracted, such as systolic and diastolic peaks from PPG or R-peak intervals from ECG. These characteristics are essential for evaluating heart rate variability and vascular health, as well as for identifying diseases like arrhythmias, hypertension, and arterial stenosis. The accuracy and effectiveness of parameter extraction have been improved by recent developments, such as machine learning and efficient signal processing techniques, allowing for reliable and real-time monitoring in wearable and clinical contexts. Personalized healthcare and non-invasive diagnostics are based on the analysis of ECG and PPG signals.

3.1 MIMIC III dataset

Hospitals have made a determined effort to implement digital health record systems in recent years. Despite these developments, there are still issues with digital system compatibility, which makes data integration difficult. Because of this, the full potential of hospital data to comprehend and enhance care has not yet been achieved. Simultaneously, the scientific community is under growing criticism for their findings' lack of reproducibility. Under a data usage agreement, MIMIC-III unifies the deidentified, full clinical data of patients admitted to Boston, Massachusetts' Beth Israel Deaconess Medical Centre and makes it publicly available to researchers worldwide (Fig. 1). Clinical research can be improved and

replicated in ways that would not be feasible otherwise due to the open nature of the data. A massive single-center database called MIMIC-III (the "Medical Information Mart for Intensive Care") contains data about patients admitted to intensive care units at fairly large tertiary care hospitals. Applications such as higher education courses, quality improvement projects, and academic and industrial research are supported by the database.

Data from 53,423 unique hospital admissions of adults (16 years of age or older) to critical care units between 2001 and 2012 are included in MIMIC-III. It also includes information on 7870 newborns who were admitted between 2001 and 2008. The information includes 38,597 unique adults as well as 49,785 hospitalisations. In-hospital mortality is 11.5%, the median age of adult patients is 65.8 years, and 55.9% of patients are male. The typical duration of a hospital stay is 6.9 days, while the median duration of an intensive care unit stay is 2.1 days.

Depending on the decisions made by the ICU personnel, different waveforms and numbers are recorded. Waveforms nearly always contain one or more ECG signals, and they frequently incorporate breathing, fingertip photoplethysmogram (PPG) signals, continuous arterial blood pressure (ABP) waveforms, and other waveforms (up to eight at once) when available. Systolic, mean, and diastolic blood pressure, heart and respiration rates, SpO2, and additional data as available are commonly included in numerical values. The lengths of recordings also differ; the majority last a few days, while some are shorter and some last for several weeks. Here each ID is of 7500 samples with 1-minute recording time. All signals that are available at any point throughout a record are listed when using a viewer like the *PhysioBank ATM*, however, typically only a subset is viewable at any given moment.

Only a few publicly available datasets have the corresponding CVD diagnosis with ECG and PPG signals. Physionet's MIMIC-III [152] signal is one of them, which integrates the Lead-II [153] ECG signal into the maximum patient ID and PPG signal as well. Since Lead-II ECG is in a convenient location and contains important cardiovascular information (clear view of P and R waves), we concentrated on it over all other leads.

3.2 MITBIH Dataset

A popular public dataset, the MIT-BIH Arrhythmia Database (mitdb) was created to support biomedical signal processing research and development, specifically for the analysis and detection of arrhythmias in electrocardiogram (ECG) signals. Since studied between 1975 and 1979 and published in 1980, the dataset was created by Beth Israel Hospital (BIH) and the Massachusetts Institute of Technology (MIT) and has served as a standard for ECG analysis. The first major product of that effort was the MIT-BIH Arrhythmia Database and It has been utilized at over 500 sites across the globe for that reason as well as fundamental studies on cardiac dynamics. The database was first made available on quarter-inch IRIG-format FM analog tape and 9-track half-inch digital tape at 800 and 1600 bpi. They created a CD-ROM version of the database in August 1989.

The complete MIT-BIH Arrhythmia Database is located in this directory [154]. Since the launch of PhysioNet in September 1999, approximately half of this database—25 of the 48 complete records and reference annotation files for all 48 records—has been made publicly accessible here. In February 2005, they made available the 23 remaining signal files that had previously only been accessible on the MIT-BIH Arrhythmia Database CD-ROM.

It includes recordings from 47 people with 48 records (with one record edited), 25 of whom are men and 22 of whom are women, ranging in age from 23 to 89. In order to include less common but clinically significant arrhythmias that would not be well-represented in a small random sample, 25 recordings were selected from a set of 4000 24-hour ambulatory ECG recordings that were obtained from a mixed population of inpatients (approximately 60%) and outpatients (approximately 40%) at Boston's Beth Israel Hospital. Of these recordings, 23 were chosen at random.

To guarantee variety in cardiac patterns, a combination of healthy and arrhythmia-afflicted patients is used. It includes two-channel, 30-minute ECG recordings for every patient. High-resolution information about heart activity is provided by the 360 Hz sampling of the data. Over 110,000 beats were identified by the expert-labeled annotations. Various forms of normal and pathological heartbeats (such as normal, ventricular ectopic, and supraventricular ectopic beats) are included in the labels. The dataset is especially useful for researching abnormalities such as atrial fibrillation and ventricular tachycardia.

3.3 ICD-9-CM codes

A standardized coding system called ICD-9-CM (International Classification of Diseases, 9th Revision, Clinical Modification) was created to categorize and code medical procedures and diagnoses. Accurate documentation, billing, and analysis of health-related data have been made easier by its widespread use in the healthcare sector. Before switching to ICD-10-CM in 2015, ICD-9-CM, which was first introduced in the middle of the 20th century, was the mainstay for reporting and coding in the US healthcare system. ICD-9-CM, however, continues to be historically relevant as a fundamental instrument in the development of medical coding, impacting the creation of later coding schemes. Later WHO announced an official framework for using ICD-9-CM to assign codes for diagnosing various illnesses.

The hierarchical structure of ICD-9-CM codes guarantees that they encompass a wide range of disease categories while permitting medical diagnosis specificity. Three to five alphanumeric characters make up each code. The notations are-"Three-digit category: Indicates a sickness or condition's general classification. The fourth digit subcategory: Offers more detail on the condition. Subclass (5th digit): Provides more information, such as the clinical presentation or laterality of the illness."
For instance: "402-Hypertension heart disease, 402.9-Unspecified hypertensive heart disease, 402.91-Unspecified hypertensive heart disease with heart failure." The ICD-9-CM codes for various cardiac diseases as RBBB (426.4), Hypertension (402.91), Arrhythmia (427.31), CHB (426.0), and DCM (425.4).

ICD-9-CM codes are essential in the following domains:

- Medical Billing and Reimbursement: These codes are used by healthcare professionals to record services given and submit insurance reimbursement claims.

- Healthcare Analytics: By making it possible to aggregate data on disease prevalence, treatment trends, and results, the codes aid in statistical analysis and research.

- Public Health Surveillance: They enable public health organizations monitor and respond to health emergencies by documenting trends in morbidity and mortality.

ICD-9-CM codes have historically been used in healthcare data collecting and analysis, as evidenced by the references to datasets or research that use them in this thesis.

3.4 ECG Data Acquisition (Bipac system)

Compact, portable, and easy to use, the Biopac MP45 [155] is a physiological data acquisition system that is frequently used for research and teaching. It is made to gather, analyze, and interpret a variety of physiological signals like EEG (electroencephalogram) signals, EMG (electromyogram) signals, and EOG (electro-oculogram) signals including electrocardiogram (ECG) data. The MP45 system is especially well-suited for non-invasive heart activity monitoring, which makes it a popular option for clinical research, biomedical engineering studies, and teaching.

The Biopac MP45 system is a small, lightweight gadget made for accurate ECG data collection. It is appropriate for both laboratory and field applications since it uses electrodes to record the electrical activity of the heart in real time. The Biopac Student Lab (BSL) software and the equipment work together smoothly to make setup, recording, and analysis simple. It reliably records ECG waveforms, such as P waves, QRS complexes, and T waves, with a sampling rate of up to 1000 Hz. Simple computer integration for real-time data processing and display is ensured by USB interface. Researchers can examine fiducial points, heart rate, rhythm, and variability in the ECG data by using the Biopac BSL software.

Electrical impulses from the heart, brain, muscles, eyes, and other organs can be recorded and analyzed using the Biopac MP45, a two-channel data gathering device, where electrical signals from the body are amplified and filtered by the MP45 before being transformed into computer-readable numbers. These figures are plotted as waveforms on the computer screen using the Biopac Student Lab software. The Biopac Student Lab (BSL) system, which also consists of transducers, electrodes, and software, incorporates the MP45. The BSL system allows students to plan experiments, gather information, and evaluate the outcomes. The total set up consists of "BIOPAC Electrode Lead Set (SS2L),· BIOPAC Disposable Electrodes (EL503) 3 electrodes per subject,· BIOPAC Electrode Gel (GEL1) and Abrasive Pad (ELPAD),· Mat, cot or lab table and pillow for Supine position, Biopac Student Lab System: BSL 4 software, MP36, MP35 or MP45 hardware, Computer System (Windows or Mac)."

Fig. 3.1 (a) Biopac MP45- Two-channel data gathering device, (b) Biopac electrode Lead set (SS2L), (c) Biopac disposable electrodes (EL503).

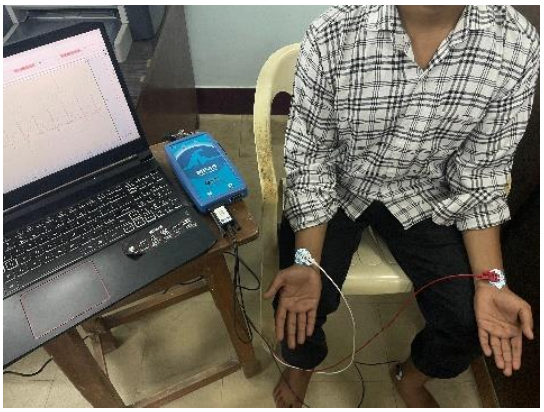

Fig. 3.2 ECG Data Acquisition system (Biopac MP45).

3.5 PPG Data Acquisition (HRM-2511E Easy pulse version 1.1)

Using a data acquisition system and a standard PPG sensor module, the HRM-2511E Easy pulse version 1.1 [156],the data was captured. With the use of an IR LED source and a photo detector, the cardiovascular system's physiological data can be obtained. Infrared light is emitted into the skin via infrared LEDs (IR LEDs) and photodetector identifies light that is transmitted or reflected through the fingertip, changing in response to variations in blood volume. PPG provides useful information about any volumetric changes in our blood, artery structure, and the illnesses and conditions that are associated with it. Using an MCP6004 Op-Amp, a two-stage filtering and amplification process is used to obtain the filtered PPG signal to reduce noise and to enhance the quality of pulse waveform Afterwards, it provides the analog voltage signal that corresponds to the heart rate. After that, the sensor was linked to the analog channel of

the embedded microcontroller (ATMEGA328) in order to record the patient signal for two minutes at a sampling frequency of 250 Hz. Finally, the microcontroller is connected to a PC via a USB cable to provide data in the.txt format.

This pulse sensor module is compact, non-invasive, and reasonably priced and compatibility with various microcontroller platforms.. Thus, it is a solution for easy-to-use heart rate monitoring that may be used for wearable health, research, and education applications.

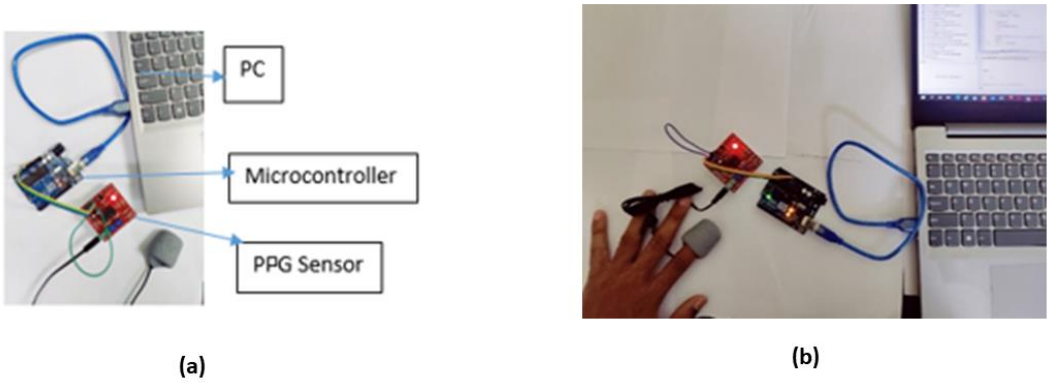

Fig. 3.3 (a) PPG sensor (HRM-2511E Easy pulse version 1.1), (b) PPG data acquisition system.

3.6 Extraction of PPG fiducial parameters

Fiducial parameters obtained from PPG signals, such as rising timings, amplitude changes, and peak-to-peak intervals, etc offer important information about cardiovascular health, including arterial stiffness, heart rate, and blood oxygen levels. The extraction procedure uses signal processing techniques to locate important waveform elements such as diastolic, systolic, and dicrotic notches. These parameters are essential for applications in blood pressure measurement, heart rate variability analysis, and vascular health monitoring. The dependability of PPG-based diagnostics is increased by sophisticated algorithms and filtering techniques that provide precise fiducial point detection even in noisy situations.

3.6.1 PPG preprocessing

Denoising ECG and PPG signals is the first step after collecting the data. The high frequency noise and baseline drift are eliminated by applying a 4th-order Butterworth band pass filter [157] with cut-off frequencies of 0.03 Hz and 10 Hz. The Pseudo code 3_1: Denoising of PPG signal illustrates how DC cancellation and scaling of the PPG signal in the [0,1] range is subsequently carried out as shown in Fig. 3.4.

Pseudo code 3_1: Denoising of PPG Signal

Input: Raw PPG signal U in the time domain with sampling frequency f_s, 4th order of Bandpass filter(BPF) with N=2 with lower cut-off frequency $f_L = o.03\ Hz$ and higher cut-off frequency $f_H = 10\ Hz$.

Output: Filtered PPG signal U_1 in the time domain.

1. Load raw PPG signal U
2. Compute the Nyquist frequency as $f_N = {f_s}/{2}$
3. Obtain the desired Butterworth filter coefficient [a b].
4. $[a\ b] = butter(N, [0.03\ 10]/f_N)$
5. $V_1 = filtfilt(a, b, U)$
6. // **DC Cancellation and Normalization**
7. $V_2 = V_1 - mean(V_1)$
8. $U_1 = V_2 / (\max(abs(V_2))$

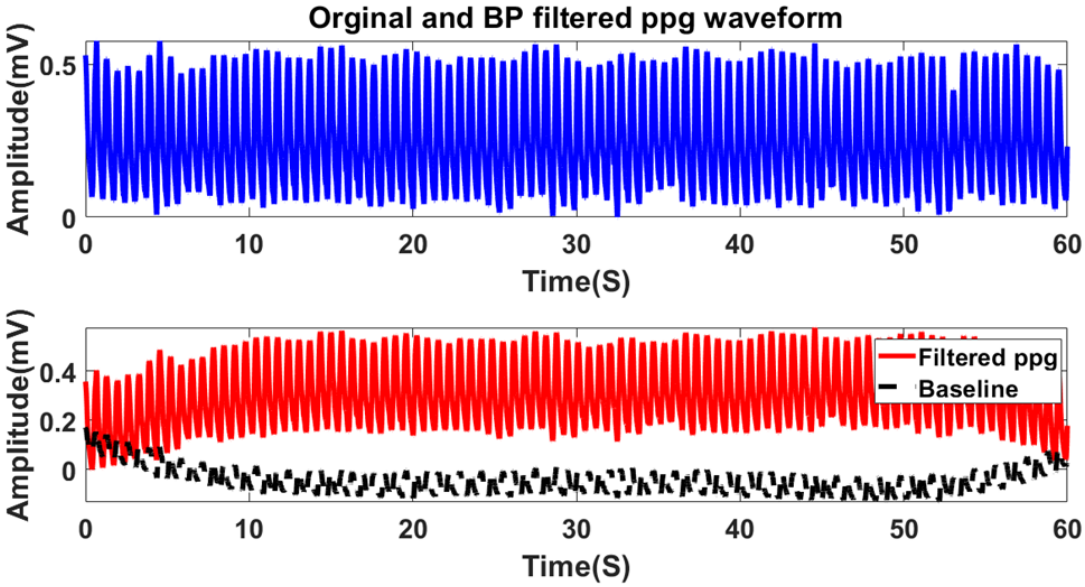

Fig. 3.4 Raw original PPG signal (blue colored) and corresponding filtered signal (red colored) with baseline noise removal.

3.6.2 PPG beat extraction

Two successive index values will produce one PPG cycle or beat, and the local minima spot and accompanying amplitude peak values were identified concerning the index number for the filtered PPG signal. The sampled data for each beat is contained in a single column of a two-dimensional matrix, with the output being recorded as a two-dimensional array format, as shown in Pseudo code 3_2: Beat extraction of PPG Signal. The simulation result shows in Fig. 3.5.

Pseudo code 3_2: Beat extraction of PPG Signal

Input: Filtered PPG signal U_1 in the time domain, sampling frequency f_s

Output: Beat wise PPG signal matrix 'BEAT'

1. $[max_{peak} \;\; loc_1] = findpeaks(U_1)$
2. $U_{1-inv} = -1 * (U_1 - \text{mean}(U_1))$
3. $[min_{peak} \;\; loc_2] = findpeaks(U_{1-inv})$
4. $S = size(min_{peak})$

   // **Beat formation**
5. $for \;\; k = 1 \; to \; S(1,1) - 1$
6. $M_1 = loc_2(k)$
7. $M_2 = loc_2(k+1)$
8. $beat = U_1(M_1 : M_2)$
9. $eval(['BEAT' \; num2str(k) \; ' = \; beat'])$
10. $end \; for$

    // **Count the number of samples in each beat**
11. $for \;\; g = 1 \; to \; k$
12. $j = size(eval(['BEAT' \; num2str(g)]))$
13. $T = [T; j(1,1)]$
14. $end \; for$

    //**Padding extra zeros**
15. $M_x = max(T)$
16. $for \; g = 1 \; to \; k$
17. $p(g) = M_x - T(g)$

18. $end\ for$
19. $for\ \ i = 1\ to\ k$
20. $\quad BEAT = [BEAT\ [eval(['BEAT'\ num2str(i)]); zeros(p(i)]]$
21. $end\ for$

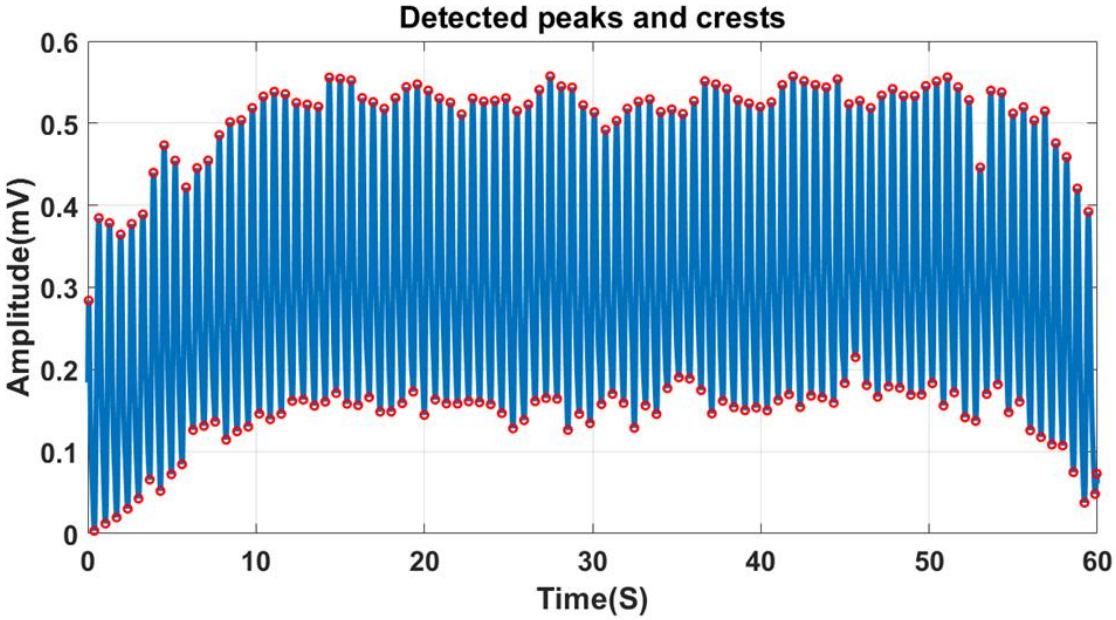

Fig. 3.5 Filtered PPG signal with peaks and crests.

3.6.3 Fiducial parameters of PPG

The systolic (time, peak), dicrotic (time, peak), diastolic (time, peak), pulse wave time (PT), diastolic phase (DLP), and PPG augmentation index (PPGAI) are widely acknowledged to provide adequate cardiovascular information for clinical diagnosis in numerous published works [158]. Acceleration PPG (APG) and velocity PPG (VPG) can be used to determine the inflection points (Systolic, Dicrotic, and Diastolic) [159–162]. Similarly, DLP is computed by subtracting pulse time (PT) from systolic time (ST). All fiducial parameters are recovered and shown in Pseudo code 3_3: Beat–wise fiducial parameter extraction of PPG Signal, and PPGAI is computed [159] using Eq. (3.1). Fig. 1.10 shows PPG signal with fiducial parameter for one beat.

$$PPGAI = \frac{(x-y)}{x} \qquad (3.1)$$

Pseudo code 3_3: Beat–wise fiducial parameter extraction of PPG Signal

---

Input: Beat matrix U_2, sampling frequency f_s.

Output: 10 number of the fiducial parameter as Beat no: f, Systolic time:ST, Systolic peak:$ST(2)$, Dichrotic time:$DR(1)$, Dichrotic peak: $DR(2)$, Diastolic time: $DS(1)$, Diastolic peak: $DS(2)$, Diastolic phase: DLP, PPGAI, Pulse time: PT.

1. $N = size(U_2)$
2. $b = N(1,2)$
3. $for\ \ f = 1\ to\ b$
4. $\quad ppg = U_2(:, f)$
5. $\quad N = size(ppg)$
6. $\quad for\ i = 1{:}\ N(1,1)$
7. $\quad\quad if\ \ ppg(i) \neq 0\ \ then$
8. $\quad\quad\quad y = [y\,; ppg(i)]$
9. $\quad\quad end\ \ if$
10. $\quad end\ \ for$
11. $\quad S = size(y)$
12. $\quad ppg = \mathrm{y}$
13. $\quad for\ i = 1{:}\ S(1,1)$
14. $\quad\quad ppg_{d1} = ppg(i+1) - ppg(i)$
15. $\quad end\ \ for$
16. $\quad N1 = size(ppg_{d1})$
17. $\quad for\ i = 1{:}\ N1(1,1)$
18. $\quad\quad ppg_{d2} = ppg_{d1}(i+1) - ppg_{d1}(i)$
19. $\quad end\ \ for$

/ /Systolic peak

20. $\quad MX = max(ppg)$
21. $\quad I = find(ppg == MX)$
22. $\quad ST = [I\ MX]$

// Diastolic peak

23. $ppg_{d3} = -ppg_{d2}$
24. $[max_{peak2}, loc_2] = findpeaks(ppg_{d3})$
25. $P = size(max_{peak2})$
26. $I = loc_2\,(P(1,1))$
27. $DS = [I \;\; ppg(I)]$

// Dicrotic peak, PT, DLP, PPGAI

28. $[max_{peak3}, loc_3] = findpeaks(ppg_{d2})$
29. $n = size(loc_3)$
30. $n = n(1,1)$
31. $DR = [\, loc_3\,(n) \quad ppg(loc_3(n))]$
32. $PT = N(1,1) * f_s$
33. $DLP = PT - ST(1)$
34. $PPGAI = (ST(2) - DS(2))/ST(2)$

// Beat –wise fiducial parameters

35. $M = [f \;\; ST(1) \;\; ST(2)\; DR(1) \;\; DR(2)\; DS(1)\; DS(2)\; DLP\; PPGAI\; PT]$
36. $end \;\; for$

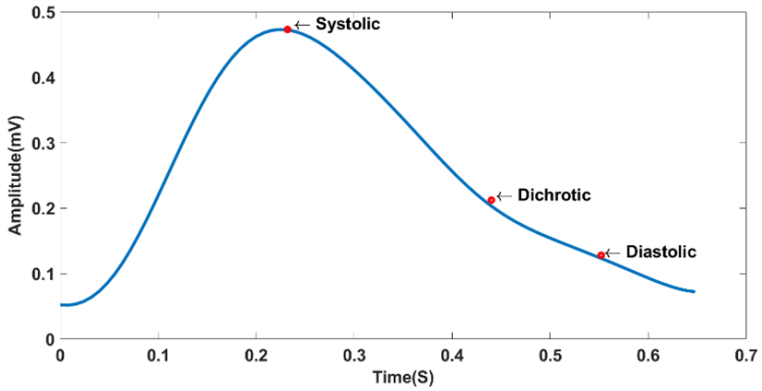

Fig. 3.6 Showing PPG signal with fiducial parameter for one beat.

3.7 Extraction of ECG fiducial parameters

The P wave, QRS complex, and T wave are fiducial characteristics that are taken from ECG signals and offer crucial details on cardiac rhythm, conduction problems, and general heart health. Finding important

characteristics like R-peaks, wave onset and offset locations, and intervals like PR, QT, and RR are all part of the extraction process. Even when noise or artifacts are present, these features can be reliably identified using sophisticated signal processing techniques like filtering and peak detection algorithms. Heart rate variability analysis, cardiac event monitoring, and clinical diagnosis all depend on these fiducial factors.

3.7.1 ECG preprocessing

We have employed an 8-level wavelet decomposition using a discrete Biorthogonal ('bior3.7') wavelet [163] family as the signal frequency of 125 Hz to eliminate the baseline noise of the ECG at 0.5 Hz. The second-order IIR notch filter eliminates power line noise at 50 Hz. As demonstrated in the pseudo code 3_4: Denoising of ECG Signal, DC cancellation and scaling of the ECG signal in the [0,1] range [164] are then carried out and showed in Fig. 3.7 and Fig. 3.8.

Pseudo code 3_4: Denoising of ECG Signal

Input: Raw ECG signal X in the time domain with sampling frequency f_s of 125 Hz, Notch frequency f_n of 50 Hz, Bandwidth BW and passband gain A.

Output: Filtered ECG signal X_1 in the time domain.

1. Load raw ECG signal X
2. // **Baseline noise removal at 0.5 Hz**
3. Take wavelet as Biorthogonal DWT ('bior3.7')
4. Perform the 8- level wavelet decomposition of X.
5. Store the approximate and detailed coefficients of step 4.
6. Reconstruct detailed components $d_8, d_7, d_6, d_5, d_4, d_3, d_2, d_1$.
7. Find $y_{baseline\_remove} = Y_1 = d_8 + d_7 + d_6 + d_5 + d_4 + d_3 + d_2 + d_1$
8. // **Power line noise removal at 50 Hz**
9. Obtain the desired 2nd-order IIR notch filter coefficient [b a].
10. $[b\ a] = iirnotch(f_s, f_n, BW, A)$
11. $Hd1 = dfilt.df2(b, a)$
12. Find $y_{powerline\_remove} = Y_2 = filter(Hd1,\ Y_1)$
13. // **DC Cancellation and Normalization**
14. $Y_2 = Y_2 - mean(Y_2)$
15. $X_1 = Y_2 / (\max(abs(Y_2))$

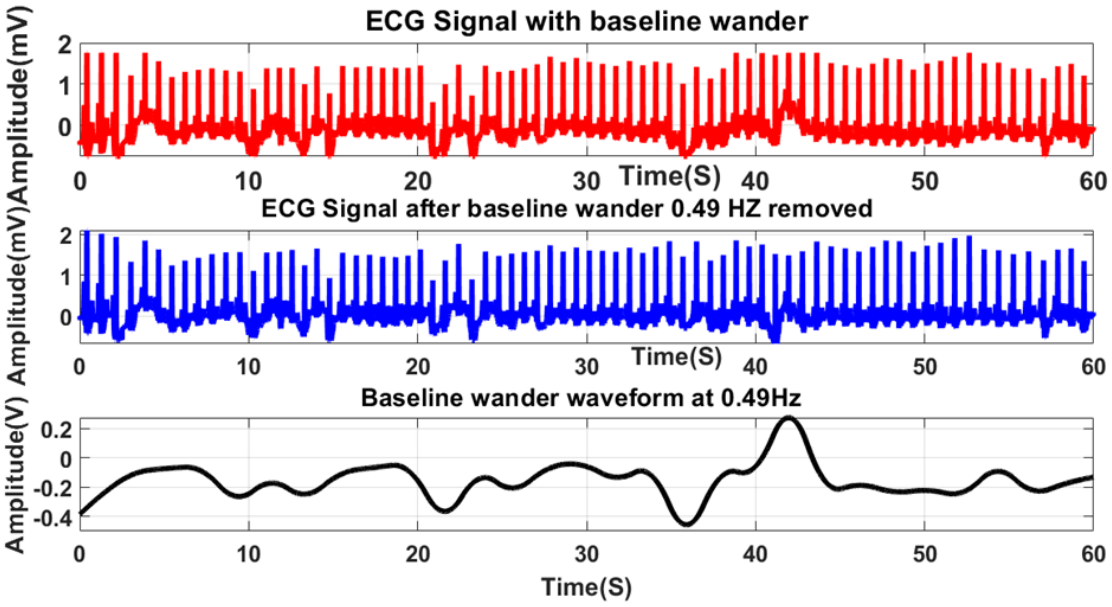

Fig. 3.7 Raw original ECG signal (red colored) and corresponding filtered signal (blue colored) with baseline noise removal.

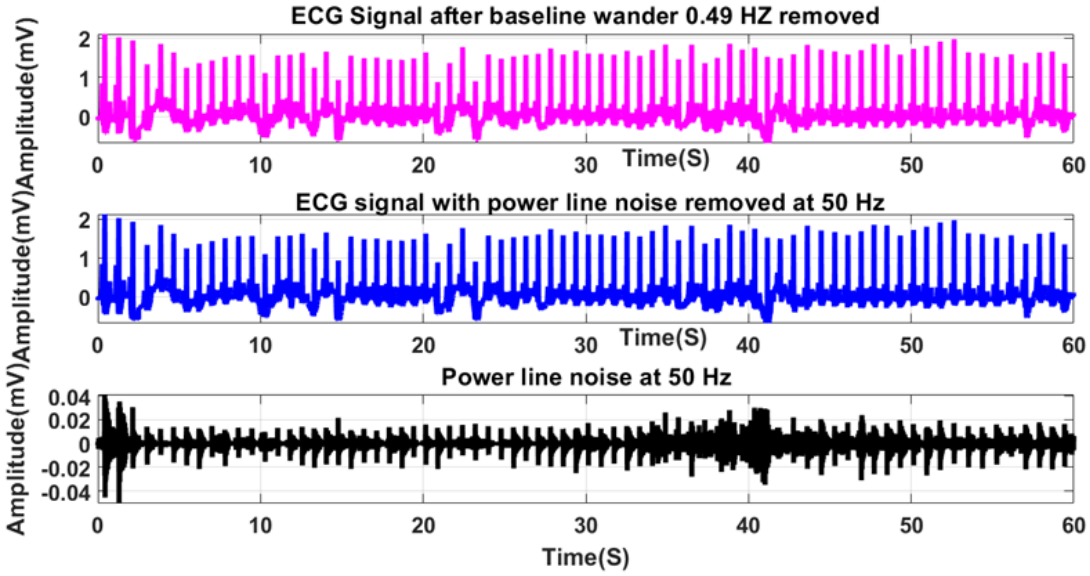

Fig. 3.8 Filtered ECG signal showing baseline noise removal and powerline noise removal.

3.7.2 Beat-wise fiducial parameter extraction of ECG

Following filtering, the credible Pan-Tompkins method [34] has identified the QRS using our panwindow function, which sequentially performs low-pass, high-pass, derivative, squaring, moving window integration, and thresholding operations. As demonstrated in Pseudo Code Beat-wise fiducial parameter

extraction of ECG Signal, the remaining P and T points can be recovered after marking the Q, R, and S fiducial points of the ECG. Pseudo code 3_5: Beat-wise fiducial parameter extraction of ECG Signal describes the beat-wise fiducial points [165–166], which provide all the cardiovascular information about the heart's functioning and is illustrated in Fig. 3.9.

Pseudo code 3_5: Beat–wise fiducial parameter extraction of ECG Signal

---

Input: Filtered ECG signal X_1 in the time domain, No of samples N, sampling frequency f_s

Output: No of beats N_B, for each beat $[P_{loc}\ P_{val}\ Q_{loc}\ Q_{val}\ R_{loc}\ R_{val}\ S_{loc}\ S_{val}\ T_{loc}\ T_{val}]$

1.$[left\ \ right] = panwindow(X_1, N, f_s)$

// Computing QRS

2. *for* i=1 to length(left)

3. $[\ R_{val}(i)\ R_{loc}(i)] =\ \max(X_1(left(i):right(i)))$

4. $[Q_{val}(i)\ Q_{loc}(i)\ ] =\ \min(X_1(left(i):R_{loc}(i)))$

5. $[S_{val}(i)\ S_{loc}(i)\ ] =\ \min(X_1(left(i):right(i)))$

6. end *for*

// Computing P and T

7. $for\ j = 1\ to(\ length(R_{loc}) - 1)$

8. $mid =\ ceil[R_{loc}(j+1) - R_{loc}(j)]/2$

9. $X_2 =\ X_1((mid+1) : (\ R_{loc}(j+1) - 1))$

10. $cd1 = [\ c\ d] = findpeaks(\ X_2)$

11. $cd1 = sortrows(cd1,1,'descend')$

12. $P_{val}(j) = cd1(1,1)$

13. $P_{loc}(j) = cd1(1,2)$

14. $X_3 =\ X_1((R_{loc}(j)+1) : mid)$

15. $cd2 = [\ u\ v] = findpeaks(\ X_3)$

16. $cd2 = sortrows(cd2,1,'descend')$

17. $T_{val}(j) = cd2(2,1)$

18. $T_{loc}(j) = cd2(2,2)$

19. end *for*

//Beat–wise fiducial parameters

20. $M1 = [P_{loc}\ P_{val}\ Q_{loc}\ Q_{val}\ R_{loc}\ R_{val}\ S_{loc}\ S_{val}\ T_{loc}\ T_{val}]$

21. $A = size(M)$

22. $N_B = A(1,1)$

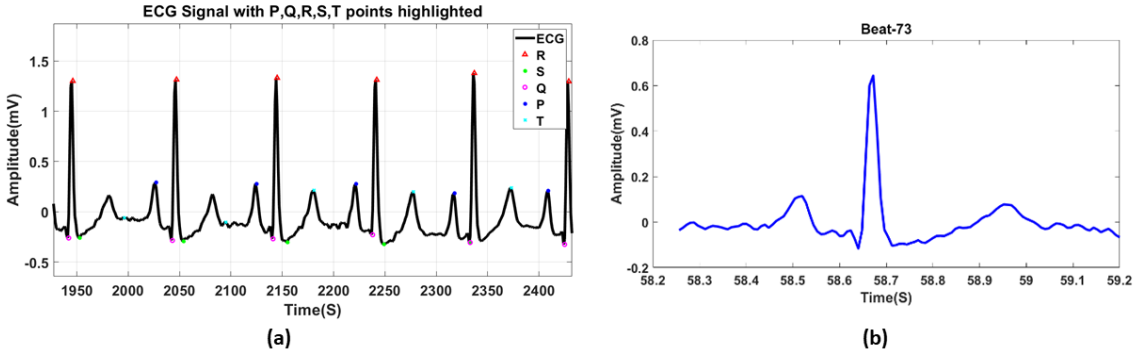

Fig. 3.9 Showing ECG signal (a) with the fiducial parameter for beatwise. (b) the individual beat.

3.8 Formation of 2-D beat matrix

Converting the processed 1-D ECG and 1-D PPG signals into a 2-D array of data independently was a crucial step to take advantage of both intrabeat and interbeat correlation. To put it simply, the goal was to identify the dependencies both inside and between ECG/PPG cycles. To create the 2-D array, each whole beat was extracted from the waveform signal and vertically aligned with the beat before it. However, zero padding was used for length normalization because each beat was not the same length [99]. First, according to the literature, zero padding was frequently utilized for irregular ECG patterns to improve efficiency and enhance compression overhead. Second, 2-D-based compression of ECG data has several advantages, including the capacity to analyze signal features such as R wave and period information and the compact visualization of long-duration ECG signals. However, from a clinical perspective, abnormal signals are more crucial for diagnosis than normal ones. Ideally, a compression algorithm should be more accurate in handling abnormal ECG signals. This problem is sufficiently addressed by the suggested zero padding strategy for length equalization, which also provides improved exposure for the 2-D correlation architecture of the data. In conclusion, this step equates the duration of each heartbeat segment to produce an accurate 2-D array. Lastly, intrabeat messages were delivered horizontally, while interbeat information was maintained vertically.

Chapter 4

Compression of ECG and PPG signals of CVD classes for Telemedicine

4.1 Introduction

The cardiovascular system is the most important organ system in the human body, producing bioelectric signals as a result of ongoing physiological activities. The heart's constant contraction and relaxation causes the cardiovascular system to malfunction, which can result in a variety of cardiovascular diseases (CVDs). The World Health Organization (WHO) estimates that in 2019, cardiovascular diseases (CVDs) will account for 32% of all deaths worldwide, killing approximately 17.9 million people [139]. Electrocardiography (ECG) and photoplethysmography (PPG) are the two types of sensors that provide different methodology-based windows for the perception and evaluation of the cardiac cycle. For clinical and portable electronic equipment, the bulk of PPG spectrum energy is contained within 15 Hz [167], indicating a notable amount of information redundancy in raw data. PPG usually has a sampling rate of 100–1000 samples per second. Raw PPG waveforms are usually problematic to store, especially when using wearable health monitoring devices with limited memory. For example, a normal PPG captured with a sample frequency of 500 Hz and 16-bit resolution will yield 2.4 Mbit of data in 5 minutes [24] . Similarly, a typical ECG monitoring equipment generates massive amounts of digital data per sensor every minute, ranging from 7.5 kB (sampling frequency 125 Hz, quantizer resolution 8 bit) to 45 kB (sampling frequency 500 Hz, 12-bit quantizer) [168]. Just 10.8 MB to 64.8 MB of storage space per day are needed for each ECG sensor. It is very challenging to store such a large amount of data locally for a long time (at least one day). System maintenance will also be hampered by years of uncompressed raw data from many patients stored on hospital local computers. Once more, it is believed that data transmission is the primary source of energy loss because power is lost while transmitting and receiving vast amounts of data for remote healthcare monitoring devices. By removing redundancies, signal data compression lowers the amount of data being sent or stored, which is one way to address this important problem.

Despite its many advantages, data compression has drawbacks of its own. Depending on the needs of the particular application, the main objective is to attain high compression ratios and retain as much

information as feasible. Even a small amount of information loss can be unacceptable in applications like scientific data analysis or medical imaging. Therefore, a significant issue is to achieve large compression ratios without compromising data integrity. Once more, it is crucial to strike a balance between computing resources and compression efficiency, especially for real-time or resource-constrained applications. A balance between compression efficiency and signal fidelity is crucial to ensure that critical diagnostic information is not lost. Furthermore, it can be difficult to develop compression methods that can adjust to various data attributes as well as distribution patterns. Last but not least, processing massive amounts of data necessitates the creation of a compression technique that can manage massive datasets efficiently while maintaining reasonable compression and decompression speeds.

With an emphasis on its use in telemedicine for CVD diagnosis, this chapter examines the state-of-the-art in ECG and PPG compression. It addresses future directions for enhancing diagnostic reliability and compression efficiency while highlighting important methods, measures, and difficulties.

4.2 Modeling-based compression

To achieve effective data representation while maintaining crucial diagnostic information, modeling ECG and PPG signals for compression is important. Both signals have distinct properties that necessitate customized modeling techniques to guarantee the efficiency of compression methods. For the diagnosis of cardiovascular diseases (CVDs), the relevant characteristics are essential. Reducing redundancy while maintaining the temporal and spectral properties of ECG and PPG signals is the main goal of effective modeling. In chapter-1.5.9, various models have been discussed for ECG and PPG signals. In this chapter Gaussian modeling (GM) and Fourier modeling-based (FM) approaches have been developed with different CVD patient data for both ECG and PPG signals for compression purposes.

4.2.1 Fourier modeling (FM)-based compression

The basic principle of operation is already discussed in chapter-1.5.8. By utilizing the frequency domain properties of ECG and PPG signals, Fourier modeling is an effective technique for compressing these signals. Although Fourier approaches work well on their own for many applications, their resilience and adaptability are increased when combined with more sophisticated techniques like wavelets or deep learning. Fourier-based compression is a crucial part of telemedicine solutions since it guarantees excellent compression efficiency without sacrificing the diagnostic quality of data.

4.2.2 Gaussian model (GM)-based compression

In chapter-1.5.9 already elaborated on the basics of the GM model in general. But the choice of number of Gauss functions required to synthesize the type of signal depends on its pattern and complexity. Medical professionals interpret the ECG to evaluate cardiac cycles, making it an essential diagnostic tool for cardiovascular health. Each of the three main waves—the P, QRS, and T—offers information about how the heart works. Diagnostic hints are provided by variations in wave morphology and intervals; for example, large QRS durations imply bundle branch block, many P waves suggest heart block and absent P waves indicate arrhythmia [122]. A more straightforward approach is suggested to improve utility and clarity. In contrast to two Gauss pulses for the P and T wave, a waveform that resembles the ECG for the QRS complex can be produced by combining six Gaussian pulses with varying amplitudes, variances, and time positions. Once more, cardiovascular surrogates are evaluated using the GM model with a six-Gaussian pulses formulation-based approach, which divides the PPG pulse into its forward and reflection waves for the compression procedure. An explanation of why ECG signal segmentation is necessary is provided below. This is done by visualizing the pattern and complexity of the ECG and PPG.

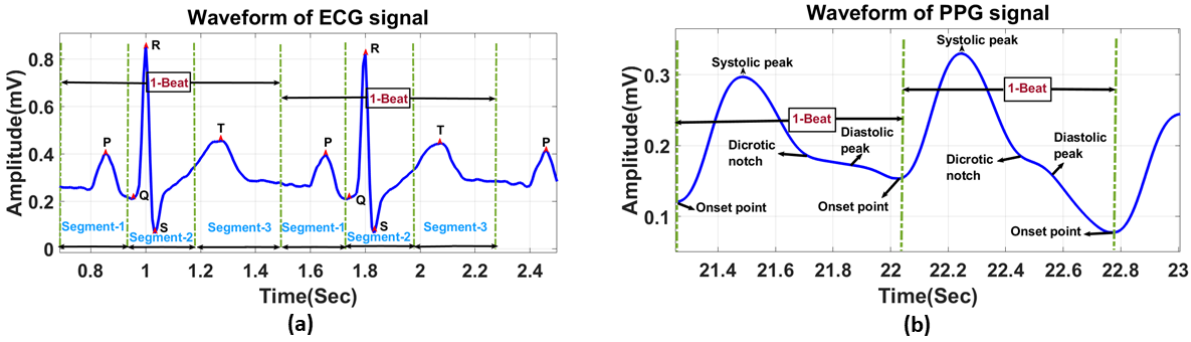

Fig. 4.1. (a) Beat segmentation of ECG waveform. (b) No beat segmentation of PPG waveform

4.2.2.1 GM-based compression of ECG signal (with segmentation)

Typically, the ECG signals are quasiperiodic[169] . One ECG signal period [101-170-171] can be divided into three continuous segments based on the waveform's morphological pattern: Segment 1 (P-block), which is from the beat starting point to Q-onset; Segment 2 (complex QRS block), which is from Q-onset to S-offset; and Segment 3 (T block), which is from S-offset to beat ending point, as shown in Fig. 4.1. (a). Cardiologists typically employ the QRS complex wave as a clinical component to detect arrhythmias

[170] . According to the compression ratio, segment partitioning once more yields a greater reconstructed signal quality for a given beat than non-segment partitioning [170] . Since the QRS complex block contains more information than the other two blocks, three segmentations were carried out to maximize the number of modeling coefficients and have a high compression ratio without compromising generosity. It is possible to give more modeling coefficients (less compression) to the complex block, which has more information, and less modeling coefficients (more compression) to the other two blocks, which have less information. Because the complexity of the waveform is directly connected to the number of Gaussian pulses needed for signal encoding, an imperfect diagnostic approach was used. Since the ratio of the two blocks' standard deviations is sufficiently large, applying two separate coding techniques to two different types of blocks clearly increased compression. Naturally, our suggested approach used two-Gaussian pulses for the other two segments and six-Gaussian pulses for the complex parts. All three segments' segregation and accumulation make use of effective data transmission or reception.

4.2.2.2 GM-based compression of PPG signal

In general, a single cardiac period of the PPG waveform can be approximated by matching the forward and backward waves of the PPG pulse with two sets of Gaussian functions. As shown in Fig. 4.1. (b), we presented the heart action from ventricular injection to the end capillary point and modeled it by six Gaussian pulses for a whole beat in order to illustrate the many cardiac anomaly kinds with various morphological patterns. Therefore, left ventricle contraction and ventricular ejection (first rapid ejection phase and last rapid ejection phase) can be used to represent the first two Gauss functions in accordance with the physiology of heart motion. Once more, the third Gaussian function represents the initial pulse reflection at the thoracic and abdominal aortic junctions. The fourth and fifth Gauss functions, respectively, are produced by additional reflection and re-reflection in the physical structure of the systemic arteries at the point where the Aorta and the common iliac split into external and internal iliac arteries [172]. Finally, the reflection at arterioles and end capillaries is represented by the sixth Gauss function.

4.2.2.3 Working principle of GM-based compression

To fit the ECG/PPG waves with fewer modeling coefficients, this methodology models beatwise using a combination of Gaussian functions. That is, according to Eq. 1.5, one Gauss function will produce three

coefficients. Therefore, the number of coefficients will be determined by the number of Gauss functions used. The beat number, GM coefficients, and sample count for the complete signal are then delivered and stored together with the model coefficients. Eq. 1.5 then reconstructs the signal from these modeling coefficients for various irregular morphological CVD pattern types. Pseudo codes 4_1: Proposed Gaussian model-based compression for PPG signal and 4_2: Proposed Gaussian model-based compression and reconstruction for ECG signal provide detailed examples of how the compression process works.

To optimize bit usage through segmentation, the suggested GM-based compression has the following advantages:

- Flexibility and the ability to handle a variety of data patterns with ease;
- The ability to apply a variable compression rate to data areas with high variability that might need more bits for representation, while those with low variability can get by with fewer bits to optimize bit usage through segmentation.
- Capable of capturing the fundamental structure of data distribution and robustness against baseline wander and noise issues.

Pseudo code 4_1: Proposed Gaussian model-based compression for PPG signal

---

Input: Beat matrix $BEAT$, sampling frequency f_s, Gauss order O, number of beats b

Output: Beat-wise Gaussian model store matrix M and Reconstructed PPG signal Y, compression ratio CR

1. $N = size(BEAT)$ and $b = N(1,2)$
2. $for\ \ i = 1\ to\ b$
3. $ppg = BEAT(:, i),\ \ N1 = size(ppg),\ \ S = N1(1,1),$

// **Trim trailing zeros to get the original PPG signal**

4. $for\ j = 1\ to\ S$
5. $if\ \ ppg(j)\ \neq 0\ \ then\ y = [y\ ; ppg(j)]$
6. $end\ \ if$
7. $end\ \ for$

// **Curve fitting and get Gaussian modeling coefficients**

8. $ppg = \mathrm{y}\ \ and\ N2 = size(y)$

9. $x = 1\ to\ (S-1) * 1/f_s$
10. $mname\ = \{'gauss1','\ gauss2','\ gauss3','\ gauss4','\ gauss5',\ so\ on\ \ldots\}\%\ Gauss\ order$
11. $f = fit(x, y, mname(O))$
12. $C = coefvalues(f)$
13. $M = [M; i\ \ C\ \ N2(1,1)\ \ ]$

// **Reconstruction of PPG signal**

14. $for\ k\ =\ 1\ to\ O$
15. $d\ =\ (x\ -\ C(3 * (k-1) + 2))\ /\ C(3 * (k-1) + 3);$
16. $Y\ =\ Y\ +\ C(3 * (k-1) + 1)\ *\ exp(-d.\hat{}2);$
17. $end\ for$
18. $end\ for$

// **Calculate CR**

19. $N4\ =\ b\ *\ (O\ *\ 3\ +\ 2);$
20. $CR\ =\ N2(1,1)\ /\ N4;$
21. $Calculate\ other\ evaluation\ indices\ like\ PRD, PRDN, RMSE, SNR\ \ CC, QC\ using\ equation.\ 4.1\ to\ equation.\ 4.7.$

Pseudo code 4_2: Proposed Gaussian model-based compression and reconstruction for ECG signal

---

Input: ECG Beat matrix $BECG$, sampling frequency f_s, Gauss order $O1$ for P wave, Gauss order $O2$ for QRS wave, Gauss order $O3$ for T wave and number of beats b

Output: Beat-wise Gaussian model store matrix $M2$ and Reconstructed ECG signal $Y1$, compression ratio CR

1. $N = size(BECG)$ and $b = N(1,2)$
2. $for\ \ i = 1\ to\ b$
3. $ecg\ =\ BECG(:, i),\ \ N1 = size(ecg),\ \ S\ =\ N1(1,1),$

// **Trim trailing zeros to get original PPG signal**

4. $for\ j = 1\ to\ S$
5. $if\ \ ecg(j)\ \neq 0\ \ then\ y = [y\ ; ecg(j)]$
6. $end\ \ if$
7. $end\ \ for$
8. $t = 1\ to\ (S-1) * 1/f_s\ ,\ x = t'\ , Z = [x\ y],\ \ L = size(t)\ ,\ l = round(L(1,1)/3)$

9. $S1 = Z(1{:}\,l,:), S2 = Z(l+1{:}\,2*l,:)\ and\ S3 = Z(2*l+1{:}\,end,:)$

// **Modeling P wave or first segment**

10. $x = S1(:,1),\ \ y = S1(:,2)\ \ and\ \ N2 = size(y)$

11. $mname\ = \{'gauss1','\ gauss2','\ gauss3','\ gauss4','\ gauss5',\ so\ on\ \ldots\}\%\ Gauss\ order$

12. $f1 = fit\big(x, y, mname(O1)\big)\ and\ \ C1 = coefvalues(f1)$

13. $M1 = [\ M1\ \ i\ \ C1\ \ N2(1,1)\ ]$

// **Modeling QRS wave or second segment**

14. $x = S2(:,1),\ \ M = max\big(S1(:,1)\big), x = x - M, y = S2(:,2)\ and\ N3 = size(y)$

15. $f2 = fit\big(x, y, mname(O2)\big)\ \ and\ \ C2 = coefvalues(f2)$

16. $M1 = [\ M1\ \ C2\ \ N3(1,1)\ ]$

// **Modeling T wave or third segment**

17. $x = S3(:,1),\ \ M = max\big(S2(:,1)\big), x = x - M, y = S3(:,2)\ and\ N4 = size(y)$

18. $f3 = fit\big(x, y, mname(O3)\big)\ \ and\ \ C3 = coefvalues(f3)$

19. $M1 = [\ M1\ \ C3\ \ N4(1,1)\ ]$

20. $M2 = [M1; M1]\ \ and\ \ N5(1,1) = N2(1,1) + N3(1,1) + N4(1,1)$

// **Three segments retrieving and merging them for beat and reconstruction of ECG signal**

21. $for\ j\ =\ 1\ to\ 3$

22. $\quad for\ k\ =\ 1{:}\,eval(['O', num2str(j)]$

23. $\quad\quad d\ =\ (x\ -\ C(3*(k-1)+2))\ /\ C(3*(k-1)+3)$

24. $\quad\quad Yj\ =\ Yj\ +\ C(3*(k-1)+1)\ *\ exp(-d.\hat{}2)$

25. $\quad end\ for$

26. $\quad Y\ =\ Y\ +\ Yj$

27. $\quad end\ for$

28. $Y1 = [Y, Y\ \ldots]$

29. $end\ for$

// **Calculate CR**

30. $N6\ =\ b\ *\{1+\ (O1*3+1)+\ (O2*3+1)+\ (O3*3+1)\};$

31. $CR\ =\ N5(1,1)\ /\ N6$

32. $Calculate\ other\ evaluation\ indices\ like\ PRD, PRDN, RMSE, SNR\ \ CC, QC\ using\ equation.\ 4.1\ to\ equation.\ 4.7.$

4.3 Quality evaluation indices for compression

Numerous commonly used global quality evaluation metrics are available, including the Compression Ratio (CR), the Pearson Correlation (CC) coefficient, the Signal-to-Noise Ratio (SNR in dB), the Percent Root Mean Square Difference (PRD in %), and the Quality Score (QS).

- ***Compression Ratio (CR):***

The degree of compression reveals the amount of redundant data that the compressor suppresses, which is represented by CR in equation (4.1). A higher CR means that less bandwidth or storage space was used to send the compressed signal.

$$CR = \frac{Number\ of\ samples\ of\ original\ signal}{Total\ number\ of\ samples\ of\ Gauss\ model\ parameters} \qquad (4.1)$$

- ***Percent root mean square difference (PRD)***

According to the description of the records from MIMIC III signals, it is the PRD with the baseline signal eliminated; it is obtained for each patient ID, which is specified in equation (4.2). It is a gauge of the proper level of fidelity and distortion brought about by the compressed data reconstruction method.

$$PRD = 100 \times \sqrt{\frac{\sum_{k=1}^{N}[X(k) - \hat{X}(k)]^2}{\sum_{k=1}^{N}[X(k) - baseline]^2}} \qquad (4.2)$$

The real and reconstructed ECG/PPG signals, with a number of samples N, are denoted by $X(k)$ and $\hat{X}(k)$. The root mean square difference between the real and reconstructed signals is calculated statistically, and the result is expressed as a percentage of the value of the original signal. A lower PRD is a good sign of compression, and research [126] indicates that it is unacceptable to have a PRD above 9%.

- ***Percentage Root Mean Square Difference Normalized (PRDN)***

Equation (4.3) defines the normalized PRD, which is identical to the PRD with the extra inclusion of $\bar{X}$, which is the mean of the actual ECG/PPG signal.

$$PRDN = 100 \times \sqrt{\frac{\sum_{k=1}^{N}[X(k) - \hat{X}(k)]^2}{\sum_{k=1}^{N}[X(k) - \bar{X}]^2}} \quad (4.3)$$

- ***Root Mean Square Error(RMSE)***

Equation (4.4) represents RMSE, another statistical technique for diagnosing errors in real and reconstructed ECG/PPG signals.

$$RMSE = \sqrt{\frac{\sum_{k=1}^{N}[X(k) - \hat{X}(k)]^2}{N}} \quad (4.4)$$

Because it indicates a higher match between the original and reconstructed signals, a lower RMSE value indicates better reconstruction quality and more diagnostic utility.

- ***Signal-to-noise Ratio (SNR)***

SNR, represented by equation (4.5), measures the noise energy (in dB) introduced into a signal by compression and decompression procedures.

$$SNR = 10 \times log_{10} \times \left(\frac{\sum_{k=1}^{N}[X(k) - \bar{X}]^2}{\sum_{k=1}^{N}[X(k) - \hat{X}(k)]^2}\right) \quad (4.5)$$

- ***Pearson correlation coefficient(cc)***

Equation (4.6) represents the Pearson correlation coefficient, which is useful for variables with linear correlations [119].

$$cc = \frac{\sum_{k=1}^{N}\{ X(k) - \overline{X(k)} \} \sum_{k=1}^{N}\{ \hat{X}(k) - \bar{\hat{X}} \}}{\sqrt{\sum_{k=1}^{N}\{ X(k) - \overline{X(k)} \}^2} \sqrt{\sum_{k=1}^{N}\{ \hat{X}(k) - \bar{\hat{X}} \}^2}} \quad (4.6)$$

It measures the correlation between variables that change continuously in statistics, with 0 signifying no concordance and cc (±1) representing the highest degree of concordance.

- ***Quality score (QS)***

The compression technique's overall performance is evaluated using QS. A high QS and low distortion are signs of good compression performance, as shown in equation (4.7).

$$QS = CR/PRD \tag{4.7}$$

The visual examination of the error signal $e(k)$, which is provided in equation (4.8), is an additional method that even a non-expert can use.

$$e(k) = X(k) - \hat{X}(k) \tag{4.8}$$

4.4 Gaussian mixture model-based data compression of ECG and PPG for CVD monitoring

In the field of biomedical signal processing, research on ECG/PPG compression is still in its infancy, despite the growing popularity of telemedicine healthcare systems. Fig. 4.2 shows the suggested GM for compressing and decompressing PPG and ECG bioelectric signals.

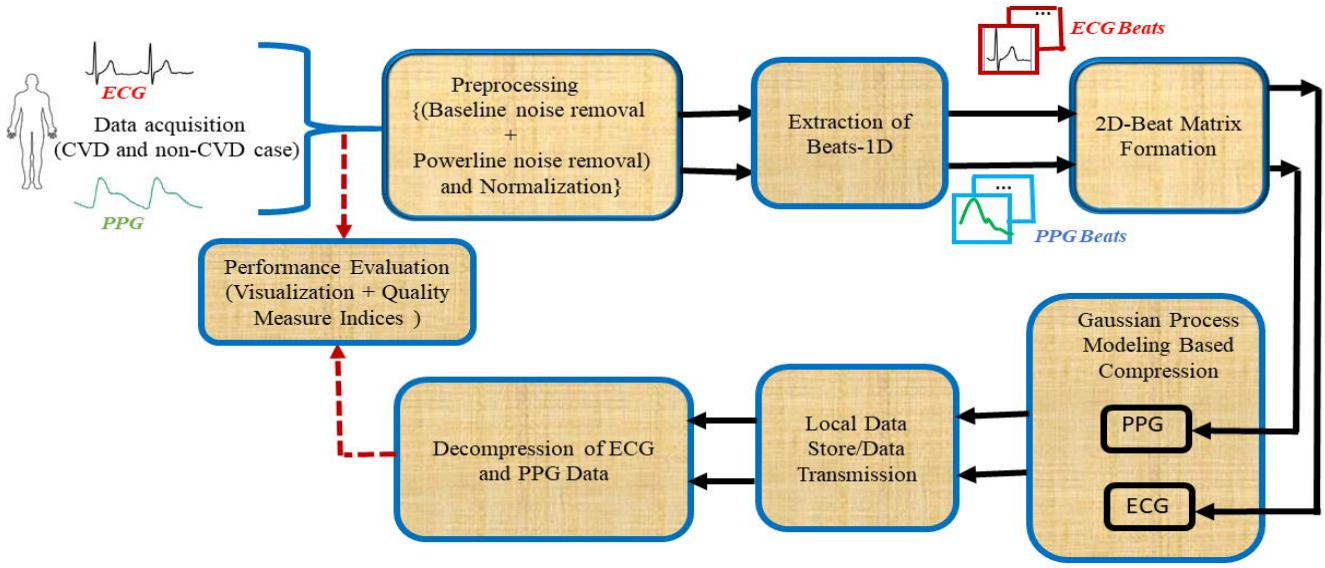

Fig. 4.2. Process flow diagram of GM-based data compression and decompression scheme of ECG and PPG for CVD monitoring.

4.4.1 Dataset description for compression

Few publicly available datasets include CVD diagnoses with correlated ECG and PPG signals. Physionet's MIMIC-III dataset integrates Lead-II ECG signals, known for their clear P and R waves, and PPG signals for cardiovascular analysis. We analyzed four CVD classes (RBBB, hypertension, arrhythmia, DCM) and one normal class to identify morphological signal patterns during compression. The ICD-9-CM codes for different CVDs are –" RBBB (426.4), Hypertension (402.91), Arrhythmia (427.31), and DCM (425.4)." RBBB is characterized by a delayed electrical signal in the heart's right bundle branch, seen as a widened QRS complex on an ECG. Hypertension presents a high R-value, while atrial fibrillation lacks P waves due to erratic atrial activity. DCM features an enlarged, weaker heart with extended QRS duration. The normal class indicates no significant cardiac abnormalities from sepsis and pneumonia illnesses people from MIMIC-III Dataset. Each recording is one minute long with signals sampled at 125 Hz, featuring participants aged 42–88 years. Resilience was validated using the MIT-BIH dataset (360 Hz). Additionally, Biopac Systems [41] collected real-world data from volunteers and hospital patients utilizing a PPG sensor module with a 125 Hz sampling frequency (HRM-2511E Easy pulse version 1.1) and an ECG transducer (BSLINTRO with SS2LB). The required signal processing and beat extraction is being carried out as described in chapter-3.

MATLAB (R2021a) was used to apply the methodology on a Windows 10 Pro machine equipped with an Intel Core i3 CPU (3.50 GHz) and 12 GB of RAM.

4.4.2 Hyperparameter sensitivity for ECG and PPG

Though the literature has revealed the five-Gauss (G-5)[172] for PPG, we have incorporated six-Gauss(G-6) by changing the parameter N, which is the number of Gaussian pulses. Keeping in mind to capture the various complex morphological patterns of cardiac persons we have proposed this value and the results shown in Table 4.1 and Table 4.2. Table 4.1 and Table 4.2 report that the values of PRD and SNR of G-6 and G-7 are very close. But G-7 consumes more computational resources, resulting in slower decompression time with CR degradation. So, we have taken G-6 throughout the study.

Table 4.1

Quality evaluation indices for selection of hyperparameter of ECG using various cardiac signals.

Disease	**Metrics**	**G-2**	**G-3**	**G-4**	**G-5**	**G-6**	**G-7**
RBBB (ID-1)	CR	24.894	23.657	22.895	22.015	21.758	19.560
	PRD	5.787	4.984	4.684	3.518	2.930	2.931
	SNR	48.527	49.951	51.547	52.009	54.687	54.625
	Exe.time(s)	3.985	4.358	4.954	5.457	5.890	6.458
Hyper (ID-3)	CR	28.998	28.842	28.049	27.654	26.234	24.521
	PRD	4.951	4.367	4.059	3.684	3.254	3.251
	SNR	36.651	37.054	37.543	38.567	39.254	39.254
	Exe.time(s)	4.028	4.156	4.854	5.157	5.684	6.214
Ary-atrfab (ID-1)	CR	21.359	20.896	20.158	19.526	18.936	16.235
	PRD	6.577	5.977	5.258	4.961	4.502	4.500
	SNR	44.891	45.128	45.637	46.251	47.558	47.551
	Exe.time(s)	5.124	5.857	6.124	6.548	7.094	8.569
DCM (ID-2)	CR	28.891	27.989	27.484	26.658	25.568	24.541
	PRD	4.589	4.221	3.895	3.124	2.859	2.859
	SNR	44.126	45.256	46.322	47.124	47.777	47.771
	Exe.time(s)	4.127	4.652	5.123	5.216	5.951	6.328
Normal (ID-2)	CR	19.128	18.567	17.995	17.327	16.897	15.254
	PRD	4.867	4.251	3.951	3.156	2.246	2.241
	SNR	35.546	36.254	37.457	38.562	39.258	39.251
	Exe.time(s)	3.268	3.856	4.012	4.651	5.214	5.895

Table 4.2

Quality evaluation indices for selection of hyperparameter of PPG using various cardiac signals.

Disease	**Metrics**	**G-2**	**G-3**	**G-4**	**G-5**	**G-6**	**G-7**
RBBB (ID-1)	CR	33.016	32.658	31.991	31.016	30.721	29.235
	PRD	3.011	2.564	1.956	1.342	0.907	0.904
	SNR	43.219	44.138	44.752	45.126	45.624	45.629
	Exe.time(s)	3.152	3.456	3.951	4.251	4.985	5.589
Hyper (ID-3)	CR	28.034	27.213	26.895	26.126	25.658	24.568
	PRD	2.851	2.246	1.945	1.114	0.982	0.980
	SNR	43.158	43.865	44.435	45.013	45.529	45.524
	Exe.time(s)	3.149	3.628	4.016	4.361	4.892	5.689
Ary-atrfab (ID-4)	CR	21.847	22.989	23.784	24.157	23.689	22.234
	PRD	2.894	2.333	1.898	1.256	0.998	0.998
	SNR	39.516	40.256	40.995	41.751	42.895	42.891
	Exe.time(s)	4.158	4.468	4.951	5.216	5.786	6.785
DCM (ID-3)	CR	34.716	33.984	33.521	32.896	32.329	31.562
	PRD	2.689	1.458	1.008	0.899	0.748	0.742
	SNR	41.632	42.995	43.524	44.158	44.959	44.951
	Exe.time(s)	4.128	4.625	5.018	5.246	6.012	7.007
Normal (ID-5)	CR	22.896	22.035	21.621	20.548	19.787	18.562
	PRD	2.628	1.864	1.358	0.995	0.647	0.648
	SNR	41.265	42.038	42.651	43.521	44.651	44.654
	Exe.time(s)	3.018	3.216	3.652	4.123	4.518	5.128

4.4.3 Result and discussion

The compression-based results are discussed in below subsections.

4.4.3.1 Result on ECG compression

The values of the aforesaid quality evaluation indices for each of the five patient IDs of four disease class CVD and one non-CVD class in the MIMIC III database throughout one minute are reported in Table 4.3 for ECG signal. The average values for CR, PRD (%), PRDN (%), QS (%^-1), SNR (dB), RMSE, CC, and execution time (Exe. Time (s)) are reported in Table 4.3 as being 20.956, 3.131, 5.403, 6.960747,

45.702, 0.0116, 0.999464, and 6.114, respectively, in that order. These compression findings, much outperform the many compression techniques that have been documented in the literature. Based on these performance matrices, it is evident that these techniques provide high compression at acceptable reconstruction errors. The obtained findings from the employed GM based compression methodology are compiled in Fig. 4.3 as box plot presentation format for better comparative analysis for all class patients. The results acquired persistently indicate that normal signal has comparatively low CR (lowest value of 16.28 to highest value of 18.213), low PRD (lowest value of 1.998 to highest value of 3.005), and execution time (lowest value of 4.682s to highest value of 5.741s) than the CVD signals. Execution time is the total time required from preprocessing to completely reconstruct the total beats. The results acquired emphatically demonstrate the conclusion that among the CVD classes, Ary-Atrfab class has poor CR, QS, SNR, CC, RMSE, and PRD values. Fig. 4.4 provides a credible visual representation of the original, reconstructed, and error signals for various ECG signal morphological patterns, including those with and without cardiovascular disease.

Fig. 4.5 gives a visual insight of the original ECG signal, GM coefficients, reconstructed GM coefficients, and, reconstructed ECG signal for the three segments for one complete beat. To assess the methodology's efficacy against three distinct segmentations for an entire beat, another study was also carried out using CVD class and normal class data. As an example, Fig. 4.6. (a) shows RBBB class without segmentation having CR = 56.047 and PRD = 11.275%, and Fig. 4.6. (b) shows the same signal with segmentation having CR = 22.634 and PRD = 3.125%. Additionally, the results are presented with great precision in Figs. 4.6(c) and 6(d), taking into account the segmentation of data for the normal class. It's quite evident that segmentation performance is much superior with less error. Therefore, the Table 4.3 findings are done with proper segmentation. Fig. 4.7. shows the variation of PRD with CR for CVD and normal classes.

The presence of noise is also an important factor. The reconstruction performance of Signal Ary-atrfab-ID-5 is the lowest and it is distorted by noise. Although CR is sufficient, the lowest QS (4.194314) is the consequence of its greater PRD (4.678).

Another vital information associated with Table 4.3 is that the combined duration of the compression and decomposition processes, i.e., execution time, is around 6.114 seconds, which is comparatively small when considering the signal of 1-minute duration. Also, the memory requirement for each ID was calculated. i.e. RBBB1-ID1 requires 1880 MB of memory, Hyper-ID2 requires 1750 MB, and normal-

ID2 requires 1677MB of memory for total compression and decompression process. For the entire dataset, it requires an average of 1784MB of memory. The overall computational complexity is calculated as such.

MIT-BIH data with different anomalies' performance are also shown in Table 4.4. Record 100 (Atrial premature beat (A)), record 107(ventricular premature beat (V)), record 111 (LBBB), record 112 (A), record 124 (RBBB), record 217 (V). Record 107 and 217 bear higher paced rhythm with poor QS of 4.126 and 4.256 respectively concerning other signals. Taking into account ten cardiac records an average CR is achieved as 22.228. PRD of 2.568.

Compression performance measure of ECG signals of real-world healthcare data and volunteers' is also shown in Table 4.5. Subjects S1, S4, and S6 belong to the DCM type with CR 24.118, 25.775, and 23.135 respectively. Normal subjects S9 and S10 have lower CR with values 16.797 and 17.887 respectively.

Compression performance evaluation of different class ECG signals GM and a transform domain approach, such as the fast Walsh-Hadamard transform (FWHT) shown in Table 6. RBBB-ID1 gives CR values of 21.758 and 16.254 for the GM model and FWHT respectively. Memory required for Table6 all data average value is 1790MB for GM model, whereas FWHT requires average value of 1240 MB of space.

4.4.3.2 Discussion on ECG compression

The compression performance findings shown in Table 4.3 and Table 4.5 demonstrate that non-CVD classes outperform CVD classes in terms of low PRD and low RMSE because the segmented Gauss model is large enough to coordinate with the non-CVD class regular pattern ECG, and its morphological characteristics vary less than those of CVD classes.

The Ary-atrfab class signals exhibit a higher pace rhythm and substantially lower QS [99] values of 4.20613, 5.332642, 5.474076, 4.831619, and 4.194314, respectively, as compared to other signals as per Table 1. As a result, signals with a faster rhythm are probably not going to compress well. This is mostly because the Gauss-modeling coefficients are unable to fit the increasing R-R variability, which is caused by the lack of a P' wave with beats of 100(±20) per minute, leading to poorer compression performance.

Amplitude a_m , center b_m, and variance c_m are the three model parameters needed for one Gauss function, as previously we have mentioned. If we were to model the ECG signal without segmentation and use six-gauss for a single beat, we would need twenty modeling coefficients. According to the distribution, six Gauss will yield eighteen coefficients, sample number will yield one, and beat number will yield one. In contrast, thirty-four modeling coefficients will be needed if we use two, six, and two-gauss for three segments progressively over the course of a beat while segmenting. The distribution of the first and third segments is as follows: Two-Gauss will provide six coefficients, the number of samples will provide one coefficient with a total of seven coefficients, Six-Gauss will provide eighteen coefficients, and the number of samples will provide one coefficient with a total of nineteen coefficients. Finally, using a single beat number, the beat as a whole is represented by thirty-four coefficients. In brief, when segmentation is omitted, a lower number of modeling coefficients is used, accomplishing satisfactory CR at the expense of PRD in the range of 5–9%. According to the literature [99] , PRD is within an acceptable range for high-quality reconstruction in the compression field but is inappropriate for the biomedical field's diagnosis of CVD patients. A wrong disease diagnosis and potential threat to human life could arise from taking into account a morphological signal pattern that was recovered incorrectly during reconstruction. From Fig. 4.7 it's quite evident that PRD increases with CR for both normal and CVD classes and reconstruction quality degrades.

Ary-atrfab-ID-5 is a noisy signal, and this noise can be eliminated by using an appropriate sophisticated preprocessing method. Table 4.6 result reveals that FWHT is faster than the GM model, but compression performance is inferior as a whole. so, we can conclude that it is not suitable for complex waveforms and results in inferior performance.

The qualitative evaluation of the suggested compression technique with various anomalies is displayed in Fig. 4.4. These records' 5-s duration is displayed there for improved comparison and visual representation. This analysis clearly shows that the shape of the P wave, QRS complex, and T wave, which are the three crucial components of ECG signals, have been preserved. As a result, the suggested approach is capable of recreating the signal with relatively little distortion.

As execution time is minimal, real-time compression and transmission could be accomplished using the suggested method for e-health applications. The average performance of the suggested framework in comparison to current state-of-the-art methods is displayed in Table 4.7. Here, it is evident that the

suggested compression method is more effective in terms of compression and lower PRD and lower RMSE when compared to reported works. While [113] has a lower PRD, its SNR (34.66) and CR (19.92) are also relatively low without providing the execution time. The previously reported work [115] had adequate PRD and QS values, but it did not take the baseline signal into account, which led to a low CR of 15.56 and a short execution time of 6.89 seconds. In contrast to [115], our suggested methodology yields better outcomes as CR, i.e., 20.956, and execution time, i.e., 6.114 seconds. Henceforth by taking all evaluation indices into account, the suggested technique is effective in compressing the ECG signal at a greater rate while maintaining a tolerable level of signal distortion, as demonstrated by the overall analysis.

Table 4.3

Compression performance evaluation of different class ECG signals.

Disease	**ID**	**CR**	**PRD(%)**	**PRDN**	**QS(%^-1)**	**SNR**	**RMSE**	**CC**	**Exe. time(s)**
RBBB	1	21.758	2.930	5.642	7.425939	54.687	0.0124	0.999947	5.890
	2	22.634	3.125	5.245	7.242880	52.258	0.0127	0.999864	5.987
	3	21.362	2.897	5.365	7.373835	51.258	0.0111	0.999951	6.458
	4	26.248	3.275	6.568	8.014656	49.325	0.0104	0.999953	6.254
	5	19.254	2.987	5.996	6.445932	47.258	0.0144	0.999950	5.984
Hyper	1	20.215	3.685	6.568	5.485753	52.265	0.0112	0.999954	6.127
	2	22.231	2.851	5.567	7.797615	47.258	0.0115	0.998974	6.125
	3	26.234	3.254	4.562	8.062077	39.254	0.0120	0.999957	5.684
	4	21.315	2.643	5.235	8.064699	45.787	0.0116	0.999979	5.694
	5	19.423	3.042	6.235	6.384944	44.258	0.0118	0.999891	6.214
Ary-atrfab	1	18.936	4.502	7.893	4.206130	47.558	0.0119	0.997578	7.094
	2	20.568	3.857	7.245	5.332642	39.258	0.0125	0.998493	6.947
	3	21.327	3.896	7.356	5.474076	42.259	0.0123	0.997954	7.147
	4	19.254	3.985	7.025	4.831619	44.258	0.0107	0.998999	7.125
	5	19.621	4.678	6.654	4.194314	44.757	0.0111	0.998579	7.018
DCM	1	23.235	2.407	3.569	9.653095	48.235	0.0120	0.999708	5.965
	2	25.568	2.859	4.528	8.942987	47.777	0.0108	0.998963	5.951
	3	22.327	3.704	5.899	6.027808	39.527	0.0115	0.999000	6.345

	4	21.698	2.786	4.258	7.788227	45.254	0.0112	0.999357	6.235
	5	24.658	3.128	4.458	7.882992	41.989	0.0121	0.999956	6.427
Normal	1	18.213	2.045	3.687	8.906112	47.558	0.0101	0.999846	5.154
	2	16.897	2.246	4.254	7.523152	39.258	0.0111	0.999841	5.214
	3	17.357	1.998	4.254	8.687187	42.259	0.0125	0.999994	5.741
	4	17.295	3.005	3.801	5.755408	44.258	0.0111	0.999931	5.408
	5	16.280	2.499	3.235	6.514606	44.757	0.0104	0.999982	4.682
Average		20.956	3.131	5.403	6.960747	45.702	0.0116	0.999464	6.114

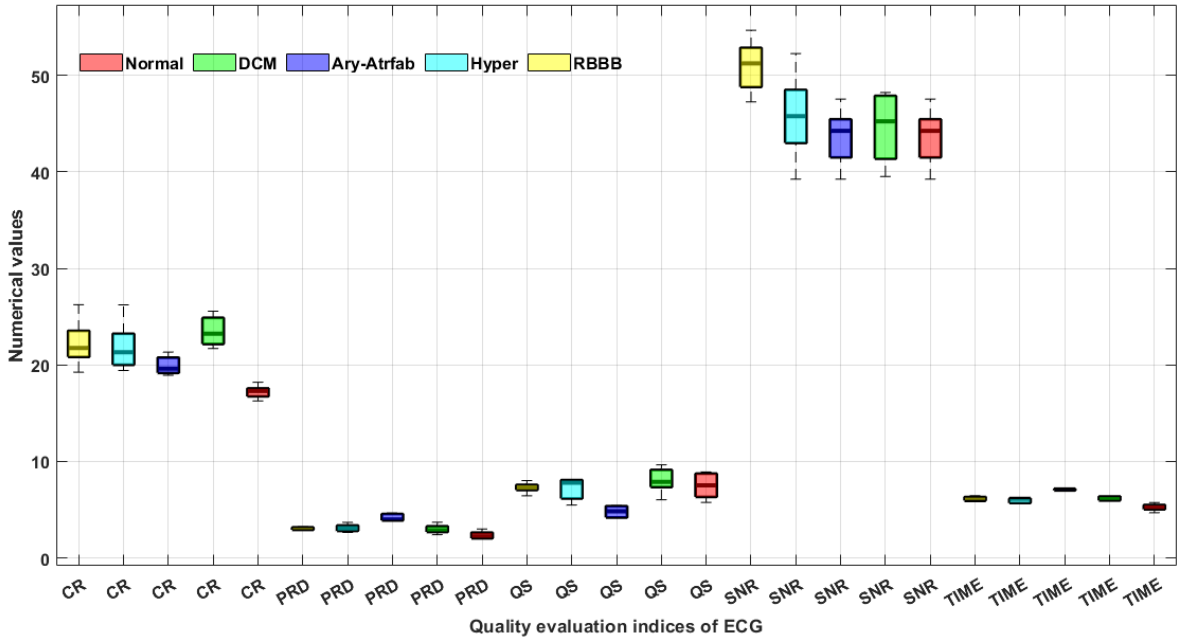

Fig. 4.3. Comparative analysis of compression performance of ECG in box plot form for CVD and non-CVD cases.

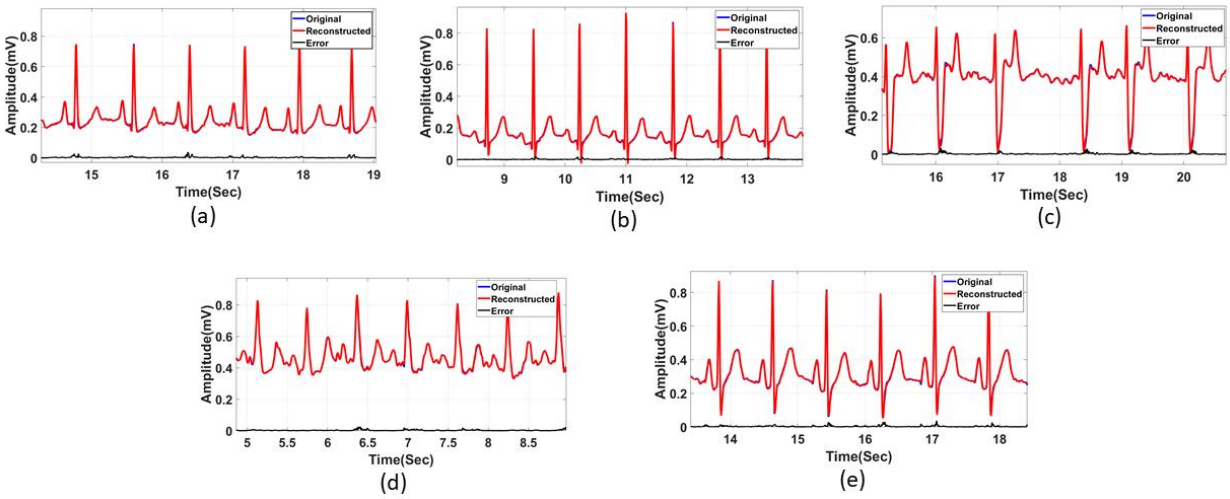

Fig. 4.4. Original, reconstructed and error signal for all four CVD and one non-CVD class of ECG using the proposed methodology: (a) RBBB-ID-2 (CR = 22.634 and PRD = 3.125%), (b) Hyper-ID-5 (CR = 19.423 and PRD = 3.042%), (c) Ary-atrfab-ID-5 (CR = 19.621 and PRD = 4.678%), (d) DCM-ID-5 (CR = 24.658 and PRD = 3.128%), (e) Normal-ID-2 (CR = 16.897 and PRD = 2.246%)

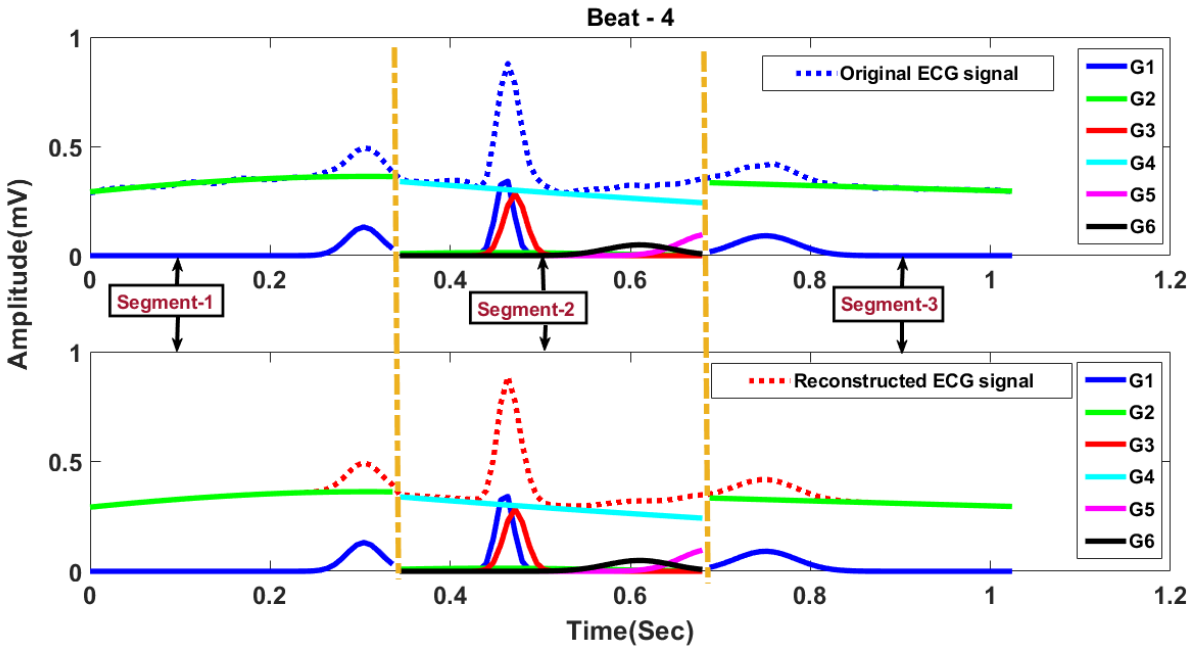

Fig. 4.5. Original ECG signal, GM coefficients, reconstructed GM coefficients and reconstructed ECG signal for the three segments of one complete beat.

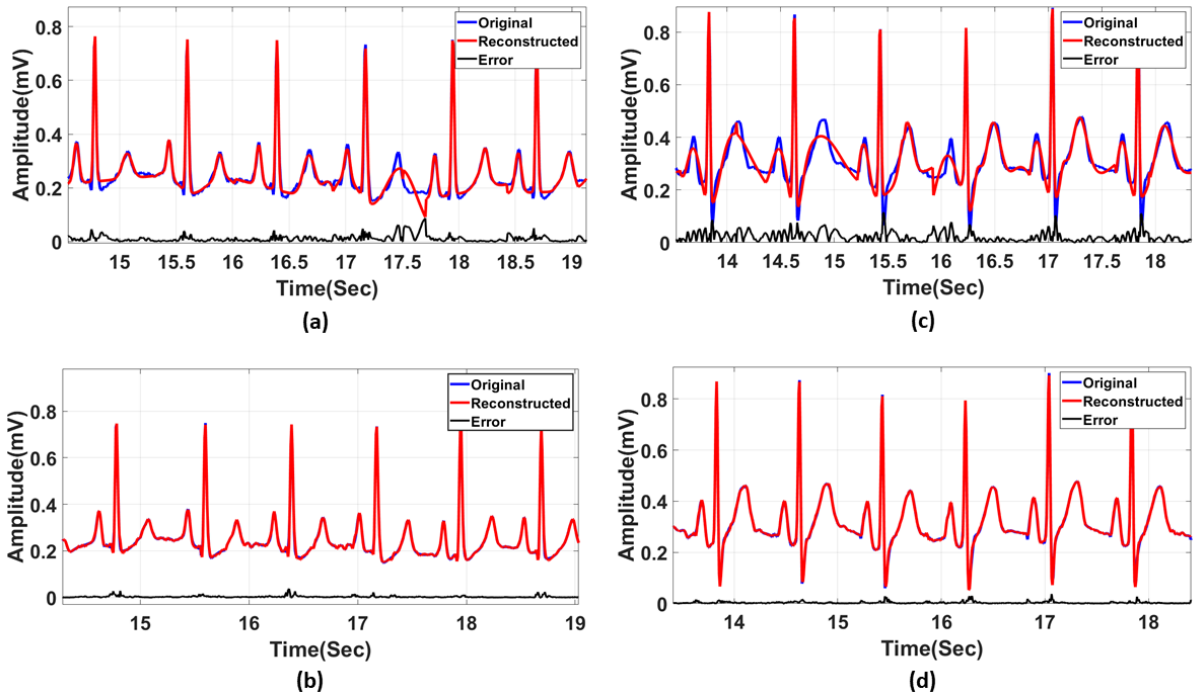

Fig. 4.6. Original, reconstructed, and error signal for one CVD and one non-CVD class of ECG using the proposed methodology: (a) RBBB-without segmentation-ID-2 (CR = 38.477 and PRD = 6.101% and QS= 6.306671), (b) RBBB-with segmentation-ID-2 (CR = 22.634, PRD = 3.125%, and QS = 7.242880), (c) Normal-without segmentation -ID-2 (CR = 28.724, PRD = 5.017%, and QS = 5.725333), (d) Normal-with segmentation-ID-2 (CR = 16.897, PRD = 2.246%, and QS = 7.523152)

Table 4.4

Compression performance evaluation of different cardiac syndrome ECG signals of MIT-BIH records.

ECG record	CR	PRD(%)	PRDN	QS(%^-1)	SNR	RMSE	CC	Exe. time(s)
100	27.017	3.548	5.991	4.352	37.918	0.018	0.999801	5.958
101	22.358	3.267	5.569	4.865	37.859	0.016	0.999912	6.421
103	23.187	3.854	5.611	4.981	38.946	0.017	0.999647	6.102
107	16.051	2.246	4.126	4.126	39.458	0.011	0.999716	7.148
111	18.561	5.217	7.771	3.008	34.251	0.019	0.999518	6.128
112	25.958	2.218	4.627	8.624	34.746	0.009	0.999618	6.007
117	26.857	2.005	4.852	9.018	41.287	0.001	0.999845	6.248
123	24.561	1.906	4.216	7.426	40.561	0.009	0.999715	6.511
124	20.877	1.956	4.448	7.851	40.958	0.01	0.999814	6.128
217	16.854	2.568	4.851	4.256	40.231	0.014	0.999812	6.923
Average	22.228	2.878	5.206	5.850	38.621	0.012	0.99974	6.357

Table 4.5

Compression performance measure of ECG signals of real-world healthcare data and volunteers

Subject (Age, Sex)	**CR**	**PRD(%)**	**PRDN**	**QS(%^-1)**	**SNR**	**RMSE**	**CC**	**Exe. time(s)**
S1(50,M)	24.118	2.666	4.418	7.754831	46.757	0.0108	0.998888	5.884
S2(62,M)	23.235	2.651	5.326	7.797615	47.558	0.0119	0.999841	6.006
S3(85,M)	26.774	3.008	5.562	7.082077	40.254	0.0116	0.999801	5.886
S4(68,M)	25.775	2.999	4.016	7.005876	44.773	0.0104	0.999956	6.124
S5(33,M)	22.315	2.844	5.009	8.746699	46.527	0.0107	0.999969	5.321
S6(26,F)	23.135	2.008	3.258	8.658095	49.265	0.0112	0.999708	5.657
S7(22,M)	19.884	4.506	7.888	4.254131	40.002	0.0124	0.997224	7.124
S8(42,F)	20.558	4.157	7.245	5.332642	40.258	0.0120	0.998001	6.928
S9(30,F)	16.797	2.117	4.004	7.425872	39.999	0.0107	0.999875	5.524
S10(60,M)	17.887	1.998	4.254	8.000458	42.019	0.0112	0.999984	5.211
Average	22.047	2.895	5.098	7.20583	43.741	0.0113	0.999325	5.966

Table 4.6

Compression performance evaluation of different class ECG signals GM and FWHT.

		Gaussian mixture based model				**Fast Walsh-Hadamard transform**			
Disease	ID	CR	PRD(%)	SNR	Exe. time(s)	CR	PRD(%)	SNR	Exe. time(s)
RBBB	1	21.758	2.930	54.687	5.890	16.254	2.885	57.568	4.358
	2	22.634	3.125	52.258	5.987	14.985	3.457	54.787	4.125
	3	21.362	2.897	51.258	6.458	16.567	2.562	52.354	4.851
Hyper	1	20.215	3.685	52.265	6.127	13.254	3.254	52.857	5.413
	2	22.231	2.851	47.258	6.125	15.247	2.616	48.251	5.319
	3	26.234	3.254	39.254	5.684	18.596	3.128	39.009	5.167
Ary-atrfab	1	18.936	4.502	47.558	7.094	13.542	4.126	49.235	6.517
	2	20.568	3.857	39.258	6.947	14.236	3.124	40.334	5.968
	3	21.327	3.896	42.259	7.147	12.568	3.127	43.568	6.746
DCM	1	23.235	2.407	48.235	5.965	17.258	2.124	48.899	5.419
	2	25.568	2.859	47.777	5.951	19.007	2.167	49.658	5.207
	3	22.327	3.704	39.527	6.345	15.049	3.138	40.538	6.041
Normal	1	18.213	2.045	47.558	5.154	12.348	1.999	48.996	4.856
	2	16.897	2.246	39.258	5.214	10.357	2.124	42.357	4.759
	3	17.357	1.998	42.259	5.741	12.859	1.425	43.569	5.017

Table 4.7

Comparison of the proposed Gaussian based modelling compression with the existing state-of-the-art methodologies for ECG.

ECG compression principle(year)	**SNR**	**RMSE**	**PRD**	**PRDN**	**CR**	**QS**	**CC**	**Exe. time(s)**
Hybrid encoding (2016) [108]	-	-	2.43	3.27	10.99	4.52	-	-
DCT+RLE+HC (2017)[109]	60.11	0.012	3.43	5.51	11.49	3.82	-	-
Wavelet+modified RLE (2022)[111]	28.27	-	3.92	6.36	17.18	4.37	-	-
CS+ Kronecker-based recovery (2020) [112]	-	-	9.72	-	~8	-	-	-
SVD+EZW(2016) [113]	34.66	-	1.99	-	19.92	-	0.999	-
DCT-based discrete orthogonal Stockwell transform (2018)[114]	22.68	0.03	5.37	7.95	6.27	1.49	-	-
Discrete Krawtchouk moments+AALO (2022))[115]	44.52	-	0.69 (base line not taken)	-	15.56	23.92	-	6.89
TQWT+CHIO(2023 [119]	31.984		2.8869		13.722	7.2820	0.9991	
B-spline+ACO (2023)[120]			2.3		7.8	3.4		
Proposed work (MIMIC III)	45.702	0.011	3.131	5.403	20.956	6.960	0.99946	6.114 (1784 MB memory)

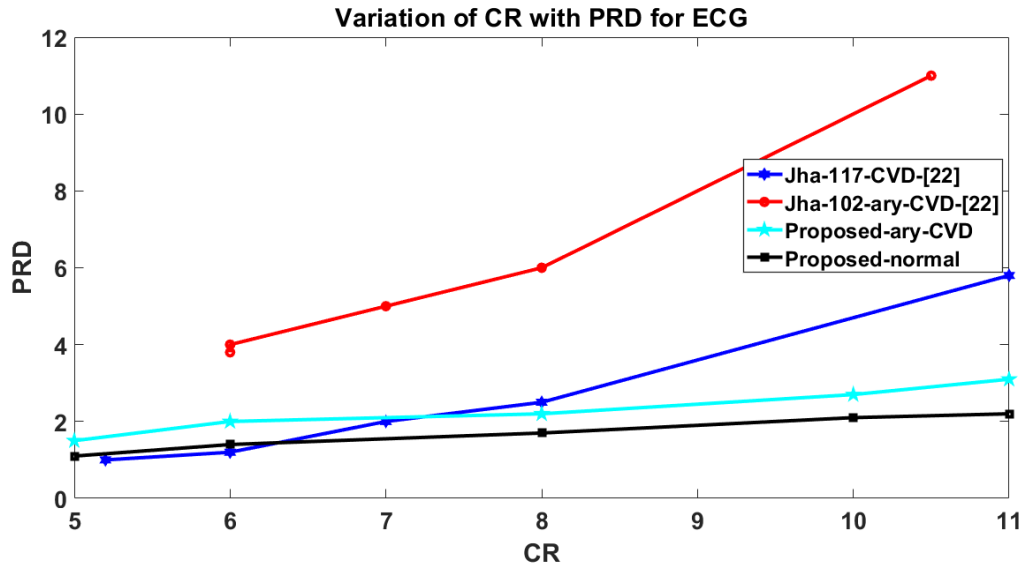

Fig. 4.7. Variation of PRD with CR for normal and CVD patients for ECG signal.

4.4.3.3 Result on PPG compression

Table 4.8 provides a summary of the results of testing the compression method on a large number of digitized PPG data with various types of cardiac syndromes. It is evident from findings on these enormous amounts of samples that the algorithm produces average values for CR, PRD (%), PRDN (%), QS (%^-1), SNR (dB), RMSE, CC, and Exe. Time (s) of about 26.051, 0.954, 2.691, 28.355,45.135, 0.008, 0.999634, and 5.293, respectively. For improved comparative analysis for all class patients, the results of the GM-based compression methods are collected in Fig. 4.8 and presented as a box plot. The results acquired persistently indicate that the normal signal has comparatively lower CR (lowest value of 19.787 to highest value of 22.005), lower PRD (lowest value of 0.647 to highest value of 0.83), and execution time (lowest value of 4.518s to highest value of 5.235s) than the CVD signals. Like ECG, among the CVD classes, the Ary-Atrfab class has the lowest CR, QS, SNR, CC, RMSE, and PRD values, as the outcomes obtained clearly show as in Table 4.8.

For a variety of PPG signal morphology patterns, including those with and without cardiovascular illness, Fig. 4.9 offers a reliable qualitative visual depiction of the original, reconstructed, and error signals. The discrepancies between the original and reconstructed signal are usually estimated using PRD (PRDN) and RMSE values. Our result outperforms average PRD (%) values for CVD, non-CVD, and both (CVD and non-CVD) as 0.763, 1.002, and 0.954, respectively.

A visual representation of the original PPG signal, GM coefficients, reconstructed GM coefficients, and

reconstructed PPG signal for a single beat is also provided in Fig. 4.10 for better understanding. The execution time of 5.293 seconds is relatively short when compared to the signal's minute duration. Fig. 4.11 shows the variation of PRD with CR for CVD and normal classes.

Compression performance measure of PPG signals of real-world healthcare data and volunteers' is also shown in Table 4.9. Subject S1, S4, S6 belong to DCM type with CR 29.884, 31.004and 28.543respectively. Normal subject S9 and S10 have lower CR with values 20.458and 19.124respectively.

Compression performance evaluation of different class PPG signals GM and a transform domain approach, such as the fast Walsh-Hadamard transform (FWHT) shown in Table 4.10. RBBB-ID1 gives CR value as 30.721and 27.038 for GM model and FWHT respectively.

4.4.3.4 Discussion on PPG Compression

Because of the six-Gauss model's ability to coordinate with the non-CVD class regular pattern PPG, as well as its less variable w.r.t. the morphological characteristics compared to CVD classes, the compression performance findings presented in Table 4.8 show that non-CVD classes outperform CVD classes in terms of low PRD and low RMSE.Poorer compression performance for the Ary-Atrfab class because of the inability of Gauss-modeling coefficients to fit the faster systolic-to-systolic peak arrival, resulting in a higher beat rate. Again, from Fig. 4.11 it's quite evident that PRD increases with CR for both normal and CVD classes and reconstruction quality degrades.

According to work [173], numerical evaluation of the reconstructed bio-signals' clinical acceptability concerning PRD less than 2%, the reconstructed signal is regarded as "very good," as our result is 0.954. However, in contrast as per literature [174], these metrics do not offer an optimal assessment of the retention of all clinically meaningful information in the rebuilt PPG data. For that, we have ensured that all therapeutically significant wave features are retained by independently evaluating the reconstruction quality of all classes of signal by the suggested compression strategy. The most significant characteristic points of the PPG signal are shown in Fig. 4.1.(b) are mostly used to extract the pertinent clinical fiducial parameters such as onset points, which represent the minimum blood volume change corresponding to the start of ventricular contraction; systolic peaks, which represent the maximum blood volume change corresponding to the end of systole; lower body arteries reflect the pressure wave, causing the diastolic peak, and dicrotic notch, where the information about the aortic valve closer is expressed. The waveform

shown in Fig. 4.8 has preserved all the fiducial points in the reconstructed signal because by overlapping both signals, fairly we mark any discrimination of the original and reconstructed signal in peak positions or onset points or in the morphological pattern. For visual cross-inspection, the hospital's skilled medical professional has also shown the original signal obtained from the MIMIC III dataset patients as well as the reconstructed signal following compression-decompression using the methodology suggested. In his view, the reconstructed data effectively preserves all relevant clinical information on cardiovascular syndrome.

Table 4.10 result reveals that FWHT is faster than the GM model, but compression performance is inferior as a whole. so, we can conclude that it is not suitable for complex waveforms and results in inferior performance.

The proposed method for e-health applications might achieve real-time compression and transmission because of its short execution time.

Table 4.8

Compression performance evaluation of different class PPG signals.

Disease	ID	CR	PRD(%)	PRDN	QS(%^-1)	SNR	RMSE	CC	Exe. Time
RBBB	1	30.721	0.907	2.135	33.871003	45.624	0.0014	0.999985	4.985
	2	28.965	1.065	3.569	27.197183	45.567	0.0037	0.999964	5.012
	3	27.328	0.888	2.789	30.77477	49.256	0.0051	0.999941	5.147
	4	29.654	1.125	3.014	26.35911	48.031	0.0048	0.999969	4.845
	5	29.367	0.897	2.568	32.73913	48.678	0.0054	0.998795	4.985
Hyper	1	28.568	1.114	3.564	25.64452	47.361	0.0028	0.999964	5.126
	2	26.351	1.509	2.851	17.46256	44.657	0.0118	0.998978	5.453
	3	25.658	0.982	1.095	26.12831	45.529	0.0035	0.999937	4.892
	4	27.359	0.767	1.652	35.67014	43.325	0.0032	0.999979	4.657
	5	26.027	0.632	1.563	41.18196	44.057	0.0031	0.999897	5.857
Ary-atrfab	1	23.357	1.126	3.612	20.74334	39.356	0.0178	0.999571	6.213
	2	23.048	1.115	3.242	20.67085	41.257	0.0098	0.999494	5.954
	3	24.934	1.047	2.781	23.81471	42.605	0.0064	0.999831	5.994
	4	23.689	0.998	1.138	23.73647	42.895	0.0088	0.998909	5.786

	5	24.506	1.358	1.998	18.04566	40.657	0.0751	0.999311	6.459
DCM	1	29.327	0.921	2.945	31.84256	45.376	0.0047	0.999908	4.857
	2	27.024	0.769	2.616	35.14174	44.658	0.0159	0.998008	5.568
	3	32.329	0.748	3.285	43.22059	44.959	0.004	0.999894	6.012
	4	28.597	1.091	4.123	26.21173	42.657	0.0053	0.999953	5.347
	5	28.704	0.987	2.517	29.08207	49.651	0.0058	0.999952	4.666
Normal	1	21.658	0.755	2.448	28.68609	42.369	0.0016	0.999755	5.011
	2	20.987	0.754	3.664	27.83422	45.678	0.0011	0.999833	5.237
	3	22.005	0.829	2.693	26.54403	48.888	0.0025	0.999994	4.999
	4	21.326	0.83	3.201	25.69398	47.654	0.0038	0.999064	4.751
	5	19.787	0.647	2.235	30.58268	44.651	0.0017	0.999957	4.518
Average		26.05104	0.95444	2.6919	28.35517	45.135	0.0083	0.999634	5.2932

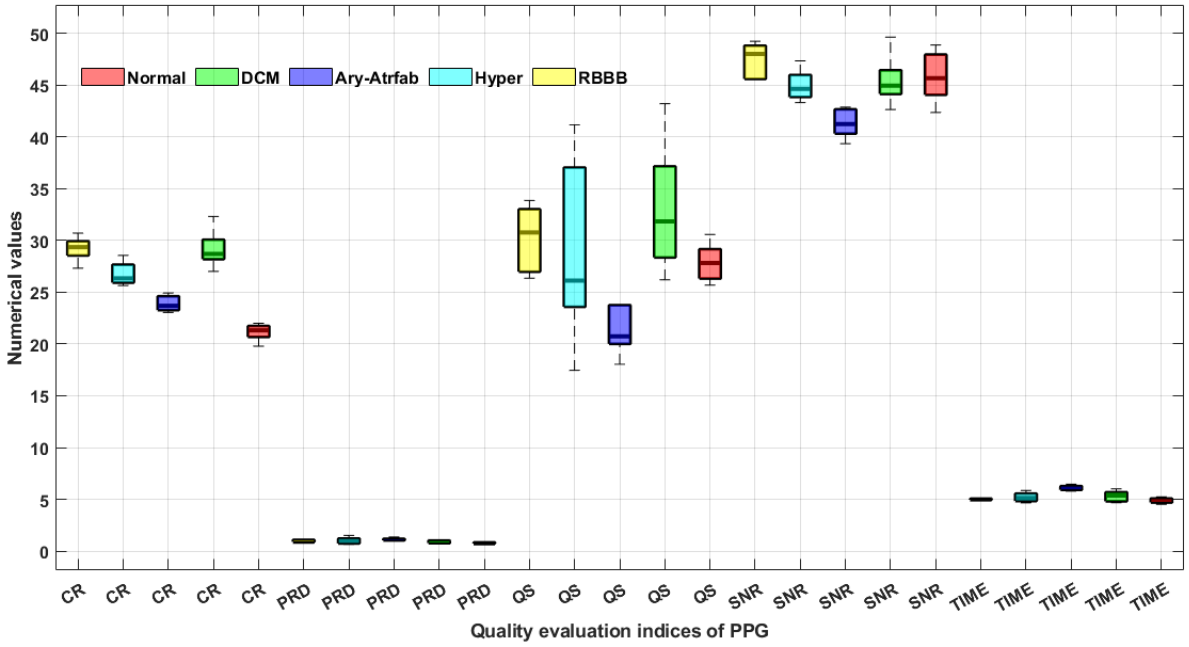

Fig. 4.8. Comparative analysis of compression performance of PPG in box plot form for CVD and non-CVD cases.

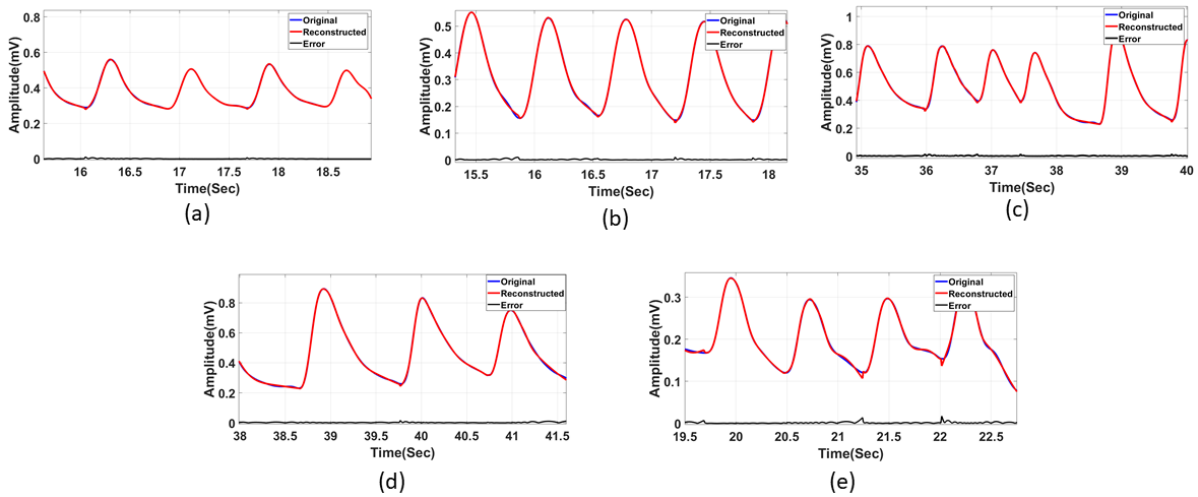

Fig. 4.9. Original, reconstructed and error signal for all four CVD and one non-CVD class of PPG using the proposed methodology: (a) RBBB-ID-2 (CR = 28.965 and PRD = 1.065%), (b) Hyper-ID-1 (CR = 28.568 and PRD = 1.114%), (c) Ary-atrfab-ID-2 (CR = 23.048 and PRD = 1.115%), (d) DCM-ID-2 (CR = 27.024 and PRD = 0.769%), (e) Normal-ID-1 (CR = 21.658 and PRD = 0.755%).

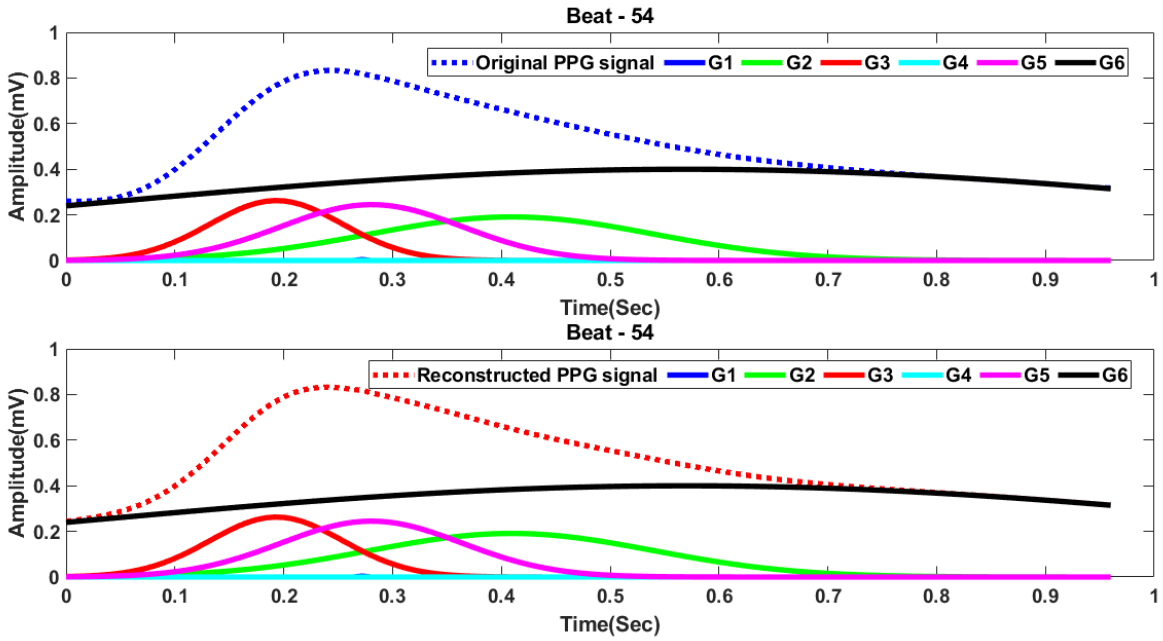

Fig. 4.10. Original PPG signal, GM coefficients, reconstructed GM coefficients and reconstructed PPG signal for one complete beat.

Table 4.9

Compression performance measure of PPG signals of real-world healthcare data and volunteers

Subject (Age, Sex)	CR	PRD(%)	PRDN	QS(%^-1)	SNR	RMSE	CC	Exe. time(s)
S1(50,M)	29.884	0.988	2.624	30.62256	44.851	0.0039	0.999921	4.955
S2(62,M)	25.528	0.994	1.254	29.12842	43.324	0.0041	0.999931	4.894
S3(85,M)	26.675	0.804	1.452	35.54014	45.322	0.0035	0.999979	4.757
S4(68,M)	31.004	0.867	3.128	38.25248	45.009	0.0032	0.999891	5.826
S5(33,M)	26.346	0.635	1.566	42.18666	47.055	0.0024	0.999897	5.757
S6(26,F)	28.543	0.906	2.891	32.08214	45.628	0.0081	0.999904	4.527
S7(22,M)	23.326	0.998	1.538	24.73647	42.995	0.0048	0.998904	5.286
S8(42,F)	23.906	1.128	2.269	21.04566	37.657	0.0744	0.999411	6.124
S9(30,F)	20.458	0.842	3.008	25.21588	46.622	0.0125	0.999158	4.4561
S10(60,M)	19.124	0.7004	2.645	30.44468	44.651	0.0025	0.999928	4.234
Average	25.479	0.88624	2.2375	30.92551	44.311	0.0119	0.999692	5.0816

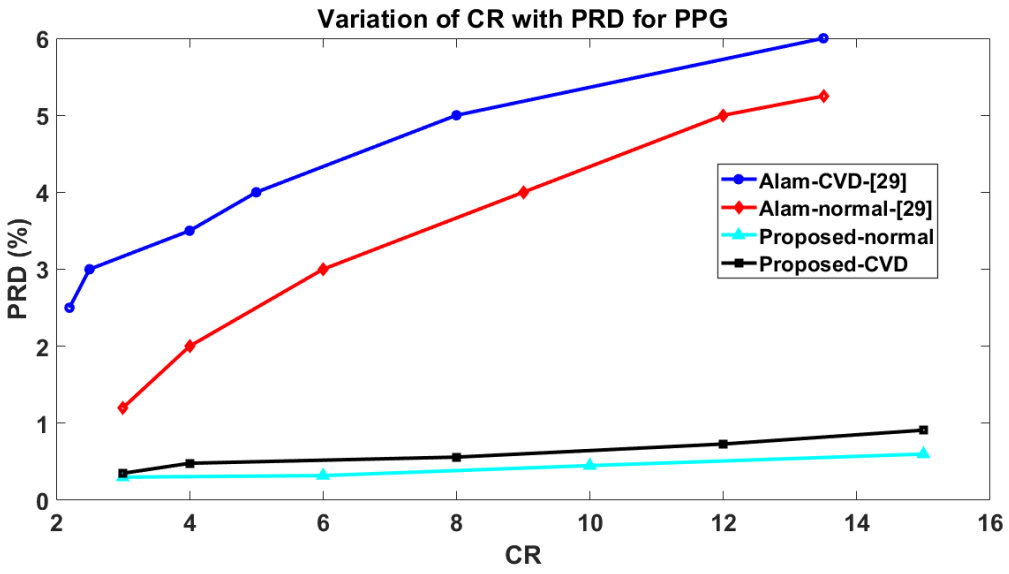

Fig. 4.11. Variation of PRD with CR for normal and CVD patients for PPG signal.

Table 4.11 shows the average performance of the proposed framework compared to the state-of-the-art techniques currently in use, taking into CVD and non-CVD classes separately. The table shows that the suggested approach produced respectable results for every numerical measurement. In particular, the CR

that the algorithm has produced is excellent. Certain areas in the table designated for the corresponding measurements of the corresponding methods remain unfilled due to the absence of data in the original publications.

Table 4.10

Compression performance evaluation of different class PPG signals GM and FWHT.

		Gaussian mixture based model				**Fast Walsh-Hadamard transform**			
Disease	ID	CR	PRD(%)	SNR	Exe. Time	CR	PRD(%)	SNR	Exe. Time
RBBB	1	30.721	0.907	45.624	4.985	27.038	0.891	46.628	4.128
	2	28.965	1.065	45.567	5.012	26.327	0.957	47.028	4.607
	3	27.328	0.888	49.256	5.147	25.367	0.807	49.997	4.384
Hyper	1	28.568	1.114	47.361	5.126	25.634	1.045	48.016	4.985
	2	26.351	1.509	44.657	5.453	22.608	1.267	44.138	5.243
	3	25.658	0.982	45.529	4.892	21.568	0.954	46.509	4.526
Ary-atrfab	1	23.357	1.126	39.356	6.213	20.057	1.105	39.555	5.661
	2	23.048	1.115	41.257	5.954	21.359	1.009	41.987	5.558
	3	24.934	1.047	42.605	5.994	22.651	1.007	43.009	5.342
DCM	1	29.327	0.921	45.376	4.857	26.348	0.845	46.887	4.126
	2	27.024	0.769	44.658	5.568	24.857	0.668	44.239	5.108
	3	32.329	0.748	44.959	6.012	27.651	0.708	45.987	5.341
Normal	1	21.658	0.755	42.369	5.011	18.551	0.669	44.658	4.882
	2	20.987	0.754	45.678	5.237	19.007	0.718	47.851	5.008
	3	22.005	0.829	48.888	4.999	20.346	0.811	49.651	4.338

Table 4.11
Comparison of the proposed Gaussian-based modeling compression with the existing state-of-the-art methodologies for PPG.

PPG compression principle(year)	**SNR**	**RMSE**	**PRD**	**PRDN**	**CR**	**QS**	**CC**	**Exe. time(s)**
Second order delta modulation + HC (2015) [122]	-	-	0.127	0.187	2.223	17.5	-	-
quality-aware quality-control data compression (QAQCDC)(2019) [124]{a)CapnoBase database,b)MIMIC-II}			a) 5.97		18.41			
			b) 5.97		25.93			
Delta encoding (2015)[125]			5.82	7.57	3.84	0.659		
Principal component analysis(PCA),2018 [121]			2.41	4.98	5.65(N)			
			3.33	5.9	6.76 (CVD)			
Fourier series analysis(2009) [126]					12			
Vector quantization with residual encoder(2021) [127]			0.31		15.8			
Second order delta encoding+RLE+buffer array(2023) [128]					2.49			
Proposed work a) Normal only	45.848	0.002	0.763	2.848	21.152	27.868	0.999721	4.903 (1425 MB memory)
b) CVD only	44.957	0.009	1.0023	2.652	27.275	28.476	0.999612	5.390 (1527 MB memory)
c) Both (Normal + CVD)	45.135	0.008	0.954	2.691	26.051	28.355	0.999634	5.293 (1501 MB memory)

4.4.3.5 Case study of compression on CVD patients

For a better illustration of the compression steps, we have shown it on the MIMIC III dataset in Fig. 4.12 for the ECG signal. It is easy to observe that baseline noise is removed at 0.49 Hz as shown in Fig. 4.12. (a), followed by power noise removal at 50 Hz as shown in Fig. 4.12. (b). The very next step is done with the representation of fiducial points (P, Q, R, S, and T) as illustrated in Fig. 4.12. (c). Then beat wise signals were retrieved for the entire 1-minute duration signal as shown in Fig. 4.12.(d). A two-dimensional matrix is formed by arranging all beats one after another sequentially in text form. After this, the matrix is fed to GM modeling for compression as shown in Fig.4. 5. Finally, through the modeling coefficients the reconstructed signal is achieved with minimal error shown in Fig. 4.12. (e).

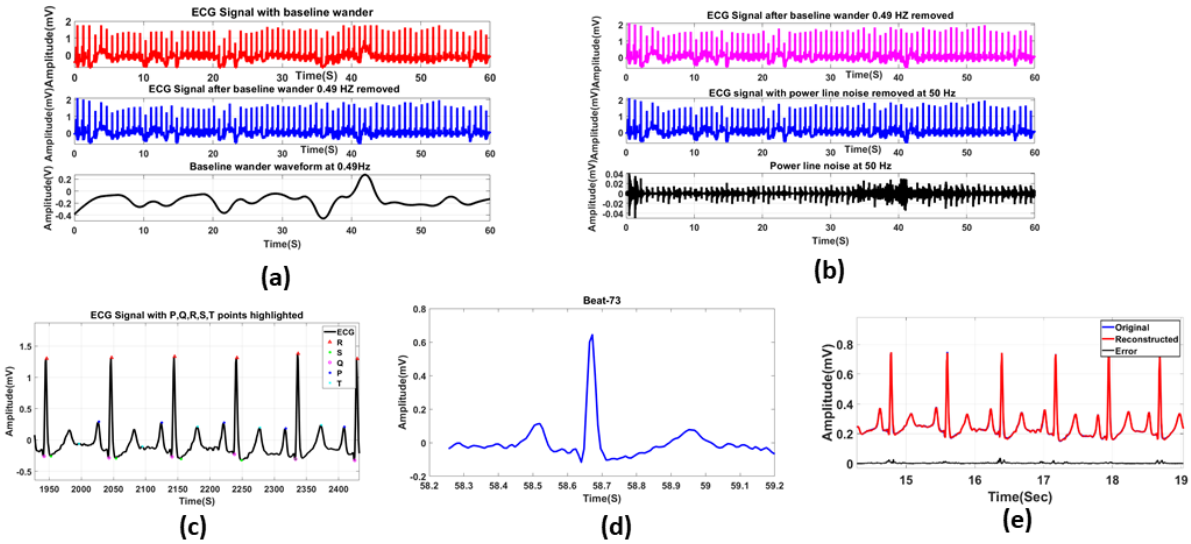

Fig. 4.12. Visualization of compression steps of ECG on MIMIC III dataset. (a) Visualization of raw input sample RBBB-ID2, (b) Visualization of removal of baseline wander and power noise, (c) Visualization of clean ECG with fiducial points, (d) Visualization of individual beat, (e) Visualization of the original and reconstructed signal after decompression with error signal.

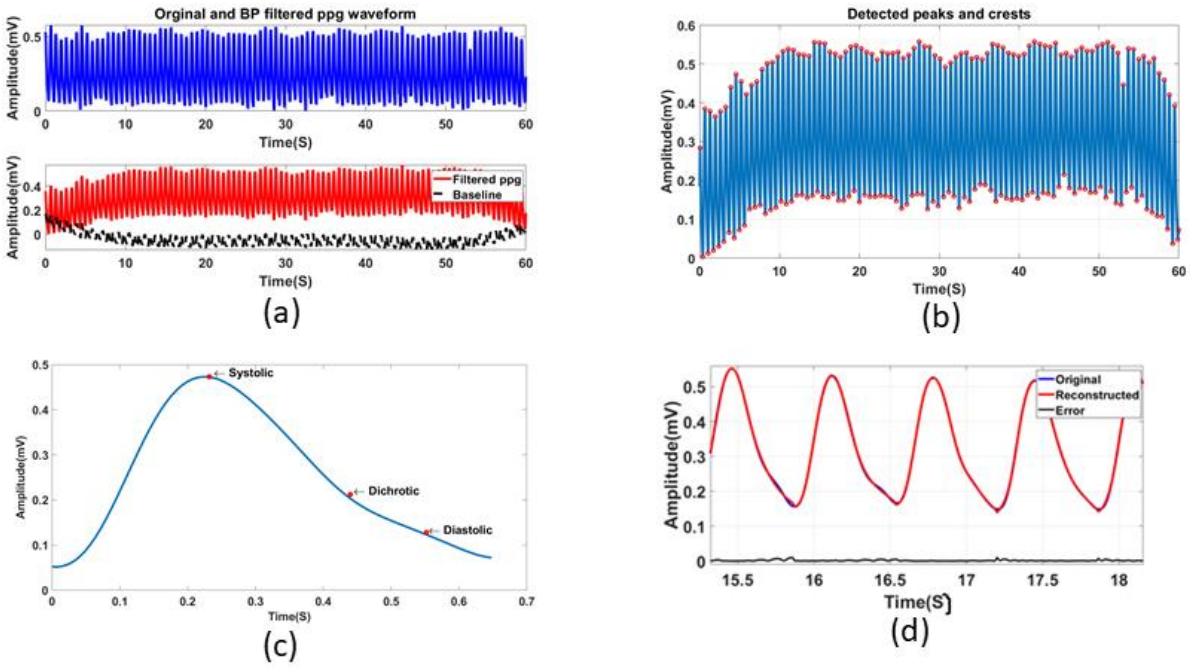

Fig. 4.13. Visualization of compression steps of PPG on MIMIC III dataset. (a) Visualization of raw input sample Hyper-ID1 and filtered signal with baseline noise removed, (b) Visualization of entire signal showing peaks and crests, (c) Visualization of clean PPG with fiducial points for beat wise (d) Visualization of the original and reconstructed signal after decompression with error signal.

Similarly, for a clearer representation of the compression stages, we have used the PPG signal from the MIMIC III dataset in Figure 4.13. The pre-processing of PPG is done by a bandpass filter to remove the baseline signal as shown in Fig. 4.13(a). crests and troughs are shown for the entire 1-minute duration period shown in Fig. 4.13(b). Consequently, beats are retrieved with all the fiducial points (systolic, dichrotic, and diastolic) illustrated in Fig. 4.13. (c). The beat matrix is formed by taking all the beats one by one and forming a 2-D matrix. Then the GM based compression is done as shown in Fig.10. Ultimately, as demonstrated in Fig. 4.13. (d), the reconstructed signal is obtained with little error by virtue to the modeling coefficients.

4.5 Data compression of PPG signal for CVD monitoring in IoT-based platform

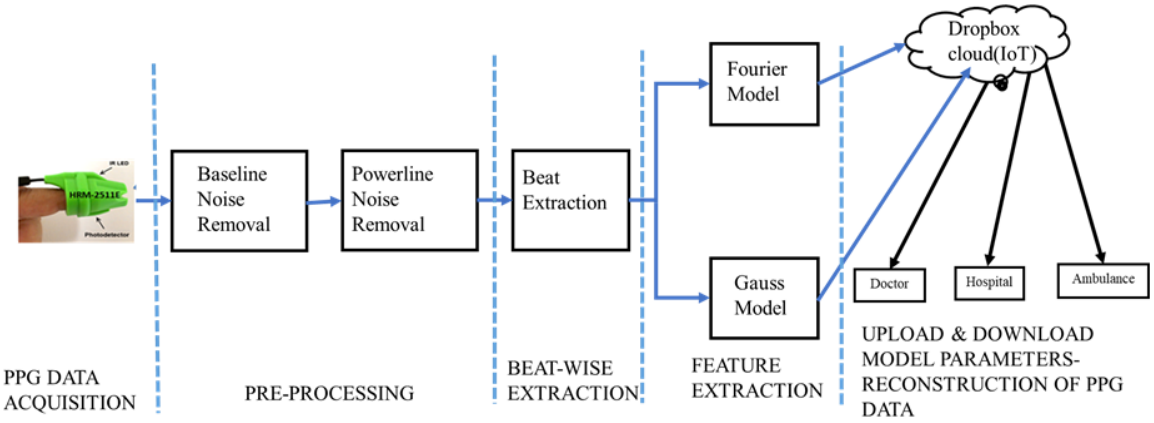

Fig. 4.14 Workflow diagram of the proposed model for PPG monitoring in IoT platform.

The novelty of the work, is to use data compression of PPG signal in the IoT cloud, where any patient's PPG signal can be sent via Bluetooth or other wireless information technologies across the Internet. Connected devices may gather and share information with each other using IoT technologies, which is more secured. The enormous data set of various cardiac patients contains some vital information for which the implementation of such a robust data-compressing tool or data compressing mechanism is necessary so that time and cost required for the storage i.e. less memory space requirement and maintenance of such a huge data set can be significantly reduced without compromising accuracy. The proposed solution is the implementation of Gaussian and Fourier models. Instead of storing the PPG raw sample values, the beat-wise characteristic model parameters are stored and uploaded into a database called Dropbox. Thus, the information that we have gathered over the time period can be accessed globally with the help of the high speed internet connection and the unique configuration that has been set from the user side (Unique Patient ID). Hence compression plays a significant role for data storing and accessing in IoT cloud. Our case study covers 3 class cardiac abnormalities and one normal class. Where, Class1 -Hypertension (too high blood pressure), Class2-Ischemic (insufficient flow of O_2 to some organ of our body), Class3- Myocardial Infarction or Heart Attack (when coronary artery is deprived of sufficient blood flow).

The proposed IoT based non-invasive PPG monitoring topology is shown in Fig. 4.14. The main thought is to model beat-wise PPG signal through Gaussian and Fourier models and consequently compressing and downloading the data of particular Patient ID at the time of requirement

4.5.1 ***PPG Data Acquisition***

The proposed methodology is developed by using data acquisition system with a typical PPG sensor module i.e. HRM-2511E Easy pulse version 1.1. The physiological information of cardiovascular system can be retrieved in assistance ship of IR LED source and a photo detector. It (PPG) obtain a valuable information regarding any volumetric changes in our blood, manifests arterial structure and its related diseases and disorders. The filtered PPG signal is acquired by two stage filtering and amplification using MCP6004 Op-Amp. Afterwards the analog channel of embedded microcontroller (ATMEGA328) was connected with the sensor to capture the patient signal at sampling frequency of 250 Hz for a duration of 2 minutes. Last but not the least via a USB cable the microcontroller is connected to a PC to give data (.txt) format. The PPG signals are captured from 20 different persons -cardiac abnormal of 3 different classes such as Hypertension, Ischemia, Myocardial Infraction and normal.The subjects are male and female from age group of 38 years to 79 years of NH Rabindranath Tagore, International Institute of Cardiac Sciences, Kolkata.

4.5.2 Dropbox to store PPG data in IoT systems

Dropbox is a cloud storage platform that lets users safely store, sync, and share data online. It is beneficial for applications that need distant data storage and retrieval, including Internet of Things-based healthcare monitoring systems, because it enables file access from multiple devices. It is a useful tool for PPG signal compression and retrieval in cardiovascular disease (CVD) patient monitoring because of Dropbox.

Following are the steps of IoT-based CVD monitoring through Dropbox:

- PPG signals are captured via wearable IoT devices.
- Data size reduction occurs with the Fourier series/Gaussian model-based compression technique.
- Dropbox receives the compressed PPG file.
- The PPG data is retrieved and decompressed for CVD analysis by a physician or artificial intelligence system.
- An alert is provided to the clinician for prompt action if anomalies are found.

4.5.3 Result and Discussion

The PPG signal is represented using a mixture of Gaussian functions after simulation-based signal processing, which is an additive signal of two independent Gaussian functions. Each cycle of the PPG has a systolic peak and a diastolic peak for better reconstruction and accuracy. This model is recommended for initialization of random data and centred at around a value i.e. the mean and usually set as zero [176].

The model parameters $\{(a_1, b_1, c_1)$ and $(a_2, b_2, c_2)\}$ were determined and reconstructed over time period of recording as per GM based approach as explained in chapter 1.5. For easy reconstruction, we proposed for each beat or cycle of PPG is modelled with the eight model parameters {Beat no.,(a_1, b_1, c_1)) and (a_2, b_2, c_2) and N}. Where N is the total no. of samples for a single beat. The said eight model parameters are extracted with the help of Curve Fitting Toolbox (CFT) in MATLAB.

Twelve model parameters for FM based are proposed for each beat of PPG if it is of 4th order are: {Beat no., C_0, (A_1, A_2, A_3, A_4), (B_1, B_2, B_3, B_4) (a_2, b_2, c_2), ω_0 and N}. Where N is the total no. of samples for a single beat. The said twelve model parameters are extracted with the help of Curve Fitting Toolbox (CFT) in MATLAB.

4.5.3.1 Result of FM and GM based compression

After modelling throgh Gaussian and Fourier medels of each beat of every patient is uploaded to the IoT clooud and saved thereafter.Again at the time of need the model parameters of the particular patient is downloaded from the folder where it was saved.while saved data aws also compressed to have less memory space.Eventually the during reconstruction all the betas are concanated to form the dataset for the particular patient.The statistical performance parameters give the valuable authentication of reconstruction signal.These parameters[171] are Root mean square error (RMSE), signal to noise ratio (SNR), percentage root mean squared difference normalized (PRDN) were determined. Uncompressed files demand substantially more storage space than compressed files, hence compressed files significantly reduce storage costs. Data compression ratio (CR) is defined as the ratio between the uncompressed size and compressed size as in (4.9) and (4.10). For Gauss and Fourier CR is expressed in (4.11) and (4.12).

$$Compression\ ratio\ (CR) = \frac{Uncompressed\ size}{Compressed\ size} \quad (4.9)$$

$$Space\ saving = 1 - \frac{Uncompressed\ size}{Compressed\ size} \quad (4.10)$$

$$CR_{fourier} = \frac{No.of\ samples\ beatwise}{No.of\ fourier\ model\ parameters} \quad (4.11)$$

$$CR_{gauss} = \frac{No.of\ samples\ beatwise}{No.of\ Gauss\ model\ parameters} \quad (4.12)$$

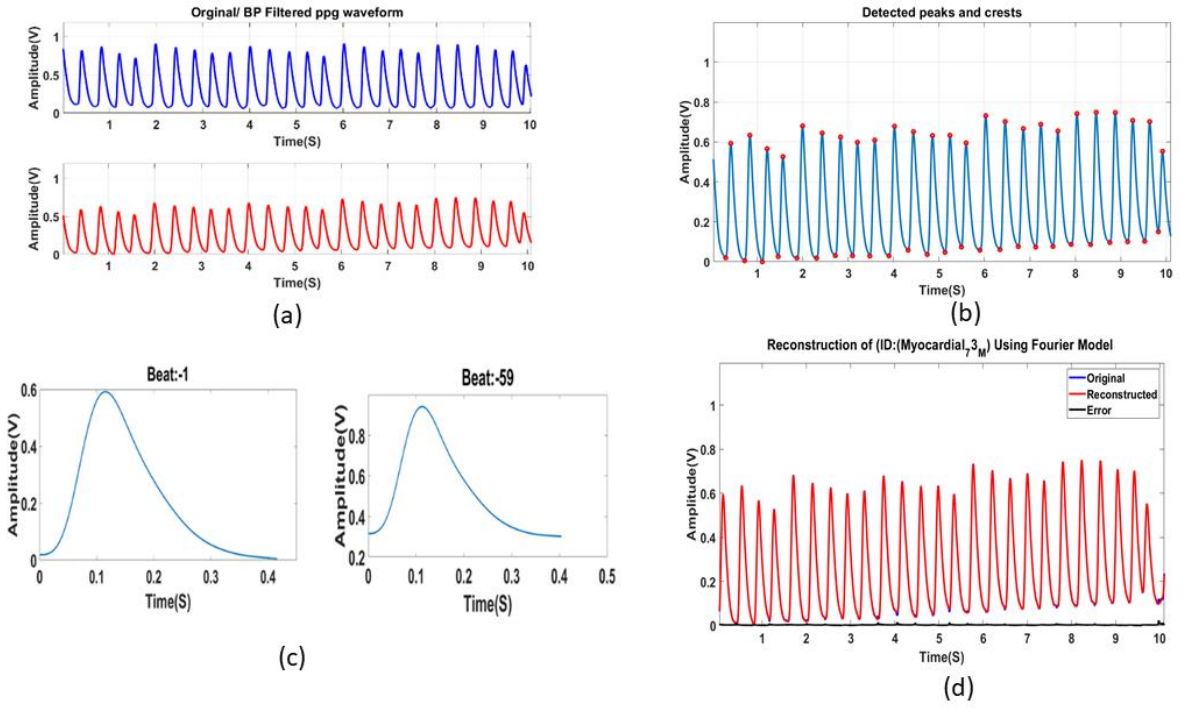

Fig. 4.15. (a) Class 1: Myocardial_(73_M) (a) raw and filtered PPG, (b) peak and crest for 6000 samples (c) Two beats shown (1st, Last), (d)Reconstruction Using Fourier model.

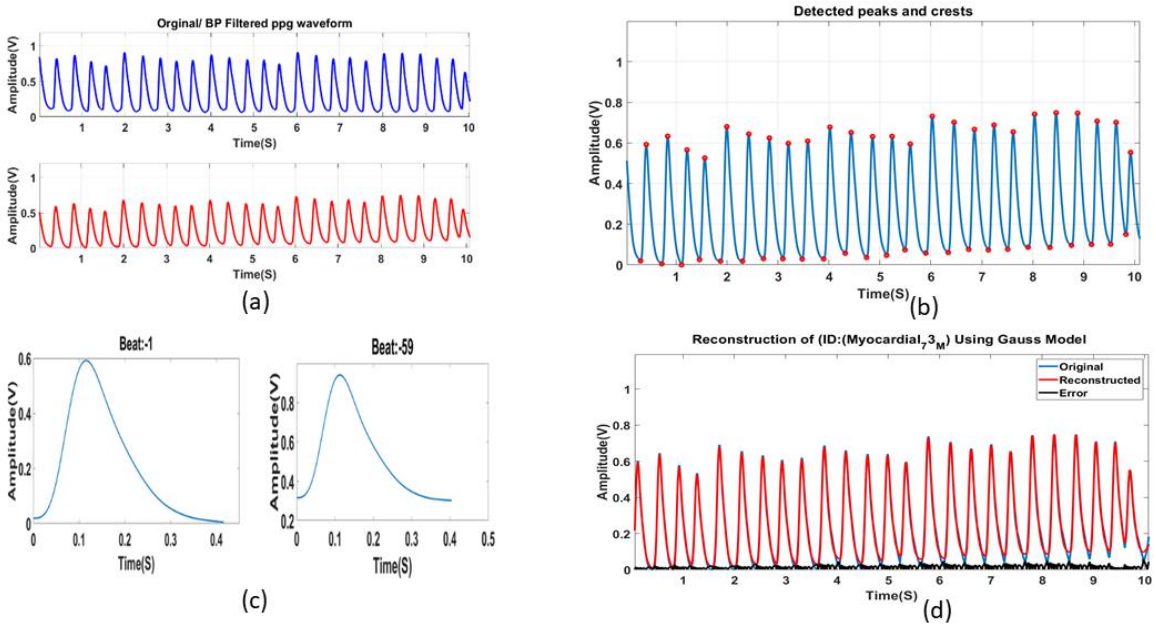

Fig. 4.16. (a) Class 1: Myocardial_(73_M) (a) raw and filtered PPG, (b) peak and crest for 6000 samples (c) Two beats shown (1st, Last), (d) Reconstruction Using Gauss model.

The work is done by transmitting the PPG data of Normal as well as 3 classes of cardiac syndrome patients (taken as case study) to the IoT cloud and the relevant Patient ID data can be accessed or downloaded in emergency by Fourier and Gauss model. The performance of the proposed models is evaluated using the statistical parameters such as RMSE, SNR and PRDN. The CR value signifies the memory space occupancy by both models. Fig. 4.15(a) shows the original and filtered PPG signal followed by the peak-crest detection and beat extraction shown in Fig. 4.15 (b) and Fig. 4.15 (c) respectively. The reconstruction of the original signal is done by Fourier model (FM) as in Fig. 4.15 (d) and Gauss model (GM) as in Fig. 4.16 (d). It's clearly visible from Fig. 4.15 (d) that the performance of FM is significantly better than GM. The Fourier and Gaussian model parameters are demonstrated beat wise in Table 4.12 and Table 4.13 respectively. Table 4.14 clearly illustrates that SNR, RMSE and PRDN performance for FM streets ahead GM. As GM is taken care by 2nd order [175] the performance efficiency is low, in other side increasing the order will accumulate more no of coefficients and acquiring more memory space in cloud. Here we have to go for a trade-off between accuracy and memory space. Table 4.15 shows a comparison of our work with the related work. The work[125-183-173] , does not show the different class of cardiac syndrome, whereas work [121] though shows cardiac syndrome, but without particular class of cardiac disease.

Table 4.12

Beat wise Fourier model parameters of PPG signal.

lass 1 : Myocardial_(73_M)											
Beat No	C_0	A_1	B_1	A_2	B_2	A_3	B_3	A_4	B_4	ω_0	N
1	0.212	-0.145	0.212	-0.081	-0.053	0.010	-0.038	0.014	-0.0003	15.681	105
----	----	----	----	----	----	----	----	----	----	----	----
59	0.527	-0.156	0.233	-0.090	-0.054	0.011	-0.042	0.014	-0.0001	16.045	102
Class 2: Ischemic_(53_M)											
1	0.449	-0.100	0.204	-0.076	-0.062	0.025	-0.033	0.0142	0.0033	16.357	85
----	----	----	----	----	----	----	----	----	----	----	----
70	0.290	-0.265	0.282	-0.050	-0.143	0.048	-0.010	0.0047	0.0118	18.184	83
Class 3: Hypertension_(53_F)											
1	1.978	-0.675	-0.042	0.27	0.034	-0.075	-0.0113	-0.0005	-0.0095	18.860	73
----	----	----	----	----	----	----	----	----	----	----	----
72	1.160	0.606	-0.484	0.005	0.347	0.049	-0.0883	-0.0057	0.0109	17.583	89
Class 4: Normal_(55_F)											
1	-0.73	0.9526	3.3988	1.6759	-0.393	-0.975	-0.9754	-0.7133	0.1813	4.8657	159
----	----	----	----	----	----	----	----	----	----	----	----
39	1.667	-0.5988	0.9337	-0.4267	-0.252	0.036	-0.0184	-0.0209	-0.0376	10.227	141

Table 4.13

Beat wise Gauss model parameters of PPG signal.

Class 1 : Myocardial_(73_M)							
Beat No.	a_1	μ_1	σ_1	a_2	μ_2	σ_2	N
1	0.42757	0.10853	0.051885	0.27893	0.17549	0.092012	105
----	----	----	----	----	----	----	----
59	0.56105	0.1165	0.06923	0.41698	0.21208	0.27457	102
Class 2: Ischemic_(53_M)							
1	0.45771	0.11523	0.056457	0.37212	0.16382	0.29038	85
----	----	----	----	----	----	----	----
70	0.60853	0.11073	0.048425	0.36247	0.15344	0.073179	83
Class 3: Hypertension_(53_F)							
1	1.4258	0.16988	0.055737	1.5855	0.16858	0.6849	73
----	----	----	----	----	----	----	----
72	1.6454	0.22101	0.056255	0.76767	0.17716	0.33755	89
Class 4: Normal_(55_F)							
1	2.6911	0.18637	0.11873	0.73919	0.43656	0.18736	159
----	----	----	----	----	----	----	----
39	2.3578	0.18197	0.11195	1.1676	0.35165	0.35248	141

Table 4.14
Reconstruction performance with Gaussian and Fourier modeling

Class and Patient ID	**Fourier Model**				**Gaussian Model**			
	SNR	RMSE	PRDN	CR	SNR	RMSE	PRDN	CR
Cla ss 1: Myocardial_(73_M)	42.2941	0.0032	0.0203	8.3277	25.1971	0.0231	1.0329	12.4915
Class 2: Ischemic_(53_M)	46.0429	0.0022	0.0089	7.1190	28.8262	0.0160	0.4685	10.6786
Class 3: Hypertension_(53_F)	50.9691	0.0050	0.0050	6.9132	29.0922	0.0617	0.7691	10.3698
Class 4: Normal_(55_F)	38.9380	0.0191	0.0474	5.7308	25.8545	0.0862	0.9635	8.0962

Table 4.15
Performance comparison. With state-of-art methods.

Compression method	**Dataset illustration**			**Distortion Metrics**			**Compression Metrics**
	PPG recordings	Sampling frequency (Hz)	Bit-size	SNR	RMSE	PRDN	CR
[125]	MIMIC-II	125	10	-	-	9.19	2.84
	In-House	125	10	-	-	7.57	3.84
[183]	MIMIC-II	125	10	-	-	0.214	1.601
	In-House	125	10	-	-	0.187	2.223
[173]	MIMICDB	125-500	12-16		0.06	0.33	30.27
[121]	In-House	60	10	-	-	4.15 to 6.09 (Normal) 3.84 to 6.81(CV D)	13.28(Normal) 13.31(CVD)
Proposed (Fourier Model)	In-House	250	10	42.29 to 50.96 (CVD)	0.0022 to 0050(CVD)	0.005 to 0.0203 (CVD)	6.9132 to 8.3277(CVD)
				38.9380 (Normal)	0.0191 (Normal)	0.0474 (Normal)	5.7308 (Normal)
Proposed (Gauss Model)	In-House	250	10	25.19 to 29.09 (CVD)	0.016 to 0.0617 (CVD)	0.4685 to 1.0329 (CVD)	10.3698 to 12.4915(CVD)
				25.8545 (Normal)	0.0862 (Normal)	0.9635 (Normal)	8.0962 (Normal)

4.5.3.2 Discussion on FM and GM based compression

The notion for a remote PPG monitoring system with IoT assistance is illustrated in the current study. The suggested design can be put into practice for remote patient health monitoring with myocardial infarction[177-178], ischemic heart disease [179], hypertension[180], heart failure [179], which could make it easier to measure PPG, blood pressure, heart rate [181,182] and oxygen saturation levels for clinical diagnosis. As a result, PPG waveform data were sent to the IoT cloud using fast Wi-Fi networks with extensive coverage. Users could access the IoT cloud to store the PPG model parameters with the least amount of storage space and use it for normal or cardiovascular disease diagnosis and prognostics. PPG signals can be added to the proposed system to increase its functionality and enable the assessment of heart rate variability parameters as a function of model parameters. Instead of storing the PPG data continuously, which needs a large memory storage device, the model parameters over each cycle or beat of the PPG signal are stored. Thus, PPG waveform data are compressed using Fourier and Gaussian modelling method. The performance of data compression is accessed after reconstruction PPG waveform at the receiving end of the IoT cloud server station.

The dependability of the wireless communication route is essential to IoT cloud services. SNR, RMSE, PRD, and CR are just a few of the metrics functions that are used to evaluate compression performance (Compression ratio). The Compression Ratio (CR) is a metric for signal compression that takes into account data compactness and encoding techniques. It gauges the algorithm's effectiveness at saving storage space but does not offer information on the quality of the compressed signal. PRDN, RMSE, SNR are the metric for assessing inaccuracy or variation between the original. It appears from the result (Table 4.14) that the CR values are greater in case of data compression by Gaussian method than by Fourier method as the number of model parameters in gauss method (i.e. 8) is less than that by Fourier method (i.e. 12). But with respect to accuracy (Table 4.14) Fourier method is much superior. So, there is a trade-off between accuracy and memory space occupancy in drop box. Table 4.14 shows clearly that CR value is for CVD patients is higher than that of normal persons.

Suppose, by taking the ID: Class 1 Myocardial_(73_M) case has 5896 samples and 59 beats in total. In case of, GM having 8 model parameters for 59 beats require 472 samples. Hence CR is found to be 5896/472 i.e. 12.4915. Hence to save memory space in IoT cloud, we are storing 472 samples instead of 5896 samples. Likewise, FM having 12 model parameters (as shown in the Table 4.12), for 59 beats require 708 samples. Calculated CR found to be 5896/708 i.e. 8.3277. Simply, data is compressed 8.3277 times and occupies less space/memory in IoT cloud**.**

4.6 Summary

This chapter proposes a data reduction methodology for ECG and PPG signals based on Gaussian modeling to increase storage efficiency and telemonitoring for cardiac patients. The method preserves good compression performance while successfully reducing intrabeat and interbeat redundancy. The method's stability and effectiveness across various signal types such as four CVD classes (RBBB, hypertension, arrhythmia, DCM) and one normal class are confirmed by evaluations using the MIMIC-III and MIT-BIH databases and actual hospital data. The results show that because of their simpler structure, PPG signals have a higher compression efficiency than ECG signals.

Additionally, an IoT-assisted remote PPG monitoring system is proposed for tracking heart conditions such as myocardial infarction, ischemic heart disease, and hypertension. PPG waveform data is compressed using Fourier and Gaussian modeling before being transmitted to the IoT cloud via fast Wi-Fi networks. The Gaussian method achieves higher compression ratios (CR), requiring fewer model parameters than the Fourier method, making it ideal for reducing memory usage in cloud storage. However, the Fourier method offers superior accuracy, highlighting a trade-off between accuracy and storage efficiency. Future work aims to optimize compression techniques by incorporating dimensionality reduction methods (e.g., PCA) and regularization strategies to enhance computational efficiency and prevent overfitting.

So, depending upon the complexity of the CVD morphological patterns the order of Gauss functions and Fourier functions can be considered for the compression and decompression process.

Chapter 5

Prediction of ECG Fiducial Parameters from PPG for CVD Diagnosis

5.1 Introduction

Across the entire world, cardiovascular diseases (CVDs) are the main cause of death. In 2019, 32% of all fatalities worldwide—including all ages, genders, and nationalities—were predicted to have been caused by CVDs, killing approximately 17.9 million people [139] worldwide as per the World Health Organization (WHO) report. The unavailability of enough health care systems and the work stress and casual lifestyle hinder routine health check-ups and precise diagnoses. A key issue has been the requirement for a prompt, affordable and precise diagnosis, treatment and cure at the early stage at a fair price to enhance human health.

Electrocardiography (ECG) and photoplethysmography (PPG) are the two types of sensors to provide a different methodology-based window for the perception and estimation of the cardiac cycle. These ultimately include continuous blood pressure monitoring, and monitoring of heart rhythm [184]. ECG is the direct continuous recording method having salient features with major 5 peak points (P, Q, R, S, T) and the intervals correspond to the different electrical activity of the heart. Placing 12-lead ECG electrodes in various skin locations including the chest [185] for prolonged duration, could lead to user inconvenience and discomfort, which makes the recording process cumbersome. However, brief cardiac monitoring exposes patients to the risk of missing important asymptomatic, infrequent and irregular signals. Meanwhile, PPG is an indirect non-invasive optical recording method to measure changes in blood volume in tissue vessels to assess various heart performance measures. According to Beer-Lambert's law, PPG signals are captured by a photoresistor after an IR light transmitter is illuminated [186]. This low-cost, tiny, wearable, skin-compatible continuous cardiovascular status monitoring method has flourished as an alternative to ECG.

ECG and PPG are intrinsically highly physiologically correlated as they give two different visualization windows for the same cardiac activity as shown in Fig.1 with pulse transit time

(PTT) [187]. Electrical impulses are normally produced by the natural pacemaker known as the sinoatrial node (SA node) and are conducted throughout the heart to start each heartbeat known as the cardiac cycle. The previous studies explored, that heart rate variability assessed by PPG signals and ECG signals have a strong correlation [188]. Prominent dicrotic notch person's RR interval, PR, QRS, and QT interval can be better extracted from some fiducial features of PPG [131]. An excellent performance [132] was achieved by BIDMC datasets for a strong correlation of ECG with PPG (the RR interval of ECG corresponds to a peak-peak interval of PPG, the P-peak maps to the onset of PPG, PR interval refers to the systolic peak of PPG, RP interval correlates to the diastolic phase of PPG, the onset of PPG is lagging behind 600-700 ms of P-peak and the systolic peak of PPG is lagging behind 600-700 ms of R-peak).

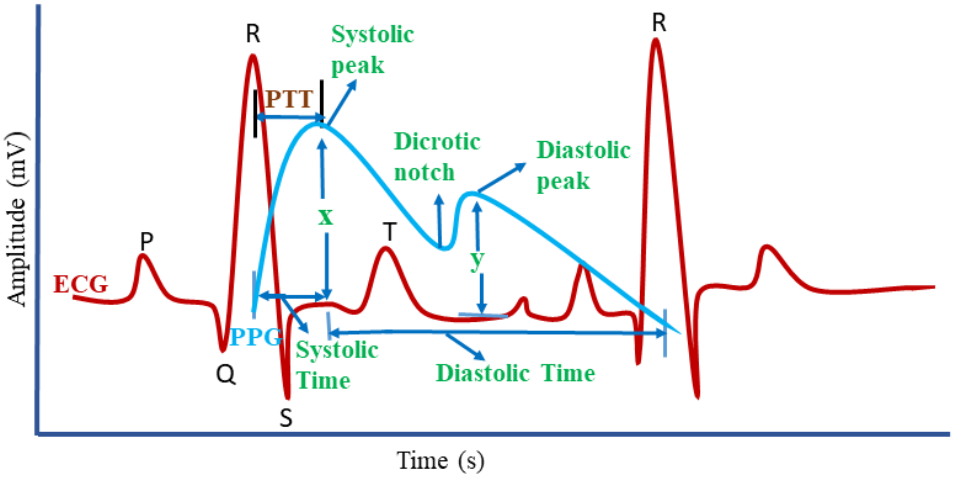

Fig. 5.1. A typical ECG and PPG signal waveform with pulse transit time (PTT).

This chapter discusses a Gaussian process regression (GPR)-based model to predict the ECG fiducial parameters from PPG signals. Contrary to earlier research, it will just forecast the fiducial points rather than creating the ECG waveform. The motivation behind this proposed work is that fiducial parameters have fewer data sizes in comparison to the entire ECG waveform [168], by which not only reduces the storage overhead but also is efficient in the use of transmission bandwidth in real-time telemonitoring application over wire/ wireless communication network may be in Internet of Things (IoT) platform. Moreover, reduces processing time and energy consumption to work with remote health care monitoring systems and is clinically relevant for automated analysis. The crucial aspect is that fiducial parameters are quite straightforward and easily comprehensible also insensitive to noise and baseline wander. Major discriminating events and the intervals of ECG fiducial parameters in terms of signal amplitude and time instances will give sufficient information about the CVD case and

help in identifying cardiovascular abnormalities in the early stage. In comparison to state-of-the-art technologies [134,137,138] that require enormous data sizes, the proposed work incorporates fewer data samples. Hence, the suggested work aims to mitigate the cost and easy diagnosis by doctors with the use of low cost PPG. Corresponding to the type (RBBB, HYPER, ARYTH-ATRFAB, DCM, CHB) of CVD the precautionary major can be carried out to save the life at an early stage. This technology might make it possible for continuous, long-term cardiac monitoring that is more user-friendly, affordable, and can support and promote public health, especially for the essentially needy people. Also this chapter highlights the prediction of PPG fiducial parameters from PPG signal by using Neural network for blood pressure patients.

5.2 Necessity of prediction of ECG fiducial parameters

The technique of estimating or predicting future events using past data, trends, and patterns is known as prediction. In order to evaluate data and create defensible predictions about the future, it makes use of statistical methods, machine learning algorithms, and mathematical models. These Predictive models can be used in medical applications to examine physiological signals and detect potential health risk factors before they become life-threatening. So, this prediction of ECG and PPG fiducial parameters is required for the following reasons.

- *Early CVD Risk Detection*: By anticipating anomalies in PPG and ECG signals, medical professionals can identify myocardial infarction, arrhythmias, ischemic heart disease, and hypertension early on and take appropriateaction.

- *Continuous and Remote Monitoring*: Patients can be continually monitored in real-time by combining predictive models with Internet of Things-based health monitoring devices. This eliminates the need for frequent hospital visits and enhances access to healthcare in remote places.
- *Automated Diagnosis and Decision Support*: AI-powered prediction models help physicians by examining fiducial parameters, spotting anomalous trends, and making potential diagnosis recommendations. This lowers human error and increases diagnostic precision.

- *Customized Treatment and Risk Assessment*: Using a patient's past PPG and ECG data, predictive models assist in determining their risk profile, allowing for tailored treatment regimens that reduce the chance of serious cardiac events.
- *Better Healthcare Efficiency*: Predictive care improves preventive care, optimizes resource allocation, and lowers hospital admissions, all of which lead to better patient outcomes and cheaper healthcare costs.

5.3 Different prediction models

5.3.1 Hidden Markov model (HMM)

Short-term memory was introduced with the introduction of hidden Markov models (HMMs) [189] . Based on the Markov property, which states that the probability of changing to a future state depends only on the current state and not on past states, HMMs are probabilistic models that explain observable events that depend on unobservable internal elements.

5.3.2 Empirical Mode Decomposition (EMD)

It is a signal processing method called Empirical Mode Decomposition (EMD) that breaks down a complicated signal, like PPG, into a collection of intrinsic mode functions (IMFs) [131]. Slow-frequency changes are captured by low-frequency IMFs.Rapid frequency changes are captured by high-frequency IMFs. PPG signals can be converted into ECG fiducial parameters, and it is frequently used to reveal hidden patterns in biological signals. Its good aspects include nonlinear and adaptive decomposition. However, it is less suitable for real-time applications because to its drawbacks, which include mode mixing, noise sensitivity, lengthy computation times, and lack of stability. Accuracy can be increased by using hybrid techniques that include statistical filtering, deep learning, and wavelet transforms.

5.3.3 Deep Learning-Based Methods

PPG-ECG mapping uses Convolutional Neural Networks (CNNs) to identify spatial patterns. PPG and ECG fiducial points show temporal correlations with Recurrent Neural Networks (RNN) and Long Short-Term Memory (LSTM). Graph Neural Networks (GNNs) use graph

data to model PPG-ECG connections. ECG prediction accuracy is quite high, but computational power is extremely high.

5.3.4 Gaussian process regression–based model

Gaussian Process Regression(GPR) is a non-linear regression approach for nonparametric data sets. It is well-fitted on small datasets and measures the uncertainty over prediction. It is a nonparametric kernel-based probabilistic model that employs a finite collection of random variables with a multivariate distribution and is shown in Fig. 5.2. It is equally distributed among each linear combination. Statistical modeling, the study of mapping in higher dimensions, and regression to multiple target values are all applications of Gaussian processes.

Simply this approach can be used to solve challenging issues including high dimension, small sample size, and nonlinearity [190]. The GPR parameters are calculated by parameters decided by the algorithm itself; the user is not required. Additionally, the model may interpret the projected results in terms of probability [191,192] and assess the model's accuracy. As a result, the model has been extensively used in numerous fields.

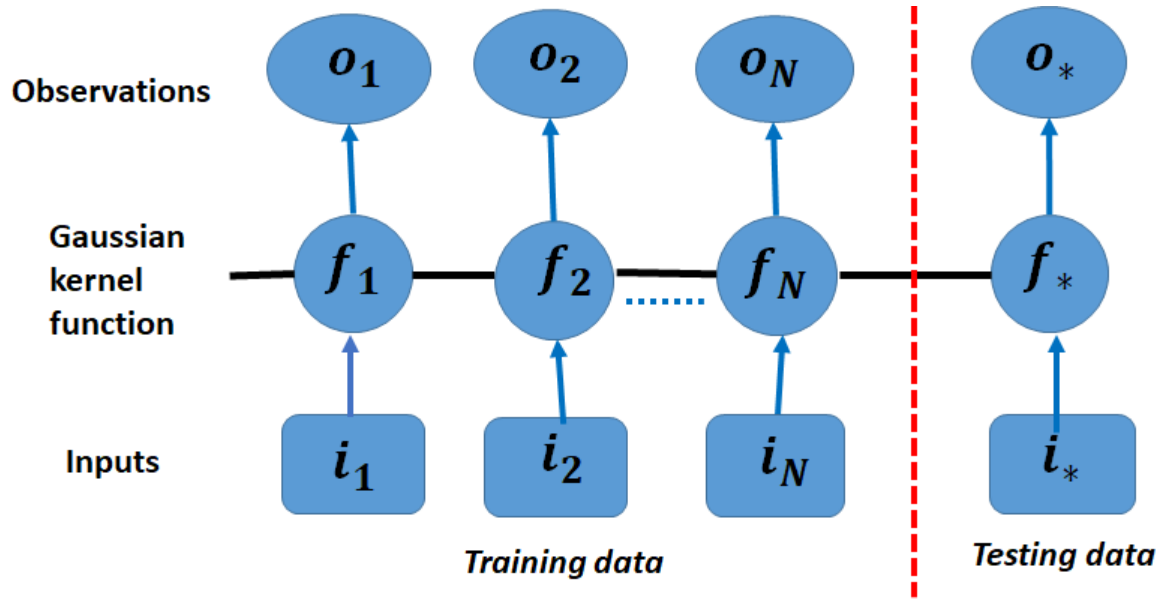

Fig. 5.2. Gaussian process regression-based model.

Suppose, we want to do the regression process of the fiducial dataset: $D_f = \{ i_n , o_n \}_{n=1}^{N}$,

where PPG fiducial as inputs: $I = \{ i_n \}_{n=1}^{N}$ and corresponding ECG fiducial as target: $O = \{ o_n \}_{n=1}^{N}$. N is considered as no of input-output pairs. Where, $i_n \in \mathbb{R}^{\mathcal{F}}$, $o_n \in \mathbb{R}$ and $\mathcal{F}$ is the dimension of the feature vector. Each observation in GPR is thought to be produced by mixing of a latent function $f(i)$ and Gaussian noise as: $o(i_n) = f(i_n) + e_n$, Where, $e \sim \mathbb{N}(0, \sigma^2)$ is the zero-mean Gaussian noise having variance as σ^2.

Limited expressiveness is a problem for the Bayesian linear model. One extremely straightforward solution to this issue is to project the inputs into the feature space and use kernel trick with a set of basis functions. Simply, the linear model is applied in space rather than upon the inputs directly. so, a Gaussian process is used as a basis function.

The mean function and covariance function are all that are needed to fully describe a Gaussian process. Hence for our real process of PPG to ECG prediction, the Gaussian process can be expressed as

$$f(i) \sim \mathbb{G}\left(m(i), k(i, i'; \hbar)\right) \qquad (5.1)$$

Where, $m(i)$ is the mean function, $k(i, i'; \hbar)$ is the arbitrary covariance function. Here are the values of $k(.\ ,.\ ; \hbar)$ not only depends on inputs (i, i') but also the free parameters well known as hyperparameters shown as $\hbar$. The total function values can be written in row matrix form as corresponding to any number of input points n are jointly Gaussian.

$$f = [f_1, f_2, f_3, \ldots\ldots, f_N] \qquad (5.2)$$

Now, for a multivariate Gaussian prior, for (inputs: I, zero mean for simplicity with covariance K_N), the predictive distributor can be written as

$$p(f|I) = N(f|0, K_N) \qquad (5.3)$$

In combination with the regression model, the Gaussian noise assumption yields the Gaussian likelihood and can be expressed as $p(O|f) = N(O|f, \sigma^2 \mathbb{I}_N)$. Here $\mathbb{I}_N$ is the N x N identity matrix and

$$O = [o_1, o_2, o_3, \ldots\ldots, o_N] \qquad (5.4)$$

Maximizing the marginal likelihood (evidence) allows for the estimation of the GPR hyper-parameters by integrating the latent function in a noisy environment given by

$$p(O|I\ ,\hbar) = N(O|0, K_N + \sigma^2 \mathbb{I}_N) \qquad (5.5)$$

The marginal likelihood is maximized using the gradient descent approach. After the estimation of hyper-parameters, the posterior distribution for new test sample data i_* is denoted as

$$p(O_*) = N(O_*|\omega_*\ , {\sigma_*}^2) \qquad (5.6)$$

where $\omega_* = k_{*N}(K_N + \sigma^2\ \mathbb{I})^{-1}\ O$ and ${\sigma_*}^2 = k_{**} - k_{*N}(K_N + \sigma^2\ \mathbb{I})^{-1}\ k_{*N} + \sigma^2$.

Where $[K_{*N}]_j = k(i_*\ , i_j; \hbar)$ and $k_{**} = k(i_*\ , i_*\ ; \hbar)$. Here ω_* and ${\sigma_*}^2$ are the predicted and estimates of its variance respectively. By using a loss function $(o_{true}, o_{guess})$the predictive distribution's decision is taken optimally. Table 5.1 gives the detailed internal structure of the proposed model for all six classes. The learning steps [191] of the GPR model were followed and worked for the prediction of ECG fiducials parameters. The GPR algorithm is illustrated through the Pseudo code 5_1**:** Gaussian procession regression.

Pseudo code 5_1: Gaussian procession regression

Input: N number of Fiducial parameters of PPG $(x1)$ and N number of Fiducial parameters of ECG$(y11)$.

Output: Predicted ECG values : $y21\_pred$.

1. $X = [x1, y11]$
2. $hpartition = cvpartition(size(X, 1), 'Holdout', 0.3)$
3. $trainId = training(hpartition)$
4. $testId = test(hpartition)$
5. $trainData = X(trainId, :)$
6. $testData = X(testId, :)$

7. $x1\_new = trainData(:,1:N)$
8. $y11\_new = trainData(:,N+1:2N)$
9. $for\ L = 1\ to\ N$
10. $y_{old} = trainData(:,N+L)$
11. $sigma0 = sigmaF0 = std(yold)$
12. $gprMdl = fitrgp(x1\_new, yold, 'Basis', 'linear', 'FitMethod', 'exact', \ldots$
$'PredictMethod', 'exact', 'KernelFunction', 'ardsquaredexponential', \ldots$
$'KernelParameters', [sigmaM0; sigmaF0], 'Sigma', sigma0, 'Standardize', 1)$
13. $x2\_new = testData(:,1:N)$
14. $y_{new} = testData(:,N+L)$
15. $y21\_pred = predict(gprMdl, x2\_new)$
16. $end\ for$

Table 5.1

Working model of GPR for all six classes of CVD.

Sl. No.	**Disease Class**	**Kernel Function**	**Basis**	**Equation**	**Hyper parameter**
1.	ARYTH-ATRFAB	Squared Exponential	Linear	$k_{SE}(i,i') = {\sigma_s}^2 \exp[-\frac{(i-i')^T (i-i')}{2l^2}]$	σ_s = scaling parameter l =length parameter
2.	RBBB				
3.	NORMAL				
4.	CHB	Squared Exponential	Constant		
5.	DCM				
6.	HYPER	Exponential	Constant	$k_E(i,i') = {\sigma_s}^2 \exp[-\frac{\sqrt{(i-i')^T (i-i')}}{l}]$	

5.4 Performance evaluation indices

To calculate the prediction accuracy some evaluation metrics as described below.

- ***Root mean square error (RMSE) and relative root mean square error (rRMSE)***

The most commonly revealing metric for describing the discrepancies between true and predicted values is predicted by an estimator or model quantified by RMSE and rRMSE. In our case of the GPR model, lower values of RMSE and rRMSE indicate that close correlation between two-time series ECG and the predicted ECG data samples.

- ***Pearson's correlation coefficient (ρ)***

When used with variables that have linear correlations, the Pearson correlation coefficient is a versatile measure of the correlation between those continuously changing variables in statistics. The value range: ρ [+1, -1], where ρ (±1), means the highest degree of concordance and 0 means no concordance.

- ***Coefficient of determination (R^2)***

A statistical model's ability to properly predict an outcome is quantified by the coefficient of determination , which has a range of 0 to 1. In our Gaussian regression model R^2 value nearer to 1 tells that, the more accurate it is in forecasting the ECG fiducial parameters.

- ***Dynamic time warping (DTW) distance***

Dynamic time warping (DTW) is one method used in to assess the degree of resemblance that exists between continuous momentary sequences of events, which may differ in speed. This technique determines the most optimal feasible match between any two series of time events that are specified. Denoted as d and the lesser the value (range from 0 to infinity) more similarity between them.

- ***Scatter plot***

In a Cartesian system, scatter plots are the graphical representation to demonstrate the correlation between two sets of data points. A negative correlation is seen if the arrangement of dots slopes from higher left to lower right.

- ***Bland-Altman plot***

Bland-Altman plots are utilized in biomedical signals for clinical purposes, usually to look for any connections between the differences, between the predicted and the ground truth value. When the difference in the model lies between the lower limit of agreement (LOA) and upper limit of agreement (UOA) we can visualize the data accumulation and correlate the relationship between the true and predicted ECG parameters. The mean difference's 95% Confidence Interval (CI), i.e. ±1.96 demonstrates the size of the systematic discrepancy. A large systematic difference exists if the line of equality is not within the interval.

5.5 Prediction of ECG fiducial parameters from PPG signal using GPR model

The suggested non-invasive cardiac monitoring system is depicted in Fig. 5.3. The main essence of the proposed model is to visualize the ECG fiducial parameters from PPG through the Gaussian process regression-based model predictor for 5 class CVD cases and one normal (NORMAL) class.

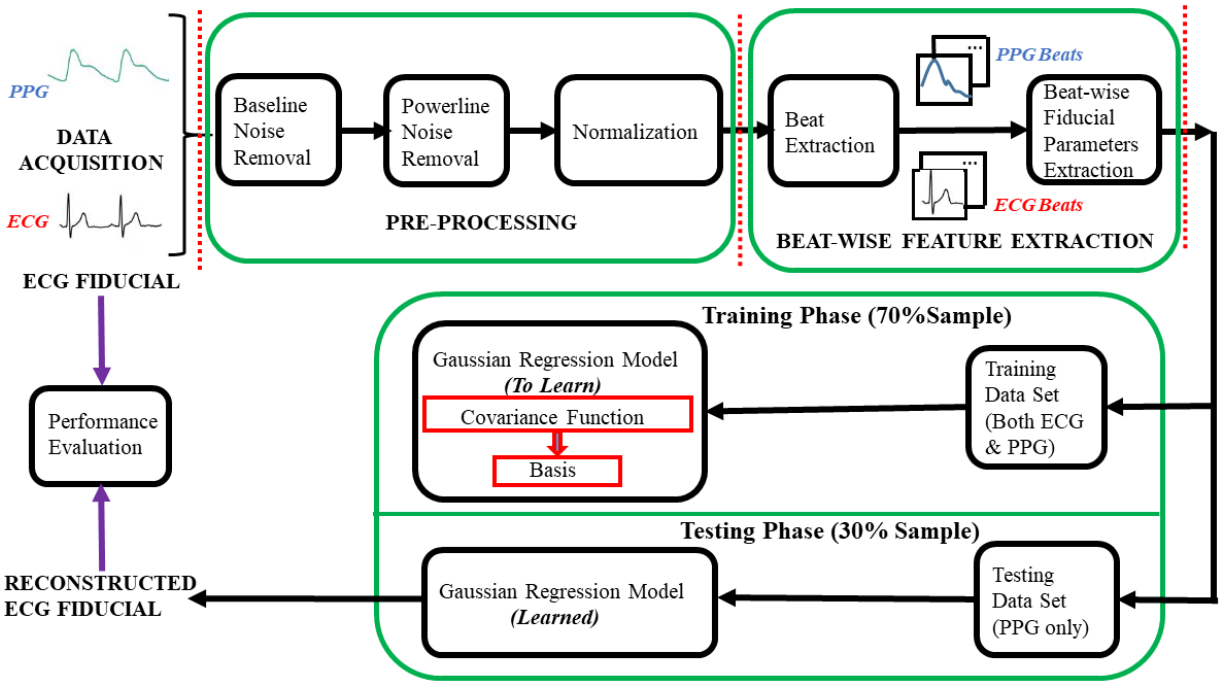

Fig. 5.3. Workflow diagram of the proposed model for ECG fiducial monitoring for analysis of CVD from PPG signal.

5.5.1 ECG/PPG dataset description

Few publicly accessible datasets include both matched paired PPG/ECG signals and the associated CVD diagnosis. MIMIC-III from Physionet is one of them with the inclusion of Lead-II ECG signal in maximum subject ID. Here we have selected the CVD (5 class diseases, such as right bundle branch block (RBBB), hypertension (HYPER), arrhythmia-atrial fibrillation (ARYTH-ATRFAB), dilated cardiomyopathy (DCM), complete heart block (CHB)) and one normal (NORMAL)class data. We have selected the ICD-9-CM codes for various cardiac diseases as RBBB (426.4), Hypertension (402.91), Arrhythmia (427.31), CHB (426.0), and DCM (425.4). The normal class is taken from pneumonia and sepsis diseases from the MIMIC III dataset. We have concentrated on those subjects having only one syndrome. We then collected the subject IDs that matched ECG (Lead II) and PPG signals. Consequently, we have collected the excellent segment by visualizing the waveform plot without any sample data missing. Each class dataset contains 5 patient IDs. Here each ID is of 7500 samples with 1-minute recording time. The sampling frequency of both signals is 125 Hz. Here the dataset contains males, and females with different age groups from 42 years to 88 years. The age distribution of six classes is shown later in Section 3 of this article, for the collected 30 patients (ID) from the MIMIC-III database.

5.5.2 Results and Discussion

The proposed methodology is applied to extract ECG fiducials from the PPG signal. Now the challenging part of the work is to determine whether or not these outcomes, are precise and acceptable. In the context of this query we have gone through many performance evaluation metrics to evaluate, the outcome of our forecast and compare it with true ECG fiducial parameters. Performance evaluation is being carried out by the methods mentioned above. To get consistency throughout the system, we arbitrarily selected 70% of the data for training and the rest 30% of the data for testing. To get the repeatability of the result, we have taken the mean and standard deviation of each result by running it 15 times. The findings and discussions are as follows.

5.5.2.1 Results of ECG prediction

As per the age and disease class, the distribution of the collected 30 patients (ID) from the MIMIC-III database is shown in Fig. 5.4 using bar graphs. The typical ECG characteristic waveforms with the required fiducial parameters of all six classes are shown in Fig. 5.5 after the simulation in MATLAB R2021b environment (shown one ID from each class). The corresponding ECG signature is given in Table 5.2. The composition of data beat's/cycle's fiducial parameters fed to the proposed GPR model is given in Table 5.3.

The performance metrics are first evaluated by RMSE and rRMSE. Table 5.4 clearly shows that the P wave's value is a little higher than Q, R, S, and T. If we consider the RBBB class for P wave RMSE and rRMSE give a result of 0.127 and 0.457 respectively. Again magnitude of the R wave having the highest significance shows a very low rRMSE value compared with other waves for all classes**.** Table 5.4 shows for the CHB class, our proposed method for R wave gives a result of 0.047 for RMSE and 0.094 for rRMSE. Likewise, the T wave shows better performance than the P wave, but worse performance than the QRS complex.

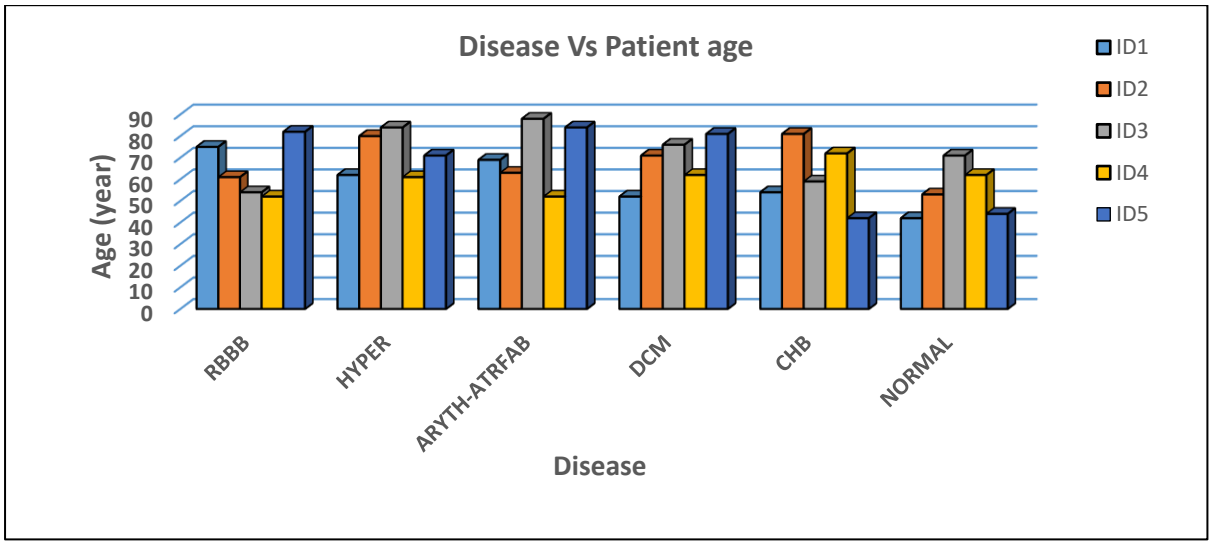

Fig. 5.4. Distribution of disease class and age is shown for all IDs.

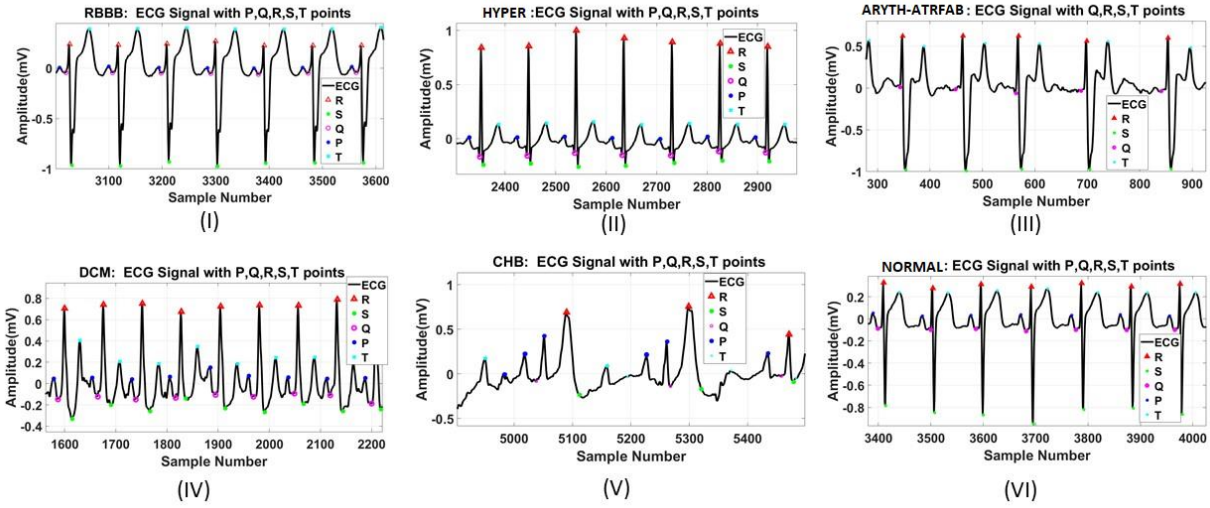

Fig. 5.5. Fiducial parameters (P, Q, R, S, and T) shown for MIMIC III data of all six classes.

Table 5.2

ECG signature for all six classes.

Disease Class	**R Amplitude (mV)**	**P Amplitude (mV)**	**No. of 'P'**	**QRS Duration (ms)**	**R-R Variability**	**HR (bpm)**
RBBB	1.0(±0.8)	0.15(±0.005)	1	120(±20)-S wide	Regular	72(±5)
HYPER	1.4(±0.8)	0.15(±0.005)	1	100(±20)	Regular	72(±5)
ARYTH-ATRFAB	1.0 (±0.5)	-	-	100(±20)	Increases	100(±20)
DCM	1.2(±0.5)	0.15(±0.005)	1	140(±20)	Regular	72(±5)
CHB	1.0(±0.8)	0.2(±0.005)	3(±1)	120(±20)	Decreases	35(±5)
NORMAL	1.2(±0.5)	0.15(±0.005)	1	100(±20)	Regular	72(±5)

Table 5.3
Composition of data cycles fed to GPR model for all six classes.

Disease class	**Number of patients**	**Number of cycles**
RBBB	5	365
HYPER	5	347
ARYTH-ATRFAB (Due to the absence of P waves and HR=100(±20)	5	493
DCM	5	350
CHB (Due to more no of P waves and HR=35(±5))	5	187
NORMAL	5	342
Total	30	2,084

Table 5.4
Performance evaluation of RMSE and rRMSE of six classes with mean and standard deviation in parenthesis. (NA used here abbreviation for Not Applicable)

	RMSE					**rRMSE**				
Class	P	Q	R	S	T	P	Q	R	S	T
RBBB	0.127 (0.029)	0.093 (0.017)	0.034 (0.004)	0.042 (0.008)	0.098 (0.012)	0.457 (0.078)	0.231 (0.054)	0.15 (0.039)	0.17 (0.041)	0.321 (0.058)
HYPER	0.109 (0.014)	0.035 (0.002)	0.033 (0.003)	0.13 (0.022)	0.082 (0.008)	0.535 (0.05)	0.351 (0.032)	0.148 (0.022)	0.306 (0.045)	0.443 (0.061)
ARYTH - ATRFA	NA	0.124 (0.019)	0.066 (0.007)	0.188 (0.028)	0.137 (0.020)	NA	0.848 (0.159)	0.164 (0.025)	0.324 (0.068)	0.656 (0.151)
DCM	0.229 (0.036)	0.166 (0.02)	0.135 (0.01)	0.209 (0.021)	0.22 (0.046)	0.588 (0.087)	0.339 (0.093)	0.314 (0.043)	0.370 (0.062)	0.578 (0.061)
CHB	0.232 (0.026)	0.061 (0.005)	0.047 (0.007)	0.096 (0.011)	0.104 (0.009)	0.665 (0.018)	0.589 (0.058)	0.094 (0.014)	0.215 (0.023)	0.578 (0.061)
NORMAL	0.060 (0.010)	0.032 (0.007)	0.025 (0.009)	0.053 (0.012)	0.057 (0.001)	0.31 (0.076)	0.281 (0.068)	0.167 (0.021)	0.172 (0.018)	0.182 (0.021)

Table 5.5

Performance evaluation of Pearson's correlation coefficient of six classes with mean and standard deviation in parenthesis. (NA used here abbreviation for Not Applicable)

	PEARSON (ρ)					**R^2**				
	P	Q	R	S	T	P	Q	R	S	T
RBBB	0.730 (0.080)	0.999 (0.003)	0.998 (0.003)	0.999 (0.003)	0.981 (0.007)	0.898 (0.035)	0.980 (0.032)	0.991 (0.003)	0.991 (0.003)	0.914 (0.053)
HYPER	0.964 (0.031)	0.979 (0.006)	0.992 (0.001)	0.992 (0.001)	0.984 (0.001)	0.964 (0.017)	0.984 (0.001)	0.984 (0.001)	0.984 (0.002)	0.979 (0.009)
ARYTH-ATRFAB	NA	0.983 (0.005)	0.984 (0.004)	0.983 (0.005)	0.973 (0.005)	NA	0.965 (0.01)	0.966 (0.009)	0.965 (0.009)	0.965 (0.01)
DCM	0.767 (0.045)	0.965 (0.012)	0.964 (0.013)	0.965 (0.012)	0.868 (0.081)	0.923 (0.023)	0.928 (0.024)	0.927 (0.025)	0.927 (0.026)	0.928 (0.023)
CHB	0.700 (0.050)	0.996 (0.001)	0.996 (0.001)	0.996 (0.001)	0.757 (0.036)	0.901 (0.028)	0.995 (0.001)	0.995 (0.001)	0.996 (0.002)	0.942 (0.029)
NORMAL	0.983 (0.003)	0.998 (0.001)	0.998 (0.001)	0.998 (0.001)	0.995 (0.001)	0.944 (0.062)	0.998 (0.001)	0.998 (0.001)	0.998 (0.001)	0.971 (0.030)

It is visible from Table 5.5 that the Person correlation coefficient is excellent in the normal class as compared to CVD classes which corresponds to all fiducial parameters, Q, R, and S fiducial parameters are very much close to 0.99 revealing that the highest degree of concordance of ECG fiducial parameter extracted from PPG signals and the true ECG signal. Whereas ρ values on P for all classes are from 0.7 to 0.98(for normal) and on T from 0.75 to 0.99(for normal) respectively. It has been observed that CVD classes (e.g., dilated cardiomyopathy (DCM)) ECG fiducial parameters show more variance in their morphological properties than non-CVD, exhibiting larger RMSE or lower Pearson correlation. Again morphological characteristics of all 5 CVD classes we have taken in the work are different

from each other in the form of the diversity of data pattern with the inclusion of ectopic beats and arrhythmia occurrences leading to exhibit larger RMSE or lower Pearson correlation. The variation in the values of RMSE and Pearson coefficients for a CVD i.e., DCM and a non-CVD case are illustrated in Fig. 5.6.

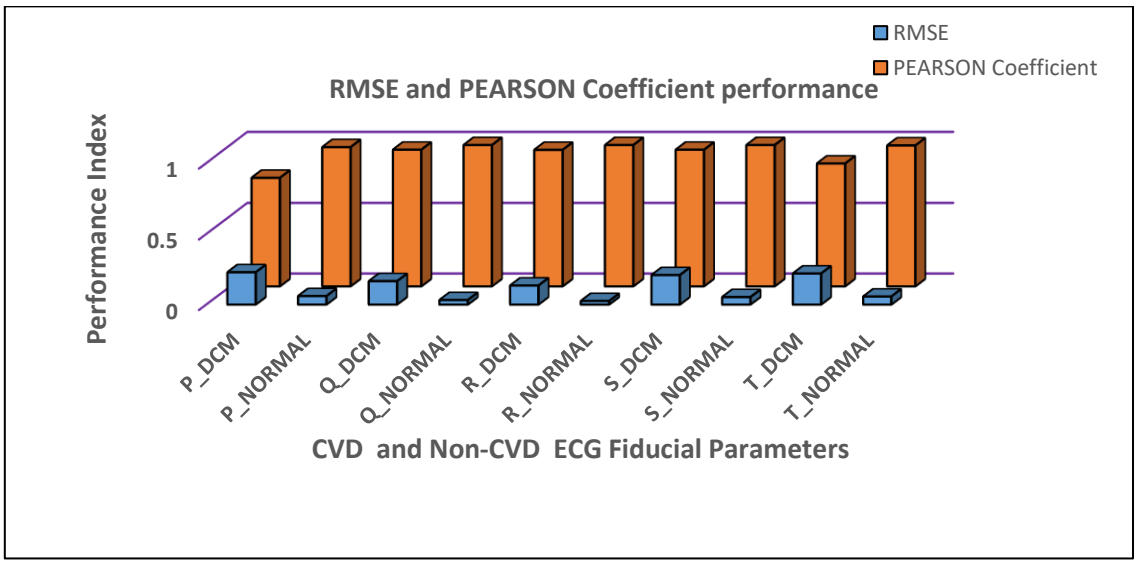

Fig. 5.6. Performance evaluation representation for CVD and non-CVD cases in terms of RMSE and Pearson coefficient.

Moreover, the accuracy of the Gaussian regression predictor model is evaluated by the coefficient of determination $R^{2.}$ Our model predicts the ECG fiducial parameters from the corresponding PPG signal are 0.91 to 0.99 for Q, R, S, and T waves for all 5 CVD classes and 0.97 to 0.99 for non-CVD classes. Likewise, the p wave gives R^2 value of 0.89 to 0.96 for 5 CVD classes and 0.94 for non-CVD classes as shown in Table 5.5.

Table 5.6

Performance evaluation of Dynamic time warping (DTW) distance (d) of six classes with mean and standard deviation in parenthesis. (NA used here abbreviation for Not Applicable)

	***d* (mV)**				
Class	P	Q	R	S	T
RBBB	1.692 (0.223)	1.222 (0.163)	3.475 (0.468)	4.671 (1.052)	3.169 (0.577)
HYPER	1.429 (0.152)	1.853 (0.196)	1.395 (0.136)	1.373 (0.178)	2.467 (0.254)
ARYTH-ATRFAB	NA	2.427 (0.309)	4.349 (0.55)	3.474 (0.468)	4.153 (0.659)
DCM	1.998 (0.329)	3.501 (0.359)	3.475 (0.468)	3.524 (0.302)	2.427 (0.309)
CHB	2.149 (0.341)	2.22 (0.219)	2.833 (0.279)	3.071 (0.313)	3.664 (0.416)
NORMAL	5.34 (0.526)	6.316 (0.561)	4.682 (0.289)	5.039 (0.621)	4.243 (0.705)

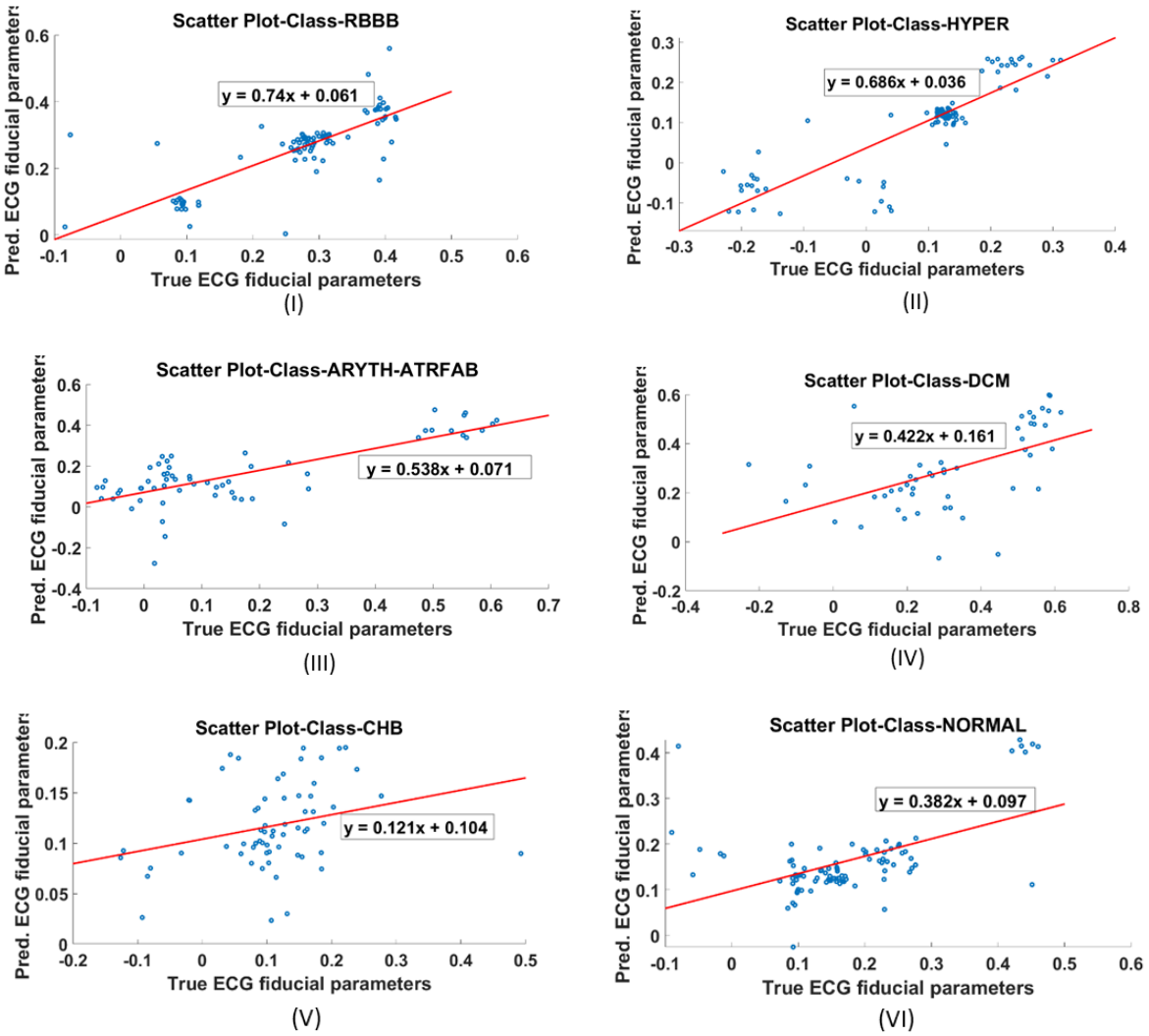

Fig. 5.7. Scatter plot of all classes.

We have included an efficient signature similarity metric, the DTW distance (d), to more accurately assess how similar the two-time series signals are. Clearly shown in Table 5.6, the optimal warping path between the ECG fiducial parameter extracted from PPG signals and the true ECG fiducial parameter, is inferior in the non-CVD class in comparison to CVD classes. Normal class for P wave gives d = 5.34 mV, whereas DCM class d=1.99 mV**.**

The scatter plots between the true and predicted ECG fiducial parameters from PPG for all six classes are displayed in Fig. 5.7. Additionally, we determined the regression line to observe the correctness of predicted results.

To examine the consistency between the ECG prediction results and true ECG fiducial values,

we have also employed the Bland-Altman plot, typically used for clinical measurement. The mean difference is zero in all classes with limits of agreement shown in terms of standard deviation (±SD) in Fig. 5.8. The majority of the result discrepancies in the proposed methodology can be seen to lay between these boundary lines. We can easily see how much our ECG fiducial prediction result deviates from the true ECG fiducial by utilizing just this plot.

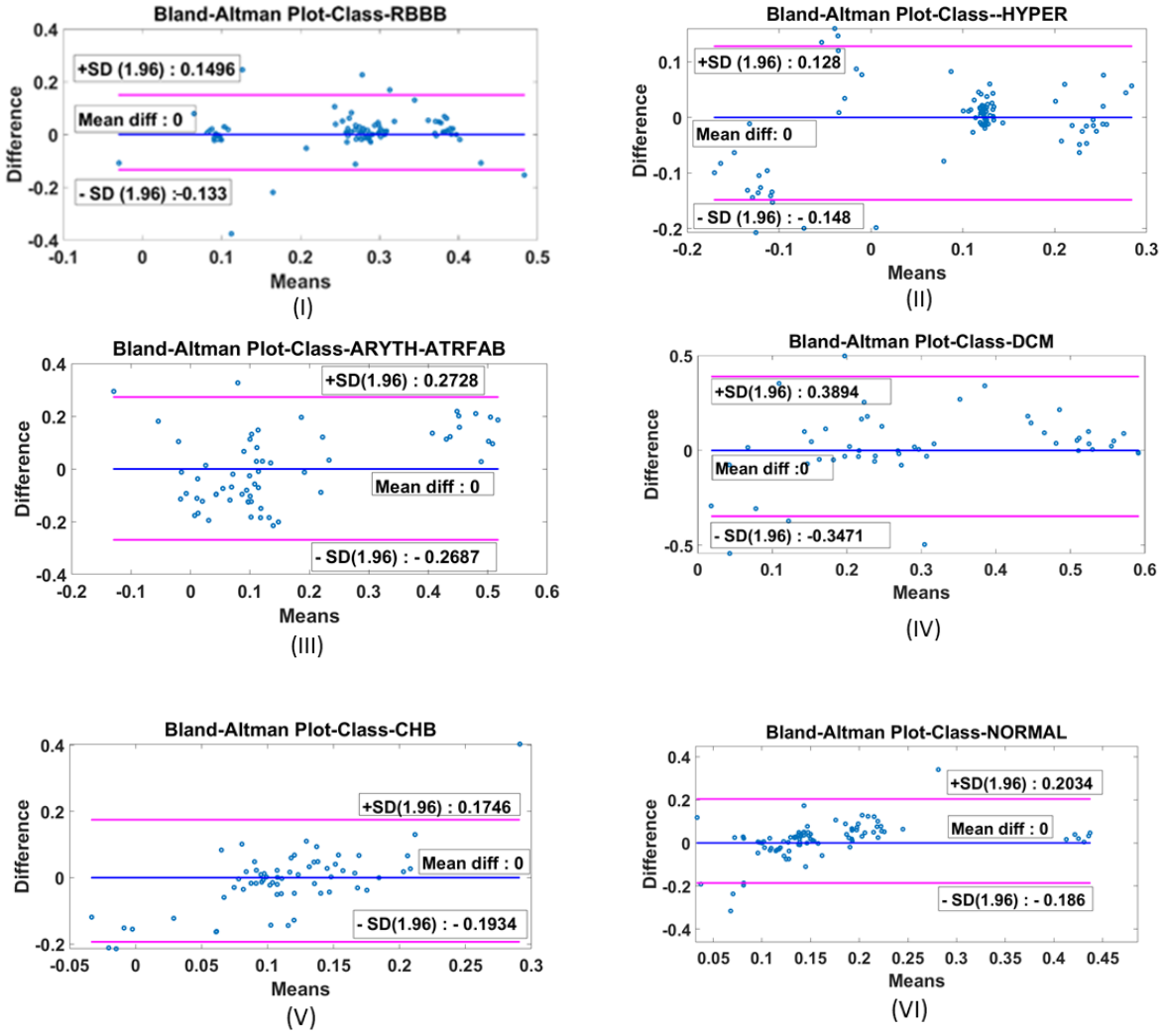

Fig. 5.8. Bland -Altman plot of all classes.

5.5.2.2 Discussion of ECG prediction

The comparison of the proposed GPR-based method with existing state-of-the-art methodologies is given in Table 5.7. The primary benefit of our study is for concentration on fiducial parameters rather than the complete ECG waveform to reduce data size, memory

storage, processing time, energy consumption, and transmission bandwidth in real-time tele-monitoring/remote healthcare monitoring applications that may be in the IoT platform. Regarding Table 4.4 explanation, possibly for the P wave's amplitude, which is considerably less than that of the QRS and T waves and by which, the P wave is more susceptible to noise and has a high RMSE and rRMSE. As a class CHB, with the presence of more no of P, leading to the highest value for rRMSE among all six classes. Statistics of Table 4.4 show that overall non-CVD classes perform better concerning RMSE and rRMSE than CVD classes because non-CVD class ECG fiducial parameters have less variation in their morphological characteristics[134].

Again the results of Table 5.5 guarantee a high value of association or correlation because of high linearity and a continuous variable of true and predicted ECG fiducial parameters. As per [134] the group model gives inferior performance to subject–specific model. The performance excellence of the GPR model proves that with a group model(taking 5 different ID data in one class) in our proposed model ρ value gives 0.88 to 0.99, whereas the subject-specific model [137] gives the value of 0.904 by using BiLSTM.

As R^2 determination has better interpretability and is more accurate and informative [193] in prediction analysis we cannot leave it. Because of the small amplitude and more susceptibility to noise P wave gives a miserable performance concerning Q, R, S, and T fiducial points. Another cause is the diversity of data, which included ectopic beats and arrhythmia occurrences. This isn't a topic of discussion for the ARYTH-ATRFAB class because of the absence of the P wave.

Considering the R wave for all classes result shows, that the lowest d = 1.39 (for HYPER class) means the best path for warping infers that the reconstructed ECG matched the reference ECG after a minimal degree of warping. The excellent performance of the CVD class may be for irregular patterns from the normal class reduces the wrapping distance of the concerned two fiducial parameters.

The best-fitted line equation in the scatterplot is individually shown for all six classes in Fig. 5.7. It is visible that true and predicted values are very close and clustered around the best-fitted line. RBBB class reports best among all with a slope value of nearly 1 and intercept value

of nearly 0 due to its morphological characteristic.

Table 5.7

Comparison of the proposed GPR-based model with the existing state-of-the-art methodologies. (NR used here abbreviation for Not Reported)

Year	Methodology	Method of Segmentation	Database Used		Performance Indices				
					$RMSE$	$rRMSE$	ρ	R^2	d
	Proposed work (Gaussian process regression predictor)	Beat	MIMIC III	RBBB	0.074	0.325	0.941	0.954	2.845
				HYPER	0.077	0.356	0.982	0.979	**1.703**
				ARYTH-ATRFAB	0.128	0.498	0.980	0.965	3.600
				DCM	0.191	0.437	0.905	0.926	2.98
				CHB	0.108	0.428	0.889	0.965	2.787
				NORMAL	**0.041**	**0.222**	**0.994**	**0.981**	5.124
2021	DCT[134]	Beat	TBME-RR		NR	0.165	0.984	NR	NR
			MIMIC III		NR	0.324	0.940	NR	NR
			Self-collected-UMD Data		NR	0.426	0.904	NR	NR
2021	CardioGAN [136]	-	BIDMC,CAPNO, DALIA,WESAD		0.364	NR	NR	NR	NR
2022	Bidirectional long short-term memory (BiLSTM) [137]	Seconds	MIMIC III		0.059	NR	0.904	NR	2.085
2020	XDJDL model [138]	Beat	MIMIC III		NR	0.39	0.880	NR	NR

5.6 Prediction of Fiducial Parameter of PPG Signal

Because of tremendous development in nanotechnology advancement in miniature device, low energy consumption, high sensitivity, mobile, and tremendous computing power fostered an exponential increase growth of interest of wearable technology. Now wearable bio-sensor [194] based systems are the emerging trend and its application covers from cardiovascular monitoring to military, battle, and patient monitoring to many more. Photoplethysmography (PPG) is a non-invasive, vivo, optical technique to detect disorders and diseases related to the cardiovascular system to measure and monitor the physiological parameters such as blood pressure, Oxygen saturation (SpO2), heart rate (beat), and respiration in the blood.

The proposal is to put the sensor i.e. IR transmitter(photodiode) which emits the light pulse periodically into the skin of finger tip, where some may be absorbed by tissue, some scattered and some reflected (Reflectance mode) to the photodetector (typically phototransistor). The absorption intensity utilizes Beer-Lambert's law ,which illustrates when the contraction of heart occurs blood comes out and enters into the blood vessel(artery) in accordance to the blood pressure. Haemoglobin (Hb) absorbs more light, so less light reflects and ultimately resistance of PD (photo resistor) increases. The PPG signal not only contains AC, DC components but also some noise components due to motion artifacts. AC component caused by arterial blood in correspondence to every heart beat. PPG waveform has 3 major fiducial components . Namely: Systolic part, Diastolic part and Dicrotic notch. These 3 parts are very much prominent in second derivative PPG (SDPPG).

There are some complex problem statements, where it is not so easy to establish an input and output relationship through mathematical modeling. For those situations artificial neural network (ANN) plays a vital role. To have good prediction precision in terms of RMS error and relative error [195] leads to statistical neural network (SNN). Depending upon the statistical method and probability theory two major neural network i.e. RBNN and GRNN is being used.

The present work thrusts the applicability of artificial neural network as an estimator of these crucial fiducial parameters of PPG by using *Radial Basis Neural Network* (RBNN) [14,15,195], and *General Regression Neural Network* (GRNN)[196-197] with modeling done by a Gaussian function[198].

5.6.1 Methodology

The current work proposes the measurement of fiducial parameter like Systolic (amplitude, time), Diastolic (amplitude, time), Dicrotic phases (amplitude, time) and pulse wave time(PWT) in Photoplethysmography with experimental result [199] .The two maxima in PPG waveform shows the Systolic and Diastolic peak ,from which heart rate can be calculated. Dicrotic notch time and amplitude is calculated,when blood flows backward before the closer of aortic valve. Hence each PPG cycle(waveform) having the fiducial parameter manifests the physiological performance of cardiovascular system of human body. The measurement process is illustrated in the subsequent paragraphs.

A systolic peak amplitude, diastolic peak amplitude, Dicrotic Notch, systolic phase, Diastolic phase and Pulse wave width are considered to major fiducial parameters for clinical analysis .

5.6.1.1 Gaussian Modelling

Each PPG signal after simulation-based signal processing, were modelled with a mixer set of two independent Gaussian functions as each cycle PPG has one Systolic peak and one Diastolic peak for better reconstruction and accuracy. The widely addressed probabilistic distribution function or Gaussian function or normal function at input x is characterized as:

$$f(x) = \frac{1}{\sigma_1\sqrt{2\Pi}} e^{\frac{-(x-\mu_1)^2}{2\sigma_1^2}} + \frac{1}{\sigma_2\sqrt{2\Pi}} e^{\frac{-(x-\mu_2)^2}{2{\sigma_2}^2}} \quad (5.7)$$

Where, Mean= μ , SD = σ, Variance = σ^2.

The philosophy behind this Gaussian distribution function is that, it is highly used for initialization of random data and centered at around a value i.e. the mean and usually set as zero. The modeling parameters (A, μ and σ) were determined from sampled data as shown in Table 5.8.

5.6.1.2 Radial Basis Neural Network (RBNN)

Because of global approximation to input/output mapping Multilayer perceptron (MLP) network is not capable of fast learning. So, RBNN [198,200] was proposed by Broomhead and Lowe in 1988 and shown in Fig. 2. The network activity depends upon the activation function and weights. Generally, in RBNN uses different activation functions [201] . Out of which

Radial Basis Function (RBF) is one.

Most widely used RBF using Gaussian function [201], having *X* as input pattern, 'μ' as the center of function and radius as σ^2 is shown in Fig. 2. with weight 'w_j'. Where, Output as Y(x) (with bias b_0) and the Gaussian function (z(x)) are expressed as:

$$Y(x) = \sum_{j=1}^{n} w_j z_j(x) + w_0 b_0 \tag{5.8}$$

$$z(x) = \exp\left(\frac{-(x-\mu)^2}{2\sigma^2}\right) \tag{5.9}$$

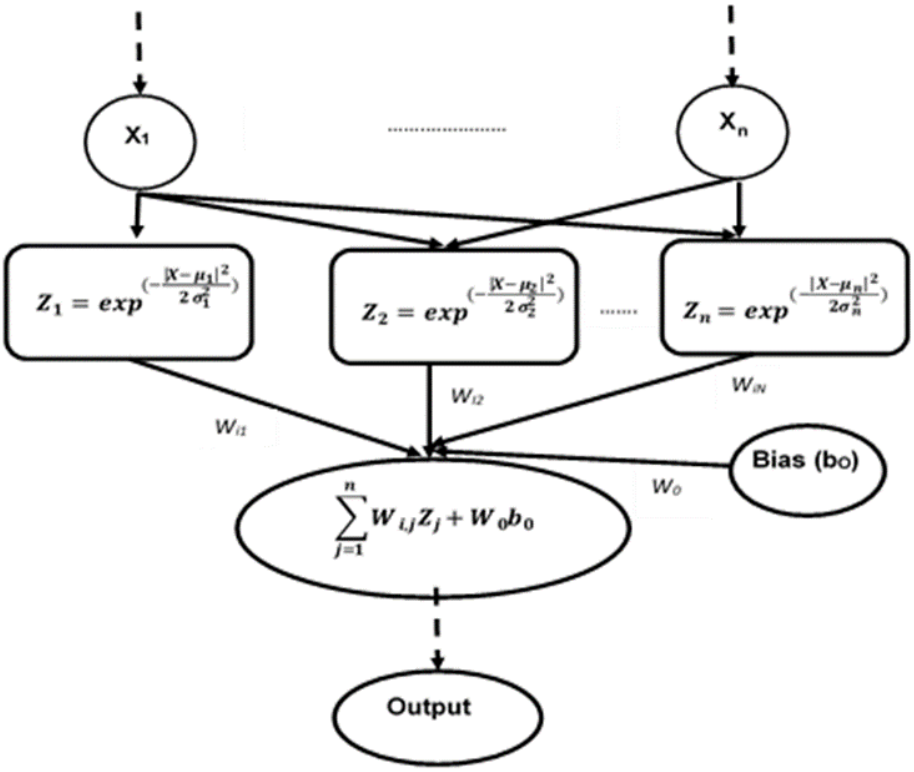

Fig. 5.9 Radial basis Neural Network

Due to additive noise, when input data are corrupted RBNNs are preferably used for function approximation and pattern reorganization [202]. The architecture is shown in Fig. 5.9. RBNNs are three layered feed forward parallel network. Input layer is the first layer where individual neuron is fed with predictor variable. Next is a single hidden layer built with RBFs centered on a point. Location of input vector is calculated by Euclidean distance. The weight associated with the corresponding output from neuron of hidden layer is multiplied and the sum gives the

output of the NN, is the last layer. In the RBNNs, first phase of the training is done in calculating RBF parameters (i.e. radius, coordinate of centre) and in the 2nd phase the weights between hidden and output unit is estimated. The σ, μ and the final weight are to be modeled.

5.6.1.3 General Regression Neural Network (GRNN)

GRNN which is coming under the category of probabilistic neural network (PNN) [200] is a feed forward supervised neural network . Because of feed forward architecture the training becomes very fast. GRNN can be applied for interpolation, regression problem, prediction and classification. GRNN can also be a good solution for online dynamical systems. GRNN is a regression estimator technique, where there is a Gaussian function to estimate the probability density function. Like BPNN, a GRNN [197] do not do repetitive training. The topology of GRNN has 4 layers. It's clearly visible in Fig. 5.10. that it has input layer, pattern layer, summation layer and output layer. The measurand X is fed to the first input layer neuron. Then 2nd layer (1st hidden layer) having N nodes for N sampled data, known as a pattern layer is connected to first layer. The squaring of difference result(D) is taken between input vector, *Xi* and the vector assigned to the node, *Xj* for jth sample in training data is fed to exponential function with a a smoothing factor(σ).This output patterns are given to the two sum units of summation layer (2nd hidden layer). First summation neuron gives the sum of product of the 2nd layer outputs and observed output y_i .Likewise 2nd summation neuron is the sum of the 2nd layer activation. Output layer is the last one to divide the result of two sum node to predict the result i.e. to estimate Y(X) as:

The output is given by:

$$\widehat{Y(X)} = \frac{\sum_{i=1}^{n} Y_i \exp(-\frac{D_i^2}{2\sigma^2})}{\sum_{i=1}^{n} \exp(-\frac{D_i^2}{2\sigma^2})} \qquad (5.10)$$

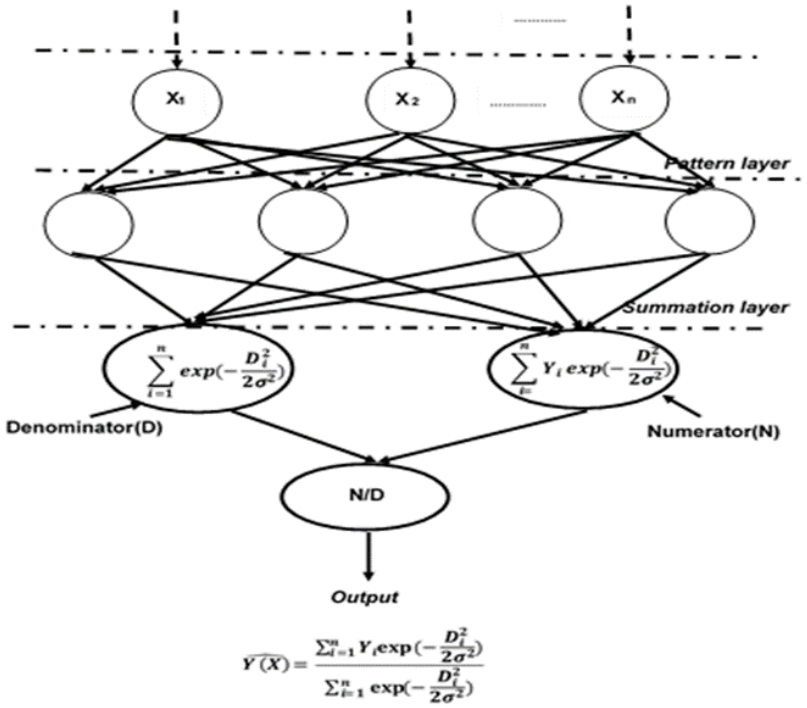

Fig. 5.10 General Regression Neural Network architecture

5.6.2 Result and Discussion

The prediction of PPG fiducial parameters are being done in the following subsections.

5.6.2.1 Result of RBNN and GRNN based prediction

PPG waveforms are recorded from fingertips of 10 subjects (five male and five female) with age group ranging from 22-57 years. The stored data sets are filtered with 2nd order band pass filter having corner frequency from 2 Hz to 40 Hz. The filtered data sets are corrected with gain adjustment multiplying factor to main peak to peak value to its original PPG waveform as shown in Fig. 5.11.(a).The local minima of filtered data set in PPG waveform are detected as shown in Fig. 5.11.(b).The sampled data sets within successive minima point are extracted and stored in an array PPG beat matrix. The1st and 2nd derivatives of sampled data sets within each beat are computed.

The filtered PPG waveform data samples for 10 subjects are converted to beat matrix array, the column of which is used as one period of PPG waveform, called pulse time and stores the total data samples in it. Thus data set for five beats (i.e. 5 PPG waveform cycles) are stored into

PPG beat matrix file. Each PPG beat is modeled with mixtures of two Gaussian functions as given by the equation 5.7, which results 6 coefficients. The model coefficients are considered the features of PPG waveform. Thus all beats are modeled by Gaussian method and are stored into data file, where each record in file consists of 6 model coefficients and the PPG pulse time period in sec.

The fiducial point of interest are computed with the help of index located at +ve and –ve zero crossing points 1st order derivative and –ve peak of 2nd order derivative of PPG waveform for all the beats as shown in Fig. 5.11.(c). The fiducial points of five subjects as Systolic peak and time, Dichotic Notch peak and time, Diastolic Peak and time are tabulated in Table 5.9. Systolic and Diastolic phase durations, Pulse wave time.

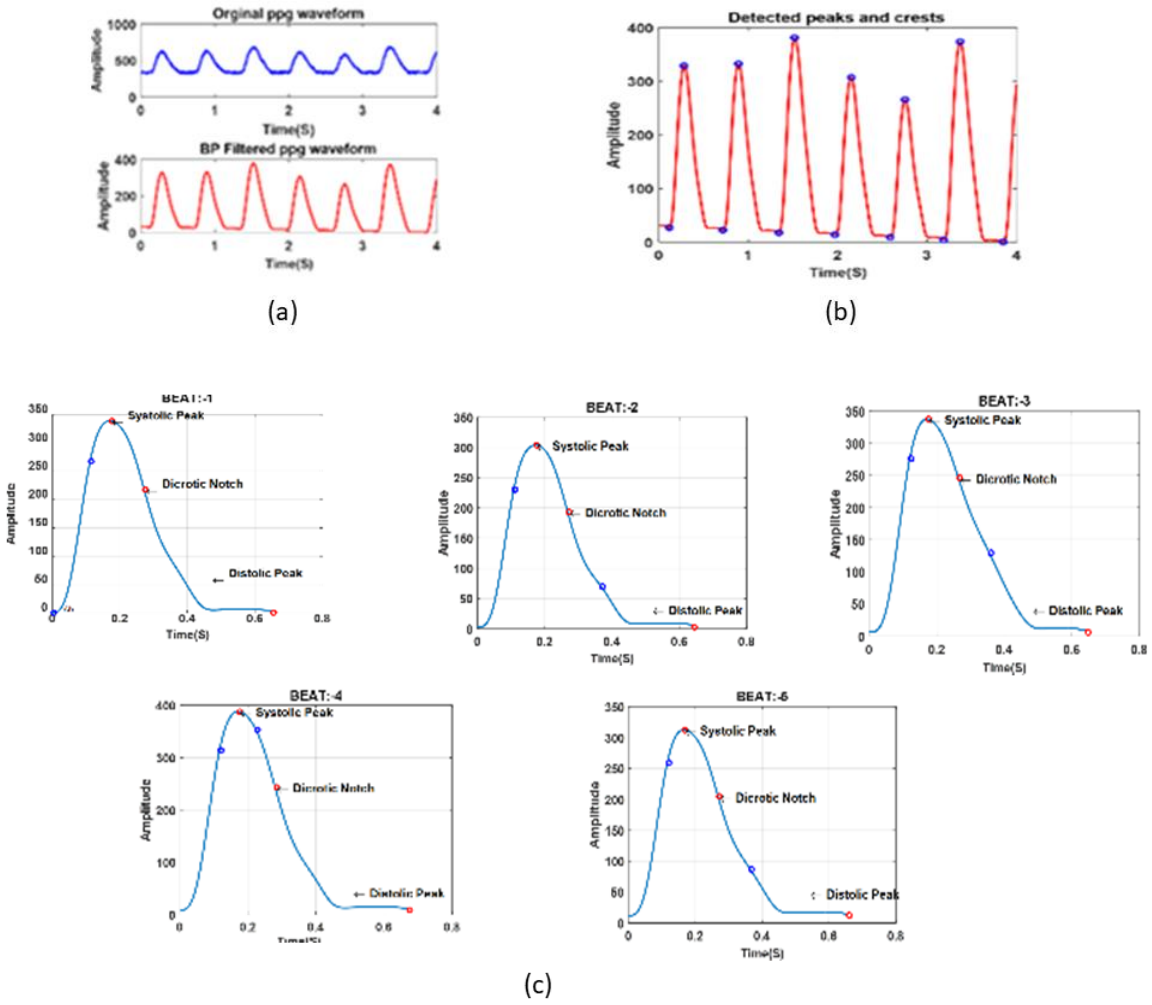

Fig. 5.11 Noisy and filtered PPG signals, (b)Detected peak and crests of PPG signal, (c) PPG waveforms of 5 beats for 50 years female subject.

The Gaussian model as features of input and fiducial parameters (time and amplitude) as target outputs are utilized for training Radial basis and generalized regression neural networks. The trained RBNN and GRNN networks are tested by applying beat wise feature input of 50 years female subject. The predicted values of fiducial parameters by RBNN and GRNN are shown in Table 5.10, 5.11 respectively. The errors w.r.t. to original value as computed for all the beats are shown in Table 5.12, 5.13 respectively. It is clearly observed that performance by GRNN is better as the errors found in case GRNN are much less that that by RBNN.

Table 5.8

2-Gauss Model Parameters and pulse wave time.

ID:50yr_high_bp_female_ppg(rest)							
Beat No.	2-Gauss Model Parameters						PTIME(S)
	A_1	μ_1	σ_1	A_2	μ_2	σ_2	
1	0.6280	0.1490	0.0851	0.7010	0.1380	0.6980	0.4560
2	0.6630	0.3720	0.0849	0.6560	0.3230	0.9020	0.6640
3	0.4670	0.3880	0.0815	0.7840	0.6010	1.1000	0.7760
4	0.5280	0.2650	0.0805	0.7870	-0.1340	1.6500	0.5160
5	0.6430	0.4060	0.0864	0.6940	0.1820	0.9370	0.7160
ID:50yr_high_bp_male_ppg(rest)							
1	0.8820	0.1110	0.0680	0.9050	0.2250	0.2120	0.4560
2	0.9920	0.1170	0.0687	1.0100	0.3000	0.2110	0.4440
3	0.8000	0.1120	0.0656	0.8220	0.2110	0.3740	0.4480
4	0.8610	0.1140	0.0685	0.8740	0.2500	0.2760	0.4480
5	0.8140	0.1100	0.0630	0.8030	0.2460	0.3070	0.4520

Table 5.9

Time and Amplitude of fiducial parameters and pulse wave time.

ID:50yr_high_bp_female_ppg(rest)							
Beat No.	Fiducial Parameters						PTIME(S)
	SYSTOLIC		DICROTIC		DIASTOLIC		
	TIME(S)	PEAK	TIME(S)	LEVEL	TIME(S)	LEVEL	
1	0.152	1.320	0.224	1.020	0.456	0.573	0.456

2	0.372	1.310	0.444	1.000	0.664	0.573	0.664
3	0.388	1.210	0.464	1.000	0.776	0.584	0.776
4	0.264	1.260	0.336	0.996	0.516	0.671	0.516
5	0.404	1.290	0.480	0.975	0.716	0.518	0.716
ID:50yr_high_bp_male_ppg(rest)							
1	0.124	1.560	0.180	1.240	0.456	0.235	0.456
2	0.128	1.460	0.176	1.230	0.444	0.231	0.444
3	0.120	1.550	0.180	1.150	0.448	0.517	0.448
4	0.124	1.540	0.176	1.240	0.448	0.516	0.448
5	0.116	1.460	0.172	1.120	0.452	0.493	0.452

Table 5. 10

Time and Amplitude of fiducial parameters and pulse wave time predicted by RBNN.

ID:50yr_high_bp_female_ppg(rest)							
Beat No.	Fiducial Parameters predicted by RBNN						PTIME(S)
	SYSTOLIC		DICROTIC		DIASTOLIC		
	TIME(S)	PEAK	TIME(S)	LEVEL	TIME(S)	LEVEL	
1	0.152	1.320	0.224	1.020	0.456	0.573	0.456
2	0.372	1.310	0.444	1.000	0.664	0.573	0.664
3	0.388	1.210	0.464	1.000	0.776	0.584	0.776
4	0.264	1.260	0.336	0.996	0.516	0.671	0.516
5	0.404	1.290	0.480	0.975	0.716	0.518	0.716
ID:50yr_high_bp_male_ppg(rest)							
1	0.124	1.560	0.180	1.240	0.456	0.235	0.456
2	0.128	1.460	0.176	1.230	0.444	0.231	0.444
3	0.120	1.550	0.180	1.150	0.448	0.517	0.448
4	0.124	1.540	0.176	1.240	0.448	0.516	0.448
5	0.116	1.460	0.172	1.120	0.452	0.493	0.452

Table 5. 11

Time and Amplitude of fiducial parameters and pulse wave time predicted by GRNN.

ID:50yr_high_bp_female_ppg(rest)							
Beat No.	Fiducial Parameters predicted by GRNN						PTIME(S)
	SYSTOLIC		DICROTIC		DIASTOLIC		
	TIME(S)	PEAK	TIME(S)	LEVEL	TIME(S)	LEVEL	
1	0.203	1.420	0.269	1.100	0.521	0.493	0.521
2	0.317	1.320	0.389	1.020	0.634	0.539	0.634
3	0.370	1.260	0.445	1.000	0.717	0.567	0.717
4	0.274	1.260	0.346	0.996	0.533	0.658	0.533
5	0.325	1.320	0.398	1.020	0.640	0.542	0.640
ID:50yr_high_bp_male_ppg(rest)							
1	0.145	1.630	0.207	1.270	0.484	0.275	0.484
2	0.150	1.690	0.216	1.310	0.498	0.218	0.498
3	0.146	1.570	0.207	1.220	0.478	0.350	0.478
4	0.144	1.610	0.206	1.260	0.481	0.300	0.481
5	0.144	1.580	0.205	1.240	0.477	0.334	0.477

Table 5. 12

Error in Fiducial Parameters by RBNN.

ID:50yr_high_bp_female_ppg(rest)							
Beat No.	Error (%) in Fiducial Parameters by RBNN						PTIME(S)
	SYSTOLIC		DICROTIC		DIASTOLIC		
	TIME(S)	PEAK	TIME(S)	LEVEL	TIME(S)	LEVEL	
1	5.79E-12	1.13E-12	-1.85E-11	3.91E-11	-9.50E-13	1.46E-10	-1.31E-12
2	3.86E-12	2.74E-12	1.81E-11	-1.29E-11	1.99E-12	-7.25E-12	1.49E-12
3	9.59E-13	-1.69E-12	9.01E-12	-7.34E-12	3.15E-13	1.71E-11	6.87E-13
4	1.87E-12	-2.06E-12	1.19E-11	1.32E-11	2.58E-13	2.78E-11	5.59E-13
5	1.80E-12	1.95E-12	3.89E-12	1.52E-11	1.55E-13	9.72E-11	1.86E-13
ID:50yr_high_bp_male_ppg(rest)							
1	3.18E-12	4.49E-12	-2.87E-11	1.66E-11	-2.90E-12	5.55E-10	-1.70E-12
2	2.04E-12	3.25E-12	9.75E-12	2.85E-11	-7.50E-14	2.01E-10	-8.50E-13
3	4.39E-12	2.53E-12	6.82E-12	1.86E-11	-3.15E-12	7.78E-11	-2.33E-12
4	1.75E-12	3.90E-12	-6.40E-12	2.27E-11	-7.68E-13	1.59E-10	-3.47E-13
5	4.18E-12	5.75E-12	-3.71E-12	7.27E-12	-1.06E-12	1.03E-10	-1.82E-12

Table 5. 13

Error in Fiducial Parameters by GRNN.

ID:50yr_high_bp_female_ppg(rest)							
Beat No.	Error (%) in Fiducial Parameters by GRNN						PTIME(S)
	SYSTOLIC		DICROTIC		DIASTOLIC		
	TIME(S)	PEAK	TIME(S)	LEVEL	TIME(S)	LEVEL	
1	33.6000	7.2900	20.0000	7.8600	14.2000	14.1000	-14.2000
2	14.8000	1.2800	12.5000	2.0800	4.4900	5.8700	4.4900
3	4.5500	3.8900	4.1300	-0.0472	7.6600	2.8400	7.6600
4	3.7400	-0.1770	3.0100	0.0463	3.2100	1.8200	-3.2100
5	19.5000	2.1800	17.2000	4.1800	10.6000	4.6900	10.6000
ID:50yr_high_bp_male_ppg(rest)							
1	-16.5000	4.6100	15.0000	3.1000	6.2200	17.1000	-0.0284
2	17.1000	15.6000	22.5000	6.4400	12.2000	5.4700	-0.0542
3	21.5000	1.3100	14.9000	6.0300	6.6700	32.3000	-0.0299
4	16.2000	4.8200	17.0000	1.3600	7.4000	41.9000	-0.0331
5	23.8000	8.0400	19.0000	10.0000	5.5700	32.3000	-0.0252

5.6.2.2 Discussion of RBNN and GRNN based prediction

In present work, captured PPG signal from index finger and later waveform data has been cleaned from baseline and noise. When the heart muscle contracts blood flows in peripheral tissues and changes the fiducial parameter of PPG (i.e. Systolic, Diastolic and Dicrotic index and pulse transit time) over every cycle or beat. Depending upon sex, age and movement condition/rest pulse transit time and HRV parameters varies. Hence for diagnosis of cardiovascular diseases, PPG waveform data set can be used to monitor HRV. Fiducial parameters (time and amplitudes of index points) of PPG signal was computed from 1^{st} and 2^{nd} order derivative of PPG signal [5], which requires the large computation time for processing PPG waveform data set extraction of sampled data set into beat matrix format and thereafter locating the index points at systolic, diastolic and dichroitic regions. The ANN method can reduce the computation time for determining the fiducial parameters. However instead of using raw data relating sampled data of PPG waveform, features has been extracted after modeling it by the sum of 2 Gaussian functions, which yields the 6 coefficients (e.g. A_1, $\boldsymbol{\mu}_1$, $\boldsymbol{\sigma}_1$ and A_2, $\boldsymbol{\mu}_2$, $\boldsymbol{\sigma}_2$) and pulse transit time (PTIME) . The features as input vectors with their corresponding fiducial parameter values of systolic, diastolic, dichroitic regions (e.g. time and amplitudes and pulse transit time (PTIME) as target vectors are utilised to train General regression and Radial Basis Neural networks separately. The Radial Basis (RBNN) and General regression (GRNN) network are a good alternative and advantageous to the Multilayer perception Back Propagation (MLP BP) network as these has only three-layer architecture and it has a much faster training process compared to the MLP. The trained networks are tested by feature of one subject randomly for prediction about their fiducial parameter. The percentage error w.r.t. to original values as determined analytically has been found. It is observed that the performance of RBNN is better as the error is very low compared to that by GRNN. The RBNN and GRNN method can also be used for prediction of HRV parameters (e.g. PPG augmented index for arterial stiffness measurement, mean value of P-P interval time, standard deviation of successive P-P interval time, parentage of successive P-P interval time, which differs from more than that by 50 ms, standard deviation of instantaneous and long term P-P interval variability.

5.7 Summary

This chapter suggested the novel approach of extracting the fiducial parameters from PPG signals and predicting the corresponding ECG signals using the Gaussian process regression predictor. Extensive experimental results demonstrate the feasibility of obtaining low-cost, long-term, and user-friendly ECG fiducial parameter monitoring and early diagnostic screening from PPG signals using the proposed methodology. The prediction of ECG fiducials is especially challenging since CVD follows distinct waveform shapes for different symptoms. Because blood volume, or more specifically, the quantity of blood that circulates through an individual, fluctuates depending on their size and weight. The system may perform differently in predicting ECG fiducial parameters from other types of unobserved CVD classes. Adding additional human body indices e.g., weight and height measurements in the regression model in parallel with the PPG fiducial parameters, can make the system more holistic. The proposed model finds its applications in the cases of medical diagnostics such as aberrant heart rhythms, and the identification of cardiovascular illnesses, to name a few. Additionally, creating multi-lead ECGs can be investigated to extract additional useful cardiac data that is frequently absent in single-channel ECG recordings. Also, future research investigations can be carried out by acquiring some longer spectrum of PPGs so that the chances of missing information in short-duration PPG spectrums will be reduced. The straightforward approach and convenient usability of the proposed method make it a potential candidate in extended health monitoring systems for clinical practices. This also creates the opportunity of fabricating IoT-enabled remote monitoring systems for cardiac patients as part of the telemedicine and tele-rehabilitation programmes. Also it is observed that the performance of RBNN is better as the error is very low compared to that by GRNN in predicting PPG fiducial parameters from PPG signal.

Chapter 6

Classification and authentication of CVD using composite features of ECG and PPG signals

6.1 Introduction

Globally, cardiovascular diseases (CVDs) are the most prevalent non-communicable health issues and one of the fundamental causes of death. According to World Health Organization (WHO) estimates, it killed 17.9 million people in 2019, with over 75 percent of those fatalities happening in low and middle-income nations [139]. In comparison to passive treatment, active prophylaxis is significantly more desirable. As a result, early identification of irregular heartbeats may be crucial to save lives by enabling early intervention and treatment.

Angiography, catheterization, etc. are invasive techniques that offer extremely precise and thorough information that is necessary for the diagnosis and management of intricate cardiac disorders, but entail inherent hazards including risk of fatal complications and are usually costlier and resource-intensive than the non-invasive counterpart [203] such as ultrasound, MRI and CT scan and biomedical signal analysis. Echocardiography, the most useful non-invasive diagnostic test is also not available in remote and rural areas and is largely observer dependant and hence is only reliable when done by experienced operators. The most popular non-invasive biomedical signals that infer cardiac information are phonocardiogram (PPG), electrocardiogram (ECG), and photoplethysmogram (PPG). Among these for simplicity, the ECG and the PPG are two of the primary common cardiac signals used in the healthcare systems. According to the heart's pumping action, the ECG signal depicts the heart's electrical rhythm with “P, Q, R, S, and T” waves and segments and the PPG signal manifests its blood volume changes.

Classification has numerous benefits, but it also has adverse challenges. ECG graphs and PPG waves are prone to interference from noise, motion artifacts, and other sources. Inaccurate feature extraction from low-quality signals can make it challenging for the classification algorithm to discern between normal and unhealthy cardiac states. Again composite features complexity from ECG and PPG signals may compromise the classification model's accuracy, which can produce noisy or unnecessary features. Again unproductive choice of features can overfit a model, consequently, it may work effectively with the training data/information but adversely on testing data. Adopting such design models in real-time applications or limited resource availability environments, like portable devices or remote healthcare

settings, may be limited by their high computing costs. A model's wider application may be limited if it is trained on a population with distinct age, gender, and ethnicity distributions since it might fail to function as well when deployed to other demographic groups.

6.2 Benefits of composite features for CVD classification

There are various advantages of classifying and authenticating cardiovascular diseases (CVD) using composite features of ECG and PPG signals as opposed to separate signals. These advantages include:

- **Enhanced precision and dependability**

  • *Complementary information***:** PPG measures variations in blood volume, whereas ECG records the electrical activity of the heart. When both are combined, cardiovascular function can be seen holistically.

  • ***Fewer false positives/negatives***: When ECG and PPG are analyzed together, fewer misclassifications occur than when individual signals are considered alone.

- **Improved extraction of features**

  •*Pulse Transit Time (PTT):* This parameter, which is not reliably provided by individual signals, gives information about arterial stiffness, blood pressure, and vascular health by measuring the interval between the ECG R-peak and the corresponding PPG peak.

  • *Heart Rate Variability (HRV) and Pulse Rate Variability (PRV)*: When combined, ECG-based HRV and PPG-based PRV improve classification accuracy.

- **Rresilience against artifacts and noise**

  • PPG is sensitive to temperature, skin tone, and sensor location, while ECG is susceptible to motion distortions. When one signal is distorted, a fusion-based method aids in compensating. For instance, PPG characteristics can still offer valuable cardiovascular insights even if the ECG signal is sporadic because of inadequate electrode contact.

- **Early detection and ongoing surveillance**

  • *Identification of CVD Biomarkers*: While some cardiovascular conditions, such as hypertension and arrhythmia, manifest in ECG, arterial stiffness and peripheral circulation problems are more noticeable on a PPG. Together, they enable earlier and more accurate diagnosis even multi-disease detection.

  • *Wearable integration*: Many wearables, including fitness bands and smartwatches, can record both PPG and ECG, allowing for constant, real-time monitoring.

- **Tailored and flexible medical care**

  • *Advantages of AI and Machine Learning*: A richer dataset for AI models is produced by fusing ECG and PPG information, which enhances predictive analytics and individualized treatment regimens.

  • *Adaptive decision-making*: This allows health monitoring systems to make real-time adjustments in response to the dynamic changes in both signals.

6.3 Classifiers for classification

Classifiers including 1D-CNN and machine learning approaches are depicted in this sub-sections.

6.3.1 1-D Convolutional neural network (1D-CNN)

CNNs are typically employed for image classification applications. Still, they can also be employed with sequential time series data [4] by employing the 1D convolution neural network, a variation of the vanilla CNN. Convolutional filters in 1D CNNs slide down the temporal axis of the input to catch local patterns or variations in the sequence. CNNs can learn hierarchical depiction of the data being used, capturing both high-level and low-level features, by applying numerous convolutional layers accompanied by increasing filter sizes and using the activation functions "RELU, softmax, and sigmoid function". The pooling layer: "max pooling, average pooling, sum pooling", which lowers the spatial dimensions while preserving significant features, comes after each convolutional layer. Subsequently, the flatten layer and dropout layer comes after the convolution layer to eliminate overfitting and reduce model size and computational cost. Finally, The output is produced by the dense fully connected layer, which receives the flattened output as an input. From sequential data, including time series, audio signals, and text data, these models can be used to extract relevant features as depicted in Fig. 6.1. Again, the hyperparameters for the proposed work for classification of CVDs is shown in Table 6.1.

Table 6.1

Hyperparameters of 1D-CNN for our classification work of CVDs.

Filter size	**No of filters**	**Activation function**	**Pooling layer**	**Optimizer**	**Maximum epochs**	**Learning rate**
5	32	RELU	Average	Adam	64	0.01

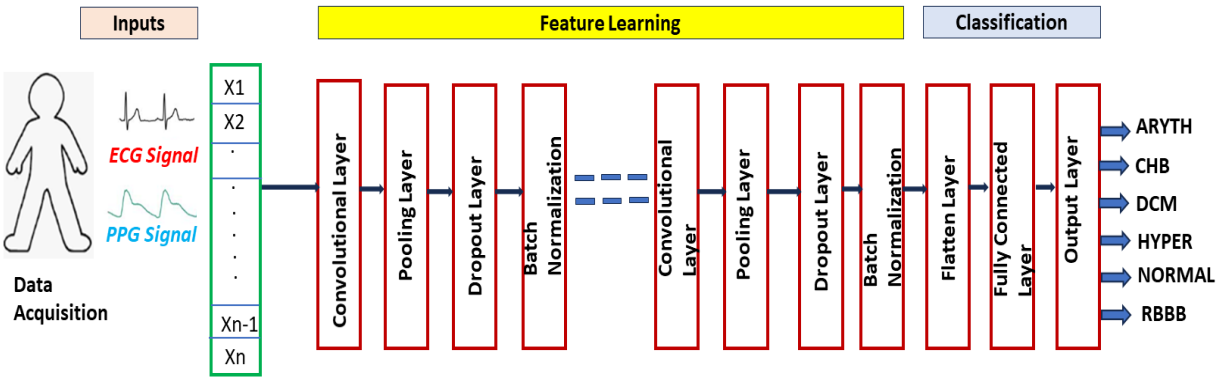

Fig. 6.1. A typical architecture of ID-CNN.

6.3.2 Machine learning approaches

An overview of the machine learning approaches employed in this work is given in this section. Based on small dataset sizes, few classical machine-learning approaches are being chosen. Furthermore, the choices of machine learning methods are chosen by taking into account the model's simplicity [143].

6.3.2.1 Support vector machines

One of the most potent supervised learning models for classification is the Support Vector Machine (SVM), which is renowned for its adaptability and capacity to handle both linear and non-linear data. Finding the hyperplane that best divides the data into two groups is the goal of support vector machines (SVM) in binary classification. To maximize the margin—also referred to as the distance between the hyperplane and the closest data points from each class—this hyperplane is selected. By employing a kernel function [204] to transfer the input vectors into a higher-dimensional feature space, SVM may nevertheless locate a separating hyperplane in cases when the data is not linearly separable in the input space. Because of this, SVM can manage non-linear decision boundaries with effectiveness.

6.3.2.2 Logistic regression

When dealing with binary classification jobs, such as those where the result variable is categorical and has just two possible outcomes, statistical methods like logistic regression are employed, where the link between input features and outcome is thought to be linear.

Equation. 6.1 [205] illustrates how the LR employs the logistic function representation to transfer a

collection of inputs X to a value between 0 and 1, which represents the likelihood of falling into the positive class.

$$p(X) = \frac{e^{\propto_0 + \propto_1 x}}{1 + e^{\propto_0 + \propto_1 x}} \quad (6.1)$$

In this case, the provided training data should be used to modify the coefficients $\propto_0$ and $\propto_1$. Maximum likelihood is one technique used to fit the LR model [205]

6.3.2.3 Linear Discriminant Analysis

A statistical technique for classification and dimensionality reduction is called linear discriminant analysis (LDA). When handling multi-class classification difficulties, it is especially helpful. The goal of LDA is to identify a linear feature combination that distinguishes or characterizes two or more classes of objects or events. Projecting the input data onto a space with fewer dimensions while maximizing the degree of separation between classes is the primary goal of LDA with an assumption of normal data distribution. It determines the axes or directions that maximize the variance between classes and minimize variance within classes [206].

6.3.2.4 Decision trees

The decision tree is one kind of supervised learning technique using sequential models for decision or classification tasks. They generate a decision tree-like model by dividing the data into subsets according to the input feature values. Upon receiving a test set, the decision tree compares a nominal characteristic to a set of options or a numeric characteristic to a threshold value. A decision tree uses its ability to identify patterns in a partitioned region to classify new data points as belonging to the most common class within that region. Various methods, such as C4.5, CART, and SPRINT, have been developed to build decision trees. Producing optimal partitioning is the primary goal of decision trees. Based on impurity, this partitioning procedure is carried out. A class is declared pure if it is the only one in the subset; if not, it is deemed impure. Because of its non-parametric, versatile, and easy to understand and interpret used widely in disease classifications [207].

6.3.2.5 Random forest

One well-liked ensemble learning technique that mainly utilized for classification is the random forest. During training, it builds several decision trees and outputs the class that is the average of the classes. The method of merging several models (decision trees in this case) to create a more accurate and reliable model. The fundamental part of the random forest is that each tree is a structure resembling a flowchart that is utilized to generate predictions based on feature values. Bootstrap aggregation is used for training to avoid overfitting. Just a random selection of features is taken into account for splitting nodes during each tree's training process. This helps to reduce the correlation between the trees by introducing another layer of randomization [208].

6.3.2.6 K-nearest neighbour

The K-nearest neighbour (KNN), a supervised machine-learning algorithm compares a given test set to the training sets to facilitate learning. Several neighbours (k) and n number of characteristics, characterize the training sets. KNN looks for the k training points in the n-dimensional space that are closest to the unknown test set whenever a new test example appears. The degree of proximity between the test data point and the training set is determined by a distance metric, most frequently the Euclidean distance. The test set is the most common class determined using a majority vote system [209].

6.3.3 Probabilistic Neural Network (PNN)

To solve the diverse group of classification problem, probabilistic neural network (PNN) is introduced in 1990s [211]. It shows excellence in classification for categorical target variable. By rapid processing and with enough training data, it guarantees to converge to Bayesian classifier to get a local optimum satisfactory solution [210], [202].

In PNN as each pattern is placed once to the NN and its training becomes faster, unlike backpropagation (BPNN) where repetitive weight adjustment and feedback error calculation which makes tedious. Because of detainment of faster learning, generalization and concurrency, the many flaws of BPNN can be overcome. The most advantage of PNNs is the probabilistic nature of output, which makes interpreting output easier. The most disadvantage part is the more memory space is occupied in storing the model.

The structural model of PNN, as in Fig.6.2 has four layers. The first layer is the input layer or simply the connection point to receive the input vector X= (X_1 X_2 …X_n), which is to be classified without performing any computation. Next comes second layer known as pattern layer, where corresponding to each training sample each pattern layer representation is done. Then for pattern layer K group division done, one for one group. Using the Gaussian kernel. Then the k-th group gives the i-th pattern, which is computed as equation (6.2).

$$f_{Ai}(X) = \frac{1}{(2\pi\sigma^2)^{\frac{P}{2}}} exp\left[-\frac{(X-X_{Ai})^T-(X-X_{Ai})}{2\sigma^2}\right] \qquad (6.2)$$

Where, i (Pattern number), p (input vector X's dimension), σ (spreading or smoothing parameter of Gaussian function), X_A (centre of the kernel).

The 3rd layer, which is the summation layer to compute the approximation of conditional class probability by virtue of the previous computed densities combinations as equation (6.3).

$$f_A(X) = \frac{1}{(2\pi\sigma^2)^{\frac{P}{2}}} \frac{1}{M}\sum_{i=1}^{M} exp[-\frac{(X-X_{Ai})^T-(X-X_{Ai})}{2\sigma^2}] \qquad (6.3)$$

The last layer (output) is the decision layer to indicate the class of the unknown current input vector(X) by thresholding as: +1 to indicating X as class A & -1 to indicate as class B.

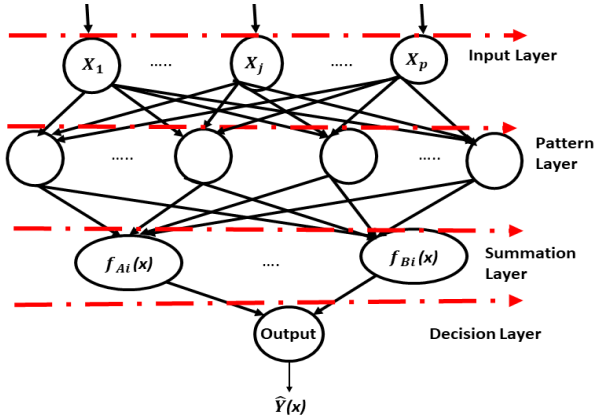

Fig. 6.2. Probabilistic neural network (PNN) structure.

6.4 Performance measurement indices

Common quantitative metrics for assessing the performance of classifiers are shown in this section. The categorization that emerged from the learning process can be referred to as a positive or negative class, depending on whether the unknown class data belongs to that correct class or other incorrect class respectively. The prediction's outcome may be either true or false, indicating a correct prediction or an incorrect prediction, in that order. As a result, classification can be summed up as follows [212] and shown

in Fig. 6.3.

1. True positive (TP): Correctly predicted positive class
2. True negative (TN): Correct negative class prediction
3. False positive (FP): Incorrect class prediction that is positive
4. False negative (FN): Incorrectly predicting a negative category

		Predicted class-->	
		Yes	No
Actual class→	Yes	TP	FN
	No	FP	TN

Fig. 6.3. Representation of 2x2 class classification considering actual class and predicted class.

Exclusively the performance evaluation is done for testing datasets as follows. We have done 6x6 class classifications. For better understanding, we have given a simple 2x2 class classification in the expression including the general expression as in equation (6.4) to equation (6.10)

- $Accuracy = \frac{All\ correct\ predictions}{Total\ predictions} = \frac{TP+TN}{TP+TN+FP+FN}$ (6.4)
- $Recall\ (Sensitivity)(True\ positive\ rate) = \frac{Correct\ 'Yes'\ prediction}{Total\ actual\ 'Yes'} = \frac{TP}{TP+FN}$ 6.5)
- $True\ negative\ rate\ (TNR)\ (Specificity) = \frac{Incorrect\ 'No'\ prediction}{Total\ actual\ 'No'} = \frac{TN}{FP+TN}$ (6.6)
- $Precision = \frac{Correct\ 'Yes'\ prediction}{Total\ predicted\ 'Yes'} = \frac{TP}{TP+FP.}$ (6.7)
- $Negative\ predictive\ value(NPV) = \frac{Correct\ 'No'\ prediction}{Total\ predicted\ 'No'} = \frac{TN}{TN+FN}$ (6.8)

- $False\ positive\ rate(FPR) = \frac{Incorrect\ 'Yes'\ prediction}{Total\ actual\ 'No'} = \frac{FP}{FP+TN}$ (6.9)

- $F1\_score = \frac{2*Precession*Recall}{Precession+Recall} = \frac{TP}{TP+\frac{1}{2}(FP+FN)}$ (6.10)

6.5 Composite feature approach for detection of CVD using ECG and PPG signals

The suggested classification model's pipeline structure is depicted in the workflow diagram as shown in Fig. 6.4 for various cardiovascular diseases.

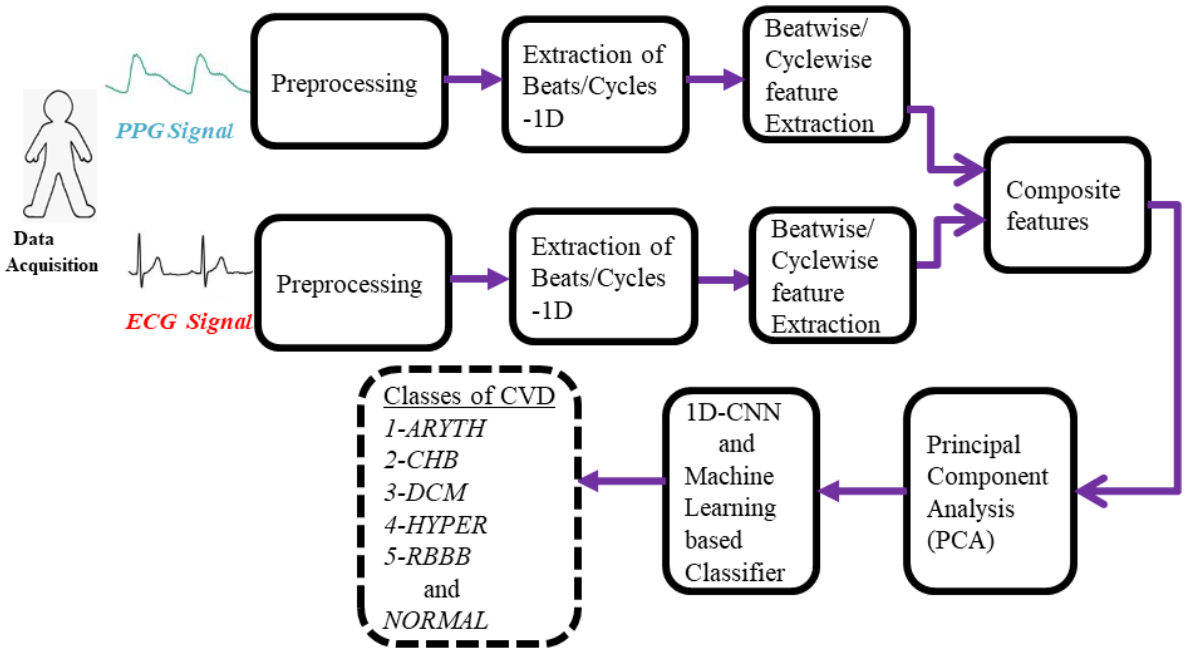

Fig. 6.4. Pipeline diagram depicting the general process flow of various CVD classifications using composite features of ECG and PPG signals.

6.5.1 Dataset description

Very few publicly accessible datasets include the coupled PPG/ECG signals and the accompanying CVD diagnosis. One MIMIC-III from Physionet incorporates the Lead-II ECG signal in the maximum subject ID. In the present scenario, "Right bundle branch block (RBBB), arrhythmia-atrial fibrillation (ARYTH), dilated cardiomyopathy (DCM), hypertension (HYPER), and complete heart block (CHB)" are among the five classes of CVD disorders that we have chosen here, along with one normal class (NORMAL). The "ICD-9-CM" codes: "RBBB (426.4), DCM (425.4), HYPER (402.91), ARYTH (427.31), and CHB (426.0)" are the ones we have selected for the variety of heart illnesses. According to

the MIMIC III dataset, the normal class is derived from sepsis and pneumonia subjects. The subjects with a single syndrome have been our focus. Five patient IDs are included in each class dataset. In this instance, one minute is recorded for every ID, consisting of 7500 samples. For both signals, 125 Hz is the sampling frequency. Men and women in various age groups, ranging from 38 to 87 years old, are included in this dataset by considering five patients for each class of disease. Furthermore, Biopac Systems collected real-world data from an ECG transducer- "BSLINTRO with SS2LB" from volunteers and hospitals with the inclusion of a PPG sensor module- "HRM-2511E Easy pulse version 1.1" with a sampling frequency of 125 Hz.

6.5.2 Composite feature formation

After ECG filtering, the widely utilized Pan-Tompkins method was used to identify the QRS. This was accomplished by progressively performing- "low-pass, high-pass, derivative, squaring, moving window integration, and thresholding operations". The rest P and T points of the ECG can be retrieved beatwise after the Q, R, and S fiducial points have been labeled and a typical waveform is shown in Fig.2. All of the cardiovascular data about the heart's operation is provided by the beat-wise fiducial points/ features extracted from entire wave beat-wise. A total of 12 time domain features are extracted from the ECG signal for this investigation including P (time, amplitude), Q (time, amplitude), R (time, amplitude), S (time, amplitude), T (time, amplitude), number of P' waves, and R-R interval for entire 1-minute duration signal length.

For every signal, peak, and valley identification, notch localization (i.e., determining the beginning and ending of the notch), and segmentation were done before feature extraction. Finding the beginning and end of each pulse is made easier by identifying valleys in the PPG signal, which is a crucial step in segmentation—that is, the procedure that comes before feature identification for each segment. The segmentation process is carried out by using the valleys to split the signals into the corresponding pulses. Fig.3 depicts a typical PPG waveform and the associated fiducial parameters/features. A total of 10 time domain features, are extracted from the PPG signal for this investigation including, "time-peak values for systolic, dicrotic, and diastolic as well as pulse wave time (PT), diastolic phase (DLP), PPG augmentation index (PPGAI), and systolic peak-peak intervals" for entire 1-minute duration signal length. Acceleration PPG (APG) and velocity PPG(VPG) are being used to determine the inflection points "Systolic, Dicrotic, and Diastolic".

Since the accuracy and dependability of this stage have been essential to obtain the best classification

performance, the feature extraction phase is the most important part of the classification process [213].

The crucial step is to form the composite feature [214] and to store it in matrix form to exploit both "interbeat and intrabeat correlation" among the ECG and PPG signals. The goal is to put it simply, to identify the dependencies both inside and between ECG, and PPG cycles. To create the 2-D array for this, the full waveform input is divided into beats, and each beat's features were then vertically aligned with the beat that preceded it. Simply speaking, 1-beat's features of ECG and PPG totaling several 22 features are arranged in one row and subsequently for the entire beats to form a 2-D array.

6.5.3 Principal component analysis

Using Principal Component Analysis (PCA), one can reduce the linear dimension that projects data in the directions of greatest variation. PCA algorithm [20] computes the covariance matrix from the extracted ECG/PPG features, decomposes the covariance matrix into eigenvalues and eigenvectors, sorts the eigenvectors in descending order of eigenvalues, and then projects the original ECG/PPGfeatures in the directions of the sorted eigenvectors. Most of the variation in the data is represented by the first few components. The first nine components are utilized in this work for pattern classification following PCA.

6.5.4 Result and Discussion

Applying the suggested methods, classification/detection of cardiovascular diseases using composite features of ECG and PPG signal are being carried out. The difficult part of the task now is figuring out whether or not these results are accurate and appropriate. About this query, we have conducted numerous performance evaluations not only through performance measurement indices but also through visualization curves. To ensure uniformity across the system, we have randomly chosen 70% of the data for training and the remaining 30% for testing. We have calculated each result's mean and standard deviation after 10 runs to determine the repeatability of the outcome. Here are the results and discussions.

6.5.4.1 Result

Our study on cardiac classification has been carried out on patients from the MIMIC-III database with several beat counts illustrated through the pie chart in Fig. 6.5.

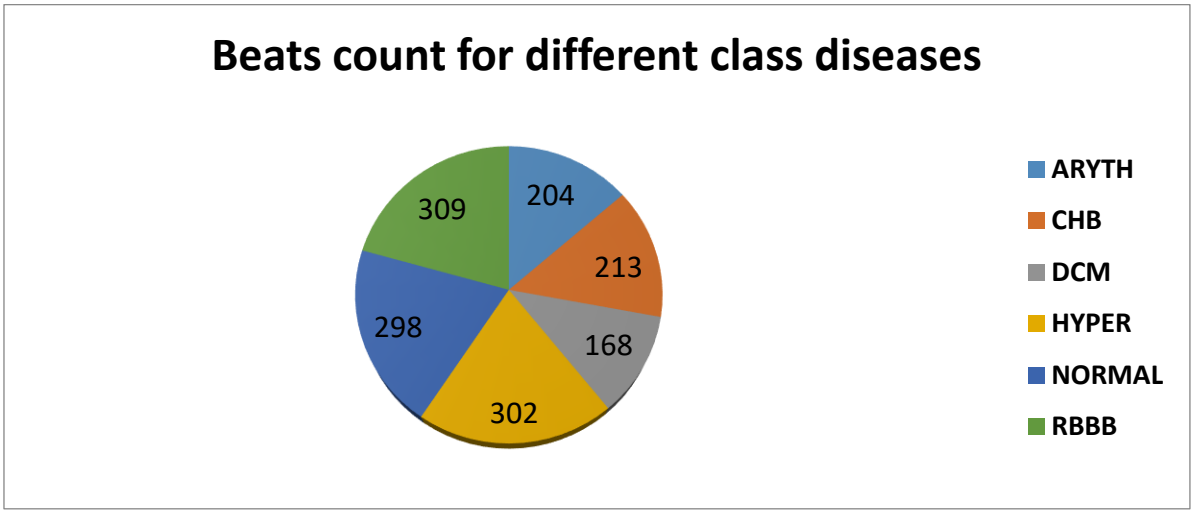

Fig. 6.5. Beats count for different class diseases using a pie chart.

The classifiers (1D-CNN, SVM, RF, LR, LDA, KNN, and DT) are being compared in Table 6.2, according to how well they perform with ECG signal only, PPG signal only, and a combination of ECG and PPG as input characteristics. For 1D-CNN, accuracy, recall, specificity, precision, negative predictive value (NPV), false positive rate (FPR), and F1-score are 0.925, 0.917, 0.926, 0.917, 0.949, 0.073, and 0.907 respectively by considering only ECG signal, 0.854, 0.872, 0.884, 0.889, 0.908, 0.115, and 0.899 respectively by considering only PPG signal moreover 0.966, 0.964, 0.993, 0.966, 0.993, 0.006, and 0.963 respectively by considering both signals. Similarly, the SVM classifier demonstrates a notable performance with an accuracy of 0.890 and an F1-score of 0.897 when using only the ECG signal. Performance slightly drops when using only PPG, with an accuracy of 0.861. However, combining both ECG and PPG features leads to improved results, achieving an accuracy of 0.949 and an F1-score of 0.949, indicating better generalization. The performance metrics of the other classifiers are detailed in Table 6.2 and visually represented in Fig. 6.6 through a bar graph. The robustness is also tested using real-time data collected from a hospital, as shown in Table 6.3. The results indicate that the 1D-CNN outperforms other machine learning approaches by considering features of both signals with accuracy, recall, specificity, precision, negative predictive value (NPV), false positive rate (FPR), and F1-score as 0.974, 0.971, 0.995, 0.966, 0.993, 0.005, and 0.975 respectively.

Table 6.2

Results of performance indices with different features for MIMIC III data.

Type of feature	**Classifier**	**Accuracy**	**Recall/TPR/ sensitivity**	**TNR/ Specificity**	**Precision**	**NPV**	**FPR**	**F1-score**
ECG	1D-CNN	0.925	0.917	0.926	0.917	0.949	0.073	0.907
PPG		0.854	0.872	0.884	0.889	0.908	0.115	0.899
ECG+PPG		0.966	0.964	0.993	0.966	0.993	0.006	0.963
ECG	SVM	0.890	0.905	0.947	0.899	0.946	0.052	0.897
PPG		0.861	0.864	0.902	0.828	0.891	0.097	0.875
ECG+PPG		0.949	0.949	0.989	0.95	0.989	0.010	0.949
ECG	RF	0.818	0.831	0.923	0.840	0.938	0.076	0.817
PPG		0.799	0.803	0.914	0.809	0.916	0.086	0.799
ECG+PPG		0.877	0.873	0.974	0.881	0.975	0.025	0.875
ECG	LR	0.805	0.809	0.914	0.816	0.925	0.085	0.799
PPG		0.784	0.799	0.908	0.795	0.913	0.091	0.771
ECG+PPG		0.853	0.848	0.969	0.857	0.97	0.03	0.851
ECG	LDA	0.584	0.537	0.883	0.694	0.896	0.116	0.564
PPG		0.569	0.524	0.847	0.671	0.873	0.152	0.536
ECG+PPG		0.62	0.576	0.921	0.721	0.925	0.078	0.589
ECG	KNN	0.861	0.847	0.943	0.867	0.914	0.056	0.851
PPG		0.841	0.831	0.905	0.833	0.883	0.094	0.806
ECG+PPG		0.89	0.883	0.977	0.893	0.959	0.022	0.887
ECG	DT	0.713	0.726	0.899	0.706	0.900	0.100	0.726
PPG		0.697	0.708	0.867	0.689	0.871	0.132	0.710
ECG+PPG		0.751	0.755	0.949	0.752	0.949	0.05	0.751

Table 6.3

Results of performance indices with different classifiers for real-time data considering both signals features.

Classifier	Accuracy	Recall	Specificity	Precision	NPV	FPR	F1-score
1D-CNN	0.974	0.971	0.995	0.966	0.993	0.005	0.975
SVM	0.935	0.928	0.968	0.94	0.982	0.032	0.937
RF	0.894	0.882	0.989	0.893	0.975	0.019	0.891
LR	0.864	0.876	0.982	0.872	0.981	0.018	0.872
LDA	0.735	0.684	0.948	0.758	0.957	0.052	0.738
KNN	0.91	0.895	0.981	0.901	0.977	0.019	0.897
DT	0.788	0.789	0.959	0.789	0.967	0.04	0.795

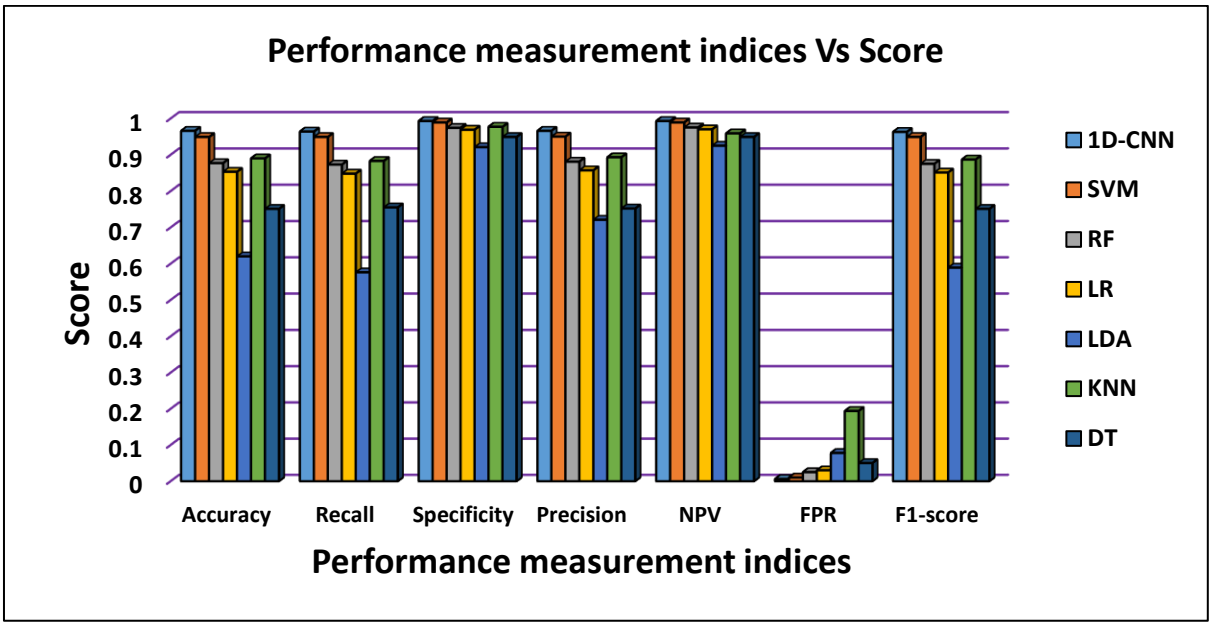

Fig. 6.6. Performance measurement using different classifiers.

According to the number of PCA components, which ranges from 1 to 22, Fig. 6.7 displays the accuracy of several classifiers (1D-CNN, SVM, RF, LR, LDA, KNN, and DT). The trends show how each classifier's performance changes as more principal components are included.1D-CNN achieves the highest overall accuracy, peaking at approximately 0.94 with 7-9 PCA components. The performance remains consistently strong, with only slight fluctuations, even as more components are added, maintaining a high level of accuracy. SVM shows competitive performance, peaking around 0.90 with 6-9 PCA components. Accuracy remained relatively stable but with little less after this peak, but slightly below than that of 1D-

CNN. KNN demonstrates consistent performance with a peak accuracy of around 0.88 at 7-10 PCA components but do not match the top performance of 1D-CNN and SVM. RF and LR show moderate accuracy, peaking at about 0.85 and 0.83 respectively with 7-9 components but do not reach the levels of the leading classifiers discussed above. DT Exhibits lower accuracy, peaking around 0.65 with 6-9 components remaining mostly flat and lower throughout, indicating less effectiveness. LDA shows lower accuracy, peaking around 0.62 with 6-9 components mostly flat, indicating less efficacy. Irrespective of classifiers as a whole results show that 9 PCA components exhibit best result.

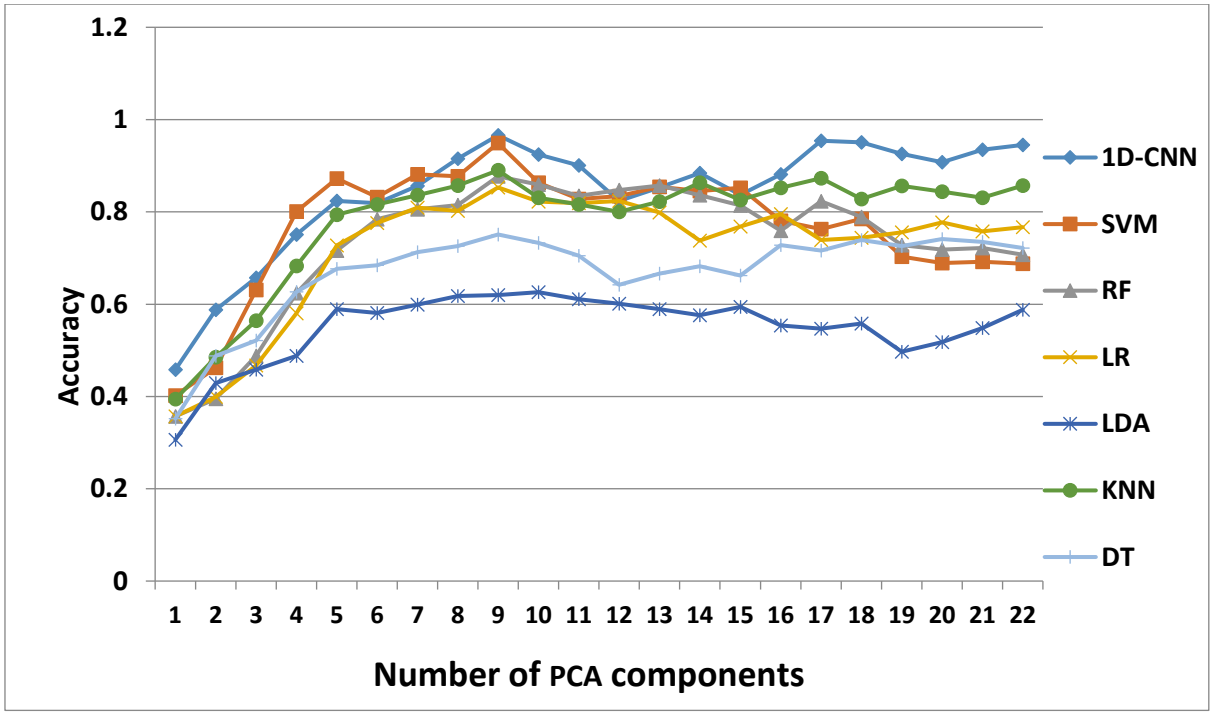

Fig. 6.7. Classification accuracy for various strategies employing various PCA components.

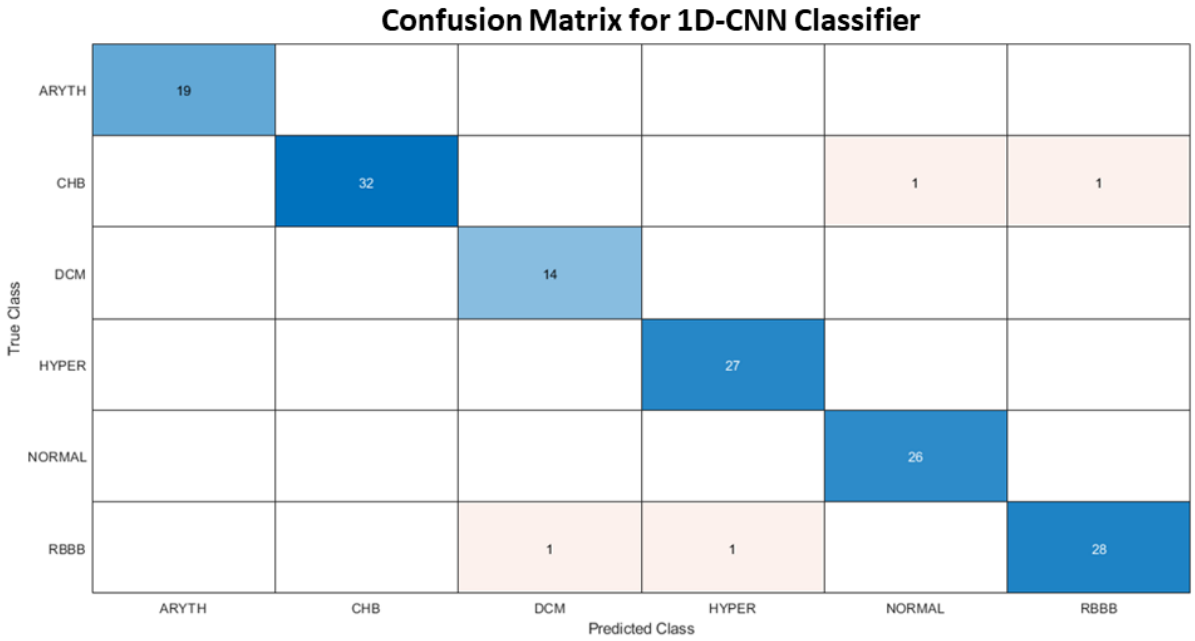

Fig. 6.8. Obtained Confusion Matrix for six classes using 1D-CNN.

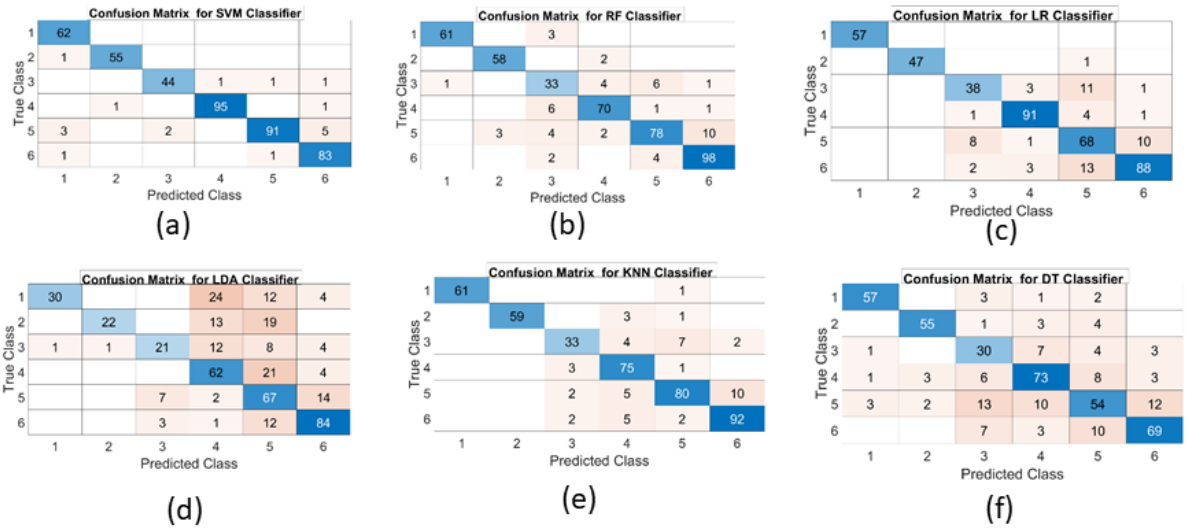

Fig. 6.9. Obtained Confusion Matrix for six classes using ML approaches (Notations for classes are as follows: 1-ARYTH, 2-CHB, 3-DCM, 4-HYPER, 5-NORMAL, 6-RBBB).

1D-CNN successfully identified 28 instances with a minor error with 1 instance incorrectly classified as CHB. CHB and ARYTH reveal no misclassifications for this class, showing good model reliability and having strong performance with 32 and 19 correct classifications respectively. Other performance inferences are very clear in Fig. 6. 8.

Confusion matrices for the six classifiers—SVM, RF, LR, LDA, KNN, and DT—are shown in Fig. 6.9. They are labelled (a) through (f), accordingly. Every matrix shows how well the classifiers performed in accurately predicting the true class of the subject across the six cardiac classes. SVM shows remarkably good performance, especially in classes 4, 5, and 6, where 95, 91, and 83 instances are successfully identified and smaller misclassifications are noted in rest three classes. RF is effective at correctly predicting class 6 with 98 instances with good results also seen in classes 4 and 5, but more noticeable misclassifications than SVM, particularly in class 3. LR reveals that 91, 68, and 88 cases are properly predicted in classes 4, 5, and 6, demonstrating high accuracy in these categories, but greater misclassifications in comparison to SVM. LDA exhibits high confusion, frequent misclassifications, and poorer accuracy across all classes. KNN performs well, especially in class 6, where 92 of the predictions were accurate. There are a few incorrect classifications, but overall, the results are consistent across most classes. Despite having respectable accuracy in classes 4, 5, and 6, DT turns out worse overall and exhibits observable misclassifications in other classes when compared to SVM, RF, and KNN.

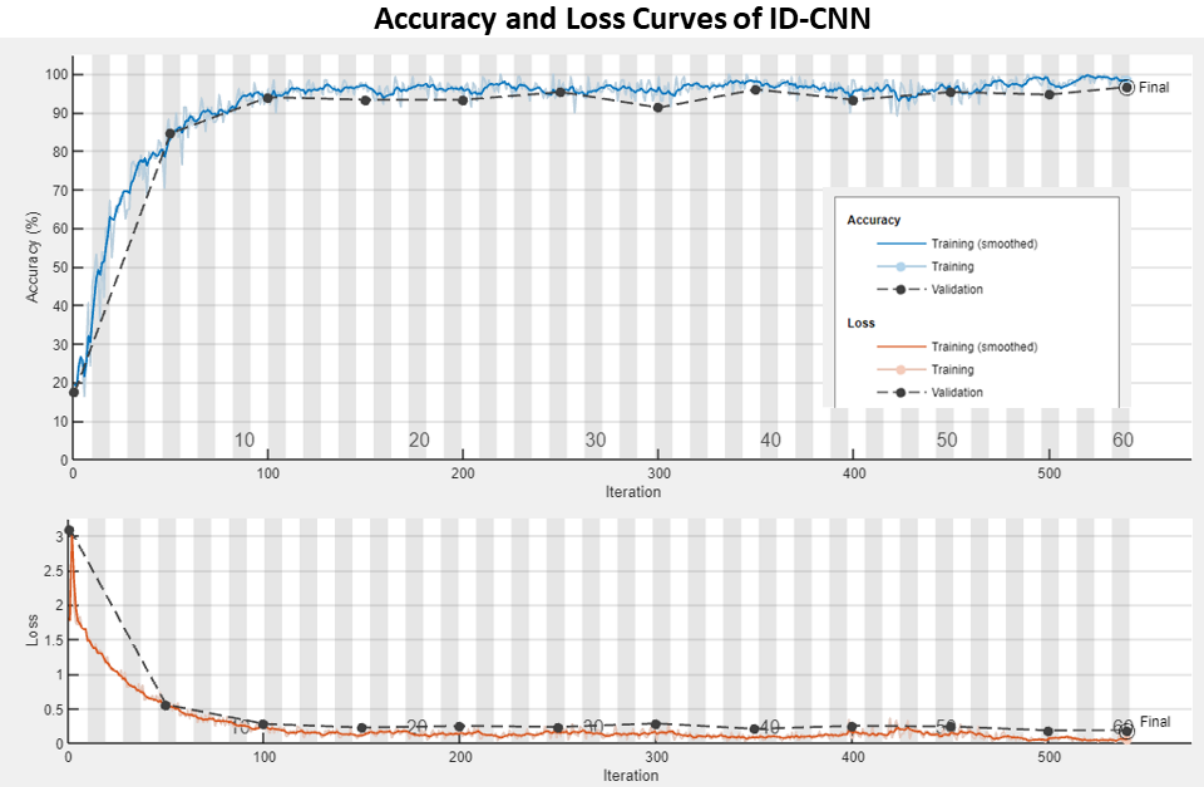

Fig. 6.10. Accuracy and loss curves of 1D-CNN methodology.

Both training and validation accuracy stabilize at 90–95% within the first few iterations in 1D-CNN. The resilience of the model's performance is further demonstrated by a finding that both training and validation losses stabilize at a low value of 0.5 and show little variation between them as shown in Fig. 6.10.

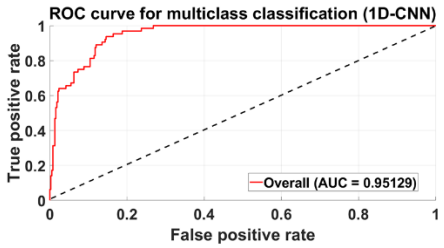

Fig. 6.11. Obtained ROC curve plots for 1D-CNN approach.

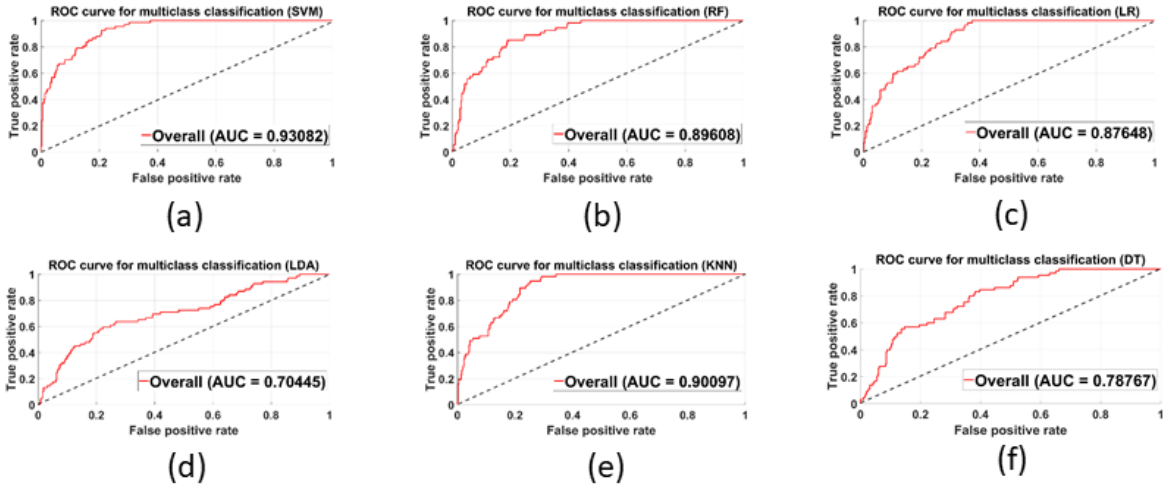

Fig. 6.12. Obtained ROC curve plots for various ML approaches.

The performance of six distinct classifiers (SVM, RF, LR, LDA, KNN, and DT) in a multiclass classification setting is depicted by the ROC (Receiver Operating Characteristic) curves in Fig. 6.12. The "True Positive Rate (TPR) and False Positive Rate (FPR)" for different threshold values are shown in each subfigure, along with the overall Area under the Curve (AUC) score. The SVM classifier achieves the highest AUC score of value 0.93082, indicating it has excellent discriminative ability as the curve's proximity to the upper-left corner indicates a high degree of class distinction. The RF classifier also performed well, with an AUC score of 0.89608 less than SVM. LR performs reasonably well, with an AUC of 0.87648. This shows that it can effectively distinguish between classes despite not being as good as SVM or RF. LDA has the lowest AUC score of 0.704, indicating limited capability to separate the classes. KNN with an AUC of 0.90097 can be effective, particularly when the dataset size or structure favors proximity-based classification. DT with a moderate AUC value of 0.787 demonstrates classification performance that is adequate but not exceptional. But, with an AUC of 0.95129, the 1D-CNN classifier demonstrates a high degree of class distinction ability as shown in Fig. 6.11.

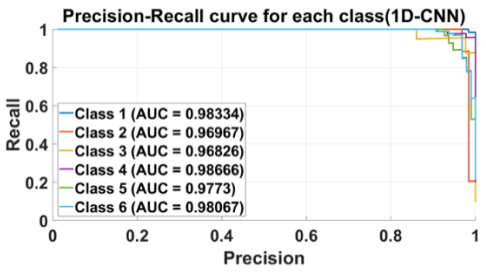

Fig. 6.13. Obtained PR curve plots for various ML approaches.

Across a range of thresholds, each PR curve shows good precision and recall values, particularly for Class 1, Class 4, and Class 6, which have the greatest AUC scores i.e. 0.98 that are more distinguishable than the other three classes in ID-CNN as shown in Fig. 6.13.

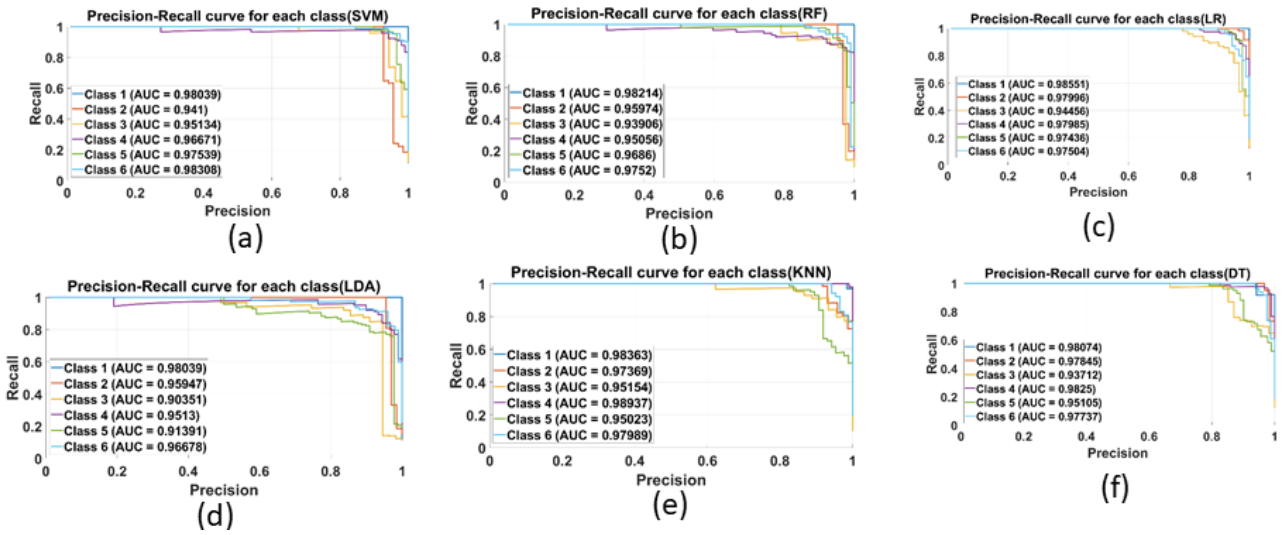

Fig. 6.14. Obtained PR curve plots for various ML approaches. (Notations are as follows: Class 1-ARYTH, Class 2-CHB, Class 3-DCM, Class 4-HYPER, Class 5-NORMAL, Class 6-RBBB).

A thorough examination of the performance of the various classifiers (SVM, RF, LR, LDA, KNN, and DT) across several classes is provided by the precision-recall (PR) curves displayed in Fig. 6.14. SVM exhibited strong precision-recall characteristics, The AUCs are above 0.94 for all classes, highlighting SVM's consistent performance. Class 1 (0.98214) and Class 6 (0.9752) both had excellent AUCs for RF, demonstrating dependable classification. Certain classes exhibit marginally lower AUCs, such as Class 3 (0.9306), indicating performance variability. LR performs exceptionally well, with AUCs for every class near or above 0.95. LDA may be less trustworthy when dealing with complicated datasets according to the lower AUCs even 0.903.KNN achieved its best AUC of 0.989 for Class 4 and varied AUC across other classes. Class 4 has the greatest AUC (0.982), but others like Class 3 are slightly lower (0.937), where the pattern might suggest that DT performs poorly in certain classes and overfits others.

6.5.4.2 Discussion

According to the findings of Table 6.2 and Table 6.3, each classifier performs better overall when ECG and PPG signals are utilized together [148]. The reason for such an improvement is that both characteristics offer complimentary information, which enables classifiers to produce more credible

predictions. In addition, 1D-CNN outperforms other ML methods, which implies that deep learning-based methods are capable of successfully identifying intricate patterns in the data. Competitive performance is also shown by SVM and KNN, particularly when integrating ECG and PPG data. Additionally, SVM and KNN perform competitively, particularly when integrating PPG and ECG inputs. Their performance is marginally inferior to 1D-CNN. RF and LR demonstrate moderate improvements when using combined features, showing their effectiveness for this task. However, their performance is less robust compared to more advanced models like 1D-CNN and SVM. LDA and DT are the least effective classifiers, as they might not be able to fully grasp the intricacy of the complex patterns of various cardiac diseases because of their comparatively straightforward decision-making procedures.

Up to a specific number of PCA components, the majority of classifiers [215], including 1D-CNN, SVM, and KNN, show increased accuracy as shown in Fig. 6.7. The advantages plateaued after this, indicating that these first components adequately capture the essential traits by the most significant nine Eigenvalues for our six cardiac class syndromes. Hence, after nine components, performance typically decreases or fluctuates, demonstrating that more dimensions could produce noise instead of helpful information. Again, across all PCA components, 1D-CNN maintained good accuracy and consistently beat other classifiers, and the strong performance probably is influenced by its capacity to pick up intricate patterns. SVM is the closest competitor, offering stable performance across components and making it ideal for tasks with dimensionality reduction. KNN and RF show moderate accuracy, with KNN slightly ahead, and both remain viable depending on dataset size and features. LDA and DT perform poorly implying these classifiers may not be as suitable for tasks requiring nuanced feature extraction.

Because of the overlap in feature representations between related classes, the diagonal dominance indicates that errors are localized and restricted in 1D-CNN as shown in Fig. 6. 8 confusion matrix. Again, due to the absence of the P wave in the ARYTH class and the presence of more P wave in the CHB class misclassification is rarely shown.

SVM is the most credible classifier in ML approaches due to its superior overall performance, which includes high accuracy across several classes and fewer misclassifications as shown in the confusion matrix in Fig. 6. 9. Similarly, KNN and RF both function well, although they exhibit greater unpredictability. Class 6 is where RF shines, but other classes are a little harder for it to classify. LR performs well in some classes and has a moderate level of accuracy, but it misclassifies more data than SVM. LDA and DT exhibit the poorest performance, with substantial class confusion, especially for LDA. For such a classification problem, these approaches might not be a satisfactory choice. SVM's consistent

performance across all classes makes it a good choice for tasks requiring great precision and stability. Alternatives like RF and KNN may be taken into consideration, particularly if interpretability or computing efficiency are top concerns. Given their reduced robustness and higher misclassification rates, LDA and DT might not be the ideal options for this task; however, they can be enhanced by more training data.

The classifier can successfully learn patterns and features in the data if it can accurately identify the majority of cases in every class. Because of excellent accuracy and low misclassification rates, 1D-CNN [212] appears to be a useful tool for medical diagnostics. Because of its consistent performance, especially for CHB, ARYTH, and RBBB, it is a good choice for practical applications where precise classification is essential. By expanding the feature set or using sophisticated methods like data augmentation or hybrid models to improve predictions for ARYTH and DCM, future developments could concentrate on lowering the few misclassifications that still exist.

The ID-CNN model generalizes effectively to unknown data and steers clear of frequent problems like overfitting or underfitting, as evidenced by its high and steady accuracy and low loss values as shown in Fig. 6.8. The steady fall in loss and increase in accuracy shows a correctly adapted learning rate and optimization approach. The validation performance fluctuated very little, indicating that the dataset is balanced and diversified enough.

Overall, the ROC results reveal that SVM performs robustly across a wide variety of datasets and is the most successful classifier for our cardiac classification job, with the greatest AUC, which represents the degree of separability. KNN and RF also do well, therefore they are good substitutes based on interpretability and computational cost requirements. The worse performance is demonstrated by LDA, indicating that linear approaches might not be as appropriate for this situation. Selecting the best classifier is aided by the variations in AUC ratings; classifiers that perform better overall are preferred when their AUC is closer to 1. Fig. 6.11 and Fig. 6.12 clearly shows for this classification assignment, 1D-CNN [212] is quite dependable since it accurately detects positive cases while reducing false positives and outperforming other models (like SVM, RF, LR, etc.) due to the ability to capture intricate patterns in the data, leading to improved generalization and accuracy from deep learning approaches.

The model's effectiveness in minimizing false positives is reflected in the high precision values, while the high recall values indicate a corresponding reduction in false negatives in 1D-CNN by taking in consideration of PR.

PR results imply that the specific class imbalances and the necessary balance between precision and recall [148] will determine the best classifier choice. According to Fig. 6. 13 and Fig. 6,14, while RF provides a dependable substitute, LR and SVM, would be better for tasks needing high overall accuracy. While KNN and DT exhibit moderate efficacy, LDA seems to have trouble with intricate class separations, suggesting that it might not be as useful for this particular task.

When working with imbalanced (each class has a roughly unequal number of samples) datasets, the ROC curve is less relevant and offers a global perspective of the model's performance across all potential thresholds. When the emphasis is on the performance of positive predictions, particularly in imbalanced datasets, PR curves are more helpful than ROC curves. They also aid in understanding the trade-off between precision and recall, particularly for tasks where false positives (low precision) or false negatives (low recall) have substantial repercussions.

So, despite the high AUC values, further information from metrics like the confusion matrix, F1-score, or misclassification analysis can help improve performance for poorly performed classes.

Because it sees that pattern more frequently, a model trained on this dataset may consistently predict that class and reach high accuracy, but fall short of what counts—identifying the lesser sample containing classes.

Table 6.4

Evaluation of the suggested classification model with the existing state-of-the-art techniques/approaches. (Notations are as follows: Accuracy-Accu, Sensitivity-Sens, Specificity-Spec, Precision-Prec, Area under ROC curve- A-ROC, and Area under PR curve- A-PR)

Year	**Methodology**	**Database Used**	**Performance Indices**						
			Accu	**Recall/ Sens**	**Spec**	**Prec**	**F1-score**	**A-ROC**	**A-PR**
2023	DCNN [148]	Hospital data	0.800	0.750	0.85	0.730	0.78	0.79	0.76
2023	1D-CNN+ BiLSTM [4]	MIMIC III	0.950	0.85	NR	0.880	0.84	0.99	NR
2023	ANN [150]	Hospital data	0.925	100	0.818	NR	NR	0.926	NR
2022	GACNN [151]	Hospital data	0.92	0.91	0.900	0.91	0.92	0.93	0.92
	*Proposed (1D-CNN)	MIMIC III	0.966	0.964	0.993	0.966	0.963	0.951	0.977
	*Proposed (SVM)		0.949	0.949	0.989	0.95	0.949	0.930	0.966
	*Proposed (RF)		0.877	0.873	0.974	0.881	0.875	0.896	0.962
	*Proposed (KNN)		0.89	0.883	0.977	0.893	0.887	0.900	0.970
	*Proposed (1D-CNN)	Hospital data	0.974	0.971	0.995	0.966	0.975	0.957	0.981

We quantitatively contrast our approach with state-of-the-art techniques/approaches discussed in earlier related publications to show how well our suggested method classifies cardiac diseases. Table 6.3 briefly shows the outcomes of related works. Pal et al. [148] in the first row achieved the least performance with Accu=0.800, Sens=0.75, Spec=0.85, Prec=0.73, F1-score=0.78, A-ROC=0.79, A-PR=0.76 by using fused ECG and PPG signals through DCNN. Little better performance was achieved in [4] , [150]. Again performance was enhanced by using Graph attentive CNN (GACNN) [151]. The last part of Table 6.3

shows that our suggested network outperforms all of the earlier approaches, displaying the greatest values for the shown performance indices including MIMIC III data and real-time hospital data. The 1D-CNN model's resilience in managing multiclass classification assignments is undoubtedly better than SVM, RF, and KNN classifiers. The performance results of LDA, DT, and LR, are not that credible and hence are not shown in Table 6.4, but in the result and discussion part, we have included them for study purposes.

6.6 Classification of Cardiac Abnormality using PPG Fiducial Parameters and Probabilistic Neural Network

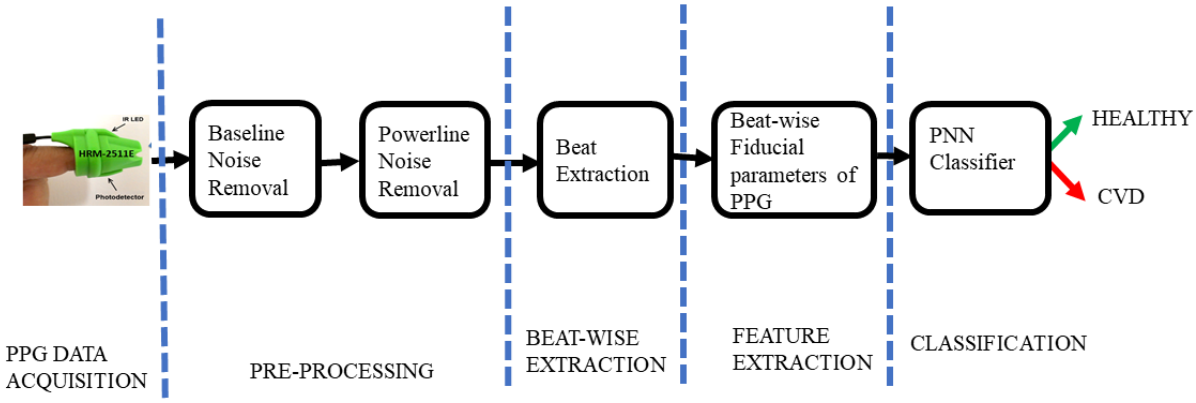

Fig. 6.15. Detail work flow diagram of the proposed work for classification of cardiac abnormalities.

Physiological activities of organisms are the various biomedical signal's observations. Processing of these signals help in finding various cardiovascular diseases and other heart related cardiac syndromes.

PPG is an optical biosensor used in measuring the amount of light absorption and reflection by blood vessels or tissues in our flesh, which quantifies the presence of blood in the optical path. It is a high informative signal, not only covering the activity of the heart's systolic and diastolic phases, but also the hemodynamicity and related network information of the peripheral microcirculation system. Thus, it is externally manifesting of various important physiological parameters in the cardiovascular system like heart rate, BP, cardiac output, and microcirculatory blood flow. A typical PPG waveform contains the systolic phase and diastolic phase separated by dicrotic notch. The systolic peak defined by the amplitude of PPG waveform is used to calculate heart rate. The pulsatile changes in blood volume are indicated in systolic amplitude. Stiffness index is a measure of arterial stiffness and depends on the age and height of the subject/person . It is obtained from systolic peak and diastolic peak. Crest time is defined as duration

of time from the base of PPG waveform to its peak. In various time-domain processing methods these parameters of PPG signal are used, like peak detection, transition point calculation etc. Pulse transit time (PTT) [216-218] , gives information of BP. Cardiovascular disease is a sort of disease that involves blood vessels (arteries) and blood pumping station (heart). Cardiovascular disease includes Hypertension, Heart failure, Ischemia, Myocardial infarction, Chronic obstructive pulmonary disease (COPD) and many more. Hypertension occurs when heart pumps more blood and the arteries are narrow causing high force against the artery wall and highly changes the systolic and diastolic pressure. It may be prehypertension (mild), stage 1 (moderate) and stage 2 (severe**).** Heart failure happens, when according to the body requirement, if the heart muscle is inefficient to pump such amount. Ischemia causes mainly for stiffening of arteries (atherosclerosis) due to fat deposition and ultimately narrowing the artery causing restricted or reduced blood flow in the different parts of the body. Heart attack, which is medically termed as Myocardial infarction is a deadly cardiac abnormality causes as plaque deposits inside the artery and consequently the heart muscle deprives of sufficient blood. Chronic obstructive pulmonary disease (COPD) is an inflammatory lungs disease, which progressively damages the lungs. Severe COPD can lead to heart failure in the ventricle part of the heart.

The vital risk factors [219] for heart diseases cause due to obesity, physical inactivity, unhealthy food habit, previous family history of cardiac syndrome, consumption of alcohol, gender, age etc. raised not only blood pressure (hypertension) but also raised blood sugar (diabetes mellitus) and raised blood cholesterol (hyperlipidemia).

Principal component analysis (PCA) can Classify and authenticate the cardiac abnormality, where the fiducial parameters of PPG (e.g., features) are dimensionally reduced. For automated diagnosis, these dimensionally reduced features were fed to the Support Vector Machine (SVM) [220-221], neural network (NN) [221, 211] and probabilistic neural network (PNN) classifiers [222-223] for automated diagnosis. In the present work, our proposed cardiac abnormality detection approach comprises several stages as (1) Remove motion artefacts and noise from raw PPG signals, (2) Determination of fiducial parameters (e.g., Systolic, Diastolic Dicrotic notch time and amplitude, Diastolic phase time PPG augmented index and pulse transit time) of PPG waveform for each cycle of patients having different cardiac abnormalities. These fiducial parameters are considered as features of cardiac abnormality. Here five types of cardiac disorders (e.g. Hypertension, Heart failure, Ischemia, myocardial infarction, Chronic obstructive pulmonary disease (COPD)) are considered .The class labels (e.g. Class-1 as Hypertension,Class-2 as Heart failure,Class-3 as Ischemia, Class-4 as Myocardial Infarction and Class-5 as COPD) are assigned against each cardiac abnormality, (3) training PNN with these fiducial parameters as input and target

classes as output and (4) lastly, for given fiducial parameters of unknown PPG waveform , prediction of the class which may fall into known classes. This unsupervised approach allows us to recognize anomalies without going through explicitly any complex analysis. Here for each cardiac disorder, PPG waveforms of 5 patients are captured over 2 minutes of time span. The fiducial parameters for each cycle are computed using alignment by 2nd order derivative method. The accuracy of PNN classifier is found to be very high as > 95%.

Arrhythmia (cardiac abnormality) detection algorithms from the features of PPG may potentially serve as a viable alternative to ECG based algorithms [224] [225] and gained the traction in current years. As PPG devices are wearable cum handy, tiny size and can be worn continuously with much comfort, PPG based cardiac disorder detection algorithms are potentially advantageous over ECG-based methods, so motivate us in a novel way to classify the 5 class disorders with better accuracy with PNN classifier. As the antiarrhythmic therapies are not analogous, Knowing the type of arrhythmia causing the stroke is much better solution to rescue life.

6.6.1 PPG Data Acquisition

Here five types of cardiac disorders (e.g. Hypertension, Heart failure, Ischemia, myocardial infarction, Chronic obstructive pulmonary disease (COPD)) are considered. Here for each cardiac disorder, PPG waveforms of 5 patients are captured over 2 minutes of time span. Placement of LED and PD shown in Figure 1(a) and its corresponding light attenuation by tissue is shown in Figure 1(b). Our work is done with a typical Photoplethysmography (PPG) sensor (HRM- 2511E Easy pulse version 1.1) topology shown in Figure 2. It is used to illuminate the index finger i.e., from skin surface by a IR LED source in one side and placed a photodetector in opposite side in a non-invasive manner to capture the change in transmitted light intensity to retrieve the vital information of cardiovascular system. The photo detector variation signal is a function of volumetric blood change in the tissue. The clean PPG signal is acquired by two stage filtering and amplification using MCP6004 Op-Amp. Then the analog channel of embedded microcontroller (ATMEGA328) was connected with the sensor signal to capture the human subject signal at sampling frequency of 250 Hz for a duration of 2 minutes. Through a USB cable the microcontroller is connected to a PC to give data file (.txt) format. The rest noise part is eliminated by band pass filtering using wavelet method in MATLAB. The PPG signals are captured from 5 normal and 25 cardiac abnormal persons of 5 different classes such as Hypertension, Heart failure, Ischemia, Myocardia, COPD .The subjects are male and female from age group of 40 years to 74 years of NH Rabindranath Tagore, International Institute of Cardiac Sciences, Kolkata.

6.6.2 Result and analysis

6.6.2.1 Result of PNN classification

The PPG waveforms are captured for 2 minutes with sampling frequency of 250 Hz, from right index finger with almost no movement of hand, from 25 patients (5 patients from each class) covering a age group of 40-74 years both male and female. Then these data is filtered with a BPF at 2 Hz and 40 Hz. As shown in Fig. 6.16. (a).

Then to extract each beats or cycles from the waveform, peaks and crests are marked as shown in Fig. 6.16. (b). Subsequently first and second derivative [23-24] of each beat is calculated to show the inflection points of systolic, diastolic and dicrotic notch as shown in Fig. 6.16. (c). After getting these points all other 9 fiducial points are calculated as shown in Table I and stored in a beat-matrix form. If the PPGAI value is like: (If, PPGAI >0.75, then non-CVD, If 0.5<PPGAI<0.7 there is probability of CVD and if PPGAI<0.5, then a cardiac patient [226]. As all our cases are CVD, we are getting PPGAI<0.5. These 9 fiducial parameters for all 5 classes are taken as the training input to the PNN network. The testing is done with the unknown class, and the accuracy result is > 95% as shown in Table 6.6. The comparison of the work done in this paper has been compared with the existing work as shown in the Table 6.7.

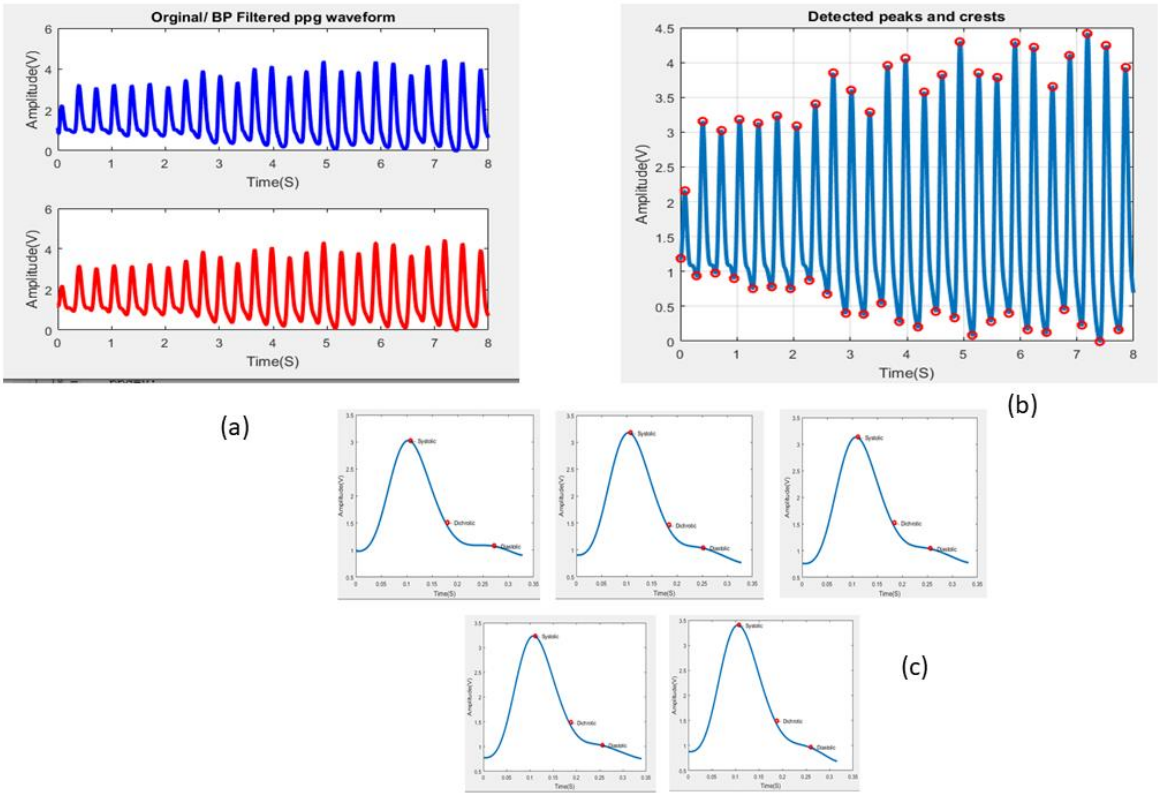

Figure. 6.16. Class 1 (Hypertension): ID: 66_Year_Male (a) raw and filtered PPG Figure 7. (b). peak and crest for 2000 samples Figure 7. (c). 5 beats shown with systolic, diastolic and dicrotic fiducial points.

Table 6.5.

Results showing fiducial parameter values for 5 beats

Class 1 (Hypertension): ID: 66_Year_Male_ppg									
Beat No.	**Fiducial Parameters as feature Target**								
	SYSTOLIC		***DICROTIC***		***DIASTOLIC***		***DLP(S)***	***PPGAI***	***PTIME(S)***
	TIME(S)	***PEAK(V)***	***TIME(S)***	***PEAK(V)***	***TIME(S)***	***PEAK(V)***			
1	0.112	3.150	0.184	1.629	0.288	1.084	0.176	0.516	0.332
2	0.108	3.020	0.180	1.514	0.272	1.078	0.164	0.500	0.332
3	0.116	3.086	0.196	1.420	0.276	1.064	0.160	0.460	0.336
4	0.108	3.404	0.188	1.496	0.260	0.961	0.152	0.439	0.320
5	0.116	3.292	0.188	1.446	0.256	0.848	0.140	0.439	0.324
Class 2 (Heart Failure): ID: 59_Year_Female_ppg									
1	0.128	1.223	0.200	0.560	0.332	0.1237	0.204	0.457	0.352
2	0.132	1.231	0.200	0.565	0.332	0.1175	0.200	0.459	0.344
3	0.136	1.259	0.208	0.597	0.336	0.1428	0.200	0.474	0.352
4	0.132	1.219	0.276	0.125	0.336	0.0536	0.204	0.102	0.348
5	0.136	1.250	0.208	0.557	0.332	0.143	0.196	0.445	0.348
Class 3 (Ischemic): ID: 67_Year_Male_ppg									
1	0.108	0.316	0.176	0.113	0.280	0.0181	0.172	0.357	0.312
2	0.108	0.324	0.180	0.106	0.284	0.0125	0.176	0.329	0.316
3	0.112	0.289	0.172	0.133	0.280	0.0334	0.168	0.460	0.316
4	0.112	0.288	0.176	0.140	0.268	0.0523	0.156	0.488	0.308
5	0.104	0.306	0.172	0.133	0.272	0.0431	0.168	0.434	0.308
Class 4 (Myocardia): ID:73_Year_Male_ppg									
1	0.136	0.844	0.276	0.193	0.420	0.0144	0.284	0.228	0.444
2	0.124	0.802	0.252	0.220	0.380	0.0342	0.256	0.274	0.408
3	0.120	0.752	0.256	0.169	0.360	0.0268	0.240	0.224	0.392
4	0.116	0.774	0.260	0.159	0.348	0.0319	0.232	0.206	0.380
5	0.116	0.726	0.260	0.132	0.392	0.0176	0.276	0.182	0.408
Class 5 (COPD): ID: 40_Year_Female_ppg									
1	0.104	1.350	0.168	0.821	0.212	0.4513	0.108	0.608	0.260
2	0.104	1.316	0.168	0.826	0.220	0.4095	0.116	0.627	0.272
3	0.104	1.364	0.172	0.802	0.216	0.4484	0.112	0.588	0.264
4	0.108	1.424	0.172	0.859	0.220	0.4344	0.112	0.603	0.280
5	0.108	1.491	0.172	0.918	0.220	0.4962	0.112	0.615	0.272
Normal: ID: Normal_51_Year_Male_ppg									
1	0.156	0.631	0.432	0.165	0.544	0.0458	0.388	0.792	0.580
2	0.176	0.788	0.428	0.261	0.588	0.0782	0.412	0.740	0.632
3	0.172	0.774	0.404	0.280	0.592	0.0424	0.420	0.823	0.644
4	0.164	0.720	0.428	0.212	0.548	0.0730	0.384	0.799	0.600
5	0.164	0.699	0.396	0.288	0.556	0.0753	0.392	0.724	0.060

Table 6.6

Classification results obtained using PNN

Sl No.	**Nature of cardiac abnormality**	**Unknown (e.g.)**	**Accuracy (%)**
1	Hypertension	ID: 50_Years_Female_ppg	98
2	Heart failure	ID: 71_years_Male_ppg	100
3	Ischemia	ID: 42_Years_Female_ppg	97
4	Myocardia	ID: 58_Years_Female_ppg	96
5	COPD	ID: 40_Years_Male_ppg	95
6	Normal	ID: _51_Year_Male_ppg	98

6.6.2.2 Discussion

In present work, the PPG signal has been considered for classification and authentication of cardiovascular disease (CVD) by PNN classifier, without ECG signal as it is known that, PPG signal captured by optical non-invasive method is easy and simple than that in ECG signal. In present work, which captures PPG signal from right hand index finger for 2 minutes has been processed by removing baseline wonder and noise. Then fiducial parameters (e.g., Systolic, Diastolic, Dicrotic, PPGAI and PTT etc.) of PPG signal have been noted beat(cycle) -wise. The attempt has been made to analysis the cardiac abnormality against fiducial parameters (e.g. Systolic, Diastolic, Dicrotic, PPGAI and PTT etc.) of PPG as necessary features by experiences of practicing cardiologists. When the heart muscle starts contraction, as a result blood flows in the peripheral tissues and then, subsequently changes the mentioned fiducial parameter of PPG over every cycle or beat. A PNN is used for classification of CVD due to its obvious robustness.

The PNN is trained with feature data and target class with suitable spread parameter (e.g., 0.8). The target class index value corresponds to the CVD abnormality (e.g., Hypertension, Heart failure, Ischemia, Myocardial infarction, Chronic obstructive pulmonary disease *(*COPD)). Here only 5 types of CVD abnormalities are considered. But data sets for more abnormalities can also be used in future work.

Table 6.7.

Comparison of our work with existing work.

Ref No.	**Method**	**Accuracy (%)**
[227]	SVM	97.674
	Logistic Regression	86.046
	ANN	95.348
	Decision Tree	95.338
	Random Forest Regressor	93.02
Our work	PNN	95-100

The PNN is tested by fiducial parameters of unknown PPG signal whose class will be predicted. The result shows that accuracy of authentication of unknown class is about 95-100%. PPGAI indirectly measures the arterial stiffness. By virtue of reduced elastic artery compliance an early return of reflected wave, which arrives to systole rather than in diastole, causing a disproportionate rise in systolic pressure and an increase in pulse pressure, with a consequent increase in left ventricular after load and a decrease in diastolic blood pressure and impaired coronary perfusion. For this vital cause, healthy people gets a higher PPGAI in comparison to the CVD people. Our result validates these 5 class classification nicely. From the analysis, it is found that the PPG can replace the ECG method of diagnosis and other heart disease detection systems. Thus, for the ease of measurement and low cost, it can be concluded that, PPG can be efficiently used for any cardiac disease assessment by combining with the advanced machine learning techniques.

6.7 Summary

To classify cardiovascular diseases (CVDs), this study proposes a CNN-based and machine-learning method that uses composite features taken from both PPG and ECG data. The model can identify more detailed patterns about heart health because of the wider feature set that resulted from the merging of these two signals. Using a 1D-CNN and machine learning techniques, the method successfully differentiates between different cardiovascular disorders. The findings indicate that composite signal analysis improves diagnostic precision since the combination of ECG and PPG data produced excellent accuracy when processed using PCA and classified using the 1D-CNN. The results indicate that 1D-CNN is the most effective classifier for data processed through PCA, particularly when utilizing nine components. For tasks where computational efficiency is a concern, SVM could serve as a robust alternative with slightly less complexity followed by RF and KNN. This dual-signal technique increased classification performance across numerous CVD categories when compared to earlier methods that just used ECG or PPG. Additionally, in wearable or portable health monitoring devices, this technique may also be a useful tool

for real-time CVD diagnosis, enabling early detection and ongoing monitoring. To enhance classification accuracy and practical applicability, future research can focus on refining feature extraction techniques, bolstering model robustness, and exploring additional signal modalities to improve performance. Efforts could also include implementing regularization methods, employing data augmentation strategies, or developing hybrid models to minimize the remaining instances of misclassification. By using this paradigm to determine the most prevalent cardiac illnesses doctors will be more competent and spend less time treating those struggling with CVD. By using this paradigm to determine the most prevalent cardiac illnesses doctors will be more competent and spend less time treating those struggling with CVD. Also PNN is a good classifier for CVD or non-CVD class distinguish for some diseases like Hypertension, Heart failure, Ischemia, Myocardia, COPD with only utilizing PPG signal with good accuracy > 95 %.

Chapter 7

Conclusions and Future Scopes

7.1 Conclusions

Across the entire world, cardiovascular diseases (CVDs) are the main cause of death. The unavailability of enough health care systems and the work stress and casual lifestyle hinder routine health check-ups and precise diagnoses. A key issue has been the requirement for a prompt, affordable, and precise diagnosis, treatment and cure at the early stage at a fair price to enhance human health. ECG, phonocardiogram (PCG), and PPG are the different well-known modalities to monitor heart malfunction. ECG devices are well-established tools in clinical diagnostics. Again PPG signal is considered over the PCG signal for cardiovascular disease monitoring distinctively in respect of methods in the thesis are noted below.

- Ease of Acquisition
  - PPG: Acquired non-invasively with the use of inexpensive, basic optical sensors (such as devices worn on the wrist or fingertip).
  - PCG is more difficult to utilize outside of clinical settings because it requires sensitive Acoustic sensors (microphones) and is more vulnerable to background noise.

- Signal Quality and consistency
  - Even in ambulatory conditions, PPG offers waveforms that are comparatively clear and constant.
  - PCG: The quality varies due to its high dependence on body habitus, stethoscope location, and outside noise.

- Rich in Hemodynamic Information
  - PPG is a rich source of hemodynamic information. It provides information on heart rate variability, pulse transit time (PTT), arterial stiffness, and blood pressure trends by reflecting variations in peripheral blood volume. These characteristics are helpful in identifying CVD markers and are directly related to cardiovascular health.
  - PCG records mechanical heart sounds (S1, S2, and murmurs), which is helpful for valvular

problems in particular, but it provides less reliable hemodynamic data for wider populations.

- Easier Signal Processing
  - Systolic and diastolic peaks form distinct waveforms in PPG data, making them simpler to process with deep learning or traditional methods.
  - PCG signals require sophisticated signal separation and filtering due to their complexity and overlapping valve sounds (S1, S2, murmurs).

- Better for Remote and Wearable Monitoring
  - For wearable technology, such as fitness bands and smartwatches, PPG is perfect.
  - PCG is not as well suited for home-based or continuous monitoring.

So, While PCG remains important in diagnosing structural heart conditions (e.g., valve diseases like stenosis (narrowing), Atresia (failure to form) etc), PPG takes the lead when it comes to continuous, quantitative, and remote cardiovascular monitoring (arterial stiffness analysis, blood pressure measurement, and arrhythmia identification etc) offering rich, easily processed hemodynamic data through affordable, wearable sensors through various morphological patterns of CVDs.

The study's conclusions highlight the revolutionary possibilities of incorporating cutting-edge techniques by considering ECG and PPG signals for data reduction, prediction, and categorization of CVD into telemedicine. By providing real-time, low-power, and scalable solutions, these technologies not only increase the effectiveness and dependability of remote healthcare services but also lessen the strain on healthcare infrastructure. This thesis work presents the interaction of IoT technology, machine learning, deep learning and signal processing methods, which lays a solid basis for further developments in the health care area.The following is a list of the contributions made by this thesis enumerated as follows:

a) Chapter 4 introduces a new framework for significant progress in shrinking the PPG and ECG data sizes without sacrificing diagnostic information by employing effective compression methods. Segmented Gaussian model algorithms that can compress ECG and PPG signals are being developed to assure interoperability with various telemedicine frameworks, opening the door to improved healthcare accessibility. Additionally, combining cloud-based systems like Dropbox with Fourier and Gaussian models has made it possible to handle massive amounts of medical data in a secure and scalable manner. The major findings are noted below:

i. We have suggested using two, six, and two Gaussian functions per cardiac cycle, respectively, to fit ECG signals with three segments (P wave, QRS complex, and T wave)
ii. PPG is also fitted with six Gaussian functions that carry the systolic and diastolic peaks for each beat, without any segmentation.
iii. The robustness of the technique is illustrated by validation using a variety of cardiovascular syndromes (RBBB, Hyper, Ary-atrfab, DCM) and normal patients from the MIMIC III database, MIT-BIH database and by the real-world dataset with the performance evaluation indices i.e., CR, PRD, PRDN, QS, CC, SNR, RMSE, and execution time.
iv. Applicability of Gaussian and Fourier models on the PPG signal for data compression for IoT applications to access it by doctors from remote areas patients.
v. Various morphological pattern diversity signals like Myocardial Infarction, Ischemia, Hypertension and normal signals have been compressed and retrieved person from a data acquisition system by HRM-2511E Easy pulse version 1.1(PPG sensor).

b) Chapter 5 highlights the significance of extracting fiducial parameters from physiological signals by the prediction approaches. With the use of statistical techniques like Gaussian Process Regression and neural network models like RBNN and GRNN, this study has shown a high degree of accuracy in identifying critical indicators necessary for the diagnosis of CVD. By reducing the need for multiple monitoring devices and improving system scalability, the ability to predict ECG parameters from PPG signals has considerably simplified the diagnostic procedure. The findings and evaluations offered support the approaches' dependability and robustness in telemedicine and clinical settings. The major findings are noted below:

i. The current state of the art proposes mitigating the cost and easy diagnosis by physicians with the use of low-cost photoplethysmograph (PPG), which will deliver ECG information in terms of ECG fiducial parameters.
ii. Gaussian process regression-based approach has been applied to the dataset of MIMIC-III matched paired datasets of PPG/ Lead-II ECG signals with CVD forVarious morphological pattern diversity signals like Hypertension, DCM, CHB,RBBB, and Arythmia-atrial fibrillation and normal signals have been studied to predict ECG parameters.
iii. Radial Basis Neural Network (RBNN) and General Regression Neural Network(GRNN) based fiducial parameter extraction was done for PPG signal through Gaussian model parameters.

iv. The proposed fiducial parameter prediction system has been obtained with high BP or Hypertension cardiac syndrome person from a data acquisition system by HRM-2511E Easy pulse version 1.1(PPG sensor).

c) Chapter 6 illustrates new approaches to disease detection and classification of CVD types using machine learning and deep learning techniques. By taking advantage of the temporal and spatial characteristics of ECG and PPG signals, 1-D CNNs and composite feature engineering have improved detection capabilities. This algorithms used to categorize unknown types of CVD have shown themselves to be accurate and flexible, guaranteeing that telemedicine systems can treat a variety of patient problems. The performance measures highlight how well these methods work for early disease detection, which is essential for prompt intervention and therapy. The major findings are noted below:

i. Applicability of ML and 1D-CNN model for authentication of class of CVD and non CVD by combined features of ECG and PPG signals.
ii. Various morphological pattern diversity signals like Hypertension, DCM, CHB,RBBB, and Arythmia-atrial fibrillation and normal signals haves been studied person from the hospital, NH Rabindranath Tagore, International Institute of Cardiac Sciences, Kolkata with a data acquisition system by HRM-2511E Easy pulse version 1.1(PPG sensor) and Biopac ECG sensor and also verified by open database MIMIC III from physionet.
iii. Applicability of PNN models on the PPG signal for data classification of CVD and non CVD with various morphological pattern diversity signals like Hypertension, Heart failure, Ischemic, Myocardial Infarction, COPD and normal signals haves been studied person from the hospital, NH Rabindranath Tagore, International Institute of Cardiac Sciences, Kolkata with a data acquisition system by HRM-2511E Easy pulse version 1.1(PPG sensor)
iv. Proposed classifier system has achieved higher performance indices using PNN classifier for PPG signals only.

Deploying the suggested model in real-world, real-time contexts poses several limitations and challenges even if it performs satisfactorily in the evaluations and stands in a better position than state-of-the-art methods. They are as follows:

- Signal noise and artifacts

  Power line interference, baseline drift, motion artifacts, and other forms of noise can affect physiological signals like ECG and PPG. These distortions have the potential to decrease model accuracy, especially in ambulatory or wearable contexts. Even though this work includes preprocessing techniques like S-Golay filtering, lowpass filtering, bandpass filtering and wavelet denoising, real-time signal variability still needs adaptive filtering or artifact correction algorithms.

- Sensor Variability

  Different sensors vary in sampling rate, sensitivity, and placement accuracy. These differences can affect signal morphology and consequently model generalizability. Cross-device variability was not comprehensively addressed in this study, and future work should involve model retraining and validation across a diverse set of sensors.

- Latency in Real-Time Monitoring

  There is a delay due to signal acquisition buffer, preprocessing, and inference time. Despite its efficiency in batch processing, the existing model pipeline creates a delay when used for continuous real-time monitoring. Signal acquisition buffer, preprocessing, signal segmentation, and model inference time are the causes of this lag. Optimization strategies, including deployment on edge computing platforms and lightweight neural architectures, have yet to be explored further for clinical applications.

To sum up, the approaches created in this research offer a strong foundation for expanding the use of telemedicine in cardiovascular treatment. This study makes a substantial contribution to the development of effective, dependable, and scalable telemedicine solutions by tackling the problems of data compression, predictive modeling, and disease classification. The way cardiovascular diseases are identified, tracked, and treated might be completely changed by incorporating these methods into healthcare systems. This would ultimately improve patient outcomes and lessen the burden of CVD worldwide.

7.2 Future scopes

The findings in this dissertation may serve as a foundation for additional studies on CVD monitoring and disease diagnosis using both ECG and PPG for telemedicine applications. Despite the existence of numerous published research studies, no specific approach is ideal for CVD compression, prediction, and classification. By taking into account certain difficult instances in future research, there is perpetually scope for improvement in the early detection and diagnosis of CVD. Research can be done to further improve early detection of CVD with the aid of new technologies, even though this thesis work developed various neural network, machine learning, and deep learning-based algorithms using the morphological operations of ECG and PPG signals for the CVD diagnose system.

i. Future research can build upon this work by exploring the real-time implementation of the proposed methodologies in large-scale clinical settings with versatile morphological patterns of cardic diseases.
ii. The integration of these techniques with next-generation IoT devices and wearable technologies offers exciting possibilities for personalized healthcare. Additionally, further enhancements in machine learning models, such as the use of advanced deep learning architectures and transfer learning, can improve the accuracy and generalizability of CVD detection systems.
iii. The incorporation of multimodal data, including imaging and genetic information, can also be explored to provide a more holistic approach to CVD diagnosis and management.
iv. Future research can develop AI models integrating ECG and PPG features to identify multi-cardiac diseases of one patient for early detection and personalized treatment.

References

[1] F. Torrent-Guasp, M. Kocica, A. Corno, M. Komeda, F. Carreras-Costa, A. Flotats, J. Cosin-Aguillar, and H. Wen, "Towards new understanding of the heart structure and function," *Eur. J. Cardio-Thorac. Surg.*, vol. 27, pp. 191–201, 2005. [CrossRef] [PubMed].

[2] O. Monfredi, H. Dobrzynski, T. Mondal, M. Boyett, and G. Morris, "The anatomy and physiology of the sinoatrial node—A contemporary review," *Pacing Clin. Electrophysiol.*, vol. 33, pp. 1392–1406, 2010. [CrossRef] [PubMed].

[3] R. Drew and L. Sinoway, "Autonomic control of the heart," in *Primer on the Autonomic Nervous System*, Elsevier, Amsterdam, The Netherlands, 2012, pp. 177–180.

[4] B. Aldughayfiq, F. Ashfaq, N. Z. Jhanjhi, and M. Humayun, "A Deep Learning Approach for Atrial Fibrillation Classification Using Multi-Feature Time Series Data from ECG and PPG," *Diagnostics (Basel)*, vol. 13, no. 14, p. 2442, 2023, doi: 10.3390/diagnostics13142442.

[5] "Types of hypertension," [Online]. Available: https://www.medicalnewstoday.com/articles/types-of-hypertension.

[6] C. Antzelevitch and A. Burashnikov, "Overview of basic mechanisms of cardiac arrhythmia," *Card. Electrophysiol. Clin.*, vol. 3, pp. 23–45, 2011.

[7] D. G. Fu, "Cardiac Arrhythmias: Diagnosis, Symptoms, and Treatments," *Cell Biochem. Biophys.*, vol. 73, pp. 291–296, 2015, doi: 10.1007/s12013-015-0626-4.

[8] C. R. Wyndham, "Atrial fibrillation: the most common arrhythmia," *Texas Heart Institute Journal*, vol. 27, no. 3, pp. 257–267, 2000.

[9] R. Gupta, M. Mitra, and J. Bera, *ECG Acquisition and Automated Remote Processing*, Springer, 2014, doi: 10.1007/978-81-322-1557-8.

[10] Y. Yang, J. Zhu, and P. Zhu, "SpO2 and Heart Rate Measurement with Wearable Watch Based on PPG," in *IET International Conference on Biomedical Image and Signal Processing*, IEEE, 2015.

[11] G. Chan, P. Middleton, and G. Celler, "Automatic detection of left ventricular ejection time from a finger photoplethysmographic pulse oximetry waveform, Comparison with Doppler aortic measurement," *Physiol. Meas.*, vol. 28, pp. 1–14, 2007.

[12] T. Toshiaki, K. Tomoyuki, K. Masao, and I. Chikao, "Utility of Second Derivative of the Finger Photoplethysmogram for the Estimation of the Risk of Coronary Heart Disease in the General Population," *Circ. J.*, vol. 70, pp. 304–310, 2006.

[13] J. Hashimoto, K. Chonan, and Y. Aoki, "Pulse wave velocity and the second derivative of the finger photoplethysmogram in treated hypertensive patients: their relationship and associating factors," *J. Hypertens.*, vol. 20, no. 12, pp. 2415–2422, 2002.

[14] N. Sun, S. Zhang, T. Peng, J. Zhou, and X. Sun, "A composite uncertainty forecasting model for unstable time series: application of wind speed and streamflow forecasting," *IEEE Open Access Journal*, vol. 8, pp. 209253–209266, 2020.

[15] Y. Ge, L. Yang, and X. Ma, "A Novel Terminal Sliding Mode Control Based on RBF Neural Network for the Permanent Magnet Synchronous Motor," in *Power Electronics Electrical Drives Automation and Motion (SPEEDAM) International Symposium*, IEEE, 2018, pp. 1227–1232.

[16] Y. Choi, Q. Zhang, and S. Ko, "Noninvasive cuffless blood pressure estimation using pulse transit time and Hilbert–Huang transform," *Comput. Electr. Eng.*, vol. 39, no. 1, pp. 103–111, 2013.

[17] N. Li, F. He, W. Ma, R. Wang, L. Jiang, and X. Zhang, "The Identification of ECG Signals Using Wavelet Transform and WOA-PNN," *Sensors (Basel)*, vol. 22, no. 12, p. 4343, 2022, doi: 10.3390/s22124343.

[18] J. Lee and K. H. Chon, "An autoregressive model-based particle filtering algorithms for extraction of respiratory rates as high as 90 breaths per minute from pulse oximeter," *IEEE Trans. Biomed. Eng.*, vol. 57, no. 9, pp. 2158–2167, 2010, doi: 10.1109/TBME.2010.2051330.

[19] A. Razzaque and A. Badholia, "PCA based feature extraction and MPSO based feature selection for gene expression microarray medical data classification," *Meas. Sens.*, vol. 31, 2024, doi: 10.1016/j.measen.2023.100945.

[20] N. Neha, H. Sardana, N. Dogra, and R. Kanawade, "Dynamic time warping based arrhythmia detection using photoplethysmography signals," *Signal, Image and Video Processing*, vol. 16, pp. 1–9, 2022, doi: 10.1007/s11760-022-02152-z.

[21] R. van de Schoot, D. Kaplan, J. Denissen, J. B. Asendorpf, F. J. Neyer, and M. A. G. van Aken, "A Gentle Introduction to Bayesian Analysis: Applications to Developmental Research," [Online]. Available: https://doi.org/10.1111/cdev.12169.

[22] Z. Li, Y. Qian, F. Tang, M. Zhao, and Y. Zhu, "H-BILSTM: A Novel Bidirectional Long Short Term Memory Network Based Intelligent Early Warning Scheme in Mobile Edge Computing (MEC)," *IEEE Trans. Emerg. Topics Comput.*, vol. 11, no. 1, pp. 253–264, Jan.-Mar. 2023, doi: 10.1109/TETC.2022.3202266.

[23] J. Kubíček, M. Penhaker, and R. V. Kahankova, "Design of a synthetic ECG signal based on the Fourier series," in *Proc. Int. Conf. Advances in Computing, Communications and Informatics (ICACCI)*, IEEE, 2014, pp. 1881–1885, doi: 10.1109/ICACCI.2014.6968312.

[24] K. Xu, X. Jiang, C. Dai, and W. Chen, "Stochastic Modeling for Photoplethysmography Compression," in *Proc. 42nd Annu. Int. Conf. IEEE Eng. Med. Biol. Soc. (EMBC)*, Montreal, QC, Canada, 2020, pp. 5925–5928, doi: 10.1109/EMBC44109.2020.9175399.

[25] B. Fong, A. C. M. Fong, and C. K. Li, *Telemedicine Technologies*, Wiley, 2011.

[26] "American Telemedicine Association," [Online]. Available: http://www.americantelemed.org.

[27] D. P. Tobon, S. Jayaraman, and T. H. Falk, "Spectro-Temporal Electrocardiogram Analysis for Noise-Robust Heart Rate and Heart Rate Variability Measurement," *IEEE J. Transl. Eng. Health Med.*, vol. 5, p. 1900611, 2017, doi: 10.1109/JTEHM.2017.2767603.

[28] M. Jacobson, "Time-frequency analysis of heart rate variability," in *Proc. Int. Symp. Signal Process. and Its Applications (ISSPA)*, Sharjah, United Arab Emirates, 2007, pp. 1–4, doi: 10.1109/ISSPA.2007.4555434.

[29] M. Bootsma, C. A. Swenne, H. H. Van Bolhuis, P. C. Chang, V. M. Cats, and A. V. Bruschke, "Heart rate and heart rate variability as indexes of sympathovagal balance," *Am. J. Physiol.*, vol. 266, pp. H1565–H1571, 1994.

[30] Z. Ori, et al., "Heart Rate Variability: Frequency Domain Analysis," *Cardiology Clinics*, vol. 10, no. 3, pp. 499–507, 1992.

[31] S. Cerutti, A. M. Bianchi, and L. T. Mainardi, "Spectral Analysis of the Heart Rate Variability Signal," *Heart Rate Variability*, Futura Publishing Company, 1995.

[32] D. G. Poian, C. J. Rozell, R. Bernardini, R. Rinaldo, and G. D. Clifford, "Matched Filtering for Heart Rate Estimation on Compressive Sensing ECG Measurements," *IEEE Trans. Biomed. Eng.*, vol. 65, no. 6, pp. 1349–1358, 2018, doi: 10.1109/TBME.2017.2752422.

[33] J. Pan and W. J. Tompkins, "A real-time QRS detection algorithm," *IEEE Trans. Biomed. Eng.*, vol. BME-32, no. 3, pp. 230–236, Mar. 1985.

[34] P. S. Hamilton and W. J. Tompkins, "Quantitative investigation of QRS detection rules using the MIT/BIH arrhythmia database," *IEEE Trans. Biomed. Eng.*, vol. BME-33, no. 12, pp. 1157–1165, Dec. 1986.

[35] J. P. Madeiro, et al., "A new approach to QRS segmentation based on wavelet bases and adaptive threshold technique," *Med. Eng. Phys.*, vol. 29, no. 1, pp. 26–37, 2007.

[36] S. W. Chen, et al., "A real-time QRS detection method based on moving averaging incorporating with wavelet denoising," *Comput. Methods Programs Biomed.*, vol. 82, no. 3, pp. 187–195, 2006.

[37] A. Ruha, et al., "A real-time microprocessor QRS detector system with a 1-ms timing accuracy for the measurement of ambulatory HRV," *IEEE Trans. Biomed. Eng.*, vol. 44, no. 3, pp. 159–167, Mar. 1997.

[38] Z. Dokur, et al., "Detection of ECG waveforms by neural networks," *Med. Eng. Phys.*, vol. 19, no. 8, pp. 738–745, 1997.

[39] B.-U. Kohler, et al., "The principles of software QRS detection," *IEEE Eng. Med. Biol. Mag.*, vol. 21, no. 1, pp. 42–52, Jan./Feb. 2002.

[40] S. W. Shuai, et al., "Is 10-second electrocardiogram recording enough for accurately estimating heart rate in atrial fibrillation," *Int. J. Cardiol.*, vol. 215, pp. 175–180, Jul. 2016.

[41] M.-H. Cheng, L.-C. Chen, Y.-C. Hung, C. M. Yang, and T. L. Yang, "A Real-Time Heart-Rate Estimator from Steel Textile ECG Sensors in a Wireless Vital Wearing System," in *Proc. Int. Conf. Bioinformatics and Biomedical Engineering (ICBBE)*, 2008, pp. 1339–1342.

[42] R. V. Sharan, H. Takeuchi, A. Kishi, and Y. Yamamoto, "Macro-Sleep Staging With ECG-Derived Instantaneous Heart Rate and Respiration Signals and Multi-Input 1-D CNN–BiGRU," *IEEE Trans. Instrum. Meas.*, vol. 73, pp. 1–12, 2024, Art. no. 2535212.

[43] D. Biswas, N. Simões-Capela, C. Van Hoof, and N. Van Helleputte, "Heart Rate Estimation From Wrist-Worn Photoplethysmography: A Review," *IEEE Sensors J.*, vol. 19, no. 16, pp. 6560–6570, Aug. 15, 2019.

[44] A. Temko, "Accurate heart rate monitoring during physical exercises using PPG," *IEEE Trans. Biomed. Eng.*, vol. 64, no. 9, pp. 2016–2024, Sep. 2017.

[45] E. Grisan, et al., "A supervised learning approach for the robust detection of heart beat in plethysmographic data," in *Proc. 37th Annu. Int. Conf. IEEE Eng. Med. Biol. Soc. (EMBC)*, Aug. 2015, pp. 5825–5828.

[46] Z. Zhang, Z. Pi, and B. Liu, "TROIKA: A general framework for heart rate monitoring using wrist-type photoplethysmographic signals during intensive physical exercise," *IEEE Trans. Biomed. Eng.*, vol. 62, no. 2, pp. 522–531, Feb. 2015.

[47] Y. Kong and K. Chon, "Heart Rate Estimation using PPG signal during Treadmill Exercise," in *Proc. Annu. Int. Conf. IEEE Eng. Med. Biol. Soc. (EMBC)*, Jul. 2019, pp. 3253–3256.

[48] H. Wang, K. Siu, K. Ju, and K. H. Chon, "A high resolution approach to estimating time-frequency spectra and their amplitudes," *Ann. Biomed. Eng.*, vol. 34, no. 2, pp. 326–338, Feb. 2006.

[49] M. R. Ram, K. V. Madhav, E. H. Krishna, N. R. Komalla, and K. A. Reddy, "A novel approach for motion artifact reduction in PPG signals based on AS-LMS adaptive filter," *IEEE Trans. Instrum. Meas.*, vol. 61, no. 5, pp. 1445–1457, May 2012.

[50] A. Temko, "Estimation of heart rate from photoplethysmography during physical exercise using Wiener filtering and the phase vocoder," in *Proc. 37th Annu. Int. Conf. IEEE Eng. Med. Biol. Soc. (EMBC)*, Aug. 2015, pp. 1500–1503.

[51] R. Krishnan, B. Natarajan, and S. Warren, "Motion artifact reduction in photoplethysmography using magnitude-based frequency domain independent component analysis," in *Proc. 17th Int. Conf. Comput. Commun. Netw.*, Aug. 2008, pp. 1–5.

[52] B. Pang, M. Liu, X. Zhang, P. Li, and H. Chen, "A novel approach framework based on statistics for reconstruction and heart rate estimation from PPG with heavy motion artifacts," *Sci. China Inf. Sci.*, vol. 61, no. 2, Nov. 2017.

[53] S. Seyedtabaii and L. Seyedtabaii, "Kalman filter based adaptive reduction of motion artifact from photoplethysmographic signal," *World Acad. Sci. Eng. Technol.*, vol. 37, pp. 173–176, Feb. 2008.

[54] X. Li and B. Pu, "Strong Robustness Heart Rate Estimation Using Discrete Fourier Transform and Personality Heart Rate Characteristic," in *Proc. 36th Chinese Control Conf.*, Dalian, China, Jul. 2017.

[55] Z. Zhang, Z. Pi, and B. Liu, "TROIKA: A general framework for heart rate monitoring using wrist-type photoplethysmographic signals during intensive physical exercise," *IEEE Trans. Biomed. Eng.*, vol. 62, no. 2, pp. 522–531, 2015.

[56] R. Yousefi, "A motion-tolerant adaptive algorithm for wearable photoplethysmographic biosensors," *IEEE J. Biomed. Health Inform.*, vol. 18, no. 2, pp. 670–681, 2014.

[57] S. M. Lopez, "Heuristic algorithm for photoplethysmographic heart rate tracking during maximal exercise test," *J. Med. Biol. Eng.*, vol. 32, no. 3, pp. 181–188, 2012.

[58] Z. Zhang, "Photoplethysmography-based heart rate monitoring in physical activities via joint sparse spectrum reconstruction," *IEEE Trans. Biomed. Eng.*, vol. 62, no. 8, pp. 1902–1910, 2015.

[59] C. Yen, S. Chang, and C. Liao, "Estimation of Beat-by-Beat Blood Pressure and Heart Rate From ECG and PPG Using a Fine-Tuned Deep CNN Model," *IEEE Access*, vol. 10, pp. 85459–85469, 2022.

[60] P. Sharma, S. A. Imtiaz, and E. Rodriguez-Villegas, "Acoustic Sensing as a Novel Wearable Approach for Cardiac Monitoring at the Wrist," *Sci. Rep.*, vol. 9, no. 20079, Dec. 2019.

[61] M. Kaisti, et al., "Stand-alone heartbeat detection in multidimensional mechanocardiograms," *IEEE Sensors J.*, vol. 19, no. 1, pp. 234–242, Jan. 2019.

[62] C. Bruser, K. Stadlthanner, S. De Waele, and S. Leonhardt, "Adaptive beat-to-beat heart rate estimation in ballistocardiograms," *IEEE Trans. Inf. Technol. Biomed.*, vol. 15, no. 5, pp. 778–786, Sep. 2011.

[63] M. Nosrati and N. Tavassolian, "High-accuracy heart rate variability monitoring using Doppler radar based on Gaussian pulse train modelling and FTPR algorithm," *IEEE Trans. Microw. Theory Techn.*, vol. 66, no. 1, pp. 556–567, Jan. 2018.

[64] B.-U. Kohler, C. Hennig, and R. Orglmeister, "The principles of software QRS detection," *IEEE Eng. Med. Biol. Mag.*, vol. 21, no. 1, pp. 42–52, Aug. 2002.

[65] M. Elgendi, B. Eskofier, S. Dokos, and D. Abbott, "Revisiting QRS detection methodologies for portable, wearable, battery-operated, and wireless ECG systems," *PLoS ONE*, vol. 9, no. 1, Jan. 2014, Art. no. e84018.

[66] D. Jarchi and A. J. Casson, "Towards photoplethysmography-based estimation of instantaneous heart rate during physical activity," *IEEE Trans. Biomed. Eng.*, vol. 64, no. 9, pp. 2042–2053, Sep. 2017.

[67] C. Jiao, B.-Y. Su, P. Lyons, A. Zare, K. C. Ho, and M. Skubic, "Multiple instance dictionary learning for beat-to-beat heart rate monitoring from ballistocardiograms," *IEEE Trans. Biomed. Eng.*, vol. 65, no. 11, pp. 2634–2648, Nov. 2018.

[68] C. Brüser, K. Stadlthanner, A. Brauers, and S. Leonhardt, "Applying machine learning to detect individual heart beats in ballistocardiograms," in *Proc. Annu. Int. Conf. IEEE Eng. Med. Biol.*, Aug. 2010, pp. 1926–1930.

[69] K. Greiser, et al., "Cardiovascular disease, risk factors and heart rate variability in the elderly general population: design and objectives of the CARLA study," *BMC Cardiovasc. Disord.*, vol. 5, no. 33, Nov. 2005.

[70] T. J. Ahmad, et al., "Effect of atrioventricular conduction on heart rate variability," in *Proc. Annu. Int. Conf. IEEE Eng. Med. Biol. Soc. (EMBC)*, 2011, pp. 1953–1956.

[71] T. J. Ahmad, H. Ali, S. M. Majeed, and S. A. Khan, "Effect of atrioventricular conduction on heart rate variability," *Annu. Int. Conf. IEEE Eng. Med. Biol. Soc.*, vol. 2011, pp. 1953–1956, 2011, doi: 10.1109/IEMBS.2011.6090551. PMID: 22254715.

[72] K. Balasubramanian and A. Cellatoglu, "Applying analysis tools of heart rate variability upon determining P-Wave interval of ECG," Apr. 2008.

[73] S. González, A. K. Yi, W. Hsieh, W. Chen, C. Wang, V. C. Wu, and S. Chang, "Multi-modal Heart Failure Risk Estimation based on Short ECG and Sampled Long-Term HRV," *ArXiv*, 2024. Available: https://doi.org/10.1016/j.inffus.2024.102337.

[74] M. Moshawrab, M. Adda, A. Bouzouane, H. Ibrahim, and A. Raad, "Cardiovascular Events Prediction using Artificial Intelligence Models and Heart Rate Variability," *Procedia Comput. Sci.*, vol. 203, pp. 231–238, Jan. 2022.

[75] M. Baumert, N. Wessel, A. Schirdewan, A. Voss, and D. Abbott, "Forecasting of ventricular tachycardia using scaling characteristics and entropy of heart rate time series," in *World Congress on Medical Physics and Biomedical Engineering 2006*, Berlin, Heidelberg: Springer, 2007, pp. 1001–1004.

[76] S. Joo, K. J. Choi, and S. J. Huh, "Prediction of ventricular tachycardia by a neural network using parameters of heart rate variability," in *2010 Computing in Cardiology*, 2010, pp. 585–588.

[77] "Spontaneous Ventricular Tachyarrhythmia Database v1.0," *PhysioNet*, May 2, 2007. Available: https://physionet.org/content/mvtdb/1.0/.

[78] J. F. Ramirez-Villegas, E. Lam-Espinosa, D. F. Ramirez-Moreno, P. C. Calvo-Echeverry, and W. Agredo-Rodriguez, "Heart rate variability dynamics for the prognosis of cardiovascular risk," *PLoS One*, vol. 6, no. 2, p. e17060, 2011.

[79] T. Song et al., "Usefulness of the heart-rate variability complex for predicting cardiac mortality after acute myocardial infarction," *BMC Cardiovasc. Disord.*, vol. 14, no. 1, pp. 1–8, 2014.

[80] E. Ebrahimzadeh, M. Pooyan, and A. Bijar, "A novel approach to predict sudden cardiac death (SCD) using nonlinear and time-frequency analyses from HRV signals," *PLoS One*, vol. 9, no. 2, p. e81896, 2014.

[81] "Sudden Cardiac Death Holter Database v1.0.0," *PhysioNet*, Jul. 2, 2004. Available: https://physionet.org/content/sddb/1.0.0/.

[82] "MIT-BIH Normal Sinus Rhythm Database v1.0.0," *PhysioNet*, Aug. 3, 1999. Available: https://physionet.org/content/nsrdb/1.0.0/.

[83] L. Murukesan, M. Murugappan, M. Iqbal, and K. Saravanan, "Machine learning approach for sudden cardiac arrest prediction based on optimal heart rate variability features," *J. Med. Imaging Health Inform.*, vol. 4, no. 4, pp. 521–532, 2014.

[84] S. Mihandoost, "A Deep Neural Network Model with Spectral Correlation Function for Electrocardiogram Classification and Diagnosis of Atrial Fibrillation," *Healthcare Analytics*, p. 100370, Nov. 2024.

[85] S. Choudhary, "Heart Rate Variability Analysis From Electrocardiogram (ECG) and Photoplethysmogram (PPG) Signals By Using Soft Computing Technique," in *2023 1st International Conference on Innovations in High Speed Communication and Signal Processing (IHCSP)*, Bhopal, India, 2023, pp. 158–163, doi: 10.1109/IHCSP56702.2023.10127200.

[86] S. T. Ahamed and M. T. Islam, "An efficient method for heart rate monitoring using wrist-type photoplethysmographic signals during intensive physical exercise," in *2016 5th International*

Conference on Informatics, Electronics and Vision (ICIEV), Dhaka, Bangladesh, 2016, pp. 863–868, doi: 10.1109/ICIEV.2016.7760124.

[87] V. S. Murthy, S. Ramamoorthy, N. Srinivasan, S. Rajagopalan, and M. M. Rao, "Analysis of photoplethysmographic signals of cardiovascular patients," presented at *Conference-Proceeding*, 2001.

[88] M. F. Ihsan, S. Mandala, and M. Pramudyo, "Study of Feature Extraction Algorithms on Photoplethysmography (PPG) Signals to Detect Coronary Heart Disease," in *2022 International Conference on Data Science and Its Applications (ICoDSA)*, Bandung, Indonesia, 2022, pp. 300–304, doi: 10.1109/ICoDSA55874.2022.9862855.

[89] D. Biswas et al., "CorNET: Deep Learning Framework for PPG-Based Heart Rate Estimation and Biometric Identification in Ambulant Environment," *IEEE Trans. Biomed. Circuits Syst.*, vol. 13, no. 2, pp. 282–291, Apr. 2019, doi: 10.1109/TBCAS.2019.2892297. PMID: 30629514.

[90] H. Wang et al., "Non-invasive continuous blood pressure prediction based on ECG and PPG fusion map," *Med. Eng. Phys.*, vol. 119, p. 104037, Aug. 2023.

[91] A. Aygun, H. Ghasemzadeh, and R. Jafari, "Robust Interbeat Interval and Heart Rate Variability Estimation Method From Various Morphological Features Using Wearable Sensors," *IEEE J. Biomed. Health Inform.*, vol. 24, no. 8, pp. 2238–2250, Aug. 2020, doi: 10.1109/JBHI.2019.2962627. PMID: 31899444; PMCID: PMC11036325.

[92] N. S. Shilpa, V. J. Varghese, P. N. Sivaranjini, A. K. Panda, M. S. Manikandan, and R. B. Pachori, "Performance Evaluation of Cuffless Blood Pressure Estimation Methods Using Linear and Non-Linear Models with PTT and PR Parameters," in *2022 8th International Conference on Signal Processing and Communication (ICSC)*, Dec. 2023, pp. 397–402.

[93] J. Kerola, V. Kontra, and R. Sepponen, "Non-invasive blood pressure data acquisition employing pulse transit time detection," in *Proc. 18th Annual International Conference of the IEEE Engineering in Medicine and Biology Society*, vol. 3, 1996, pp. 1308–1309.

[94] S. Ghosh et al., "Continuous blood pressure prediction from pulse transit time using ECG and PPG signals," in *IEEE Healthcare Innovation Point-Of-Care Technologies Conference (HI-POCT)*, 2016, pp. 188–191.

[95] F. S. Cattivelli and H. Garudadri, "Noninvasive cuffless estimation of blood pressure from pulse arrival time and heart rate with adaptive calibration," in *6th International Workshop on Wearable and Implantable Body Sensor Networks*, 2009, pp. 114–119.

[96] D. Jarchi and A. J. Casson, "Towards Photoplethysmography-Based Estimation of Instantaneous Heart Rate During Physical Activity," *IEEE Trans. Biomed. Eng.*, vol. 64, no. 9, pp. 2042–2053, Sep. 2017, doi: 10.1109/TBME.2017.2668763. PMID: 28212075.

[97] S. Banerjee, R. Gupta, and J. Saha, "Compression of multilead electrocardiogram using principal component analysis and machine learning approach," in *IEEE App. Sig. Proc. Conf. (ASPCON)*, Kolkata, India, 2018, pp. 24–28, doi: 10.1109/ASPCON.2018.8748572.

[98] S. Chandra, A. Sharma, and G. K. Singh, "A comparative analysis of performance of several wavelet-based ECG data compression methodologies," *IRBM*, vol. 42, no. 4, pp. 227–244, 2021, doi: 10.1016/j.irbm.2020.05.004.

[99] H. S. Pal, A. Kumar, A. Vishwakarma, and G. K. Singh, "Optimized Tunable-Q Wavelet Transform-Based 2-D ECG Compression Technique Using DCT," *IEEE Trans. Instrum. Meas.*, vol. 72, pp. 1–13, 2023, doi: 10.1109/TIM.2023.3279885.

[100] Y. Xiao, H. Yin, Y. Zhang, H. Qi, Y. Zhang, and Z. Liu, "A dual-stage attention-based Conv-LSTM network for spatio-temporal correlation and multivariate time series prediction," *Int. J. Intell. Syst.*, vol. 36, pp. 2036–2057, 2021, doi: 10.1002/int.22370.

[101] A. Pandey, "ECG data compression using the formation of QRS-complex segment bank and integer DCT-based plateau region processing," *Biomed. Signal Process. Control*, vol. 85, 2023, pp. 1746–8094, doi: 10.1016/j.bspc.2023.104823.

[102] Z. Peric, D. Denic, J. Nikolic, A. Jocic, and A. Jovanovic, "DPCM quantizer adaptation method for efficient ECG signal compression," *J. Commun. Technol. Electron.*, vol. 58, no. 12, pp. 1241–1250, 2013, doi: 10.1134/S1064226913130068.

[103] V. Kumar, S. C. Saxena, and V. K. Giri, "Direct data compression of ECG signal for telemedicine," *Int. J. Syst. Sci.*, vol. 37, 2006, pp. 45–63, doi: 10.1080/00319100500412337.

[104] S. Dhar, S. K. Mukhopadhyay, S. Pal, and M. Mitra, "An efficient data compression and encryption technique for PPG signal," *Measurement (Lond).*, vol. 116, pp. 533–542, 2018, doi: 10.1016/j.measurement.2017.11.006.

[105] L. Brechet, M. F. Lucas, C. Doncarli, and D. Farina, "Compression of biomedical signals with mother wavelet optimization and best-basis wavelet packet selection," *IEEE Trans. Biomed. Eng.*, vol. 54, no. 12, pp. 2186–2192, 2007, doi: 10.1109/TBME.2007.896596.

[106] B. R. Reddy and I. S. Murthy, "ECG data compression using Fourier descriptors," *IEEE Trans. Biomed. Eng.*, vol. 33, no. 4, pp. 428–434, 1986, doi: 10.1109/TBME.1986.325799.

[107] G. P. Frangakis, G. Papakonstantinou, and S. G. Tzafestas, "A fast Walsh transform-based data compression multi-microprocessor system: application to ECG signals," *Math. Comput. Simul.*, vol. 27, no. 5–6, pp. 491–502, 1985, doi: 10.1016/0378-4754(85)90068-0.

[108] P. Bera and R. Gupta, "Hybrid encoding algorithm for real-time compressed electrocardiogram acquisition," *Measurement*, vol. 91, pp. 651–660, 2016, doi: 10.1016/j.measurement.2016.05.085.

[109] C. Jha and M. Kolekar, "ECG data compression algorithm for tele-monitoring of cardiac patients," *Int. J. Telemed. Clin. Pract.*, vol. 2, no. 1, pp. 31–41, 2017, doi: 10.1504/IJTMCP.2017.082106.

[110] Y. Yin, S. M. Abubakar, S. Tan, J. Shi, P. Yang, W. Yang, H. Jiang, Z. Wang, W. Jia, and S.-p. U, "A 2.63 μW ECG Processor With Adaptive Arrhythmia Detection and Data Compression for Implantable Cardiac Monitoring Device," *IEEE Trans. Biomed. Circuits Syst.*, vol. 15, pp. 777–790, 2021, doi: 10.1109/TBCAS.2021.3100434.

[111] M. H. Kolekar, C. K. Jha, and P. Kumar, "ECG data compression using modified run length encoding of wavelet coefficients for Holter monitoring," *IRBM*, vol. 43, pp. 325–332, 2022, doi: 10.1016/j.irbm.2021.10.001.

[112] D. Mitra, H. Zanddizari, and S. Rajan, "Investigation of Kronecker-based recovery of compressed ECG signal," *IEEE Trans. Instrum. Meas.*, vol. 69, no. 6, pp. 3642–3653, 2020, doi: 10.1109/TIM.2019.2936776.

[113] R. Kumar, A. Kumar, and G. K. Singh, "Hybrid method based on singular value decomposition and embedded zero tree wavelet technique for ECG signal compression," *Comput. Methods Programs Biomed.*, vol. 129, pp. 135–148, 2016, doi: 10.1016/j.cmpb.2016.01.006.

[114] C. K. Jha and M. H. Kolekar, "Electrocardiogram data compression using DCT-based discrete orthogonal Stockwell transform," *Biomed. Signal Process. Control*, vol. 46, pp. 174–181, 2018, doi: 10.1016/j.bspc.2018.06.009.

[115] I. S. Fathi, M. A. A. Makhlouf, E. Osman, and M. A. Ahmed, "An energy-efficient compression algorithm of ECG signals in remote healthcare monitoring systems," *IEEE Access*, vol. 10, pp. 39129–39144, 2022, doi: 10.1109/ACCESS.2022.3166476.

[116] Z. Xiao *et al*., "Densely knowledge-aware network for multivariate time series classification," *IEEE Trans. Syst., Man, Cybern.: Syst.*, vol. 54, no. 4, pp. 2192–2204, 2024, doi: 10.1109/TSMC.2023.3342640.

[117] Z. Xiao *et al*., "Deep contrastive representation learning with self-distillation," *IEEE Trans. Emerg. Top. Comput. Intell.*, vol. 8, no. 1, pp. 3–15, 2024, doi: 10.1109/TETCI.2023.3304948.

[118] Z. Xiao *et al*., "CapMatch: Semi-supervised contrastive transformer capsule with feature-based knowledge distillation for human activity recognition," *IEEE Trans. Neural Netw. Learn. Syst.*, pp. 1–15, 2023, doi: 10.1109/TNNLS.2023.3344294.

[119] H. S. Pal, A. Kumar, A. Vishwakarma, G. K. Singh, and H. N. Lee, "An effective ECG signal compression algorithm with self-controlled reconstruction quality," *Comput. Methods Biomech. Biomed. Eng.*, pp. 1–11, 2023, doi: 10.1080/10255842.2023.2206933.

[120] M. R. Mohebbian and K. A. Wahid, "ECG compression using optimized B-spline," *Multimed. Tools Appl.*, vol. 82, pp. 21071–21083, 2023, doi: 10.1007/s11042-023-14610-y.

[121] S. Alam, R. Gupta, and J. Bera, "Quality controlled compression technique for Photoplethysmogram monitoring applications," *Measurement*, vol. 130, pp. 236–245, 2018, doi: 10.1016/j.measurement.2018.07.091.

[122] R. Gupta, "Lossless compression technique for real-time photoplethysmographic measurements," *IEEE Trans. Instrum. Meas.*, vol. 64, no. 4, pp. 975–982, 2015, doi: 10.1109/TIM.2014.2362837.

[123] K. Xu, X. Jiang, C. Dai, and W. Chen, "Stochastic modeling for photoplethysmography compression," in *Proc. 42nd Annu. Int. Conf. IEEE Eng. Med. Biol. Soc. (EMBC)*, Montreal, QC, Canada, 2020, pp. 5925–5928, doi: 10.1109/EMBC44109.2020.9175399.

[124] S. Vadrevu and M. S. Manikandan, "A new quality-aware quality-control data compression framework for power reduction in IoT and smartphone PPG monitoring devices," *IEEE Sensors Lett.*, vol. 3, no. 7, pp. 1–4, 2019, doi: 10.1109/LSENS.2019.2920849.

[125] S. Alam and R. Gupta, "Zonal complexity-based measure for lossy compression of photoplethysmogram using delta encoding," in *Proc. IEEE Int. Conf. Signal Process., Informatics, Commun. Energy Syst. (SPICES)*, Kozhikode, India, 2015, pp. 1–5, doi: 10.1109/SPICES.2015.7091454.

[126] K. A. Reddy, B. George, and V. J. Kumar, "Use of Fourier series analysis for motion artifact reduction and data compression of photoplethysmographic signals," *IEEE Trans. Instrum. Meas.*, vol. 58, no. 5, pp. 1706–1711, 2009, doi: 10.1109/TIM.2008.2009136.

[127] S. Alam, R. Gupta, and K. D. Sharma, "On-board signal quality assessment guided compression of photoplethysmogram for personal health monitoring," *IEEE Trans. Instrum. Meas.*, vol. 70, pp. 1–9, 2021, doi: 10.1109/TIM.2021.3067238.

[128] S. Banerjee and G. K. Singh, "A new real-time lossless data compression algorithm for ECG and PPG signals," *Biomed. Signal Process. Control*, vol. 79, p. 104127, 2023, doi: 10.1016/j.bspc.2022.104127.

[129] R. R. Sahoo, A. Lala, P. K. Kundu, and S. Ghosh, "Data compression of photoplethysmogram signal for IoT application," in *Proc. IEEE Int. Conf. Electron Devices Soc. Kolkata Chapter (EDKCON)*, Kolkata, India, 2022, pp. 615–620, doi: 10.1109/EDKCON56221.2022.10032860.

[130] S. Banerjee and G. K. Singh, "A new real-time lossless data compression algorithm for ECG and PPG signals," *Biomed. Signal Process. Control*, vol. 79, p. 104127, 2015, doi: 10.1016/j.bspc.2022.104127.

[131] R. Banerjee, A. Sinha, A. D. Choudhury, and A. Visvanathan, "PhotoECG: Photoplethysmography to estimate ECG parameters," in *Proc. IEEE Int. Conf. Acoustics, Speech, Signal Process. (ICASSP)*, Florence, Italy, 2014, pp. 4404–4408.

[132] A. Panda, S. Pinisetty, and P. Roop, "A novel mapping of ECG and PPG to ensure the safety of health monitoring applications," *IEEE Embed. Syst. Lett.*, vol. 15, no. 1, pp. 49–52, 2023.

[133] D. Kosasih, B. Lee, and H. Lim, "Neural network and cloud computing for predicting ECG waves from PPG readings," *J. Multimed. Inf. Syst.*, vol. 9, no. 1, pp. 11–20, 2022.

[134] Q. Zhu, X. Tian, C.-W. Wong, and M. Wu, "Learning your heart actions from pulse: ECG waveform reconstruction from PPG," *IEEE Internet Things J.*, vol. 8, no. 23, pp. 16734–16748, 2021.

[135] H. Chiu, H. Shuai, and C. P. Chao, "Reconstructing QRS complex from PPG by transformed attentional neural networks," *IEEE Sens. J.*, vol. 20, no. 20, pp. 12374–12383, 2020.

[136] P. Sarkar and A. Etemad, "Cardiogan: Attentive generative adversarial network with dual discriminators for the synthesis of ECG from PPG," in *Proc. AAAI Conf. Artif. Intell.*, vol. 35, pp. 488–496, 2021.

[137] Q. Tang, Z. Chen, Y. Guo, Y. Liang, R. Ward, C. Menon, and M. Elgendi, "Robust reconstruction of electrocardiogram using photoplethysmography: A subject-based model," *Front. Physiol.*, vol. 13, Art. no. 25, Apr. 2022.

[138] X. Tian, Q. Zhu, Y. Li, and M. Wu, "Cross-domain joint dictionary learning for ECG reconstruction from PPG," in *Proc. IEEE Int. Conf. Acoustics, Speech, Signal Process. (ICASSP)*, Barcelona, Spain, 2020, pp. 936–940.

[139] Y. Li, J. Luo, Q. Dai, J. K. Eshraghian, B. W. Ling, C. Zheng, and X. Wang, "A deep learning approach to cardiovascular disease classification using empirical mode decomposition for ECG feature extraction," *Biomed. Signal Process. Control*, vol. 79, Art. no. 104188, 2023, doi: 10.1016/j.bspc.2022.104188.

[140] A. K. Bhoi, K. S. Sherpa, and B. Khandelwal, "Ischemia and arrhythmia classification using time-frequency domain features of QRS complex," *Procedia Comput. Sci.*, vol. 132, pp. 606–613, 2018, doi: 10.1016/j.procs.2018.05.014.

[141] K. Ramasamy, K. Balakrishnan, and D. Velusamy, "Detection of cardiac arrhythmias from ECG signals using FBSE and Jaya optimized ensemble random subspace K-nearest neighbor algorithm," *Biomed. Signal Process. Control*, vol. 76, 2022, Art. no. 103654, doi: 10.1016/j.bspc.2022.103654.

[142] L. Yao, C. Liu, P. Li, J. Wang, Y. Liu, W. Li, and H. Jhang, "Enhanced automated diagnosis of coronary artery disease using features extracted from QT interval time series and ST–T waveform," *IEEE Access*, vol. 8, pp. 129510–129524, 2020, doi: 10.1109/ACCESS.2020.3008965.

[143] E. Martinez-Ríos, L. Montesinos, and M. Alfaro-Ponce, "A machine learning approach for hypertension detection based on photoplethysmography and clinical data," *Comput. Biol. Med.*, vol. 145, 2022, Art. no. 105479, doi: 10.1016/j.compbiomed.2022.105479.

[144] Q. Qananwah, M. Ababneh, and A. Dagamseh, "Cardiac arrhythmias classification using photoplethysmography database," *Sci. Rep.*, vol. 14, no. 1, Art. no. 3355, 2024, doi: 10.1038/s41598-024-53142-9.

[145] S. Abdullah and A. Kristoffersson, "Machine learning approaches for cardiovascular hypertension stage estimation using photoplethysmography and clinical features," *Front. Cardiovasc. Med.*, vol. 10, 2023, doi: 10.3389/fcvm.2023.1285066.

[146] A. S. A. Fahoum, A. O. A. A. Haija, and H. A. Alshraideh, "Identification of coronary artery diseases using photoplethysmography signals and practical feature selection process," *Bioengineering*, vol. 10, no. 249, 2023, doi: 10.3390/bioengineering10020249.

[147] B. D. S. Praveen, D. V. N. Sandeep, I. V. V. Raghavendra, M. Yuvaraj, and S. Sarath, "Non-invasive machine learning approach for classifying blood pressure using PPG signals in COVID situation," in *Proc. 2022 13th Int. Conf. Comput. Commun. Netw. Technol. (ICCCNT)*, Jul. 2021, vol. 9, pp. 1–7.

[148] P. Pal and M. Mahadevappa, "Adaptive multidimensional dual attentive DCNN for detecting cardiac morbidities using fused ECG-PPG signals," *IEEE Trans. Artif. Intell.*, vol. 4, no. 5, pp. 1225–1235, 2023, doi: 10.1109/TAI.2022.3184656.

[149] B. Aldughayfiq, F. Ashfaq, N. Z. Jhanjhi, and M. Humayun, "A deep learning approach for atrial fibrillation classification using multi-feature time series data from ECG and PPG," *Diagnostics (Basel)*, vol. 13, no. 14, Art. no. 2442, 2023, doi: 10.3390/diagnostics13142442.

[150] M. Z. Suboh, R. Jaafar, and N. A. Nayan, "A comprehensive analysis on severity of stenosis detection in coronary arteries using synchronized electrocardiogram and photoplethysmogram," *J. Am. Coll. Cardiol.*, vol. 81, no. 16_Supplement, 2023, doi: 10.1016/j.jacc.2023.03.109.

[151] P. Pal and M. Mahadevappa, "Coronary Health Index (CHI) as a Determinant for Arterial Stenosis, Derived Using PPG and ECG Signals," in *Proc. 2022 Computing in Cardiology (CinC)*, Tampere, Finland, 2022, pp. 1–4, doi: 10.22489/CinC.2022.316.

[152] A. Johnson, T. Pollard, L. Shen, et al., "MIMIC-III, a freely accessible critical care database," *Sci Data*, vol. 3, p. 160035, 2016. https://doi.org/10.1038/sdata.2016.35.

[153] E. Lan, "Performer: A Novel PPG-to-ECG Reconstruction Transformer for a Digital Biomarker of Cardiovascular Disease Detection," in *IEEE/CVF Winter Conference on Applications of Computer Vision (WACV)*, 2023, pp. 1990-1998. https://doi.org/10.1109/WACV56688.2023.00203.

[154] G. B. Moody and R. G. Mark, "The impact of the MIT-BIH Arrhythmia Database," *IEEE Engineering in Medicine and Biology Magazine*, vol. 20, no. 3, pp. 45-50, 2001. doi:10.13026/C2F305.

[155] Biopac Systems. [Online]. Available: https://www.biopac.com.

[156] EasyPulse User Guide. [Online]. Available: https://embedded-lab.com/uploads/manuals/EasyPulse_User_Guide.pdf.

[157] S. Banerjee and G. K. Singh, "A new real-time lossless data compression algorithm for ECG and PPG signals," *Biomed. Sig. Proc. Cont.*, vol. 79, no. 1, p. 104127, 2023.

[158] C. Fischer, M. Glos, T. Penzel, and I. Fietze, "Extended algorithm for real-time pulse waveform segmentation and artifact detection in photoplethysmograms," *Somnologie*, vol. 21, pp. 110–120, 2017.

[159] M. Z. Suboh, R. Jaafar, N. A. Nayan, N. H. Harun, and M. S. F. Mohamad, "Analysis on Four Derivative Waveforms of Photoplethysmogram (PPG) for Fiducial Point Detection," *Front. Pub. Health*, vol. 10, p. 920946, 2022.

[160] N. Hasanzadeh, M. M. Ahmadi, and H. Mohammadzade, "Blood Pressure Estimation Using Photoplethysmogram Signal and Its Morphological Features," *IEEE Sensors J.*, vol. 20, no. 8, pp. 4300-4310, 2020.

[161] S. Abdullah, A. Hafid, M. Folke, M. Lindén, and A. Kristoffersson, "A Novel Fiducial Point Extraction Algorithm to Detect C and D Points from the Acceleration Photoplethysmogram (CnD)," *Electronics*, vol. 12, p. 1174, 2023.

[162] R. R. Sahoo and P. K. Kundu, "Prediction of Fiducial Parameter of PPG Signal—A Comparative Study Between Radial Basis and General Regression Neural Network Performance," *Proceedings of International Conference on Industrial Instrumentation and Control*, Lect Notes in Elect. Eng., vol. 815, pp. 99-110, 2022.

[163] X. Wang, W. Cai, and M. Wang, "A novel approach for biometric recognition based on ECG feature vectors," *Biomed. Sig. Proc. Cont.*, vol. 86, p. 104922, 2023.

[164] W. Midani, W. Ouarda, and M. B. Ayed, "DeepArr: An investigative tool for arrhythmia detection using a contextual deep neural network from electrocardiograms (ECG) signals," *Biomed. Sig. Proc. Cont.*, vol. 85, p. 104954, 2023.

[165] M. Singla, S. Azeemuddin, and P. Sistla, "Accurate Fiducial Point Detection Using Haar Wavelet for Beat-by-Beat Blood Pressure Estimation," *IEEE Jour. of Transl. Eng. in Health and Med.*, vol. 8, Art. no. 1900711, pp. 1-11, 2020.

[166] K. Friganovic, D. Kukolja, A. Jovic, M. Cifrek, and G. Krstacic, "Optimizing the Detection of Characteristic Waves in ECG Based on Processing Methods Combinations," *IEEE Access*, vol. 6, pp. 50609-50626, 2018.

[167] S. K. Mukhopadhyay, M. O. Ahmad, and M. N. S. Swamy, "Compression of steganographed PPG signal with guaranteed reconstruction quality based on optimum truncation of singular values and ASCII character encoding," *IEEE Transactions on Biomedical Engineering*, vol. 66, no. 7, pp. 2081–2090, Jul. 2019, doi: 10.1109/TBME.2018.2883396.

[168] T. H. Tsai and M. A. Hussain, "VLSI implementation of lossless ECG compression algorithm for low power devices," *IEEE Transactions on Circuits and Systems II: Express Briefs*, vol. 67, no. 12, pp. 3317–3321, Dec. 2020, doi: 10.1109/TCSII.2020.2978554.

[169] S. Suppappola, Y. Sun, and S. A. Chiaramida, "Gaussian pulse decomposition: An intuitive model of electrocardiogram waveforms," *Annals of Biomedical Engineering*, vol. 25, pp. 252–260, 1997, doi: 10.1007/BF02648039.

[170] B. S. Kim, S. K. Yoo, and M. H. Lee, "Wavelet-based low-delay ECG compression algorithm for continuous ECG transmission," *IEEE Transactions on Information Technology in Biomedicine*, vol. 10, no. 1, pp. 77–83, Jan. 2006, doi: 10.1109/TITB.2005.856854.

[171] P. Kundu and R. Gupta, "Electrocardiogram synthesis using Gaussian and Fourier models," in *Proc. IEEE Int. Conf. Research in Computational Intelligence and Communication Networks (ICRCICN)*, 2015, pp. 312–317, doi: 10.1109/ICRCICN.2015.7434256.

[172] R. Couceiro et al., "Assessment of cardiovascular function from multi-Gaussian fitting of a finger photoplethysmogram," *Physiological Measurement*, vol. 36, no. 9, pp. 1801–1825, Sep. 2015, doi: 10.1088/0967-3334/36/9/1801.

[173] S. K. Mukhopadhyay, M. O. Ahmad, and M. N. S. Swamy, "ASCII-character-encoding based PPG compression for tele-monitoring system," *Biomedical Signal Processing and Control*, vol. 31, pp. 470–482, 2017, doi: 10.1016/j.bspc.2016.09.021.

[174] D. Sadhukhan, S. Pal, and M. Mitra, "Adaptive band limit estimation based PPG data compression for portable home monitors," *Measurement*, vol. 134, pp. 153–165, 2019, doi: 10.1016/j.measurement.2018.10.061.

[175] S. Bhowmick, P. Kundu, and D. Mandal, "IoT assisted real-time PPG monitoring system for health care application," in *Proc. IEEE Second Int. Conf. Control Measurement and Instrumentation (CMI)*, 2021, pp. 122–127.

[176] *Introduction to Deep Learning: From Logical Calculus to Artificial Intelligence*, Springer, pp. 37–38, 2018.

[177] D. Sopic, A. Aminifar, and D. Atienza, "Real-time event-driven classification technique for early detection and prevention of myocardial infarction on wearable systems," *IEEE Transactions on Biomedical Circuits and Systems*, vol. 12, no. 5, pp. 982–992, Oct. 2018, doi: 10.1109/TBCAS.2018.2848477.

[178] K. Kanakapriya, A. Mandali, and M. Manivannan, "ECG simulation for myocardial infarction diagnosis in high fidelity mannequins," in *Proc. 2011 Annual IEEE India Conf. (INDICON)*, 2011, pp. 1–5, doi: 10.1109/INDCON.2011.6139634.

[179] P. Pal, S. Ghosh, B. P. Chattopadhyay, K. K. Saha, and M. Mahadevappa, "Screening of ischemic heart disease based on PPG signals using machine learning techniques," in *Proc. 2020 42nd Annu. Int. Conf. IEEE Engineering in Medicine & Biology Society (EMBC)*, 2020, pp. 5980–5983, doi: 10.1109/EMBC44109.2020.9176447.

[180] T. Aydemir, V. M. Şahin, and Ö. Aydemir, "Determination of hypertension disease with optimal frequency range of short-time photoplethysmography signals," in *Proc. 2020 Medical Technologies Congress (TIPTEKNO)*, 2020, pp. 1–4, doi: 10.1109/TIPTEKNO50054.2020.9299292.

[181] P. Mehrgardt, M. Khushi, S. Poon, and A. Withana, "Deep learning fused wearable pressure and PPG data for accurate heart rate monitoring," *IEEE Sensors Journal*, vol. 21, no. 23, pp. 27106–27115, Dec. 2021, doi: 10.1109/JSEN.2021.3123243.

[182] L. Gohlke, F. Dreyer, M. P. Álvarez, and J. Anders, "An IoT-based low-cost heart rate measurement system employing PPG sensors," in *Proc. 2020 IEEE SENSORS*, 2020, pp. 1–4, doi: 10.1109/SENSORS47125.2020.9278844.

[183] R. Gupta, "Lossless compression technique for real-time photo-plethysmographic measurements," *IEEE Transactions on Instrumentation and Measurement*, vol. 64, no. 4, pp. 975–983, Apr. 2015.

[184] M. Shabaan et al., "Survey: Smartphone-based assessment of cardiovascular diseases using ECG and PPG analysis," *BMC Medical Informatics and Decision Making*, vol. 20, no. 1, pp. 1–16, 2020.

[185**]** L. Smital et al., "Real-time quality assessment of long-term ECG signals recorded by wearables in free-living conditions," *IEEE Transactions on Biomedical Engineering*, vol. 67, no. 10, pp. 2721–2734, 2020.

[186] S. Acharya et al., "Non-Invasive Estimation of Hemoglobin Using a Multi-Model Stacking Regressor," *IEEE Journal of Biomedical and Health Informatics*, vol. 24, no. 6, pp. 1717–1726, 2020.

[187] Y. Choi, Q. Zhang, and S. Ko, "Noninvasive cuffless blood pressure estimation using pulse transit time and Hilbert–Huang transform," *Computers & Electrical Engineering*, vol. 39, no. 1, pp. 103–111, 2013.

[188] S. Weinschenk, R. Beise, and J. Lorenz, "Heart rate variability (HRV) in deep breathing tests and 5-min short-term recordings: agreement of ear photoplethysmography with ECG measurements, in 343 subjects," *European Journal of Applied Physiology*, vol. 116, pp. 1527–1535, 2016.

[189] S. Mejía, "Hidden Markov Models for early detection of cardiovascular diseases," *Ingeniería Solidaria*, vol. 20, pp. 1–31, 2023, doi: 10.16925/2357-6014.2024.01.02.

[190] J. Rhee, K. Park, J. Cho, and S. Lee, "A study of the application and the limitations of GPR investigation on underground survey of the Korean expressways," *Remote Sensing*, vol. 13, no. 9, pp. 1–23, 2021.

[191**]** L. Muñoz-Gonzalez, M. Lázaro-Gredilla, and A. R. Figueiras-Vidal, "Laplace approximation for divisive Gaussian processes for nonstationary regression," *IEEE Transactions on Pattern Analysis and Machine Intelligence*, vol. 8, no. 3, pp. 618–624, 2016.

[192**]** P. Paral, S. Ghosh, A. Chatterjee, and S. K. Pal, "Automatic relevance determination kernel-embedded Gaussian process regression for sonar-based human leg localization with a mobile robot," *IEEE Sensors Letters*, vol. 7, no. 1, pp. 1–4, 2023, Art no. 6000504.

[193**]** D. Chicco, M. J. Warrens, and G. Jurman, "The coefficient of determination R-squared is more informative than SMAPE, MAE, MAPE, MSE, and RMSE in regression analysis evaluation," *PeerJ Computer Science*, vol. 7, Art no. e623, 2021.

[194**]** V. Rawal, A. Dhamija, and S. Gupta, "Recent advances in wearable bio-sensors application," *International Journal of Scientific Research in Computer Science, Engineering and Information Technology*, vol. 1, no. 5, pp. 154–159, 2012.

[195**]** H. B. Celikoglu, "Application of radial basis function and generalized regression neural networks in non-linear utility function specification for travel mode choice modelling," *Mathematical and Computer Modelling*, vol. 44, pp. 640–658, 2006.

[196**]** S. Hannan, R. Manza, and R. Ramteke, "Generalized regression neural network and radial basis function for heart disease diagnosis," *International Journal of Computer Applications*, vol. 7, no. 13, 2010.

[197] F. Liu, Y. Si, and T. Luo, "The ECG identification based on GRNN," in *Proc. IEEE Int. Conf. Commun. Syst. (ICCS)*, 2019, ISBN: 978-1-5386-7865-7.

[198] M. Korürek and B. Doğan, "ECG beat classification using particle swarm optimization and radial basis function neural network," *Expert Systems with Applications*, vol. 37, pp. 7563–7569, 2010.

[199] Y. Qawqzeh, R. Uldis, and M. Alharbi, "Photoplethysmogram second derivative review: Analysis and applications," *Academic Journals Scientific Research and Essays*, vol. 10, no. 21, pp. 633–639, 2015.

[200] M. Blanco, V. Miranda, and G. Vargas, "Generalized regression neural networks with application in neutron spectrometry," in *Artificial Neural Networks - Models and Applications*, InTech Open Science, ch. 3, pp. 49–83, 2016.

[201] D. F. Spetch and H. Romsdhal, "Experience with adaptive probabilistic neural networks and adaptive general regression neural networks," in *Proc. IEEE Int. Conf. Neural Netw.*, vol. 2, pp. 1203–1208, 1994.

[202] D. F. Spetch and P. Shapiro, "Generalization accuracy of probabilistic neural networks compared with back propagation networks," in *Proc. IJCNN-91 Seattle Int. Joint Conf. Neural Netw.*, vol. 1, pp. 887–892, 1991.

CHAPTER-6

[203] M. M. R. K. Mamun and T. Elfouly, "Detection of cardiovascular disease from clinical parameters using a one-dimensional convolutional neural network," *Bioengineering*, vol. 10, no. 7, Art no. 796, 2023. [Online]. Available: https://doi.org/10.3390/bioengineering10070796

[204] S. Mondal, R. Maity, Y. Omo, S. Ghosh, and A. Nag, "An efficient computational risk prediction model of heart diseases based on dual-stage stacked machine learning approaches," *IEEE Access*, vol. 12, pp. 7255–7270, 2024. [Online]. Available: https://doi.org/10.1109/ACCESS.2024.3350996

[205] F. Sohil, M. U. Sohali, and J. Shabbir, "An introduction to statistical learning with applications in R: by Gareth James, Daniela Witten, Trevor Hastie, and Robert Tibshirani," *Statistical Theory and Related Fields*, vol. 6, no. 1, p. 87, 2021. [Online]. Available: https://doi.org/10.1080/24754269.2021.1980261

[206] E. Puyol-Antón et al., "Regional multi-view learning for cardiac motion analysis: Application to identification of dilated cardiomyopathy patients," *IEEE Transactions on Biomedical Engineering*, vol. 66, no. 4, pp. 956–966, 2019. [Online]. Available: https://doi.org/10.1109/TBME.2018.2865669

[207] A. Arifuddin, G. S. Buana, R. A. Vinarti, and A. Djunaidy, "Performance comparison of decision tree and support vector machine algorithms for heart failure prediction," *Procedia Computer Science*, vol. 234, pp. 628–636, 2024. [Online]. Available: https://doi.org/10.1016/j.procs.2024.03.048

[208] K. Sumwiza, C. Twizere, G. Rushingabigwi, P. Bakunzibake, and P. Bamurigire, "Enhanced cardiovascular disease prediction model using random forest algorithm," *Informatics in Medicine Unlocked*, vol. 41, 2023. [Online]. Available: https://doi.org/10.1016/j.imu.2023.101316

[209] Z. Li and H. Zhang, "Fusing deep metric learning with KNN for 12-lead multi-labelled ECG classification," *Biomedical Signal Processing and Control*, vol. 85, 2023. [Online]. Available: https://doi.org/10.1016/j.bspc.2023.104849

[210] F. Ancona, A. M. Colla, S. Rovetta, and R. Zunino, "Implementing probabilistic neural network," *Neural Computing & Applications*, vol. 7, pp. 37–51, 1998.

[211] M. Blanco, V. Miranda, and G. Vargas, "Generalized regression neural networks with application in neutron spectrometry," in *Artificial Neural Networks - Models and Applications*, InTech Open Science, ch. 3, pp. 49–83, 2016.

[212] Z. Ebrahimi, M. Loni, M. Daneshtalab, and A. Gharehbaghi, "A review on deep learning methods for ECG arrhythmia classification," *Expert Systems with Applications: X*, vol. 7, 2020. [Online]. Available: https://doi.org/10.1016/j.eswax.2020.100033

[213] Q. Qananwah, M. Ababneh, and A. Dagamseh, "Cardiac arrhythmias classification using photoplethysmography database," *Scientific Reports*, vol. 14, no. 1, Art no. 3355, 2024. [Online]. Available: https://doi.org/10.1038/s41598-024-53142-9

[214] W. F. Wang, C. Y. Yang, and Y. F. Wu, "SVM-based classification method to identify alcohol consumption using ECG and PPG monitoring," *Personal and Ubiquitous Computing*, vol. 22, pp. 275–287, 2018. [Online]. Available: https://doi.org/10.1007/s00779-017-1042-0

[215] R. J. Martis, U. R. Acharya, K. M. Mandana, A. K. Ray, and C. Chakraborty, "Application of principal component analysis to ECG signals for automated diagnosis of cardiac health," *Expert Systems with Applications*, vol. 39, pp. 11792–11800, 2012. [Online]. Available: https://doi.org/10.1016/j.eswa.2012.04.072

[216] J. Cano, L. Fácila, P. Langley, R. Zangróniz, R. Alcaraz, and J. J. Rieta, "Application of deep neural network models for blood pressure classification based on photoplethysmographic recordings," in *2021 International Conference on e-Health and Bioengineering (EHB)*, 2021, pp. 1–4. [Online]. Available: https://doi.org/10.1109/EHB52898.2021.9657658

[217] X. Ding, B. P. Yan, Y.-T. Zhang, J. Liu, N. Zhao, and H. K. Tsang, "Pulse transit time-based continuous cuffless blood pressure estimation: A new extension and a comprehensive evaluation," *Scientific Reports*, vol. 7, no. 1, Art no. 11554, Dec. 2017.

[218] Y. Liang, Z. Chen, R. Ward, and M. Elgendi, "Hypertension assessment via ECG and PPG signals: An evaluation using MIMIC database," *Diagnostics*, vol. 8, no. 3, p. 65, Sep. 2018.

[219] W. H. Lin, H. Zhang, and Y. T. Zhang, "Investigation on cardiovascular risk prediction using physiological parameters," *Computational and Mathematical Methods in Medicine*, vol. 2013, pp. 1–21, 2013.

[220] J. Kim, M. Kim, K. Park, and H. -S. Kim, "Mental stress assessment using SVM with physiological sensor data," in *2021 International Conference on Information and Communication Technology Convergence (ICTC)*, 2021, pp. 1296–1299. [Online]. Available: https://doi.org/10.1109/ICTC52510.2021.9621148.

[221] R. Kumar, Y. Aggarwal, and V. K. Nigam, "Autonomic features in prediction of coronary artery disease and myocardial infarction," *IETE Journal of Research*, Apr. 2022.

[222] S. D. Desai, I. F. Dessai, and L. Kulkarni, "Intelligent heart disease prediction system using probabilistic neural network," *International Journal of Advanced Trends in Computer Science and Engineering (IJATCSE)*, vol. 2, no. 5, pp. 22–28, 2013, Special Issue of ICCECT 2013 - Held during September 20, 2013, Bangalore, India.

[223] M. Vijayavanan, V. Rathikarani, and P. Dhanalakshmi, "Automatic classification of ECG signal for heart disease diagnosis using morphological features," *International Journal of Computer Science & Engineering Technology (IJCSET)*, vol. 5, no. 04, Apr. 2014.

[224] A. Carpenter and A. Frontera, "Smart-watches: A potential challenger to the implantable loop recorder?" *Europace*, vol. 18, no. 6, p. euv427, 2016.

[225] S. Nemati *et al.*, "Monitoring and detecting atrial fibrillation using wearable technology," in *2016 Annual International Conference of the IEEE Engineering in Medicine and Biology Society (EMBC)*, 2016.

[226] S. Balambigai and P. Jeevitha, "A survey on investigation of vital human parameters from photoplethysmography signal to predict the risk of cardiovascular diseases," in *2017 4th IEEE International Conference on Advanced Computing and Communication Systems (ICACCS)*, Coimbatore, India, Jan. 2017, pp. 1–4.

[227] N. R. Kanawade, S. Tewary, and H. K. Sardana, "Photoplethysmography-based arrhythmia detection and classification," in *2019 6th International Conference on Signal Processing and Integrated Networks (SPIN)*, 2019, pp. 944–948. [Online]. Available: https://doi.org/10.1109/SPIN.2019.8711737.

Rashmi Rekha Sethi
26/06/25